THE ROLE OF COSMICS RAYS

IN LIGHTNING INITIATION

By

NATHAN CARL LINDY

Bachelor of Science in Physics
Grand Valley State University
Allendale, Michigan
2007

Bachelor of Science in Mathematics
Grand Valley State University
Allendale, Michigan
2008

Submitted to the Faculty of the
Graduate College of the
Oklahoma State University
in partial fulfillment of
the requirements for
the Degree of
DOCTOR OF PHILOSOPHY
July, 2014

THE ROLE OF COSMIC RAYS

IN LIGHTNING INITIATION

Dissertation Approved:

Eric Benton

Dissertation Adviser

Mario Borunda

John Mintmire

Mostafa Elshahed

ACKNOWLEDGEMENTS

I would like to thank my advisor, Eric Benton, for his continued guidance throughout the course of this project and also for being an excellent mentor. I would also like to thank the current and former members of the E. V. Benton Radiation Physics Laboratory: Joel Dewitt, Tyler Collums, Rafiq Islam, Aaron Ruse, Jonathan Monson, Robert Honeyman, Meysam Tavakoli, Rajesh Panthi, and Joseph Ross. Their assistance on this project as well their camaraderie was important to me. I especially wish to thank Aaron Ruse for setting up both the Boltek Electric Field Mill and the cosmic ray muon detectors that that were used in this work and Robert Honeyman for all his help with the developing the software used analyze the cosmic ray muon detector array and Oklahoma Lightning Mapping Array data sets.

I would also like to thank William Beasley and Danyal Petersen of the University of Oklahoma's School of Meteorology for their help and support of this work. I would like to especially thank Danyal Petersen for providing many of the electrical and lightning discharge photographs, monitoring the cosmic ray muon detectors, and explaining the physics of electrical discharges in the atmosphere and the different lightning initiation models used in this work. There is very little in this work that has not been improved because of the help and support of Danyal Petersen.

Special thanks also goes to Art Lucas for the many discussions about and advice he had for this work. I also wish to thank the authors of CORSIKA for all their help and support during this project.

Finally, I wish to thank the members of my graduate committee for taking the time to review this work.

This work was part of the Oklahoma State University Radiation Physics Laboratory and University of Oklahoma's School of Meteorology collaboration supported by the DARPA Nimbus program.

Name: Nathan Carl Lindy

Date of Degree: JULY, 2014

Title of Study: THE ROLE OF COSMIC RAYS IN LIGHTNING INITIATION

Major Field: Physics

Abstract: From electric field measurements, the maximum electric fields typically found within a thunderstorm are an order of magnitude too weak to initiate a lightning discharge. Relativistic electrons produced in galactic cosmic ray (GCR) extensive air showers (EAS) in the atmosphere have been theorized to be accelerated in thunderstorm electric fields and initiate long lived Relativistic Runaway Electron Avalanches (RREA). RREAs produce an increasing number of high energy secondary electrons, which also initiate further RREAs. The RREA and hybrid lightning initiation models propose that RREAs produced in thunderstorm electric fields are able to initiate lightning discharges. The RREA model proposes that RREAs produce a sufficient number of high energy secondary electrons to generate a lightning discharge. The hybrid model proposes that the RREAs ionize the atmosphere and generate a plasma of low energy electrons that enhances the thunderstorm electric field sufficiently to that a lightning discharge can be initiated by hydrometeors. Using the Monte Carlo code CORSIKA 6.790, the fair weather EAS secondary electron environment has been simulated and has been found to have a maximum secondary electron density of ~10^5 >1 MeV secondary electrons m^{-2} and includes >1 GeV secondary electrons at an altitude of 6 km. This population of secondary electrons was then propagated through a measured thunderstorm vertical electric field profile to determine if there are a sufficient number of secondary electrons to initiate a lightning discharge according to both the RREA and hybrid models. There was not a sufficient numbers of secondary electrons for either model to initiate a lightning discharge, but the hybrid model only required an order of magnitude increase in the number of electrons in order to initiate a lightning discharge compared to the ten orders of magnitude required by the RREA model. By combining the data from a ground based cosmic ray muon detector array and the Oklahoma Lightning Mapping Array, it was found that at >90% confidence level, that lightning initiations within 1 km of the cosmic ray detector array were preceded by the passage of an EAS through the thunderstorm.

TABLE OF CONTENTS

Chapter Page

Chapter Page

LIST OF TABLES

LIST OF FIGURES

Figure Page

Figure Page

Figure Page

Figure Page

Figure Page

Figure Page

Figure Page

Figure Page

Figure Page

CHAPTER I

INTRODUCTION

Lightning is a beautiful, yet mysterious natural phenomenon. Associated with thunderstorms worldwide, lightning discharges are several kilometer long electrical discharges that propagate through the Earth's atmosphere. Worldwide, there are on average 81 lightning discharges per second being recorded by weather satellites. Thunderstorms are not evenly distributed through the world, with the majority of them occurring over coastal land areas near the equator [1]. In the United States, there is a large variation in the lightning discharge rate, i.e. the rate lightning discharges are produced, in the different geographic areas. The Gulf region, especially central Florida, has the highest lightning discharge rate within the continental United States. The Midwest, South East, Texas, and Oklahoma have the next highest lightning discharge rate [2]. Thunderstorm systems in Florida tend to contain dozens of small thunderstorms compared to the single, large (and generally severe) thunderstorm supercells that can affect more inland areas such as Oklahoma [3]. In comparison to these other areas, there is little lightning activity in the Northern and Western parts of the continental United States. On average, 25 to 30 million lightning discharges reach the ground over the continental United States every year [2].

Every year, damage to structures and property due to lightning discharges accounts for 5% of the insurance claims in the United States [4]. In Oklahoma, a typical single story house is struck by lightning approximately every 80 to 160 years [1]. The time between lightning strikes for a two story house is approximately a quarter of the time for a single story house [4]. The average insurance claim due to lightning damages for a house is $916 [5], but house fires started by lightning discharges can completely destroy a home [4]. The estimated property damage due to lightning discharges is between $300 million to $1 billion per year in the United States, making it the eighth most expensive source of property damage [4, 5].

Table 1.1: Activities with the most reported lightning related fatalities in the United States between 2006 and 2012 [Modified from 6]

Activity	Number of Reported Fatalities	Percentage of all Reported Fatalities
On or Near Water	56	24%
Non-Water Sports	29	12%
Walking	16	7%
Camping	15	6%
Farming or Ranching	11	5%
Riding Bicycle or Motorcycle	10	4%
Social Gathering	9	4%
Yard Work	8	3%

In addition to the property damage, lightning is also responsible for injuring and killing people. Between approximately 40 deaths and over 300 injuries in the United States per year are attributed [4, 6]. Table 1.1 shows the eight activities with the most reported lightning related fatalities in the United States between 2006 and 2012 [6]. Activities that occur on water such as fishing, swimming or boating have the greatest number of lightning related fatalities. Approximately half of those fatalities occur while the victims are fishing (46%) [6]. The activity with the next highest number of lightning fatalities is non-water sports such as golf and soccer. Contrary to what one might think there are more soccer related fatalities (41%) than golf related fatalities (28%) [6]. Regardless of the activity, lightning related fatalities are all preventable if the proper warnings are heeded [4].

Combining the preventable deaths and cost of property damage, lightning discharges have been deemed to be a negative effect on society by many organizations [4]. One such organization, Defense Advanced Research Projects Agency (DARPA), has made basic lightning research a priority through their Nimbus Project. The work presented in this thesis was part of the collaboration between the Oklahoma State University (OSU) Radiation Physics Laboratory and the School of Meteorology at the University of Oklahoma (OU) for the DARPA Nimbus project.

Over the years, various properties of lightning discharges, such as lightning channel propagation and thunder generation mechanisms have been successfully modeled. However, there is no current model that can accurately describe the conditions required for lightning initiation in a thunderstorm. Ground based experiments have determined that for normal thunderstorm conditions (pressure, temperature, and relative humidity) an electric field of 1500 to 2000 kV m^{-1} is required to create a conventional electric discharge. The required electric field for dielectric breakdown is an order of magnitude larger than the electric fields

measured within thunderstorms [3, 7, 8]. This discrepancy between the measured electric field within a thunderstorm and the experimentally required electric fields for electrical discharges represents a large gap in our understanding of the lightning discharge process.

Two proposed lightning initiations models are the Relativistic Runaway Electron Avalanche model presented in *Gurevich et al.* [9] and the hybrid model presented in *Petersen et al.* [10]. The RREA model theorizes that relativistic secondary electrons from galactic cosmic ray (GCR) extensive air showers (EAS) are responsible for lightning initiation [9]. GCRs are high energy particles, mostly protons and heavy ions, that originate from outside the solar system and arrive more or less isotropically at the top of the atmosphere. Within the Earth's atmosphere, GCRs initiate high energy particle cascades that generate secondary particles and photons over a several square kilometer area. The secondaries from a single GCR are collectively called an EAS [11, 12]. Within a thunderstorm, the relativistic secondary electrons of an EAS are accelerated by the thunderstorm electric fields. These accelerated relativistic electrons initiate long lived electron avalanches, i.e. an exponentially growing population of electrons, in the thunderstorm called Relativistic Runaway Electron Avalanches (RREA). According to the RREA model, the density of electrons within an RREA is sufficient to initiate a lightning discharge [9]. The hybrid model theorizes that high energy electrons inside an RREA also generate a larger population of low energy secondary electrons as they propagate through the atmosphere. This population of low energy secondary electrons creates an ionized plasma in the thunderstorm. Inside the ionized plasma, the ambient electric field is enhanced up to the dielectric breakdown electric field threshold, either directly or by means of hydrometeors, allowing initiation of conventional hydrometeor discharges [10].

There are three research objectives in this work. The first objective is to determine the fair weather, i.e. no thunderstorm, secondary energetic electron environment, i.e. flux and energy spectrum, from cosmic ray EASs. The secondary electron environment is an important input parameter for both the RREA and hybrid lightning initiation models. Because there are few published measurements of secondary electron densities at altitudes <12 km where thunderstorms occur, the secondary electron environment was modeled using the cosmic ray Monte Carlo code CORSIKA 6.790 [11, 13].

The second objective is to determine if there are enough secondary electrons from EASs to initiate lightning for either the RREA or hybrid models in typical thunderstorm electric fields. Previous studies of the RREA model had used electric fields up to the dielectric breakdown electric field strength [9, 14, 15, 16, 17, 18, 19], which are not observed in thunderstorm electric field measurements [3, 7, 20, 21]. This work uses electric fields that have been measured in thunderstorms and should provide a suitable verification of the RREA and hybrid models.

The third objective is to attempt to obtain experimental evidence correlating the passage of EASs through a thunderstorm with lightning initiation. Because the majority of secondary electrons range out, i.e. lose all of their kinetic energy and recombine with the atoms and molecules within the atmosphere, before reaching the ground [11], this work uses ground based measurements of the secondary muons, which are also produced in EASs, to detect the passage of EASs through that atmosphere [11]. Muons are leptons like electrons, but approximately two hundred times more massive, and are unstable [12]. Secondary muons from EASs are typically very energetic and reach the ground before decaying [11, 22]. The secondary muons are measured by a ground based cosmic ray muon detector array built by my collaborator, Aaron Ruse, formerly of the OSU Radiation Physics Laboratory [23]. To detect the passage of EASs, an array of four of the cosmic ray muon detectors was built and deployed in Norman, OK. EASs produce secondary muons over a large area, so coincident measurements between multiple cosmic ray muon detectors imply that an EAS has just passed through the atmosphere right above the array. The passage of an EAS through the array is then compared to nearby lightning initiation as measured by the Oklahoma Lightning Mapping Array (OKLMA) to determine if the passage of EASs through the thunderstorm coincides with lightning initiation.

CHAPTER II

EARTH'S ATMOSPHERE

Thunderstorms are meteorological systems that develop within the Earth's fair weather atmosphere. The fair weather atmosphere, including ambient electric and magnetic fields, are necessary components in the development of thunderstorms and the propagation of GCR EAS secondary particles through the atmosphere.

2.1. Composition and Layers of the Atmosphere

The Earth's atmosphere can be considered as a homogenous mixture of gases, water in all phases, and solid and liquid aerosols. Dry air, i.e. all the gases in the atmosphere except for water vapor, makes up the bulk of the atmosphere and consists primarily of N_2, O_2, Ar, and CO_2 with many other gases in trace amounts. Table 2.1 shows the molar fractions of the main components of dry air. Trace gases, like O_3 and CO_2, play a large role in the chemistry of the atmosphere, but have a negligible effect on macroscopic processes such as thunderstorm development [24, 25].

Table 2.1: Molar Fractions of Dry Air [7].

Gas	Molar Fraction
N_2	0.7809
O_2	0.2095
Ar	0.0093
CO_2	0.0003

The amount of water in the atmosphere is highly variable and has a large effect on weather in general. On a global scale, the amount of water in the atmosphere depends on the latitude, geography, and season. The mixture between water vapor and air is called moist air and has slightly different physical properties than normal dry air, e.g. the density of moist air in the middle of a thunderstorm is ~3% lower than dry air [26]. It is these slight differences between moist and dry air that account for cloud formation and thunderstorm development. Liquid water and ice can also be found in the atmosphere as precipitation, graupel (mushy hail-like ice particles inside clouds), and cloud condensation nuclei.

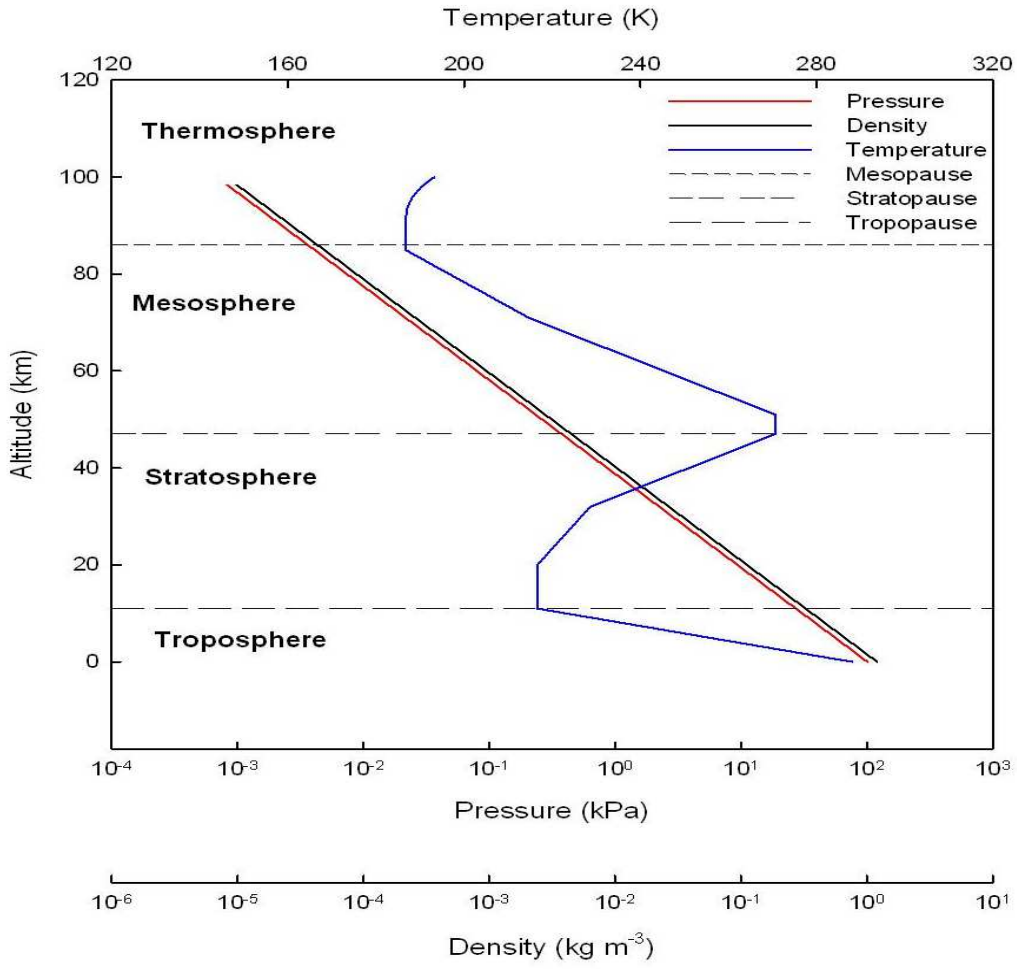

Figure 2.1. Plot of the pressure, density, and temperature profiles of the Earth's atmosphere as functions of altitude. The temperature profile determines the boundaries of the different layers of the atmosphere [7, 20].

Aerosols are non-gaseous particles, such as dust or organic compounds, and large ions, i.e. groups of neutral particles that collect around a single charged particle, that are suspended in the atmosphere. These aerosols act as condensation nuclei for water vapor in the atmosphere, effectively limiting the size and number of clouds, raindrops, and ice particles. Near the ground, most aerosols are created by pollution and by ionization from terrestrial radioactivity. The pollution travels up into the atmosphere and either directly becomes an aerosol or forms a large ion along with other neutral particles in the atmosphere. Large ions also form high in the atmosphere from particles ionized by galactic cosmic rays. At thunderstorm altitudes, aerosols make up only a tiny fraction of the entire atmosphere (aerosols have a density between 4 and 20 $\mu g\ m^{-3}$ compared to the ~1 $kg\ m^{-3}$ density of dry air [25, 27]). However, aerosols play a large role in the formation of clouds and precipitation, so any macroscopic understanding of a thunderstorm must include microscopic understanding of aerosols [25, 27].

The Earth's atmosphere is relatively well mixed between the Earth's surface and the edge of space, ~100 km above the Earth's surface. Because of the Earth's gravity, the atmosphere is not homogenous over its entire volume. Instead the density and pressure of the atmosphere decrease exponentially with altitude as expected for an ideal gas [7, 25]. Over half of the mass of the atmosphere is found below an altitude of 6 km. [13]. The temperature profile of the atmosphere does not behave as an ideal gas and is very dependent on altitude. Figure 2.1 shows atmospheric density, pressure, and temperature profiles between altitudes of 0 and 100 km from the U.S. Standard Atmosphere and *MacGorman & Rust* [7, 20].

The Earth's atmosphere can be divided into four regions based on how the temperature changes with altitude. The atmospheric region near the ground, where temperature decreases linearly with altitude, is called the troposphere. Between 10 and 20 km above the Earth's surface, the troposphere gives way to the stratosphere where temperature increases with altitude. This increase in temperature is due to the absorption of ultraviolet radiation from the sun by atmospheric ozone. The mesosphere starts around 50 km above the ground where again temperature decreases with altitude. Finally, around 80 to 90 km, the average temperature increases sharply and becomes highly variable in the thermosphere. The thermosphere trails out into space and is the first region affected by radiation from the sun. The boundaries between each layer vary with local conditions and season, and are called the tropopause, stratopause, and mesopause, respectively [28]. Thunderstorms are generally confined to the troposphere with only the largest storms extending above the tropopause.

2.2. Fair Weather Electric Field

The ultraviolet radiation from the sun causes the atmosphere in the thermosphere to ionize, creating an electrically conducting region of positive charge called the ionosphere. With the exception of charged aerosols, the atmosphere is made up of neutral gases and can be treated as a slightly lossy dielectric. The surface of the Earth is a relatively good conductor because of the salt in the oceans and metal compounds found in soil. From Wilson's measurements [8], it is known that the surface of the Earth is, on average, negatively charged. The Earth can be thought of as a spherical capacitor, with the Earth's surface and ionosphere acting as two spherical conductors and the atmosphere in between acting as the dielectric. There exists an electric field between the Earth's surface and the ionosphere called the fair weather electric field [20].

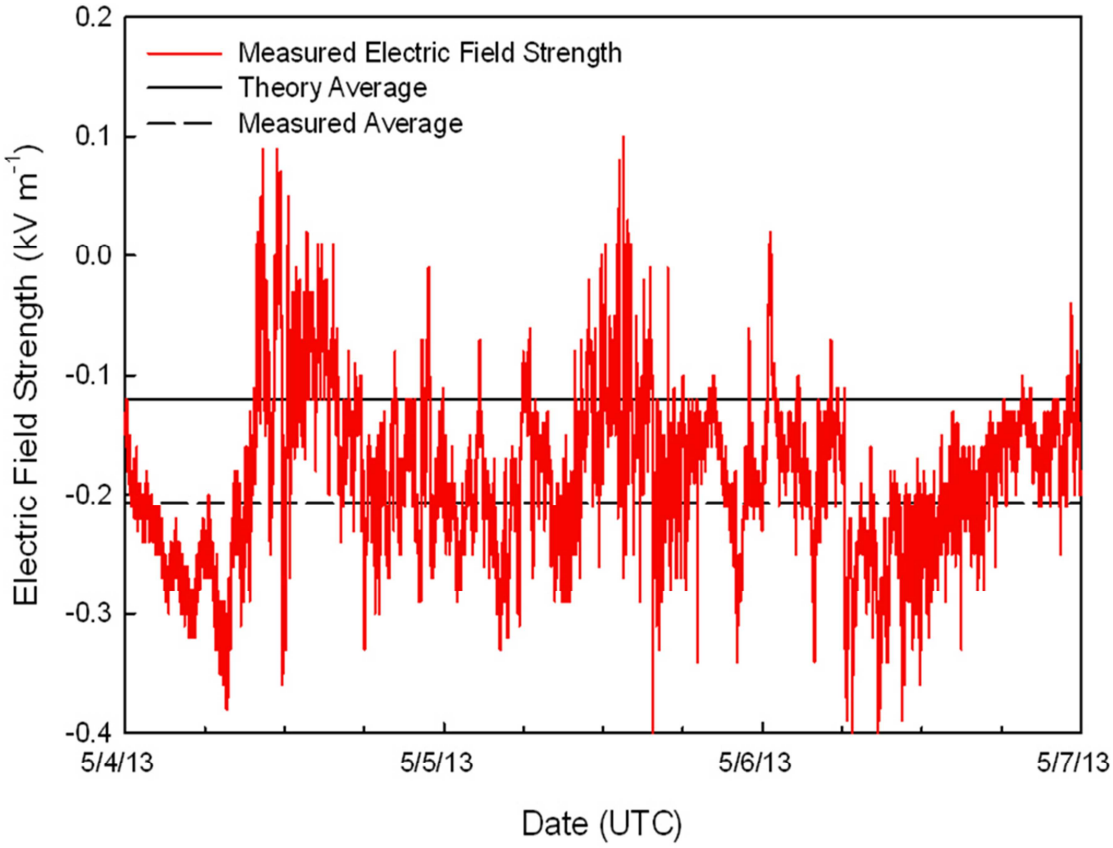

Figure 2.2. The fair weather electric field measured at the Venture 1 building in Stillwater, OK between 5/4/2013 to 5/7/2013 by a Boltek Atmospheric Electric Field Monitor [29]. The theoretical value of the fair weather electric field was taken to be -0.120 kV m^{-1} [10]. Central Standard Time (CST) is 5 hours later than Coordinated Universal Time (UTC).

The first reported measurement of the fair weather electric field was by Lemonnier in 1752, soon after Benjamin Franklin discovered the electrical nature of lightning [3, 30, 31]. The average fair weather electric field varies between -100 and -150 V m^{-1} on the ground with the negative sign indicating that the direction of the electric field is towards the Earth. An empirical formula for the fair weather electric field below 60 km is,

$$E(z) = -[93.8e^{-4.527z} + 44.4e^{-0.375z} + 11.8e^{-0.121z}], \quad (2.1)$$

where z is the altitude measured in kilometers, and $E(z)$ is the fair weather electric field measured in V m^{-1}[3]. Figure 2.2 is a plot of the fair weather electric field measured by a Boltek Atmospheric Electric Field Monitor [29] located atop the Venture 1 building in Stillwater, OK, between the dates of 5/4/2013 to 5/7/2013.

A dominant feature of the fair weather electric field shown in Figure 2.2 is the diurnal variation. The fair weather electric field reaches a maximum downward field strength near the middle of the afternoon and is at a minimum during the night. This variation is due to the changing shape (and electric potential) of the ionosphere produced by the interaction with the solar wind [30, 31].

2.3. Global Electric Circuit

In order for the fair weather electric field to be ~ –100 V m^{-1} on the ground, the potential difference between the ionosphere and Earth needs to be ~250 kV. However due to galactic cosmic rays, the atmosphere is slightly conductive with a columnar resistance of ~200 Ω between the ground and the ionosphere in fair weather conditions [30], so the atmosphere acts like an *RC* circuit. The capacitance of the spherical Earth-ionosphere capacitor can be determined by,

$$C = 4\pi\varepsilon_o \frac{r_{earth} r_{ion}}{h}, \quad (2.2)$$

where the capacitance C is measured in Farads, r_{earth} is the radius of the Earth, r_{ion} is the radius of the ionosphere, and h is the scale height of the atmosphere. The scale height, h, is the altitude where the atmospheric density is e^{-1} of its density at sea level. The scale height is used instead of the actual height of the atmosphere because the atmospheric density decreases exponentially with altitude. For Earth, the atmospheric scale height is 7 km compared to the ~100 km actual height of the atmosphere [30]. The capacitance of the Earth-ionosphere is between 0.6 and 0.7 F, depending on the location on the Earth.

The time constant for the atmospheric *RC* circuit is

$$\tau = RC \approx (0.7\ \text{F})(200\ \Omega) = 140\ \text{s}. \tag{2.3}$$

The atmospheric *RC* circuit is a discharging capacitor, so in a manner of minutes, the Earth should be completely discharged and the fair weather electric field should no longer exist. According to Figure 2.2, the fair weather electric field can be measured continuously for periods of days, so there must be some natural process that is continuously charging the Earth.

The charging mechanism, together with the Earth-ionosphere capacitor, is called the global electric circuit and is illustrated in Figure 2.3. Recent satellite data has confirmed the decades old estimates that there are ~1000 thunderstorms covering ~1% of the Earth's surface at any given time, with the majority of these thunderstorms occurring over land and near the tropics [20]. Each thunderstorm on average delivers ~-200 C of charge to the Earth and it has been proposed that it is this transfer of electric charge that keeps the Earth's surface charged and the fair weather electric field detectable. In order to complete the circuit, C.T.R. Wilson proposed that an electrical current travels from the tops of thunderstorms to the ionosphere, which is called Wilson current [30, 31].

There are still unknowns in the global electric circuit, such as the columnar resistance near mountains and elevated locations. One of the main problems with the global electric circuit is that thunderstorms are not completely understood, especially with regard to how a thunderstorm transfers charge to the Earth's surface. Originally only lightning discharges were assumed to transfer all the electric charge to the Earth, but several studies [30, 31] have shown that both charged aerosols and point discharges also deliver charge to the Earth's surface. Charged aerosols can transfer charge directly by being absorbed by falling precipitation or indirectly by being removed from the thunderstorm region by strong winds. Point discharges, otherwise known as corona discharges or St. Elmo's fire, are non-sparking electrical discharges caused by the enhancement of the local, ambient electric field. Common objects that might enhance the local electric fields during a thunderstorm are blades of grass, leaves, metal poles, and even aerosols. An object undergoing point discharge ionizes the surrounding air molecules (possibly glowing a pale blue color), but does not create enough ions to generate an electrical spark. Thunderstorms generate large numbers of point discharges near the ground, which delivers large amounts of charge directly to the Earth's surface [3, 30, 31]. Some researchers claim that up to 60% of the total current transferred to the Earth's surface comes from non-lightning sources [31].

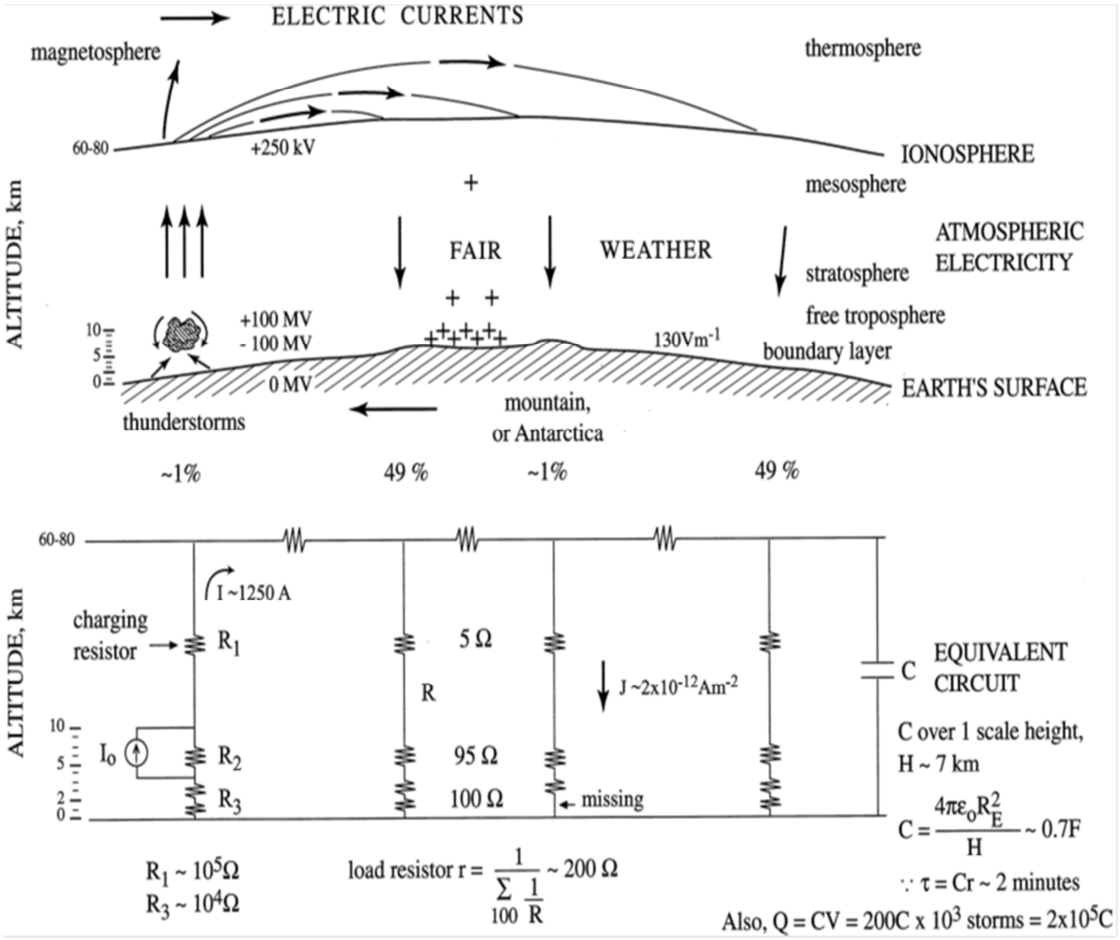

Figure 2.3: The global electric circuit both in the atmosphere and as an equivalent circuit. Numerical values are estimates of the real values and all calculations are accurate to an order of magnitude [30].

2.4. Earth's Geomagnetic Field

Within the Earth's atmosphere, the Earth's geomagnetic field can be approximated as a dipole magnet with the ends at the near North and South poles [32]. It is interesting to note that the South magnetic pole of the Earth is located in Northern Canada [33]. The Earth's magnetic field is generated by the rotation of liquid iron within the Earth's core [34]. Charged particles in motion within the atmosphere, especially low energy electrons, are deflected by the Earth's geomagnetic field [32]. Due to small variations within the Earth's core, the Earth's magnetic field varies with location and time [33, 34]. The total magnetic field strength in 2010 is shown in Figure 2.4.

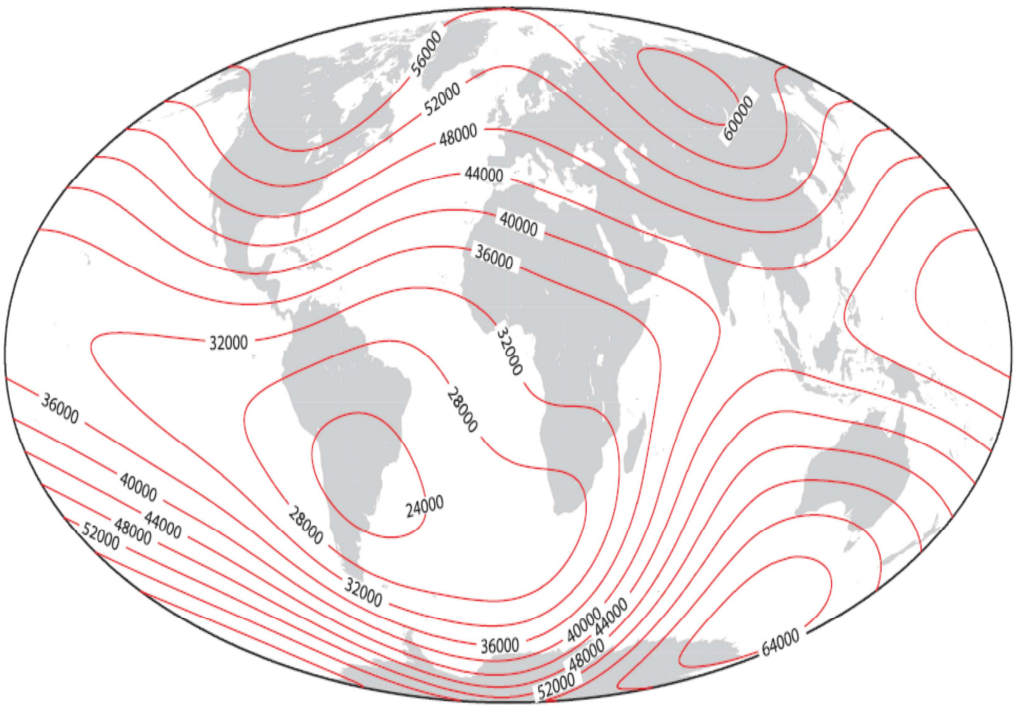

Figure 2.4: Contour map of the total strength of the Earth's magnetic field in nT for 2010 [33].

From the International Association of Geomagnetism and Aeronomy's latest IGRF 11 model, the total magnetic field strength at the muon detector telescope array in Norman, OK was 50.6969 μT on 1/29/2014 [33]. The cosmic ray Monte Carlo code CORSIKA uses the Earth's magnetic field as defined in IGRF 11 to transport secondary cosmic ray particles through the atmosphere accurately [13].

CHAPTER III

THUNDERSTORM DEVELOPMENT

Thunderstorms start to form when large amounts of moist air rise in the atmosphere through a process called convection. The rising air mass begins to cool and the water vapor within the air mass begins to condense into water droplets and freeze into ice. These water drops and ice particles continue to grow in size inside the thunderstorms until they become too large to be held in suspension within the atmosphere. Water drops and ice particles that are no longer suspended in the atmosphere begin to fall towards the ground as precipitation. In thunderstorms, lightning discharges typically occur after precipitation begins to fall [20].

Water drops and ice particles also become polarized in the fair weather electric field and become conductors in the atmosphere. Collisions between the different forms of water result in the generation of electric charge. As the thunderstorm develops, charged water drops and ice particles of different polarities are separated and collected in large regions called charge centers. The charge centers are responsible for generating the strong electric field within an active thunderstorm [20].

3.1. Convection

In order for a thunderstorm to develop, there must be an upward movement of a warm, moist air into the upper troposphere. This upward movement of moist air is an example of convection and thunderstorms are categorized by the physical process that creates this convection. Warm air is less dense than cold air, so as long as an air mass is warmer than the surrounding environment, the air mass will be buoyant in the atmosphere. As an air mass rises, it cools via adiabatic expansion and decreases in temperature. However, the atmospheric temperature also decreases with altitude within the troposphere. If the air

mass cools more rapidly than the atmosphere, its rise is inhibited. If the air mass cools less rapidly than the atmosphere, it remains buoyant and continues to rise. If the warm air mass contained only dry air, the maximum altitude reached by a buoyant air mass would be around 30 km, high in the stratosphere where atmospheric temperature increases with altitude [25].

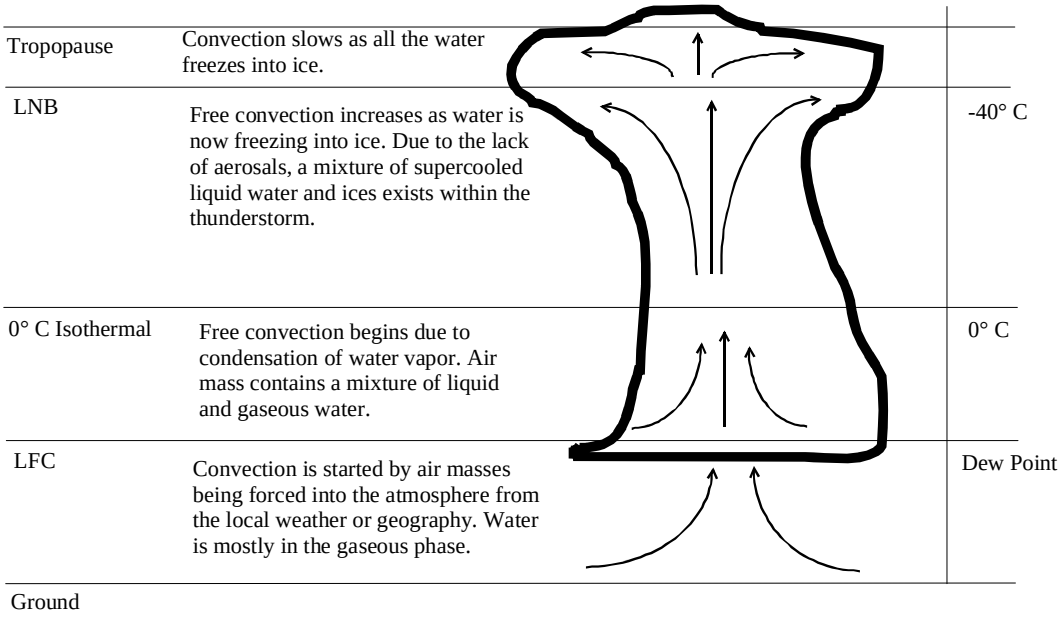

Figure 3.1. Diagram depicting convection currents within a thunderstorm: A warm, moist air mass is forced into the cooler atmosphere where the water vapor begins to condense at the LFC located at the dew point isothermal. The release of the heat of vaporization increases the rate of convection through free convection. Free convection continues above the 0°C isothermal when the gaseous and liquid water can free into ice particles and ends at the LNB at the -40°C isothermal, where all forms of water convert to ice particles [Adapted from 25].

Water vapor within a rising air mass is responsible for the formation of large cumulus and lightning producing cumulonimbus clouds. Unlike dry air, water vapor will condense into liquid water when the air mass cools to the dew point temperature. At the dew point temperature, the air mass is said to be saturated, which in meteorological terms means that liquid water is more favored to exist than water vapor. A saturated air mass would ideally condense all of its water vapor into liquid water at the dew point temperature, but typically there are not a sufficient number of aerosols (condensation nuclei) within a thunderstorm for this to occur. Without a sufficient number of aerosols acting as condensation nuclei, the air mass will contain supersaturated water vapor along with

liquid water cloud droplets [25]. The altitude which corresponds to the dew point of the ambient air is called the cloud condensation level (CCL) and is the altitude where clouds begin to form in the atmosphere. A rising, warm, moist air mass needs to cool more than the surrounding ambient air, so the altitude of its dew point is higher than the CCL. The altitude corresponding to the dew point temperature of a rising, warm, air mass is the level of free convection (LFC) and is higher than the CCL, but below the tropopause [25].

Above the LFC, water vapor from the rising air mass condenses into liquid water cloud droplets, releasing the latent energy of vaporization into the air mass. This energy raises the internal energy of the air mass and speeds the assent of the air mass, resulting in a process called free convection. In free convection, the air mass gains more energy from phase transitions of water than is lost to overcoming gravity and drag. Free convection continues to accelerate the air mass higher into the atmosphere as long as water vapor is being converted into liquid water, which is in part dependent on whether or not there are a sufficient number of aerosols and other condensation surfaces within the atmosphere [25, 35].

Once an air mass reaches the altitude of the 0° C isothermal, liquid water begins to freeze into solid ice particles called graupel and cloud ice, releasing the latent heat of freezing into the air mass. This provides another source of energy for free convection. The air mass will continue to rise in the atmosphere until all its gaseous and liquid water is converted into ice, which is the level of neutral buoyancy (LNB) [25]. Near the Earth's surface, liquid water quickly freezes into ice below 0°C due to the large availability of surfaces on to which the ice can condense in a process called heterogeneous freezing [25]. Aerosols and other ice particles are the only surfaces onto which liquid water can freeze high in the atmosphere, and, as with the condensation of water vapor to liquid water, can be relatively uncommon within a thunderstorm. Thus some of the liquid water may remain above the 0° C isothermal, the air mass becomes a mixture of supercooled liquid water and ice. Below -40° C, water molecules (both vapor and liquid) can directly freeze without any requiring condensation nuclei in a process called homogenous freezing [25]. Since water can spontaneously freeze below -40° C, air masses above the -40° C isothermal quickly lose their source of internal energy and only continue to rise due to its momentum. The most energetic air masses have been known to rise above the tropopause, which is above the -40° C isothermal [35]. Air masses above the LNB are cooler than the surrounding air and actually begin to fall back towards the ground, possibly bringing rain, hail, and strong downward winds called microbursts. Figure 3.1 shows the major steps of moist air convection in a thunderstorm. Another name for a rising air mass is a parcel and the process of thunderstorm convection as described above is called parcel theory [25, 35].

3.2. Thunderstorm Formation

Convection is the main mechanism that moves large amounts of water into the atmosphere so a thunderstorm can develop. Convection typically occurs over land where the ground heats faster than the air above. This creates a warm air mass near the ground that becomes buoyant and begins to rise. Alternatively, the geography of a region might push an air mass high into the atmosphere (for example wind pushing up the side of a mountain) and initiating convection. Both processes create what is called an air mass thunderstorm (also known as an isolated or scattered thunderstorm). Air mass thunderstorms generally do not last very long (30 minutes to an hour) and do not often produce hail and are unlikely to produce tornadoes [35]. Figure 3.2 shows the development of an air mass thunderstorm.

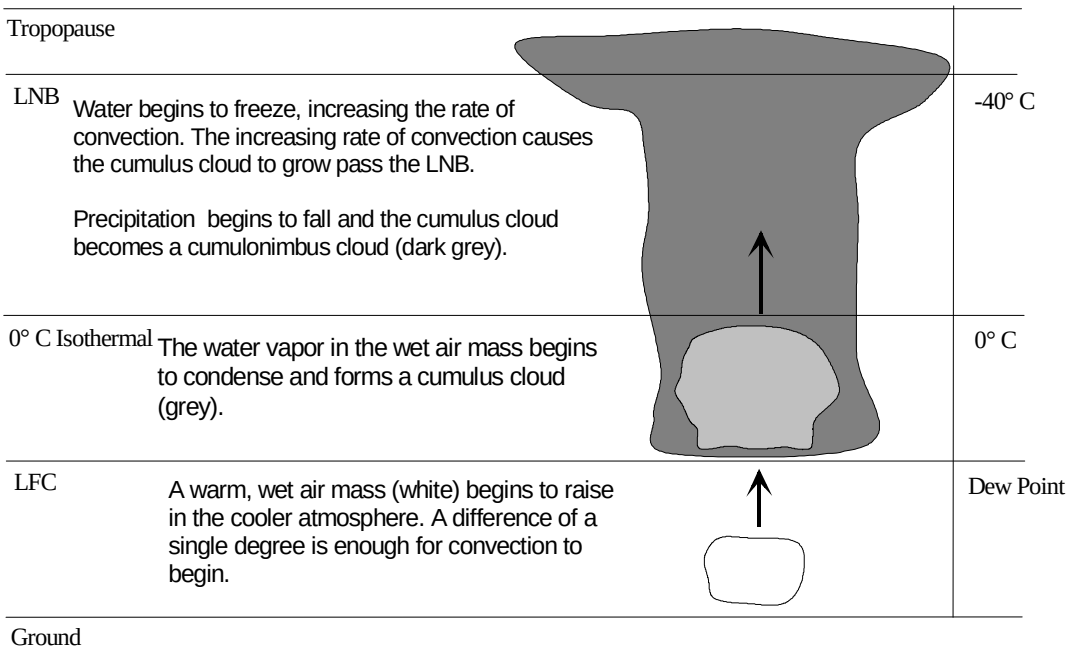

Figure 3.2. Development of an air mass thunderstorm: moist air masses are forced into the atmosphere due to convection and the water vapor begins to condense into small water droplets above the LFC. A cumulus cloud is formed by these water droplets and continues to grow in the atmosphere up to the LNB. The cumulus cloud becomes a cumulonimbus once precipitation begins to form [Adapted from 35].

Longer lived thunderstorms develop along cold and warm fronts. Along a cold front, a large mass of cold air moves toward a large mass of warm air. Since the warm air is less dense, the cold air mass pushes part of the large warm air mass high into the atmosphere, creating convection. A warm front occurs when a large mass of warm air overtakes and rises above a large mass of cold air, again creating convection. Thunderstorms can develop anywhere along the cold or warm fronts and can last for as long as the front exists. Thunderstorms produced by cold fronts are generally more severe than those from warm fronts, because the warm air is strongly forced upward along the front instead of slowly rising into the atmosphere. Figure 3.3 illustrates both cold and warm front thunderstorm convection. Because of the size of cold and warm air fronts, thunderstorms that develop along air fronts are called mesoscale thunderstorm systems [20, 35].

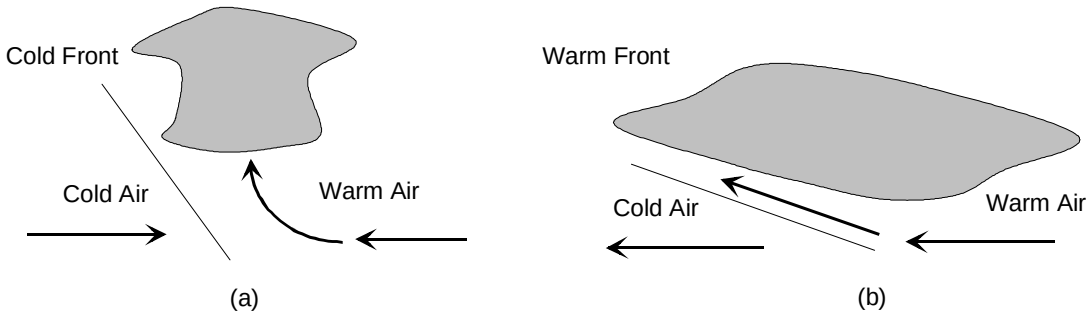

Figure 3.3. Diagrams illustrating convection along a (a) cold front and (b) warm front. (a) An advancing cold air mass forces a nearby warm air mass into the atmosphere, producing large cumulonimbus clouds. (b) An advancing warm air mass overtakes and rises above a cold air mass, producing rain-producing stratus clouds and few cumulonimbus clouds [Adapted from 35].

A strong and stable amount of convection is characteristic of severe thunderstorms, which allows them to grow taller than the tropopause and to produce hail, wind microbursts and tornados. Severe thunderstorms are generally long lived (>1 hour) [35].

All types of thunderstorms (air mass, mesoscale, and severe thunderstorms) can develop as a series of individual thunderstorm cells. Each thunderstorm cell can be >8 km in radius and move according to local wind conditions (along air mass fronts or with high winds). A dominant feature of a thunderstorm cell is a large column of upward moving air called an updraft, which is formed by a constant supply of air masses undergoing convection. Updrafts in a severe thunderstorm can have speeds of >30 m s^{-1}, but in most air mass thunderstorms updraft speeds are between 5 and 10 m s^{-1} [36]. The storm cells belonging to severe storms are called supercells due to their large size. The updraft within

a supercell can become twisted because of the wind shear, i.e. a wind strength gradient. A twisted updraft column can lead to the formation of large hail, wind microbursts, and tornadoes [36]. Figures 3.4 and 3.5 illustrate the updrafts for a typical thunderstorm cell and a supercell, respectively.

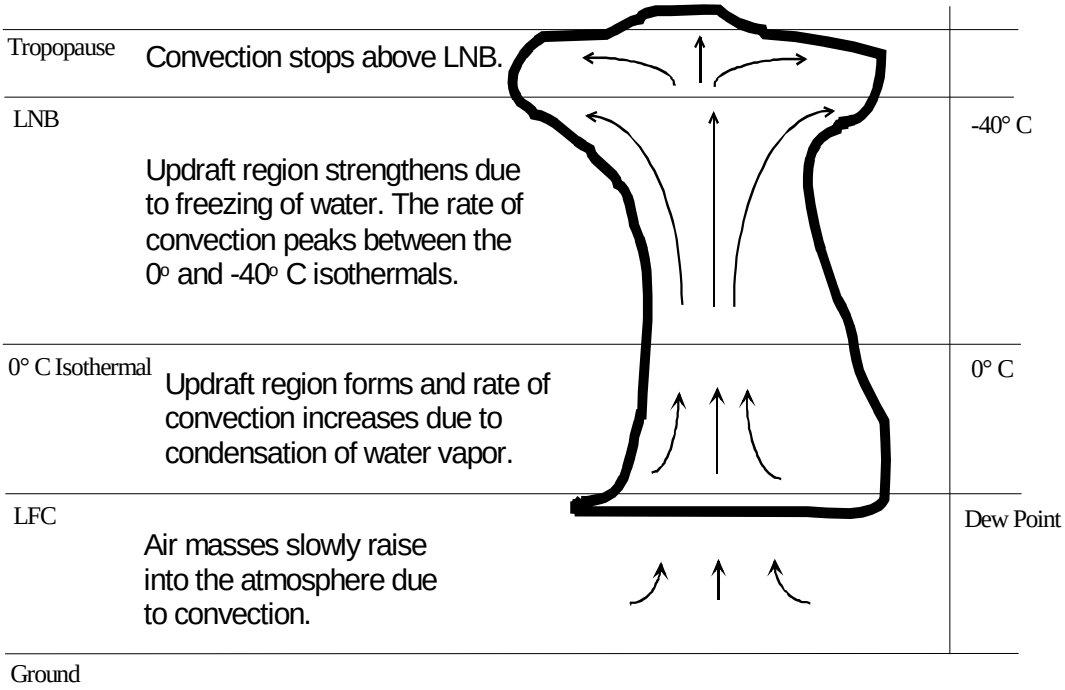

Figure 3.4. Diagram showing the strength of the updraft (arrows) in a typical thunderstorm cell. The length of the arrows represents the strength of the updraft with longer arrows representing a stronger updraft [Adapted from 20].

Regardless of type or size, a thunderstorm cell starts as a cumulus cloud. The base of the cumulus cloud rests at the CCL and builds in size with the addition of each convective air mass as water vapor condenses into cloud water and ice. As more moisture is brought into the cloud by the updraft, the water droplets become larger in a process called collision-coalescence, where small water droplets collide with one another and coalesce into one larger droplet and many tiny droplets [35, 37]. Figure 3.6 shows the relative sizes of the aerosol particles around which water droplets form (condensation nuclei), water droplets formed from the condensation of water vapor (cloud droplet), and a typical raindrop.

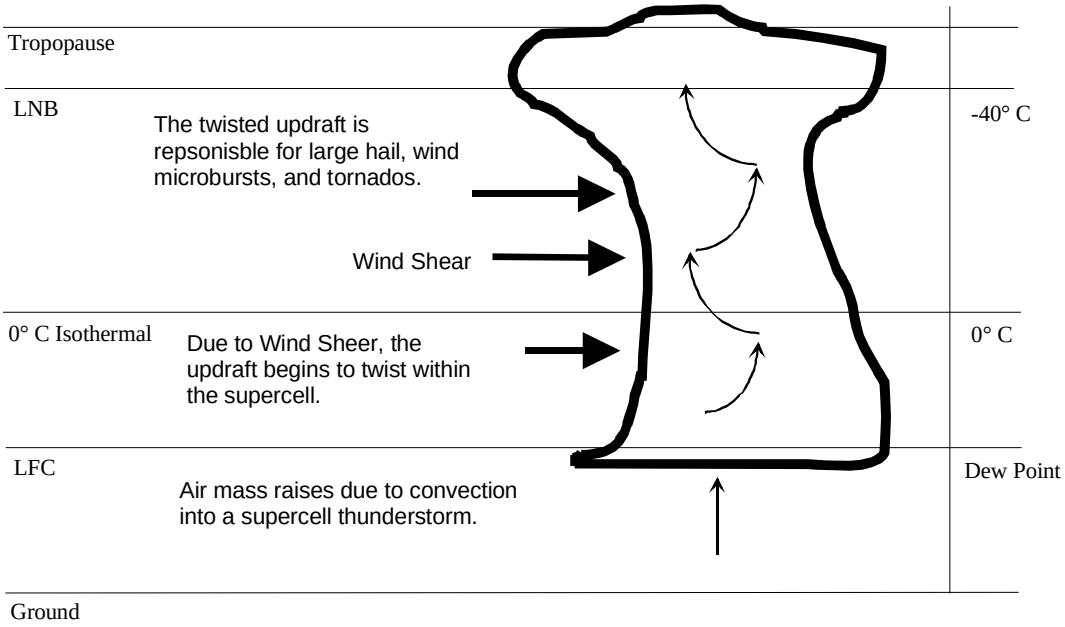

Figure 3.5. Diagram depicting the updraft (thin arrows) of a supercell thunderstorm. High lateral winds (thick arrows) twist the updraft in the supercell. This twisting allows the supercell to produce large hail, wind microbursts, and tornados [Adapted from 3 and 20].

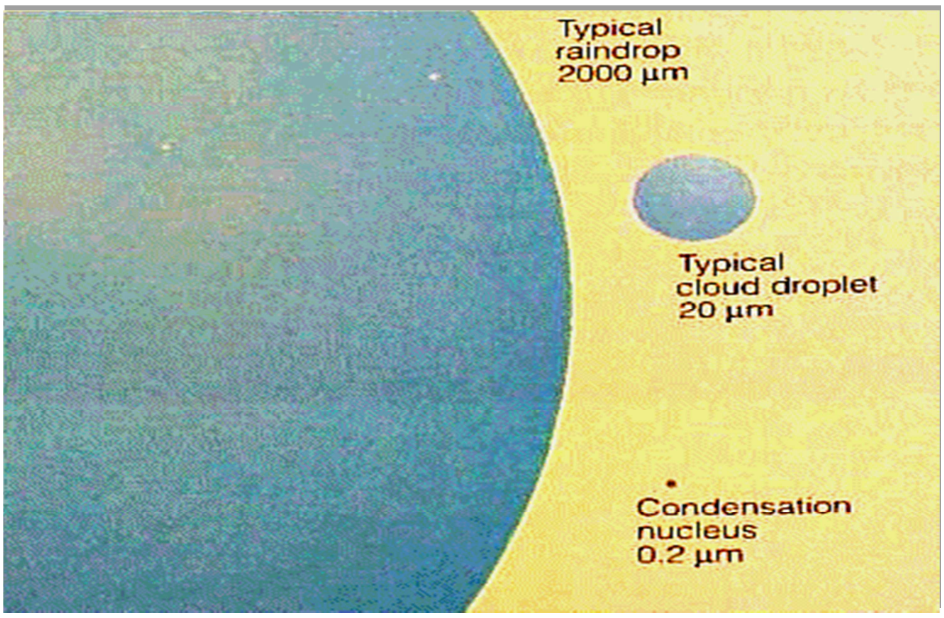

Figure 3.6. The relative sizes of raindrops, liquid cloud droplets, and aerosols (condensation nuclei) needed for the condensation of liquid water [37].

As water droplets get larger and more massive, they begin to fall out of suspension in the air mass and are kept aloft by the updraft. Once the weight of a water droplet overcomes the force of the updraft, the water droplet falls to the ground as a rain. If the cloud is above the 0° C isothermal, then graupel, which is sometimes called soft hail [25], is also often present. Graupel creates precipitation through the Bergerson process. In the Bergerson process, liquid water freezes onto graupel, making larger ice particles that fall out of suspension just like raindrops. At very cold temperatures and in strong updrafts, the Bergerson process creates hail, but in normal thunderstorm conditions it creates rain, sleet, or snow depending on how close the 0° C isothermal is to the ground [25, 35]. Figure 3.7 shows a flow chart of how different forms of precipitation are formed within thunderstorms.

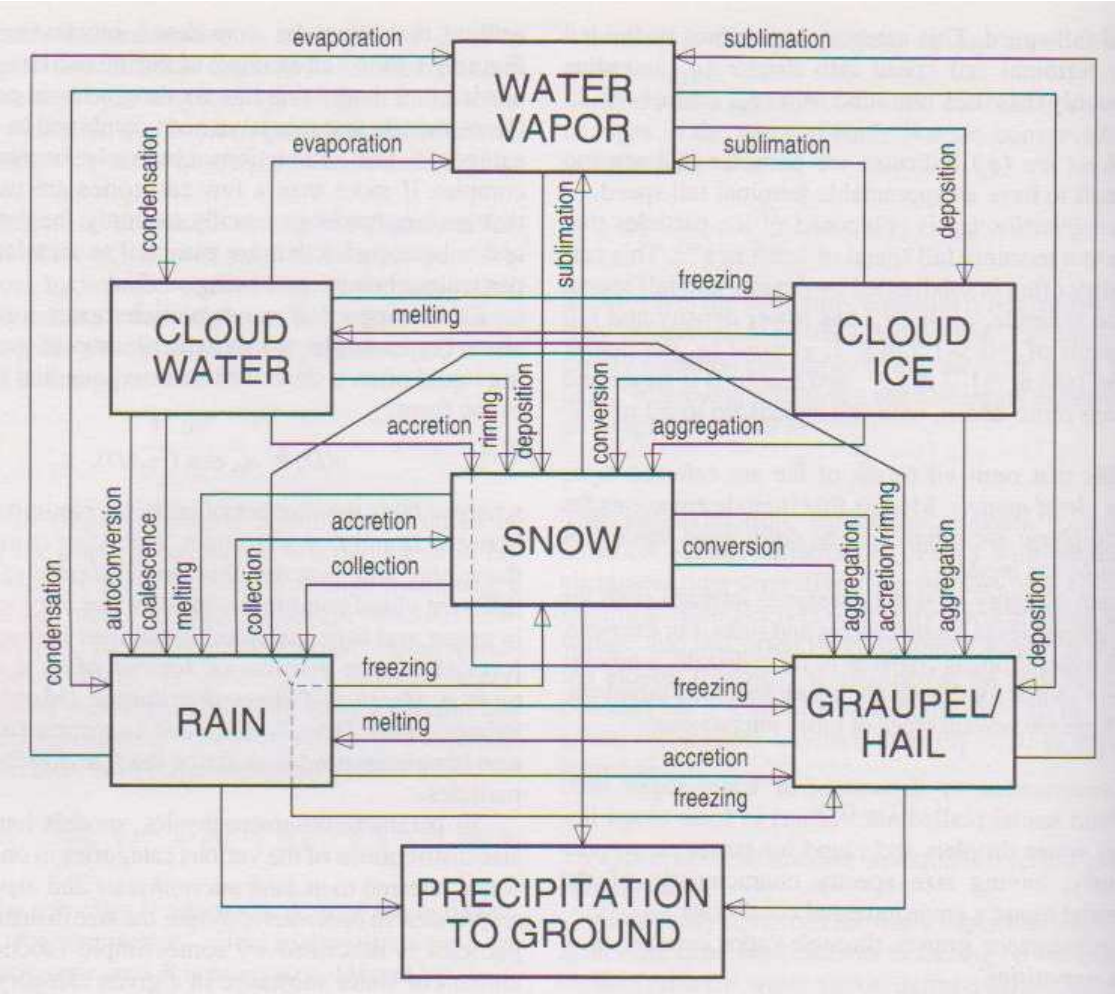

Figure 3.7. Flow chart describing how different forms of water are created within a thunderstorm. Sleet is considered a form of graupel or hail in this chart [20].

As convective air masses rise, the cumulus cloud grows in height, rising above the 0° C isotherm. As precipitation begins to fall, the thunderstorm enters the mature stage of its development. Lightning discharges also start to occur and reach a peak flash rate during the mature stage of a thunderstorm [3]. The cumulus cloud grows all the way to the LNB or possibly above the tropopause. As the precipitation begins to falls, the cumulus cloud becomes a cumulonimbus cloud. Falling precipitation also causes the surrounding air masses to fall with it, creating a downdraft. On the ground, the downdraft creates the high winds generally associated with thunderstorms. For an air mass thunderstorm, these high winds sweep away warm masses that were powering the updraft, which causes the storm to dissipate quickly. For mesoscale and severe thunderstorms, as more precipitation falls, the downdraft gets stronger and eventually overtakes the updraft, which begins the dissipating phase of the thunderstorm [35, 37].

During the dissipating phase of the thunderstorm, precipitation continues to fall, which is now being powered by the water stored in the clouds instead of convective air masses. Lightning still occurs, but is less frequent. Figure 3.8 shows a diagram for each of the different phases of a thunderstorm.

It is common to see a thunderstorm system develop, especially along fronts, with multiple storm cells in various stages of development spread over several hundred square miles. A single storm cell does not generally last for the entire length of a thunderstorm system; instead older storm cells are constantly being replaced by younger storm cells. However, supercells, once matured, can last for hours and travel hundreds of miles before dissipating [35, 36].

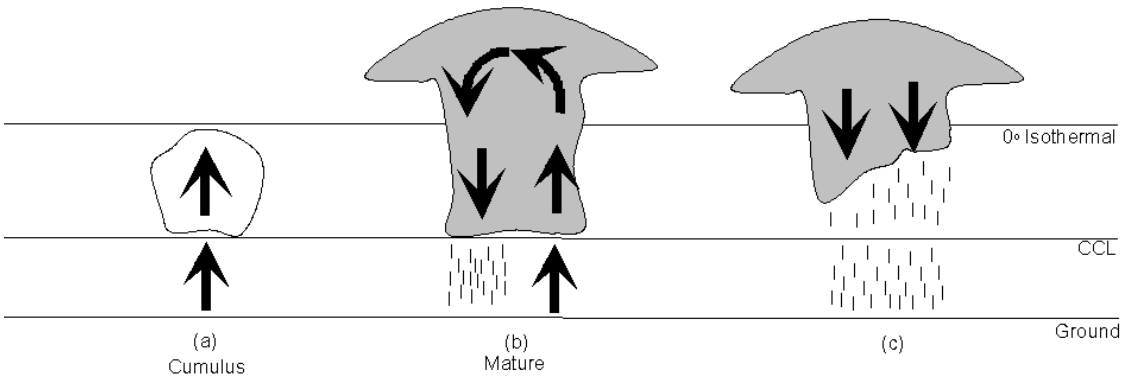

Figure 3.8. The different phases of a thunderstorm: a.) Cumulus stage, b.) Mature stage, and c.) Dissipating Stage. The arrows show the relative motion of the air masses and the vertical straight lines represent precipitation [Adapted from 35].

3.3. The Electrical Environment of a Thunderstorm

Benjamin Franklin was the first to associate thunderstorms and lightning discharges with electric charge, but because of the complex nature of thunderstorms, he could not determine the electrical charge structure of a thunderstorm [38]. Over a hundred years ago, C.T.R. Wilson using ground based electric field measurements found that thunderstorms generally have a positive charge region above a negative charge region [8]. These observations were later confirmed with weather balloons by G.C. Simpson [39]. An electrically charged region located above another charge region of the opposite charge is called a dipole [20]. In meteorology, dipoles do not necessarily require the electric charge of the charge regions to be equal and opposite [20]. Simpson's measurements from inside a storm cell also showed that a region of positive charge, smaller in magnitude than either of the main charge centers, often exists near the bottom of the storm cell [39]. The combination of a main positive dipole, named for the positive charge being above the negative charge, and the lower, smaller positive charge is called the dipole/tripole model, as illustrated in Figure 3.9.

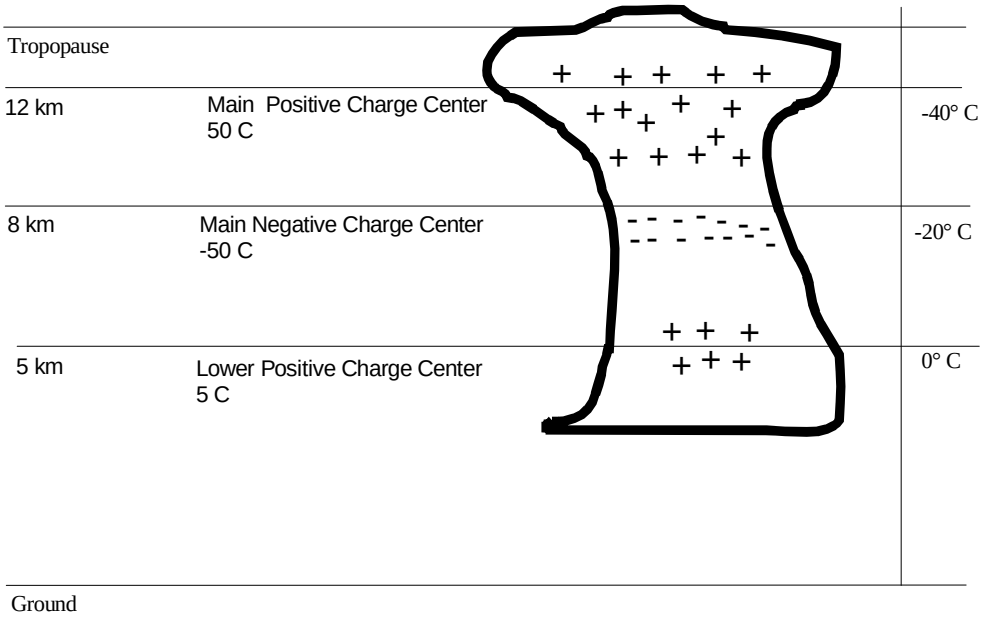

Figure 3.9. The dipole/tripole model of the electron charge structure of a thunderstorm cell [Adapted from 10].

In the dipole/tripole model, the main, upper charge regions are assumed to have the same magnitude of electric charge [3, 20]. The amount of electric charge accumulated in each of the main charge centers varies from ±20 to ±120 C [25]. Measurements have found that the upper main charges are bound between the -5° C and -40° C isothermals. The lower positive charge center is not always present in a thunderstorm, and when present is centered at the 0° C isothermal. Negative charge is generally compacted near the -10° C to -20° C isothermal, while the positive charge is widely dispersed all the way up into the top of the thunderstorm cell. The two main charge centers are separated by less than a kilometer [3, 20, 40]. The location of the charge centers depends on the altitude of the isothermals and not actual altitude as shown in Figure 3.10.

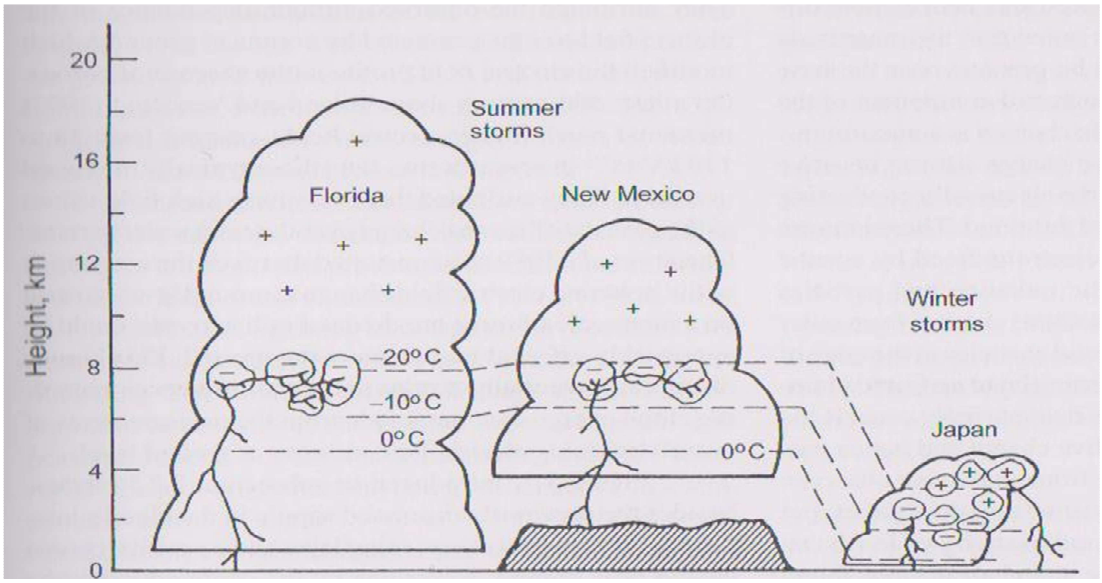

Figure 3.10. Charge centers inside a thunderstorm at different locations and during different seasons [3].

The charge structures of large thunderstorm cells can become much more complex than the basic dipole/tripole model. Additional charge centers have been measured both vertically and laterally adjacent to the main charge centers within some thunderstorm cells. It is even possible for a negative charge center to be laterally adjacent to a positive charge center, depending on the exact geometry of the thunderstorm cell. Typically, the electric charge centers within the updraft region follow the dipole/ tripole model [41]. In strong downdraft regions of a storm cell, having four or five charge regions stacked on top of one another can be common [20].

The very top of the thunderstorm has been found to contain a thin layer of negative charge called a screening layer and may be due to the upper main positive charge center and to Wilson currents, i.e. currents that travel from the top of thunderstorms towards the ionosphere [20, 31]. Originally, the lower positive charge center was also thought to be a screening layer for the main negative charge center, but currently there are no theories to explain why so much positive charge is gathered in that location. Even Feynman made the comment about the lower positive charge that, “things would be simpler if it [lower positive charge] weren’t there” [42]. Figure 3.11 depicts a more realistic electric charge structure of a thunderstorm. Individual thunderstorm cells have also been observed under some circumstances to have a negative dipole (main negative charge center above a main positive charge center) instead of the typically observed positive dipole [25, 39, 41].

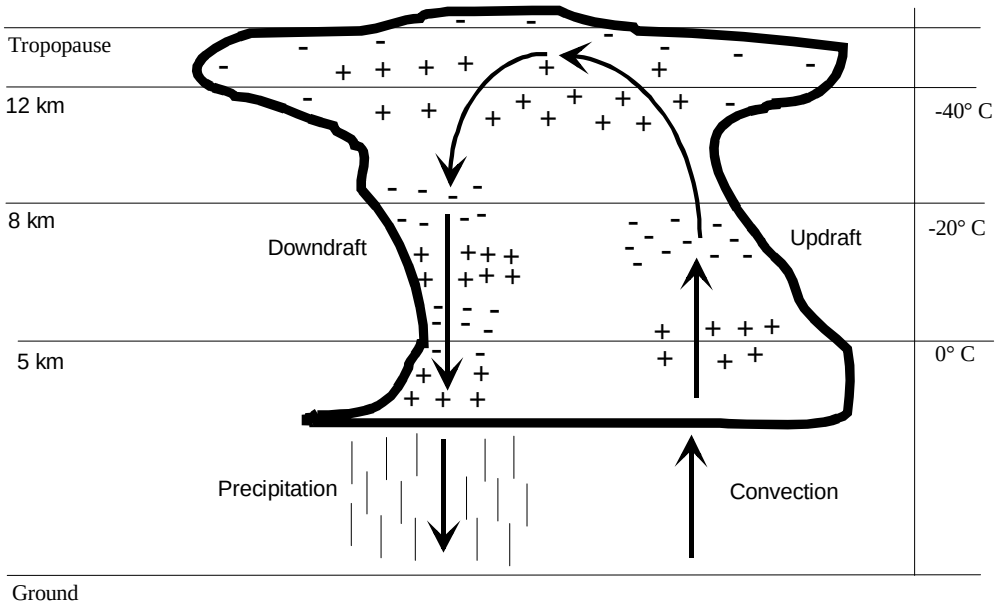

Figure 3.11. Diagram displaying the different charges found within the updraft and downdraft regions of a thunderstorm cell. A raising air mass creates an updraft (upward arrows), which continues to raise to the top of the thunderstorm and then begins to fall creating a downdraft (downward arrows). The downdraft also brings precipitation to the ground. The charge centers in the updraft region closely follow the dipole/tripole model, but there can be additional charge centers in the downdraft region [Adapted from 41].

The electric charge centers of the thunderstorm are ultimately responsible for the electric field within and outside the thunderstorm. Electric field measurements within active thunderstorm are typically made by balloon or aircraft borne electric field mills [41]. The

results from a balloon-borne electric field mill in for both the updraft and non-updraft regions of a small New Mexican thunderstorm cell are shown in Figure 3.12.

Within the updraft region, the thunderstorm can be accurately described by the dipole/tripole model with an upper negative screening layer. However, in the non-updraft regions more charge centers are needed to explain the electric field measurements. In both regions, the magnitude of the electric field reached a maximum magnitude of 100 kV m^{-1} between altitudes of 4 and 8 km. According to research using the Oklahoma Lightning Mapping Array (OKLMA), the majority of lightning discharges that reach the ground originate within this 4 and 8 km altitude [43]. Further studies have found that the average maximum electric field strength in thunderstorms is 130 kV m^{-1} [20, 44]. However, near lightning discharges the electric field rises to >200 kV m^{-1} [21]. Balloon borne instruments have measured electric fields strength >300 kV m^{-1} within a thunderstorm before being struck by lightning and destroyed [21].

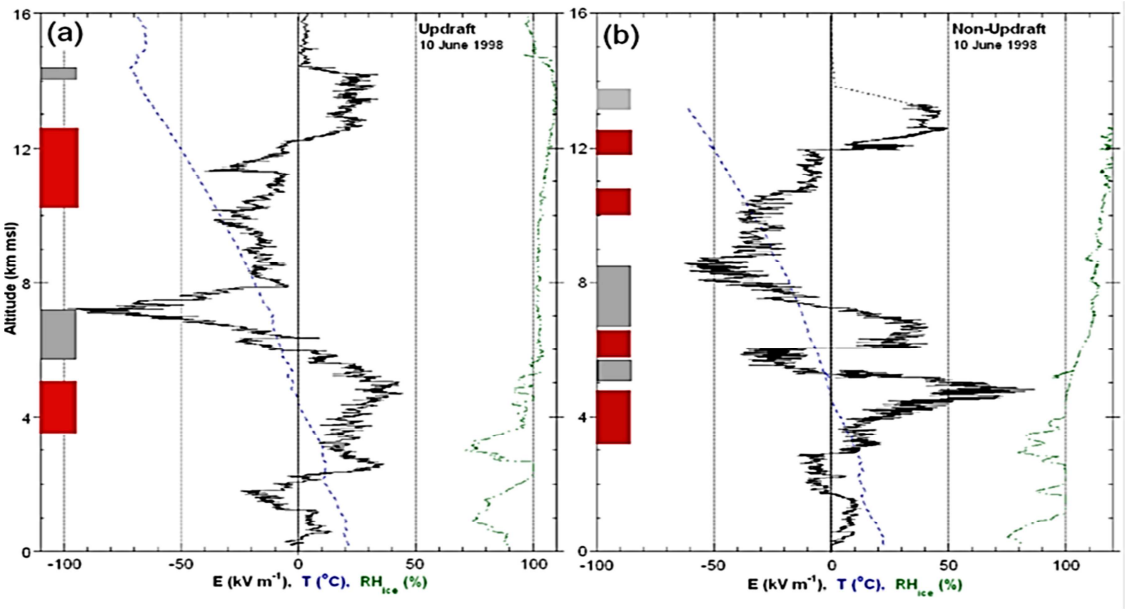

Figure 3.12. Balloon measurements of the electric field, temperature, and relative humidity within a) updraft and b) non-updraft regions of an air mass thunderstorm as a function of altitude. The black solid line is the electric field strength measured in kV m^{-1} using the atmospheric sign convention (direction of the field is opposite to the normal physics definition), the blue dashed line is the temperature of the atmosphere in °C, and the green thin line is the relative humidity with respect to liquid water for temperatures >0 °C and with respect to ice for temperatures <0 °C. The colored bars on the side of each plot are the locations of the charge centers with red being positive charge and grey being negative charge [41].

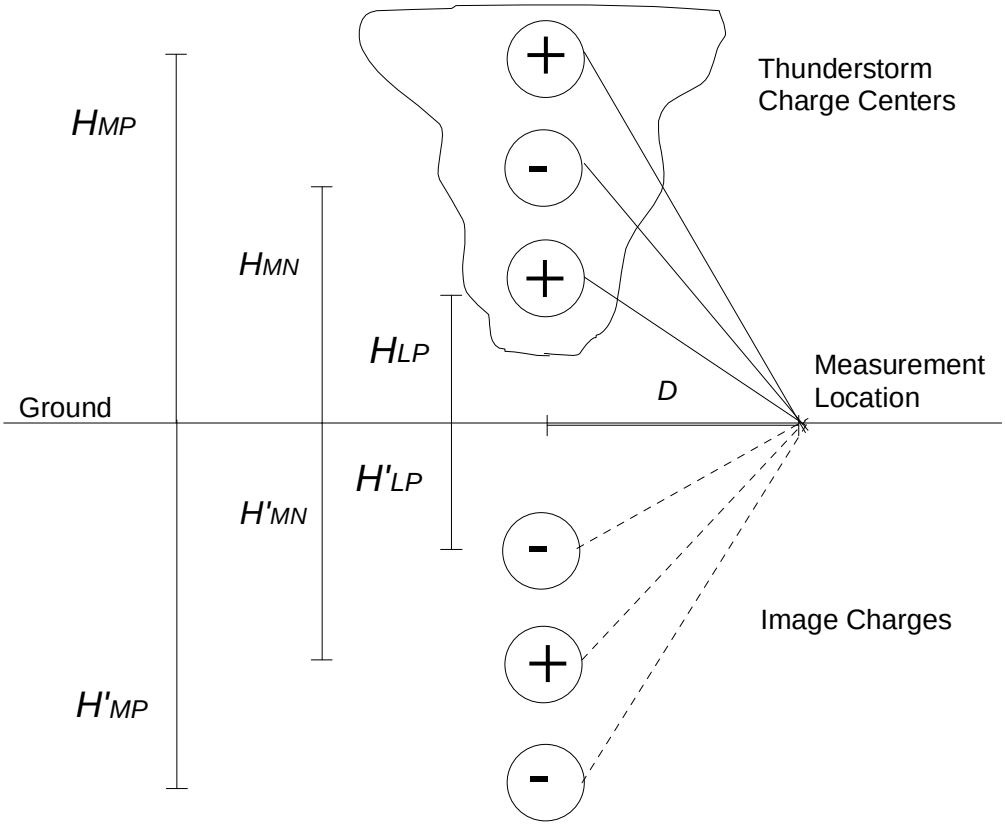

Figure 3.13. Diagram used to determine the electric field at a point on the ground at some distance *D* from a thunderstorm via the method of images. In the diagram *H* is the altitude of the charge centers above the ground and *H*' is the distance below the ground of the image charge centers for the main positive (*MP*), main negative (*MN*) and lower positive (*LP*) charge centers of a thunderstorm [Adapted from 20 and 45].

The electric field because of the thunderstorm charge centers can be measured on the ground with electric field mills. For a single thunderstorm cell with the same charge center distribution as shown in Figure 3.9, the electric field strength on the ground can be calculated by assuming that the charge centers are spherical symmetric (not a good approximation [3, 20]), that the ground is a perfect conductor (which is a good approximation [3, 20, 31, 40]), and use the method of images [45]. Figure 3.13 illustrates

the geometry assumed above and Figure 3.14 is a plot of the electric field as a function of horizontal distance from the thunderstorm.

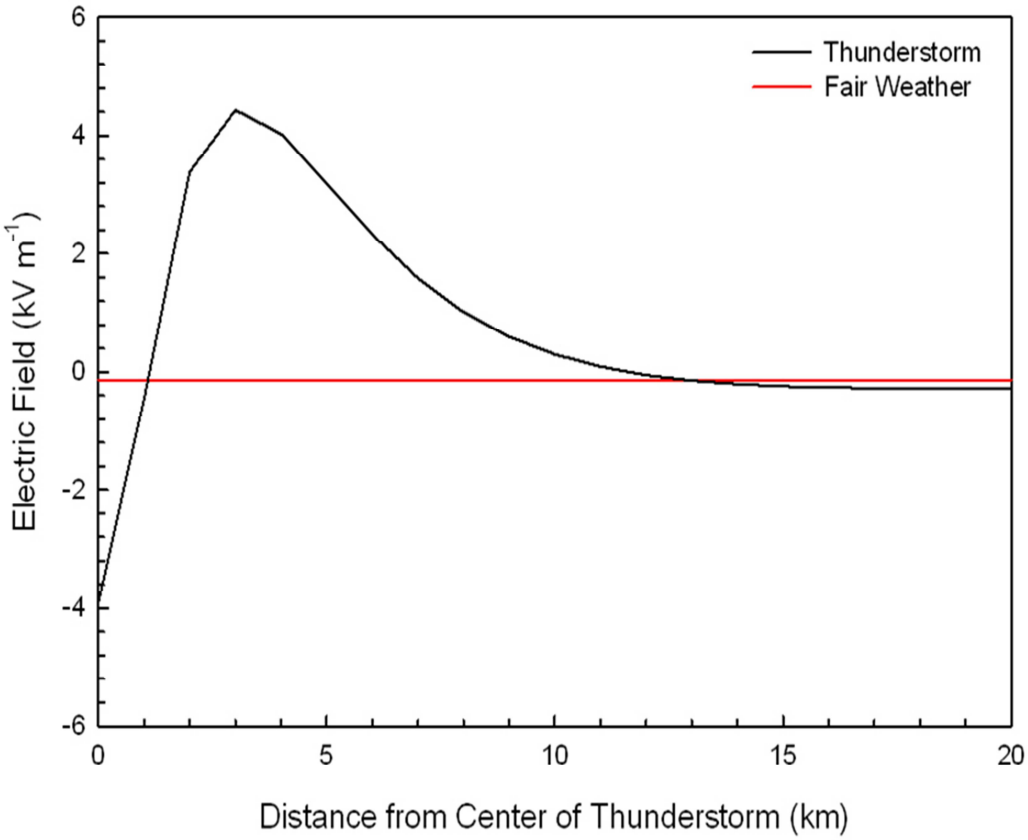

Figure 3.14. Plot of the electric field on the ground as a function of distance from the thunderstorm shown in Figure 3.9. The positive electric field is pointed away from the Earth's surface

Directly below the thunderstorm, the lower main negative center dominates and the electric field measured on the ground becomes strongly negative, i.e. pointing towards the ground. At some distance away from the thunderstorm, the direction of the field changes direction due to the combined effects of the lower secondary and upper main charge centers. Without the lower secondary positive charge center, the electric field would never change direction [3, 20]. The distance away from the thunderstorm where the electric field changes direction, is called the reversal distance [3, 20].

Actual thunderstorms are found in clusters and have more complex charge structures, so electric field measurements are never as simple as shown in Figure 3.14. An example of an actual field electric mill measurement of a nearby thunderstorm system is shown in

Figure 3.15. Figure 3.16 shows the Oklahoma Lightning Mapping Array (OKLMA) data for the same thunderstorm system shown in Figure 3.15 [46].

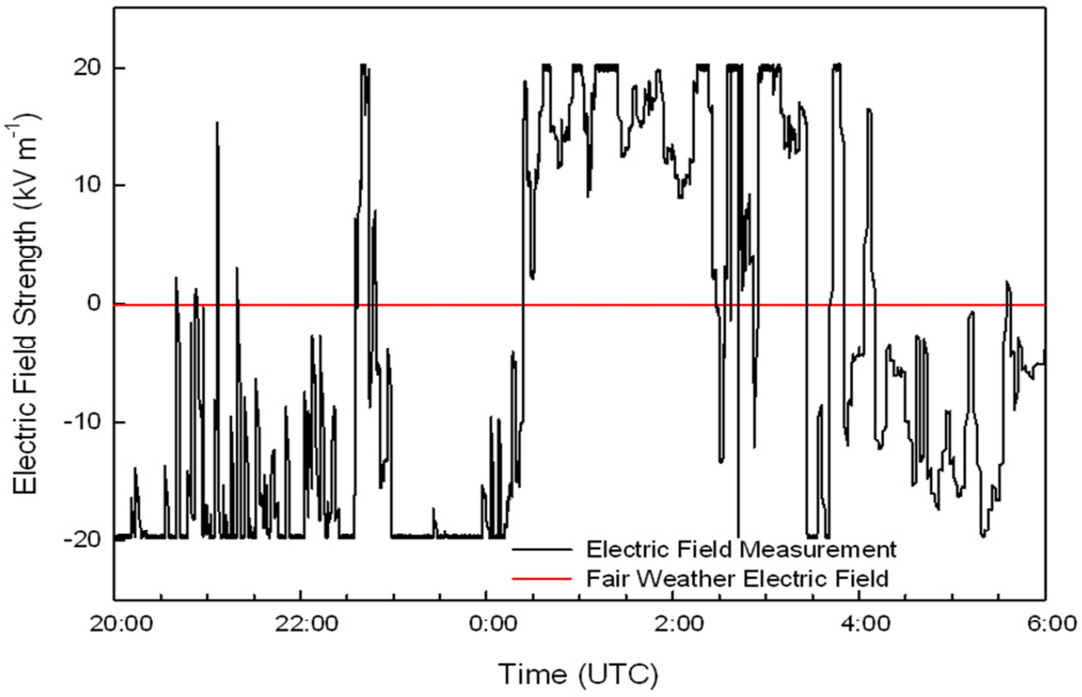

Figure 3.15. Plot of the electric field measured by a from a thunderstorm system that occurred on 5/31/2013 and 6/1/2013 by a Boltek EFM-100 Atmospheric Electric Field Monitor. The Electric Field Mill has a range of ±20 kV m^{-1}, so any electric field outside that range is cut off [29]. Note that there is a 5 hour difference between UTC and CST time zone and LMA sources are associated with lightning discharges.

On the roof of the Venture I building in Stillwater, OK are several different instruments that continuously monitor the local weather conditions, including a ground level electric field mill and a lightning detector. The bulk of the sensors are part of the WLS Digital Weather Station suite from Texas Weather Instruments Inc. which measures wind direction and speed, amount of rain, solar irradiance, temperature, humidity, and pressure [47]. Also, there is a quadrifilar antenna that receives images from National Oceanic and Atmospheric Administration (NOAA) Polar Orbiting Environment Satellite (POES) [48]. The sensor suite includes a Boltek lightning detector that can detect lightning discharges in 2D over the majority of Oklahoma [49] and a Boltek Atmospheric Electric Field Monitor (i.e. electric field mill), which measures the ground level electric field [29]. Data from the electric field monitor can be seen in Figures 3.15. This collection of different sensors has recorded several thunderstorms passing over Stillwater, OK.

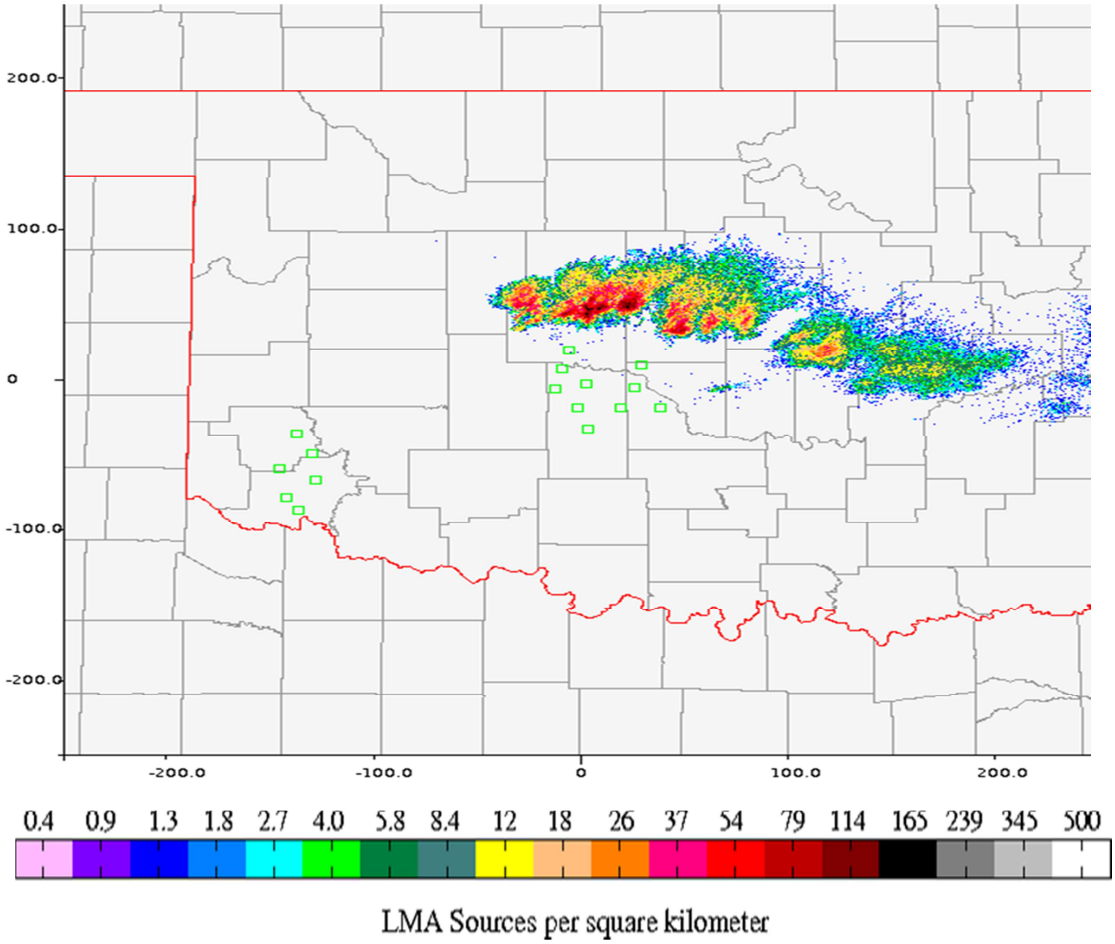

Figure 3.16. The OKLMA data from the thunderstorm system near Stillwater, OK on 5/31/13 and 6/1/13 [46].

One feature in the electric field measurements is the rapid, small decreases in electric field strength that can be seen between 20:00 and 22:00 in Figure 3.15. It was these types of decreases in the electric field strength that C.T.R. Wilson associated with lightning discharges and which led to the theoretical model of the main positive dipole within a thunderstorm [3, 8, 20]. The electric field during a thunderstorm is at least an order of magnitude larger than the fair weather electric field, and some organizations use this rapid change in the ground level electric field to predict when a thunderstorm will be overhead [4, 8].

Due to the presence of the thunderstorm electric fields, positive charge on ions accumulates between the thunderstorm and the ground. These regions of accumulated positive charge are called space charges and greatly limit the strength of the thunderstorm electric field on the ground [4, 20, 30, 31]. Large concentrations of ions in a space charge

region can undergo a point discharge, i.e. non-sparking electrical discharge, in the atmosphere [20, 30, 31]. It is believed that up to 60% of the charge required to sustain the global electric circuit comes point discharges from space charges and ground based structures [31].

Within the thunderstorm, electric charges are carried on polarized water droplets and ice particles called hydrometeors [20]. Like the space charges below the thunderstorm, hydrometeors are believed to undergo point discharge in strong electric fields. Due to the order of magnitude difference in the electric field strength between the ground and the inside of a thunderstorm, hydrometeors undergoing point discharges may be responsible for a lightning discharge [10, 20, 36].

3.4. Hydrometeors

Hydrometeors are any form of liquid or solid water within the atmosphere, including raindrops, cloud droplets (tiny water droplets), graupel (mushy hail or sleet), snow, and hail [3, 20, 36]. Lightning discharges originate above the 0° C isothermal, where both liquid water droplets (cloud droplets) and solid ice particles (graupel and hail) are common [20, 50]. Figures 3.17 is a photograph of an ice particle of the type that forms within an active thunderstorm.

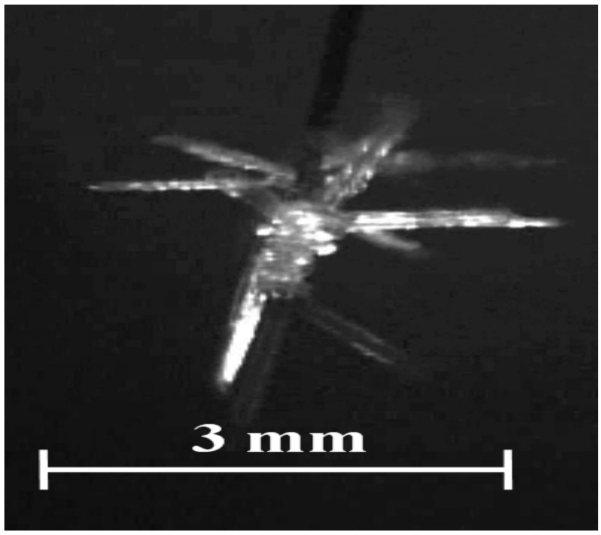

Figure 3.17: Photograph of an ice particle grown in the same conditions as those found within a thunderstorm [50].

Due to the polar nature of water, hydrometeors become polarized in ambient electric fields [20, 40]. In the fair weather electric field, the positive edge of the hydrometeor is directed towards the ground and the negative edge is towards the top of the atmosphere. In strong electric fields, the bound charges of the water drop can separate the water drop into two smaller droplets with a thin conducting channel called a filament [20, 40]. Figure 3.18 shows a drawing of a deformed water drop in a strong electric field.

Due to this polarization, all hydrometeors created below the -40°C isothermal, all hydrometeors are also electrically conducting and become the charge carriers for the entire thunderstorm. All the electric charge generated within the thunderstorm, such as in the charge centers and screening layers, is carried by hydrometeors [20, 40].

In order for the charge centers and the strong electric fields of the thunderstorm to develop, the hydrometeor must first be charged, then separated from other hydrometeors, and collected in the charge center regions [40]. The charging, separation, and collecting mechanisms within a thunderstorm are still not fully understood [10, 20, 36, 40, 50].

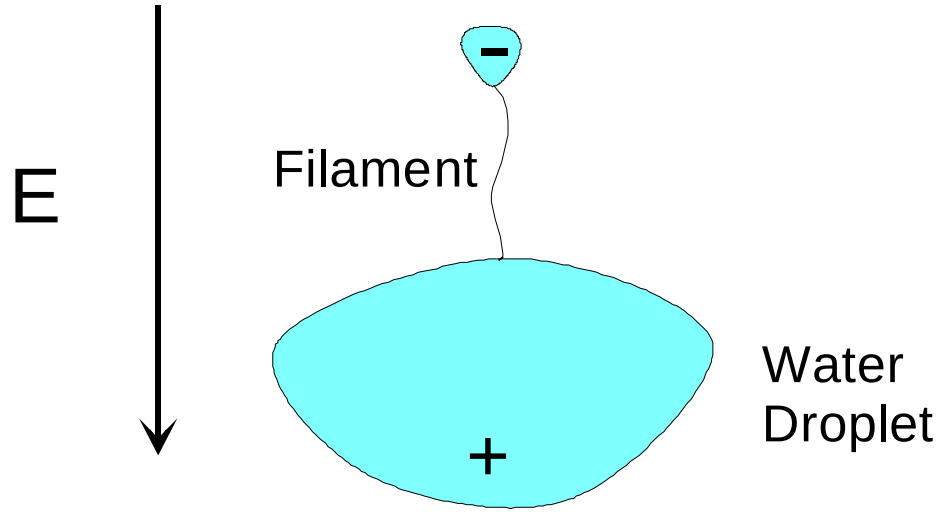

Figure 3.18: Drawing of a water drop in a strong electric field. The electric field first polarizes the water drop then the charges begin to separate into two smaller water drops joined by a very thin conducting pathway called a filament [Adapted from 20].

3.5. Thunderstorm Charging Processes

The electrical charging process begins with moist, warm air being brought into the atmosphere by some means of convection. The water vapor in the air mass begins to condense above the dew point isothermal (LFC) and freeze above the 0°C isothermal, forming hydrometeors. Due to the rarity of aerosols in the thunderstorm, there is a mixture of liquid and solid hydrometeors in the thunderstorm all the way up to the -40°C isothermal.

When created, these hydrometeors are only a few micrometers in size and are held suspended in the atmosphere by the updraft of the thunderstorm. The hydrometeors are moved around by the turbulence in the thunderstorm and collide with one another. The hydrometeors grow in size through the collision-coalescence process for water drop-on-water drop collisions and Bergerson process for water drop-on-ice or ice-on-ice collisions [20, 35]. Eventually the hydrometeors grow too large to be suspended by the updraft and begin to fall.

Falling hydrometeors provide the first method for charge generation and separation within the thunderstorm. The falling hydrometeor is polarized by the fair weather electric field, with positive charge towards the ground, as shown in Figure 3.19.

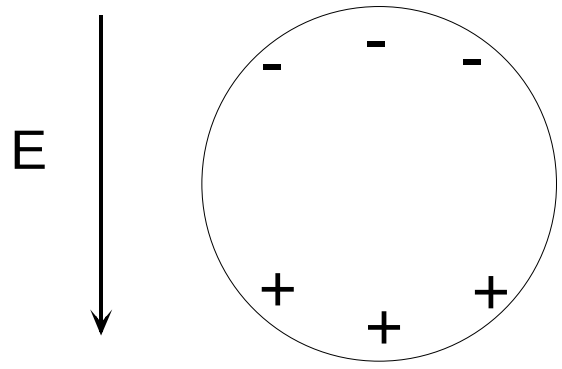

Figure 3.19: Diagram of a polarized hydrometeor in the fair weather electric field, *E* [Adapted from 20]

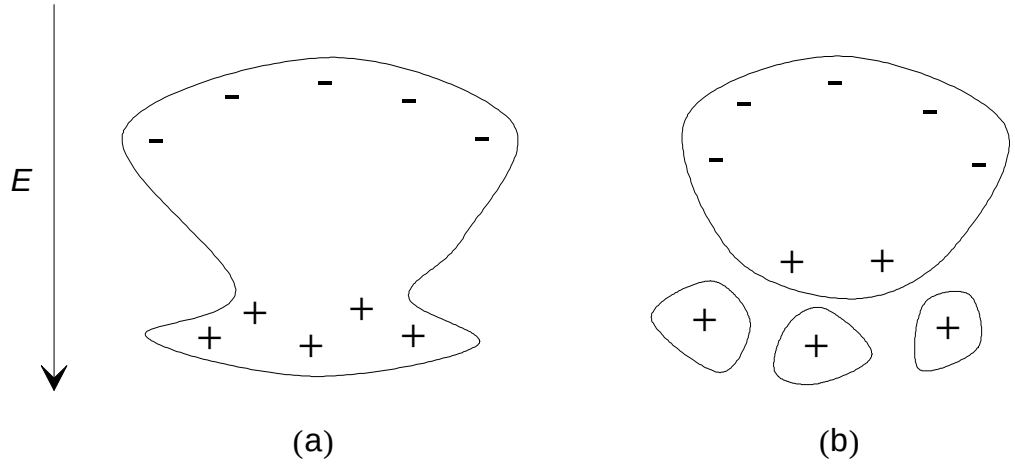

Figure 3.20: Diagram of a falling water drop breaking apart due to the Lenard (waterfall) effect: (a) a polarized, falling water drop becomes deformed due to air resistance and (b) the deformity becomes too great and the water drop breaks apart. After breaking apart, the newly formed water droplets have a positive charge and the remnant of the water drop has a net negative charge [Adapted from 35].

For very large falling liquid hydrometeors, the air resistance causes the water drop to deform. If the water drop is large enough, this deformation will cause the leading edge of the water drop to break apart, leaving many tiny, positively charge water droplets and a now negatively charged main water drop. The updraft of the thunderstorm will push the tiny positive droplets back up into the thunderstorm, thus separating positive and negative charges. The larger, negative charge will either continue to fall or will be pushed back up by the updraft, but due to the size, will be pushed up to a lower altitude than the tiny positive water droplets. This process is called the Lenard (or Waterfall) effect [35, 36] and a diagram of the process is shown in Figure 3.20.

Falling liquid hydrometeors that do not break apart due to air resistance also acquire an electric charge due to Wilson's Selective Ion Capture process [20, 39, 40]. In the Selective Ion Capture process, the polarized hydrometeor collects free ions in the atmosphere as they fall in the thunderstorm. Ions, or charged aerosols, are naturally created in the atmosphere from the passage of cosmic rays or brought up into the thunderstorm by the updraft [20, 24, 40]. The falling water drop is polarized by the fair weather electric field so that the leading edge of the water drop is positively charged. This causes positive free ions to be repelled from the leading edge of the water drop and negatively charged free ions to be attracted towards and acquired by the leading edge [20,

40]. A diagram illustrating Wilson's Selective Ion Capture process is shown in Figure 3.21.

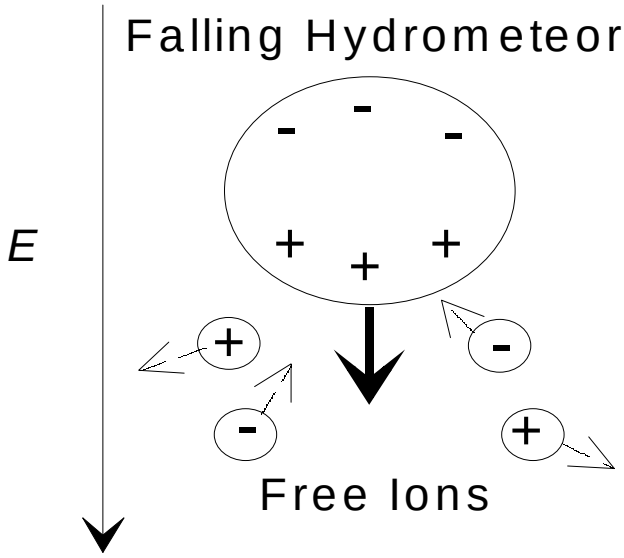

Figure 3.21: Diagram illustrating Wilson's Selective Ion Capture process: A falling hydrometeor is polarized by the fair weather electric field such that the falling edge is positively charged. Free ions in the atmosphere are accelerated by the positive charge on the falling edge and either are repelled (positive ions) or attracted (negative ions). The hydrometeor collects the attracted negative ions, which gives the hydrometeor a net negative charge, leaving only positive ions in its wake [Adapted from 35].

The Lenard effect first generates charged hydrometeors by breaking apart a polarized hydrometeor then the charged hydrometeors are separated by the updraft. Due to their smaller size, the updraft sends the positively charged water droplets higher into the thunderstorm than the negatively charged main water drop. Also, falling water drops that don't break apart will selectively remove negative free ions in the higher regions of the thunderstorm, leaving an excess of positive free ions, through Wilson's Selective Ion Capture process. Both the Lenard effect and the Wilson's Selective Ion Capture processes are responsible for the initial electrification of the thunderstorm, such as seen in warm, non-thunderstorm rain clouds [40]. The electric structure of a thunderstorm continues to develop with two additional methods of charging: inductive and non-inductive charging [20, 40].

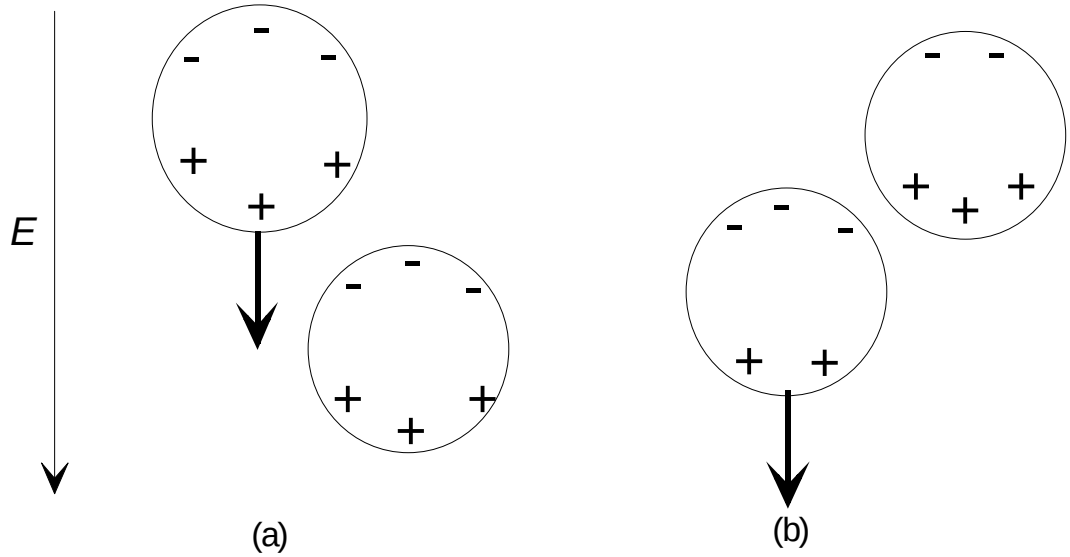

Figure 3.22: Diagram of two hydrometeors undergoing inductive charging: (a) A strong ambient electric field, *E*, polarizes the two hydrometeors. One of the hydrometeors is falling relative to the other hydrometeor. (b) After the hydrometeors collide, some of the bound charges neutralize each other, leaving the falling hydrometeor with a net negative charge and the other hydrometeor with a net positive charge [Adapted 35].

Once an ambient electric field is established within a thunderstorm cell, such as by Wilson's Selective Ion Capture process [20], the polarization of the hydrometeors strengthens and solid hydrometeors become conducting. When two charged conductors collide with one another, the charges are transferred between the two conductors in order to neutralize any excess electric charge. In the case of collisions between supercooled water drops and ice particles or between two or more ice particles, the colliding edges of the hydrometeors can exchange charges. Even without excess charge on a hydrometeor, the polarized charges on the edges of a hydrometeor can exchange in a collision [20, 40].

In the method of inductive charging of rebounding particles (i.e. inductive charging), a falling hydrometeor collides with a stationary hydrometeor while in a strong (>10 kV m^{-1}) electric field [20]. In the strong ambient electric field, the hydrometeors are strongly polarized so that the leading edge of the falling hydrometeor will have the opposite polarity as the top edge of the stationary hydrometeor. When the two hydrometeors collide, charges are transferred between the two hydrometeors in order to neutralize the bound charges. After the collision, the two hydrometeors will be left with excess electric charge of equal and opposite amounts. A diagram of the inductive charging process is shown in Figure 3.22.

Inductive charging can generate large numbers of charged hydrometeors in a relatively short period of time (~ 1 minute) compared to Wilson's Selective Ion Capture process (~10's minutes), but the required strong ambient electric field means the inductive charging method only works near the main charge centers of the thunderstorm [40]. Electric charge can be found throughout the thunderstorm cell regardless of the strength of the ambient electric field [20]. The inductive charging method does explain how the thunderstorm recovers so quickly after a lightning discharge, but not how the bulk of electric charges are generated within the thunderstorm in the first place. Non-inductive charging processes are required to explain how the bulk of the electric charge is generated within an active thunderstorm [20, 40].

Non-inductive charging processes do not require an electric field to operate and involves how hydrometeors form and grow within the thunderstorm [40]. The majority of hydrometeors within a thunderstorm are ice particles that form above the 0°C isothermal. Along with these ice particles are supercooled water droplets and water vapor [20]. Depending on the amount of liquid water and water vapor in the atmosphere, different types of solid hydrometeors can form. In typical moist conditions (liquid water > water vapor), water freezes onto aerosols or cloud ice particles to form graupel in a process called rimming [40]. In dry conditions (liquid water < water vapor), solid ice particles are formed through both heterogeneous (>-40° C) or homogeneous (<-40° C) freezing [25]. The amount of moisture in the atmosphere decreases with altitude in a thunderstorm [40]. Studies have found that riming, i.e. liquid droplets freeze onto an ice crystal, causes the hydrometeor to become negatively charged where aggregation, i.e. two ice crystals colliding and sticking together, causes the hydrometeor to acquire a positive charge [40]. Ice particles are typically found in the highest regions of the thunderstorm, where the main positive charge is observed, while the heavier graupel accumulates where the updraft is strongest, near the 0°C isothermal where the main negative charge center is observed [40]. This difference in where positive ice particles and negative graupel collects is one type of non-inductive charging.

Another example of non-inductive charging involves collisions between ice particles and graupel. Ground based experiments have found that the amount and polarity of electric charge transferred between colliding ice particles and graupel changes with temperature as shown in Figure 3.23 [40]. Above -20°C, the graupel acquires a net negative charge from the ice particles, but below -20°C, the graupel acquires a net positive charge. The -20°C isothermal has been observed to be the top edge of the main negative charge center in typical thunderstorms (See Figure 3.9) [40].

Each of the above charging processes describes a specific aspect of electric charge generation within a thunderstorm: initiation electrification for Lenard effect and Wilson's Selective Ion Capture process, rapid charge generation after a lightning discharge for

inductive charging processes, and location of charge centers for non-inductive charge processes. There is no complete theory that solves the hydrometeor problem [20, 40]. Without a complete theory of the charge generation processes in a thunderstorm, fundamental thunderstorm characteristics, e.g. electric field strength or electric charge density, can only be determined experimentally with considerable error. In regard to understanding lightning discharges in the atmosphere, the lack of a solution to the hydrometeor problem means that there are uncertainties in the electrical environment surrounding the location of a lightning discharge.

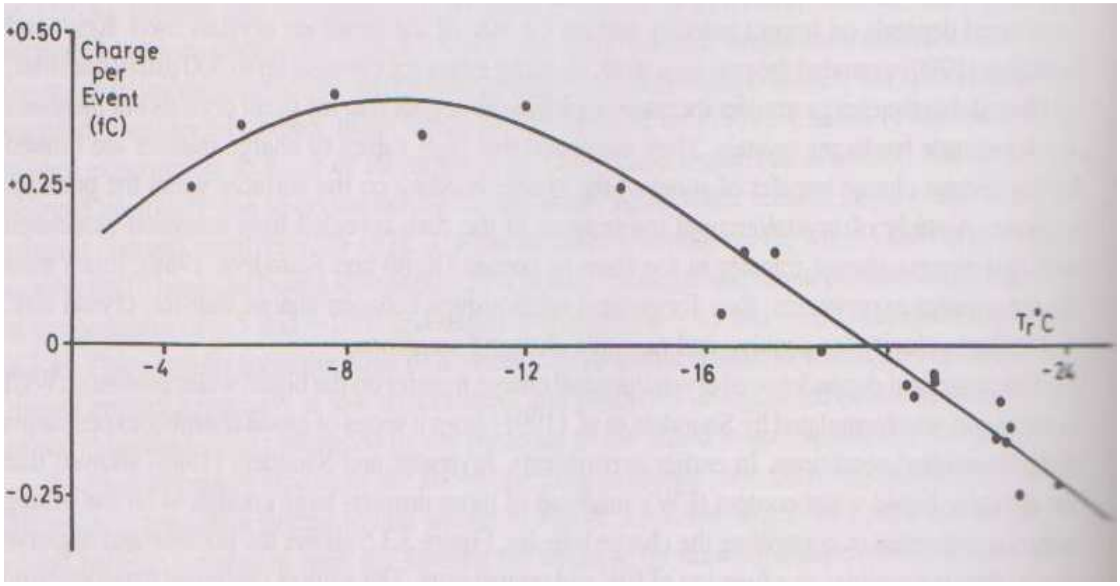

Figure 3.23: The amount of electric charge transferred to a rimming ice particle as a function of temperature [40].

CHAPTER IV

LIGHTNING DISCHARGES

Lightning discharges are naturally occurring, kilometer long electrical discharges that propagate through the atmosphere. As revealed by high speed video and photography, lightning discharges are actually made up of several different parts: point discharges, streamers, and leaders. According to the conventional lightning discharge model [10], a lightning discharge originates from a point discharge inside a thunderstorm. The point discharge ionizes the surrounding air and generates a series of electrical breakdowns called streamers. The streamers travel from the point discharge region and ionize additional regions of air until enough free electrons are generated to heat the air and form a leader. A leader is responsible for creating the several kilometers long conducting pathway of a lightning discharge [3, 20].

Lightning discharges are impossible to predict and control, so smaller scale electrical discharges, called long sparks, are studied in ground-based experiments [51]. Long sparks are atmospheric electrical discharges that are generated in facilities where the electric fields, geometry, and atmosphere can be controlled. Due to their artificial nature, long sparks are considered to be a different type of electric discharge than lightning discharges, but long sparks still represent one of the only ways to study the individual electrical discharges that make up a lightning discharge. *Bazelyan and Raizer* (1998) [51] provide an in depth summary of the properties of long sparks.

4.1. Long Sparks

Long sparks are artificially generated electrical discharges that travel through the atmosphere. Produced in ground-based electric discharge facilities, long sparks provide a controllable and reproducible method to generate electrical discharges in the atmosphere. An example of the setup required to produce a long spark is shown in Figure 4.1. Long sparks are typically generated with AC currents between two metal conductors [52, 53].

In comparison, lightning discharges are generated with a DC current and do not require the presence of metal conductors, which is why long sparks are not considered to be the same type of electrical discharge as lightning [3, 20, 51]. Long sparks are much shorter than the several kilometer long lightning discharges, with the longest spark discharges measure only tens of meters [53].

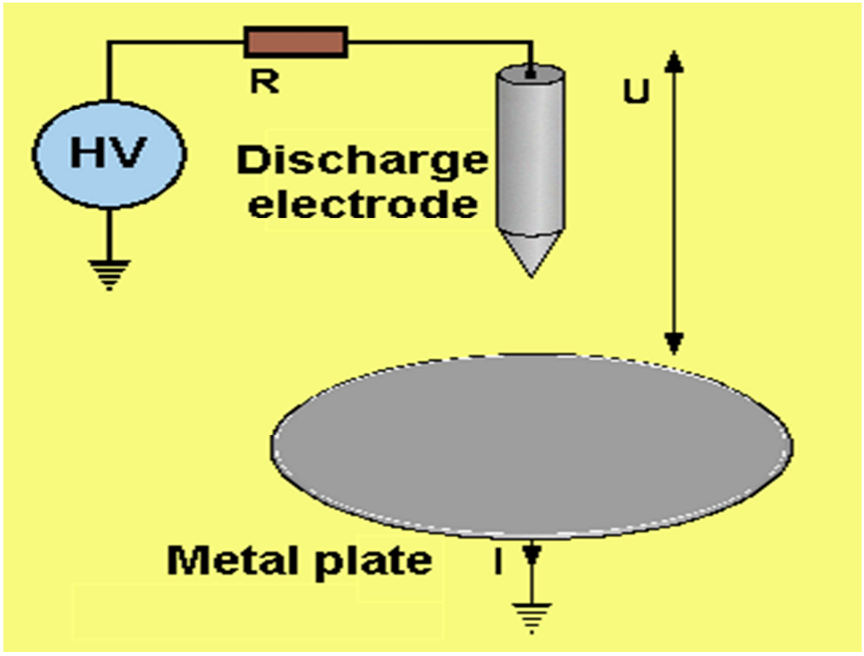

Figure 4.1. Example of the experimental setup required to generate a long spark. *U* represents the potential difference between the discharge electrode and the metal plate, *R* is the resistance between the high voltage power supply, *HV*, and *I* is the current through the metal plate [54].

Long spark studies have found that the required electric field to generate an electric discharge in dry air at sea level is 3000 kV m^{-1} [51]. An illustration of the experimental set up to determine the breakdown electric field is shown in Figure 4.2. At lightning initiation altitudes of 4-8 km, the required electric field for an electrical discharge is between 1500-2000 kV m^{-1} depending on the amount of water in the atmosphere [54]. The average maximum electric field within a thunderstorm is only 130 kV m^{-1} [20, 44], which is more than an order of magnitude weaker than the breakdown electric field measured in long spark studies. This large difference between the electric field required for breakdown and the strength of the electric field within a thunderstorm has been called the lightning initiation problem.

Long sparks are also one of the few ways to observe the development of an electrical discharge. Being able to control the different parameters (e.g. atmospheric density, electric field strength, etc.) of the long spark allows for the different types of electrical discharges (point discharge, streamers, and leaders) to be studied [51]. Long sparks can be produced in conditions similar to what is found in a thunderstorm (e.g. using hydrometeors instead of metal conductors, etc.) and can be used as a proxy for a lightning discharge [10]. Electron avalanches, which are required for any type of electrical discharge [51], can also be observed in long spark experiments [54, 55].

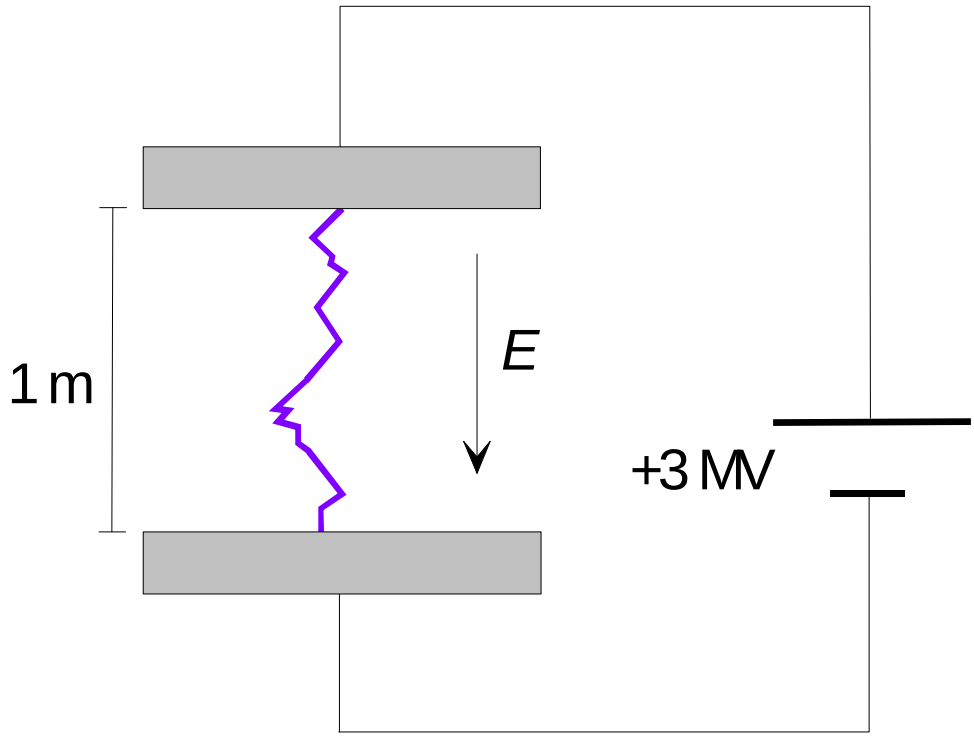

Figure 4.2: Illustration of an electrical breakdown between two parallel plates: The require potential to generate an electrical discharge between two metal parallel plate 1 m apart in dry air at sea level is 3 MV. Two parallel plates are used instead of the setup shown in Figure 4.1, because irregularity shaped electrodes enhances the electric field, making it difficult to determine the required electric field for breakdown [Modified from 51].

4.1.1. Electron Avalanches

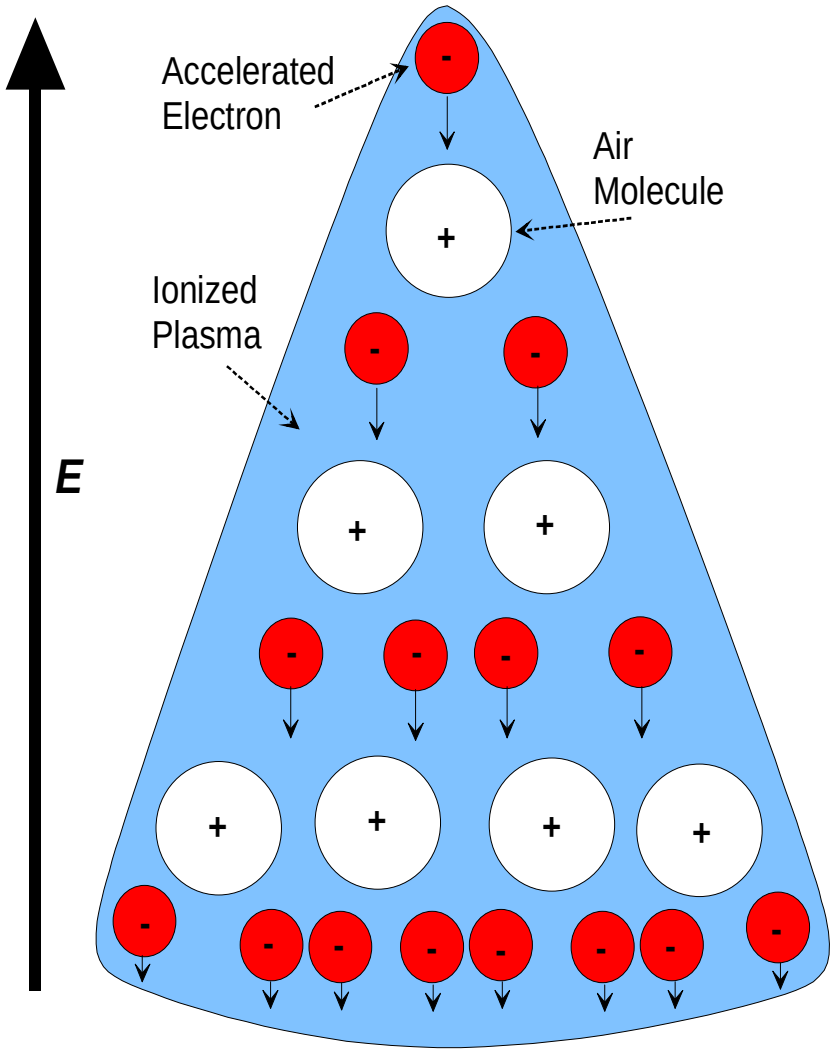

Figure 4.3. Diagram of an electron avalanche propagating through the atmosphere: The red circles are free electrons and the large white circles are air molecules. The blue surrounding the electron avalanche is the glowing ionized plasma generated by excitation photons.

While not an actual electrical breakdown, electron avalanches are produced by every type of electrical discharge in order to generate the electric charge required to sustain an electrical discharge. Electron avalanches occur in the atmosphere when a free electron, created by the passage of cosmic rays through the atmosphere [24], is accelerated in a strong electric field and begins to ionize the surrounding air molecules. In a strong

electric field, a free electron can undergo several collisions with bound electrons before ranging out, i.e. losing all its kinetic energy. The bounded electrons are either ionized and become free electrons or become excited and emit a photon, which can also ionize an bound electron through the photoelectric effect. Secondary free electrons are also accelerated in the strong electric field and can collide with other bound electrons. This exponential growth in the number of free electrons in a strong electric field is called an electron avalanche [44, 51]. Figure 4.3 shows a diagram of an electron avalanche in the atmosphere.

From ground based experiments, it has been shown that electron avalanches give off a dim glow due to the number of excitation photons produced [3]. A photograph of an electron avalanche is shown in Figure 4.4. Experiments show that it takes an average 34 eV to ionize an electron in air, but the ionization potential for N_2 and O_2 are 15.6 and 12.2 eV, respectively [51, 56]. The majority of the difference in energy between the average ionization energy and the ionization potential is given off as excitation photons [51, 55].

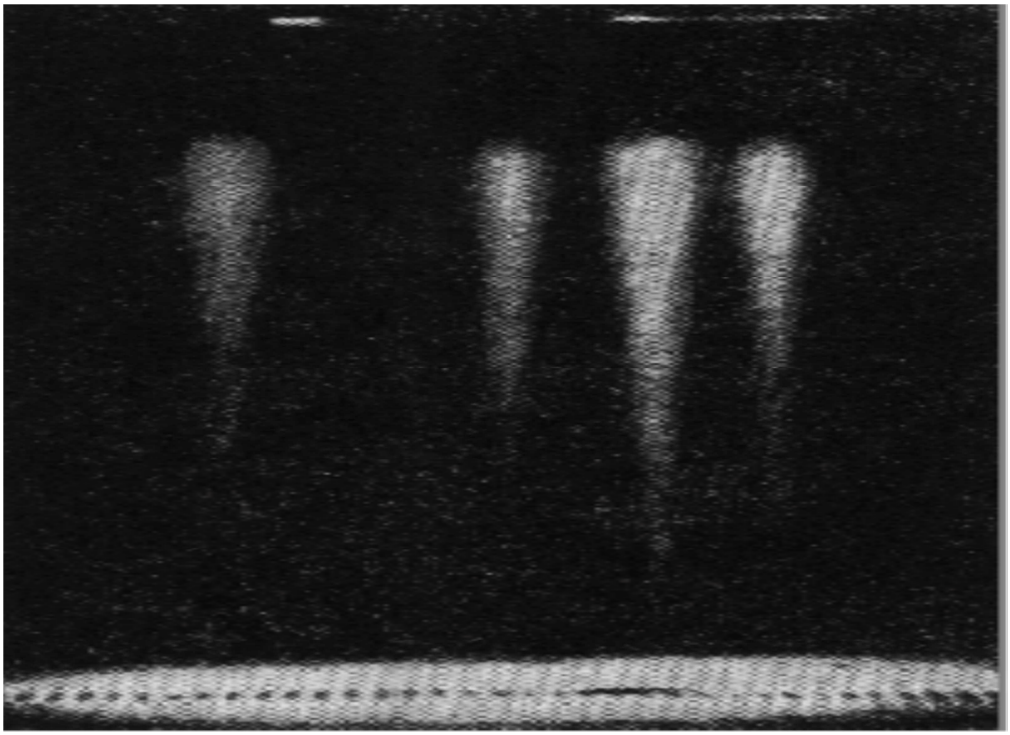

Figure 4.4: Photograph of electron avalanches produced in a ground based experiment [54].

Electron avalanches require an ambient electric field greater than the breakdown electric field in a small localized region in space in order to develop [51]. The maximum electric field within a thunderstorm is about an order of magnitude weaker than the breakdown electric field, so electron avalanches are found near regions of enhanced electric fields, i.e. hydrometeors or electrical discharges. Because of the strong electric field requirement, an electron avalanche is typically only ~1 cm in length and generates ~10^6 electrons with an average energy of 20 eV [51].

Electron avalanches are not considered electrical discharges themselves but play a major role in any electrical discharge. Electrical discharges require a large concentration of free ions, which electron avalanches provide by both generating large numbers of free electrons and regions of positively charged ions.

4.1.2. Point Discharges

In order for any sort of electrical discharge to occur, the electric field through a medium must be strong enough to cause the medium to act like a conductor instead of an insulator. For dry air, the breakdown electric field is 3000 kV m^{-1} at sea level and STP and decreases linearly with pressure [51]. The breakdown electric field at thunderstorm altitudes and conditions is approximately 1500-2000 kV m^{-1}, while the electric fields measured in thunderstorms typically range between 100-300 kV m^{-1} (average of 130 kV m^{-1}) [3, 20, 21, 36]. One possible way to enhance the electric field is to introduce conductors into the region, as shown in Figure 4.5

For ground based long spark experiments, different shaped metal conductors, such a needle tips, are placed inside the strong electric field. The ambient electric field around the conductor can be enhanced sufficiently to produce an electrical breakdown. These electrical breakdowns typically occur near the pointed tips of conductors and are called point discharges. Another name for a point discharge is a corona discharge [20, 51].

During a point discharge in air, free electrons will start an electron avalanche in the enhanced electric field region around the conductor, causing that region to ionize into a plasma and start to emit a blue or purple glow (due to the Nitrogen and Oxygen in the atmosphere). Since the enhanced electric field region only extends a short distance from the conductor, the electron avalanches do not travel far before ranging out. Depending on the polarity of any pre-existing or induced electric charge on the conductor, the electron avalanches either develop towards (positive point discharge) or away (negative point discharge) the conductor. This causes the plasma surrounding the conductor to become charged with the same polarity as the conductor [20].

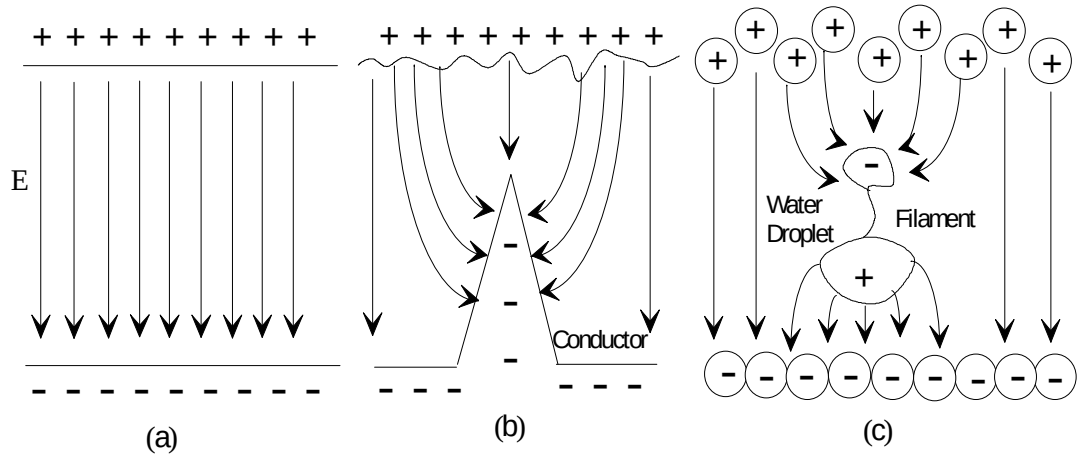

Figure 4.5. Diagram of the ambient electric field *E* (arrows) in several different situations that can result in an electrical discharge: (a) The electric field between two parallel plates. The field lines are straight and uniformly spaced. (b) The electric field between the lower positive charge region of a thunderstorm and the ground near a tall conductor (such as a metal tower or building). The electric field lines bend toward the conductor, especially near any points, enhancing the electric around the conductor. (c) The electric field near a water droplet between the upper main positive and lower main negative charge regions of a thunderstorm [Adapted from 40].

In thunderstorm conditions, water droplets and ice particle act in the same manner as the metal conductors in the long spark experiments. Point discharges can also occur near conducting man-made structures such as buildings or towers. These point discharges initiated at man-made structures are called St. Elmo's Fire after the patron saint of sailors, since it was typically seen on the masts and lines of ships at sea during thunderstorms [20, 38, 51, 57]. A photograph of an ice particle undergoing a point discharge is shown in Figure 4.6. However, point discharges typically only produce a small current (0.6 – 2.4 μA per point discharge [51]) and are localized [20, 51]. This means that point discharges are not directly responsible for high current, large scale lightning discharges. However, point discharges provide a location where other electrical discharges, such as streamers, can be initiated.

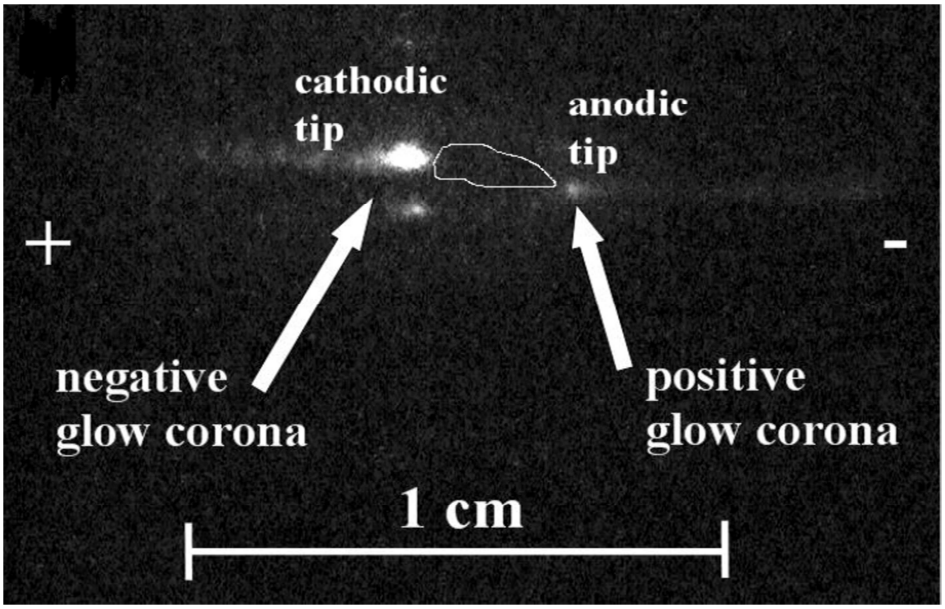

Figure 4.6. Photograph of an ice particle (white outline) undergoing two different point discharges in a ground based experiment. The glow corona is another name for the space charge [50].

4.1.3. Streamers

Hydrometeors and metal conductors enhanced the ambient electric field allowing electron avalanches to develop. Electron avalanches propagate through this enhanced electric field region, which causes the region to become an ionized plasma. The plasma polarizes in strong electric field such that its edges become charged (the same sign as the point discharge). The plasma is typically of the same shape as the original conductor. The edges of the plasma are able to undergo point discharge, just like the original conductor, and generate another region of charged plasma. As this process continues, the newly created plasma region expands farther away from the original hydrometeor in the ambient air. These regions of charged plasma that travel through the ambient environment are collectively called streamers [10, 20, 51]. Figure 4.7 shows a photograph of a point discharge generating a streamer.

The characteristics of a streamer are strongly dependent on the polarity of the most recently formed charged plasma region, which is called a streamer head [51]. In a positive streamer (which begins near a positive point discharge), electron avalanches travel toward the streamer head and down to the low conductivity streamer channel, which is the previously ionized regions of the streamer. The streamer channel is non-

conducting due to recombination and attachment processes in the atmosphere [51]. If enough positive charge is generated by the electron avalanches, the streamer will advance through the atmosphere. A diagram of the development of a positive streamer is shown in Figure 4.8.

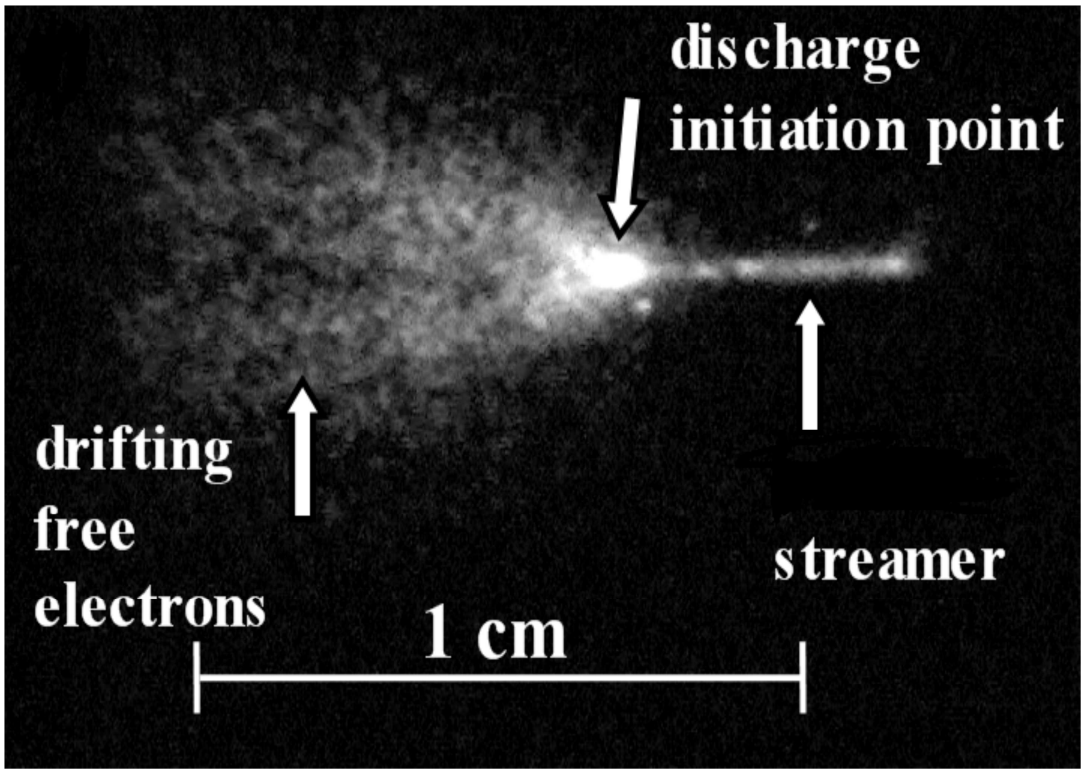

Figure 4.7. Photograph of a streamer generated by an ice particle undergoing a point discharge in a ground-based experiment [50].

The positive streamer will continue to advance through the atmosphere until it reaches a point discharge of the opposite sign or the ambient electric field, *E*, drops below an empirically determined field strength of,

$$E(d,h) = (497\ kV\ m^{-1})\left(1 + \frac{h - 11\ g\ m^{-3}}{100\ g\ m^{-3}}\right)d, \tag{4.1}$$

where *d* is the ratio of the local air density to the air density on the ground at STP and *h* is the absolute humidity of the local air in units of g m^{-3} [10]. In a 3% water atmosphere at

6 km altitude, a 260 kV m^{-1} electric field is required for a positive streamer to propagate. At the ground, the electric field needed for a positive streamer to propagate is >620 kV m^{-1}.

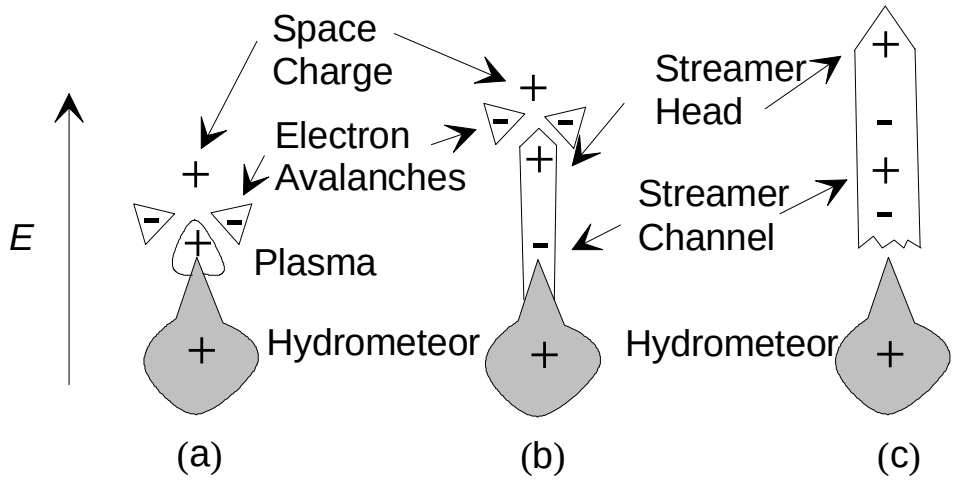

Figure 4.8. Diagram of the development of a positive streamer: (a) An irregularly shaped, positively charged hydrometeor begins to undergo a point discharge in a strong ambient electric field *E*. This point discharge generates an irregularly shaped positively charged plasma that also initiates a point discharge. Electron avalanches develop towards the edge of the plasma leaving behind a positive space charge. (b) The plasma expands into the space charge and becomes a streamer. The former positive space charge becomes the streamer head and initiates more electrons avalanches, repeating the above process. The original plasma, called a streamer channel, is where all the ions from the electron avalanches and space charges are collected. (c) As time progresses the streamer head continues to propagate through the atmosphere until the ambient electric field becomes too weak. Also, the ions in the older sections of the streamer channel recombine with the air and no longer function as a plasma. Over time, the streamer becomes detached from the original hydrometeor [Adapted from 10].

A negative streamer is generated near a negative point discharge and develops in a similar manner as a positive streamer. The main difference between a positive and negative streamer is the direction of the electron avalanches. For a negative streamer, electron avalanches develop away from the streamer head, effectively generating a positive charge region directly in front of the negatively charged streamer head. Thus, a negative streamer must travel through a positive charge region before reaching any of the electron avalanches, which is difficult without very strong ambient electric fields (about 2

to 3 times the field strength needed by a positive streamer [10, 51]). Consequently, negative streamers are not very common in normal thunderstorm electric fields.

In general, streamers require a very large amount of charge in order to develop. It has been predicted that a streamer would not develop until 10^8 ions were collected within the streamer head of approximately 30 μm radius [58]. The streamer channel can be a few centimeters in length and is approximately a centimeter in width [20, 51]. Streamers do not have to travel in straight lines while traveling through the atmosphere, but in general negative streamers are straighter than positive streamers since they need stronger electric fields to propagate [52].

In long spark theory, multiple streamers are required to cross the entire gap between the charge centers before an ionized pathway can be formed in the air that will allow a long spark to occur [51, 52]. Also, the streamers only continue to propagate through the atmosphere as long as the ambient electric field is stronger than the electric field calculated in equation (4.1). As shown in Figure 2.16, the maximum electric fields only exist within a small region of the thunderstorm and never down to the ground [21]. In normal thunderstorm conditions, streamers are not responsible for the kilometer long spark discharges. Instead these long spark discharges are a result of another type of electrical discharge called a leader [51].

4.1.4. Leaders

Without an ambient electric field significantly stronger than those typically measured in thunderstorms, streamers can only travel a few meters before dissipating and therefore cannot be responsible for kilometer long lightning discharges. However, it was found that if multiple streamers travel through the same region, all the charge generated by the streamers not only ionizes the region, but can also heat the plasma (which is typically some distance away from the hydrometeor) to over 2000 K [10]. At these temperatures, the entire plasma becomes conducting since electron recombination and attachment rates are reduced at high temperatures. In comparison, only the head of a streamer (which is a cold plasma) is conducting [10]. This heated plasma is called a leader [10, 51].

Leaders are composed of a leader tip and leader channel, which are similar to the streamer head and streamer channel, respectively. The leader tip is the location on the conductive leader where the excess charge is concentrated, generating a very strong electric field. Because of this electric field, a point discharge region develops around the leader tip and generates streamers. Similar to a point discharge, a leader has a polarity which influences the type of streamers that are generated. If a sufficient number of

streamers is generated from the leader tip, the current from each streamer travels through the entire leader and keeps the plasma heated [20, 51]. Figure 4.9 shows a photograph of the different components of a leader.

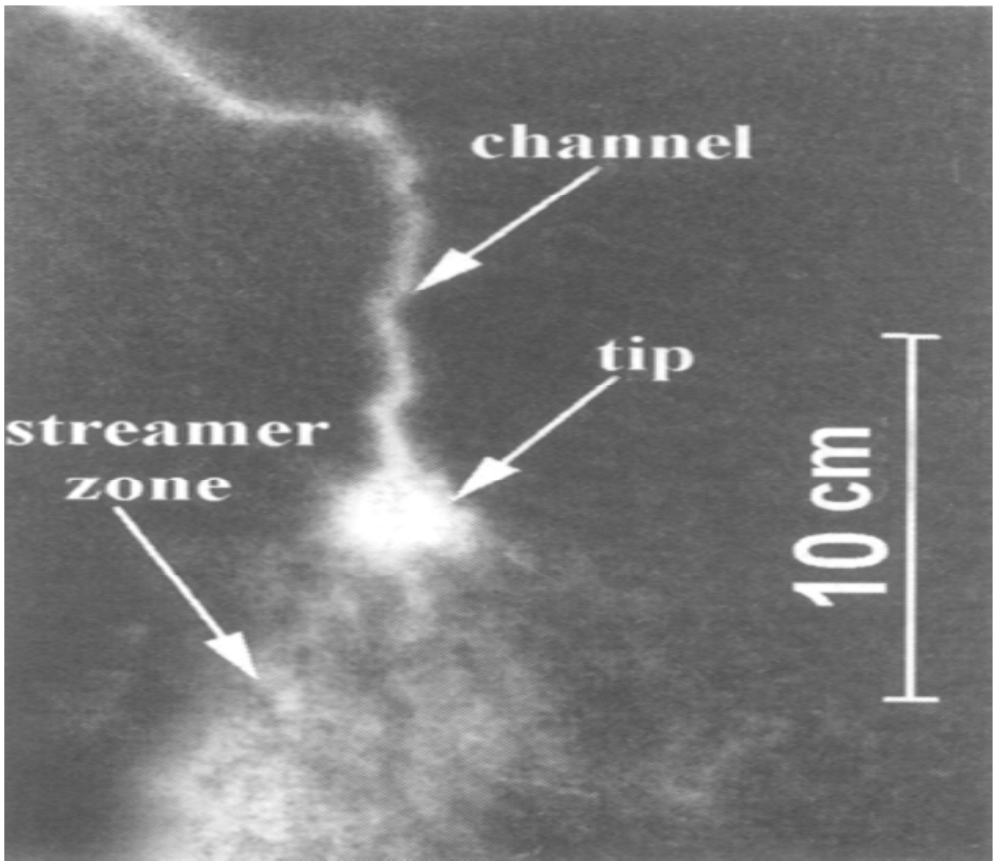

Figure 4.9. Photograph of a leader propagating through the atmosphere. A leader is made up of a hot plasma channel, an enhanced electric field region tip, and a collection of streamers that make up a streamer zone [54].

The leader channel is a heated plasma and acts as a conducting pathway from the initial hydrometeor or metal conductor to the leader tip. Because of the heated gas, the leader channel glows in the visible light region compared to the ultraviolet photons generated by point discharges and streamers [51]. However, leaders in the atmosphere are typically too dim to be seem by the unaided eye [20, 51]. Unlike a streamer channel, a leader channel remains as a conducting plasma for the entire lifetime of the leader and can be several kilometers in length [20, 44, 51].

A positive leader is initiated near a positive point discharge and generates positive streamers. A diagram of a positive leader is shown in Figure 4.10. Because of the positive streamers, the region surrounding the leader, including the leader channel, is positively charged. This charged region around a leader is called a leader cover. The combination of a conductive leader channel and the presence of the leader cover will cause point discharges to develop along the entire length of the leader channel. Point discharges only generate a small amount of current, but over the entire length of the leader channel, the total current generated around the lightning channel is comparable to the current generated in the leader tip. All current leader models require that the leader channel generate current in order to keep the leader heated and conducting [51].

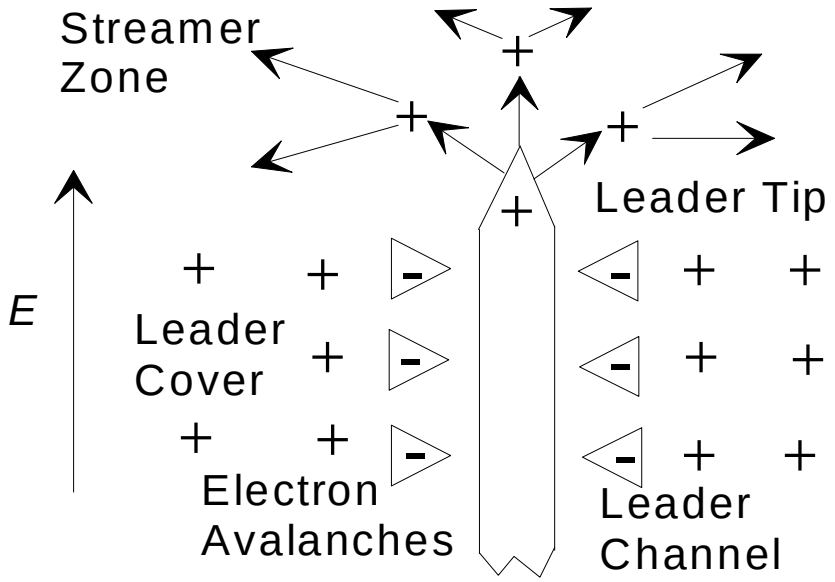

Figure 4.10. Diagram of a positive leader traveling through a region with an ambient electric field *E* (long arrow): A positive leader consists of a positively charged leader tip and a conducting leader channel. The leader tip generates a number of positive streamers (short arrows) that ionize a region of air called the streamer zone. Due to the presence of the leader tip, positive space charge in the streamer zone may also begin to produce streamers. As the leader lengthens, the space charge begins to surround the conductive leader channel in what is called the leader cover. Due to the potential difference between the positive space charges and the leader channel, electron avalanches develop away from the leader channel (providing a positive current into the leader channel). The combination of the current from the streamers in the leader tip and the electron avalanches along the leader channel keep the entire leader at temperatures greater than 2000 K [Adapted from 51].

Streamers are constantly generated from the tip of a leader, so it is possible for newly created streamers to ionize the pathway of an older streamer. When this occurs, the new streamer will possibly travel farther through the atmosphere. Also, as multiple streamers ionize the same region, that region becomes conductive and creates a pathway for the charges generated by the streamers to travel back to the leader. These conductive regions are called streamer branches and are diagramed in Figure 4.11 [59]. The leader also expands along these streamer branches in order to propagate through the atmosphere. A positive leader that propagates along these streamer branches only requires a 10-50 kV m^{-1} electric field instead of the stronger electric field needed for streamer propagation [10]. The part of the streamer branch where the leader expands is called a leader stem [60]. It is also possible for the leader to expand simultaneously along multiple streamer branches. This is called leader branching or forking [20].

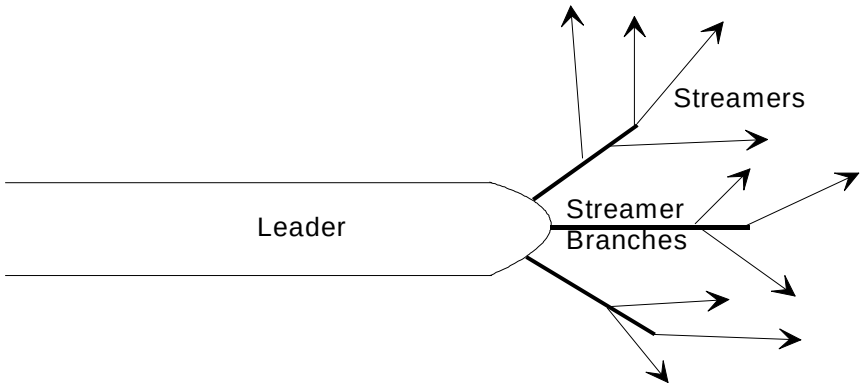

Figure 4.11. Diagram of the streamer branches of a leader: Streamers are not typically generated isotropically along the entire leader tip, but instead are focused at locations where the ambient electric field is greatly enhanced. These focused streamers create an ionized pathway through the air called a streamer branch (thick lines). Along a streamer branch, the required electric field is much lower for streamer propagation, allowing streamers (arrows) to travel further through the air. The streamer branches also provide a conducting pathway for the current generated by the streamers to the leader [Adapted from 59].

A negative charged leader functions in a similar way to a positive leader, but has a few additional features due to the unique properties of negative streamers. Negative streamers require very strong electric fields in order to propagate through the atmosphere, since the electron avalanches are always directed away from the streamer head. This creates a positive electric charge region between the negative streamer head and the electron avalanches. If multiple electron avalanches ionize the same region, the positive charge

region can become large enough to undergo a point discharge. A region that undergoes point discharge from multiple negative streamers is called a space stem, because it occurs at the base of a streamer branch and away from the leader tip [59]. Figure 4.12 illustrates the development of a negative leader.

The space stem generates positive streamers in the enhanced local electric field. These positive streamers typically travel toward the negative leader tip along the streamer branches created by the original negative streamers. The positive streamers also create electron avalanches that develop towards the space stem. From the perspective of the negative leader tip, the positive streamer acts like a backward traveling negative streamer. The direction of the positive streamers and electron avalanches generated from a space stem is illustrated in Figure 4.13. Thus, if the positive streamer from the space stem reaches the negative leader tip, the positive streamer will deposit the same amount of charge into the negative leader as if a negative streamer of the same potential had originated from the negative leader tip [10]. These positive streamers that initiate from a space stem and travel back toward the negative leader are called pilot streamers [10, 20]. The majority of the current traveling through the negative leader tip comes from pilot streamers [10].

When the current from all the streamers originating from the space stem is enough to heat the plasma sufficiently to become conducting, the space stem becomes a space leader. Like a conducting rod in a strong electric field, the space leader becomes polarized and all the built up electric charge moves to the ends. The positive charge of the space leader gathers at the edge closest to the negative leader tip. Pilot streamers continue to be generated from the positive end of the space leader, but now negative streamers can also originate at the negative edge of the space leader if the local electric field permits. Other nearby space stems can also generate positive streamers that travel to the negative edge of the space leader in a manner similar to the pilot streamer and the main negative leader. Receiving current from multiple sources allows the space leader to expand in both directions via the same process that a positive leader uses to expand [10, 51]. Once the positive edge of the space leader extends to the main negative leader, the charge of the space leader is neutralized and main negative leader tip advances up the space leader until reaches the negative edge, which becomes the new main negative leader tip. The rest of the space leader becomes part of the negative leader channel. The process of extending the negative leader along a space leader is called stepping [10, 20, 51]. Leaders that advance through the atmosphere via stepping are called stepped leaders [51]. Because the rapid neutralization of all the charge in the space leader, current pulses generate light pulses so that stepped leaders can be seen as brief flashes of light at the tip of a streamer [10, 20].

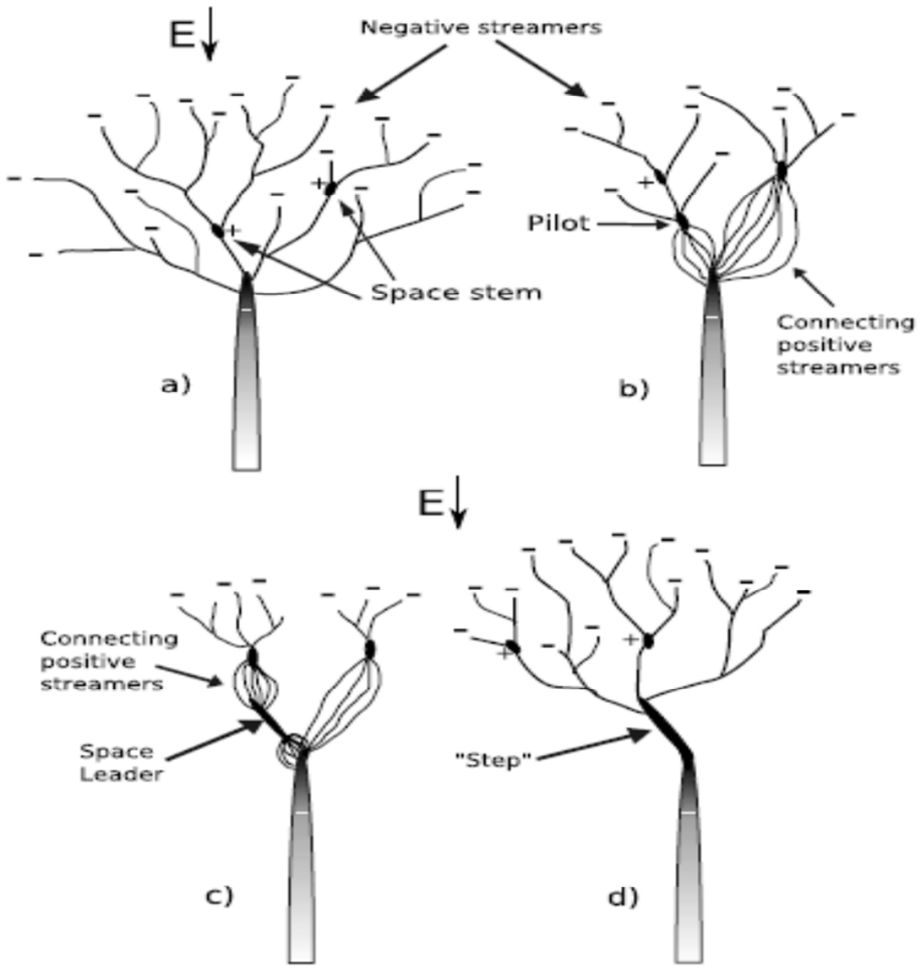

Figure 4.12. Diagram of the development of a negative leader: (a) Negative streamers create small regions of positive electric charge in the branch called space stems. (b) A space stem can generate a positive streamer that travels toward the negative leader tip. The positive streamers that travel toward the negative leader tip are called pilots. (c) Pilot streamers deliver electric charge back into the space stem which eventually heats the region enough for the space stem to become a leader. Depending on the amount of current traveling through the space leader, streamers can generate on both ends of the space leader, with positive streamers traveling toward the main negative leader tip and negative streamers toward other space stems. (d) The space leader extends into space just like a normal positive leader. Once the space leader reaches the main negative leader, the collected charge of the space leader is transferred into the negative leader and the negative leader tip travels through the space leader, extending the main negative leader. This expansion of the negative leader is called a step [10].

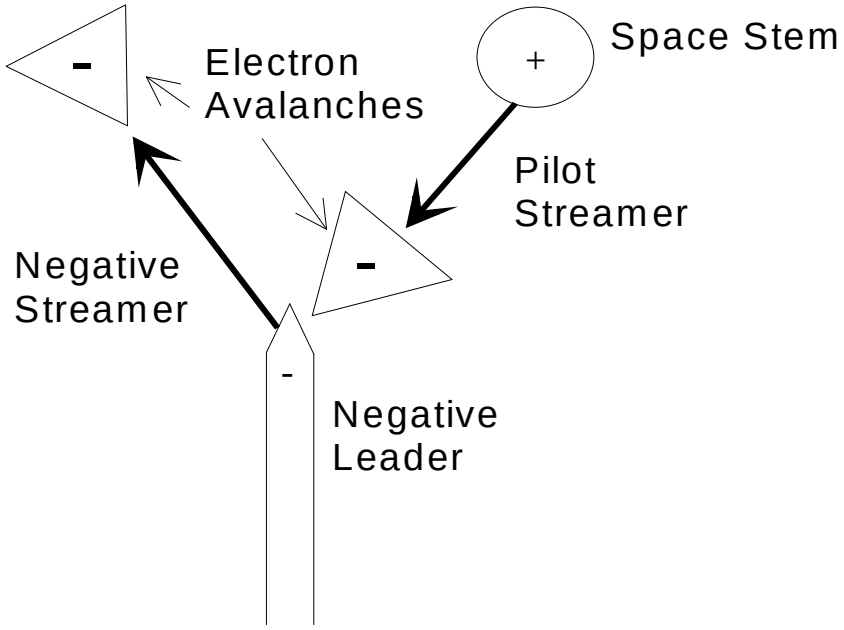

Figure 4.13. Diagram of a negative leader system: A negative leader system consists of the negative leader (rod with the pointed top), streamers (thick arrows), electron avalanches (triangles), and space stems (circle). Initially, negative streamers develop from the negative leader tips. Electron avalanches develop away from the heads of the negative streamers generating a current directed towards the negative leader tip. When multiple negative streamers ionize the same region a positive space stem may develop. The space stem produces positive pilot streamers that travel towards the negative leader tip. Electron avalanches develop towards the head of a positive streamer, which again produces a current directed toward the negative leader. The current from both the pilot and negative streamers is what keeps the temperature of the negative leader high enough to be a conducting plasma [Adapted from 59].

Leaders of both polarities continue to propagate through the atmosphere until the ambient electric field weakens or until the leader nears a large charge center of the opposite charge. When the electric field weakens to levels below that required for leader propagation, the leader is not able to generate enough streamers to supply the current required to keep the leader heated (~1 A [20]) [20, 51]. A cooling leader dissipates electric charge by allowing any excess ions to recombine or reattach within the atmosphere [10].

A leader that nears a large charge center or conductor undergoes what is called the attachment process [3]. First, as the leader nears the charge center, the charge center

begins to produce streamers that advance towards the negative leader. Some of these streamers make the transition of to a leader. When the two leaders meet, a conductive pathway is formed. The potential difference between the terminal ends of the leader generates a very large current along the former channel of the leader from the positive to the negative charge centers. The current neutralizes all the excess charge and heats the leader channel, including all leader branches, and is called a return stroke [3, 10, 20, 51]. The heated channel glows intensely and produces the loud sound of thunder (due to a rapid heating of the channel and consequent change in the air pressure) [3, 20]. The entire process of a leader connecting two charge centers is a long spark discharge [51].

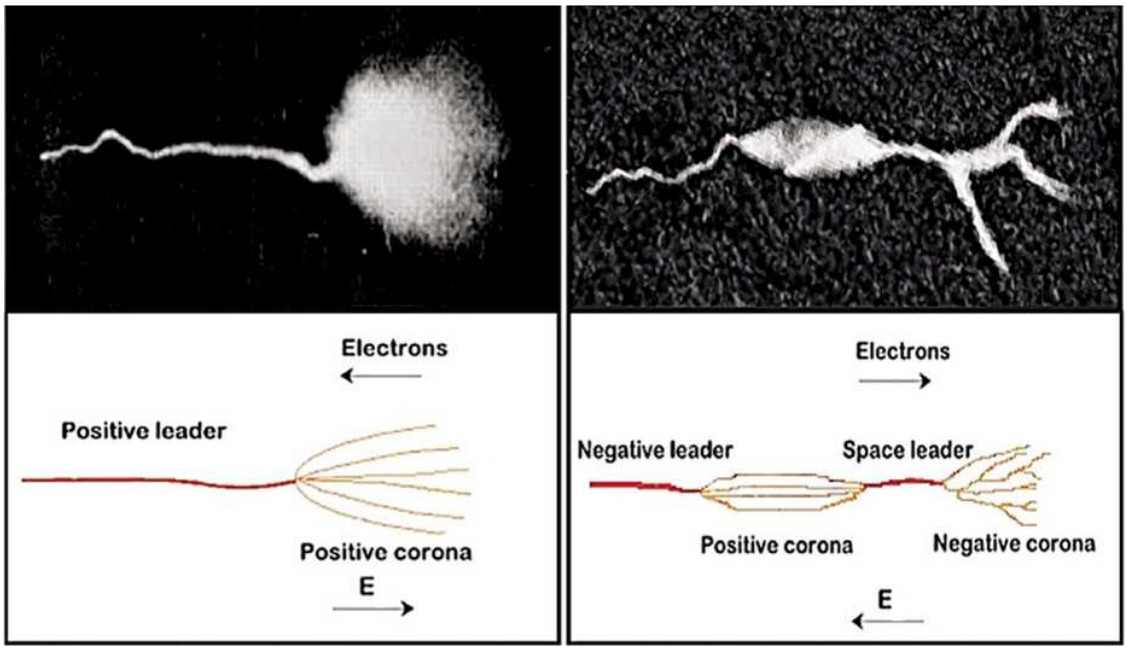

Figure 4.14: Photographs and diagrams of positive and negative leaders: (Left) A positive leader propagates continuously through the atmosphere starting from a positive streamer system (corona). (Right) A negative leader propagates via the discontinuous stepping process [54].

In summary, positive long spark leaders are easier to generate than negative long spark leaders, but both can propagate through very weak ambient electric fields as compared to those required for streamer generation. Positive leaders propagate continuously through the atmosphere while negative leaders propagate in discontinuous steps. Both types of leaders can be seen in Figure 4.14. Both polarities of leaders branch during development

and zigzag through the atmosphere (however positive leaders are generally straighter than negative leaders [51]) [51, 55].

Long spark discharges have many of the same properties (branching, zigzagging, large current transfers, etc.) associated with lightning discharges. However, lightning discharges have been observed having several different properties such as more negative leaders than positive leaders, multiple return strokes within a single discharge.

4.2. Types of Lightning Discharges

Lightning discharges are typically categorized by their observed properties, such as direction of propagation, location of the terminal end of the discharge or polarity of the lightning leader, instead of by the physical mechanism that initiated the discharge in the way long sparks are categorized [3, 4].

Lightning discharges can be divided into two large groups: discharges that reach the ground and discharges that stay completely in the atmosphere. Lightning discharges that reach the ground are called cloud-to-ground lightning or CG lightning. CG lightning discharges are further categorized by the polarity of electric charge and direction traveled by the lightning leader. The direction of the lightning leader is determined by the direction of the lightning discharge branches (downward discharges have branches towards the ground and upward discharges have branches towards the clouds) [4].

The majority of lightning discharges never reach the ground and are referred to as cloud discharges. There are three different types of cloud discharges based on where the terminal ends of the lightning discharge are located. Intercloud discharges are cloud discharges between two different storm cells. An intracloud discharge is a lightning discharge between two locations within the same storm cell. Air discharges are a type of cloud discharge in which one of the end terminals of the discharge is in clear air. Cloud discharges can be difficult to observe from the ground because the clouds block most of the lightning flash, but often the thunder can still be heard or the whole thunderstorm seems to light up briefly. The most common cloud discharge is the intracloud discharge, and in the literature, all cloud discharges are generally referred to as IC lightning [3]. Figure 4.15 illustrates the different types of lightning discharges (both CG and IC) in reference to the dipole/tripole model of a thunderstorm cell.

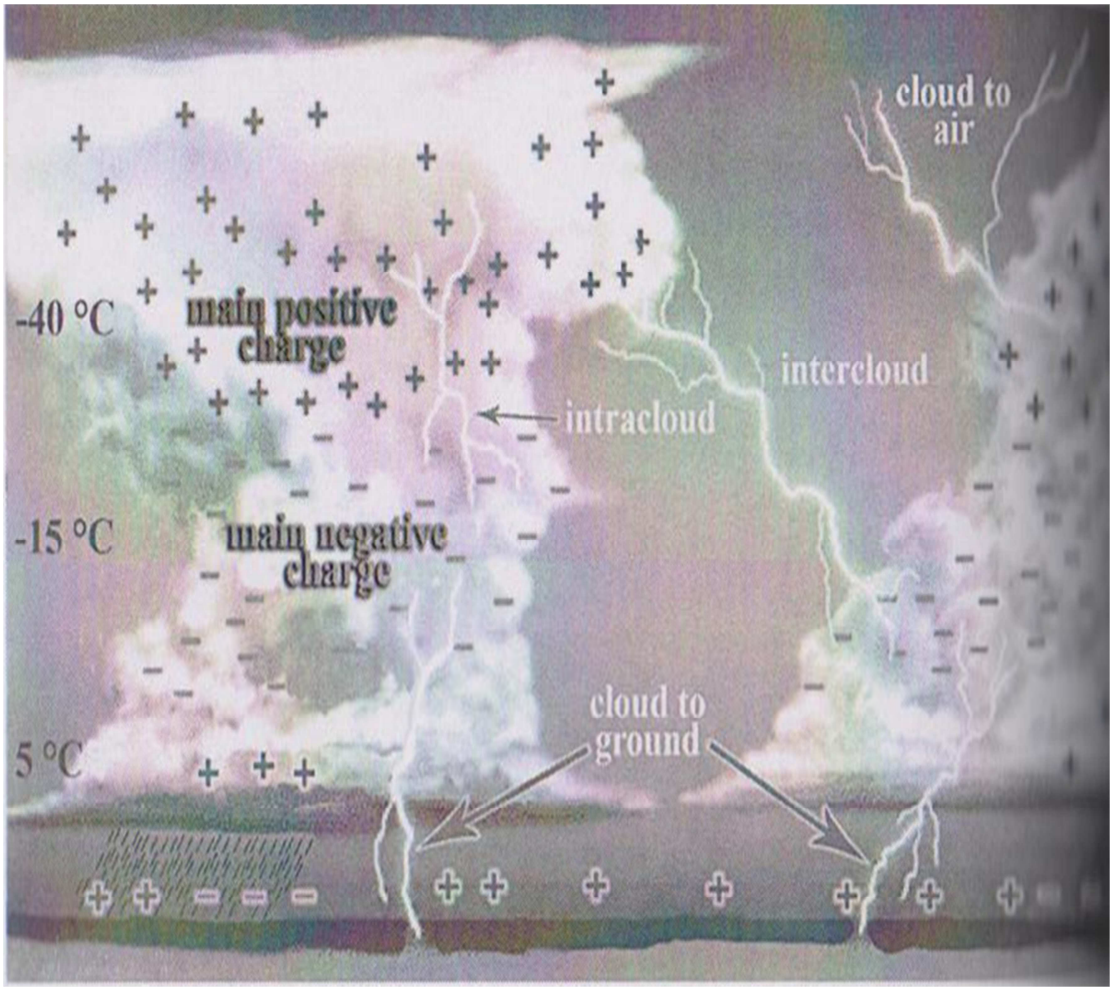

Figure 4.15. Diagram of the different types lightning discharges [4].

4.2.1. CG Lightning Discharges

CG lightning is further classified by which direction the leader branches (either toward or away from the ground) and the polarity of the leader. Figure 4.16 is a diagram of the four different types of CG lightning: downward negative, upward positive, downward positive, and upward negative [3].

The most common CG lightning discharges are the downward traveling leaders (cases a and c) and are called natural lightning, since the lightning discharge would have occurred regardless of the conditions on the ground [20]. The upward travelling leaders (cases b

and d) are examples of artificial lightning, since the leader must originate below cloud level and travel all the way up into the thunderstorm. Examples of objects that create artificial lightning are tall structures, aircraft, and rockets [4, 20]. The average relative frequencies for the different types of CG lightning discharge are listed in Table 4.1.

Table 4.1. Average relative frequency of a given type of CG lightning discharge [44]

Case of CG Discharge	Type of CG Discharge	Relative Frequency (%)
a	Downward Negative	90
b	Upward Positive	3
c	Downward Positive	5
d	Upward Negative	2

The downward, negative leader is the most common type of CG lightning discharge and is the type of lightning discharge assumed in the global electric circuit to bring negative charge to the ground [3, 4, 20, 30, 31]. Upward, positive CG lightning transfers positive charge to the thunderstorm, which is equivalent to negative charge being transferred to the ground [20]. Downward positive and upward negative CG lightning discharges both effectively bring positive charge to the ground and are usually considered separately from the more common downward negative CG lightning discharges [20]. Downward, positive CG lightning has been found to occur during the dissipating stage of a thunderstorm, winter thunderstorms, and severe thunderstorms [3], while upward, negative lightning discharges are associated with tall buildings or structures [40].

Positive leader lightning discharges are typically associated with nonstandard thunderstorm conditions such as during the dissipating stage of a thunderstorm cell or within a supercell [20]. Because of the low relative frequency of positive CG lightning discharges, this work assumes that all lightning discharges are of the negative leader type unless specified otherwise.

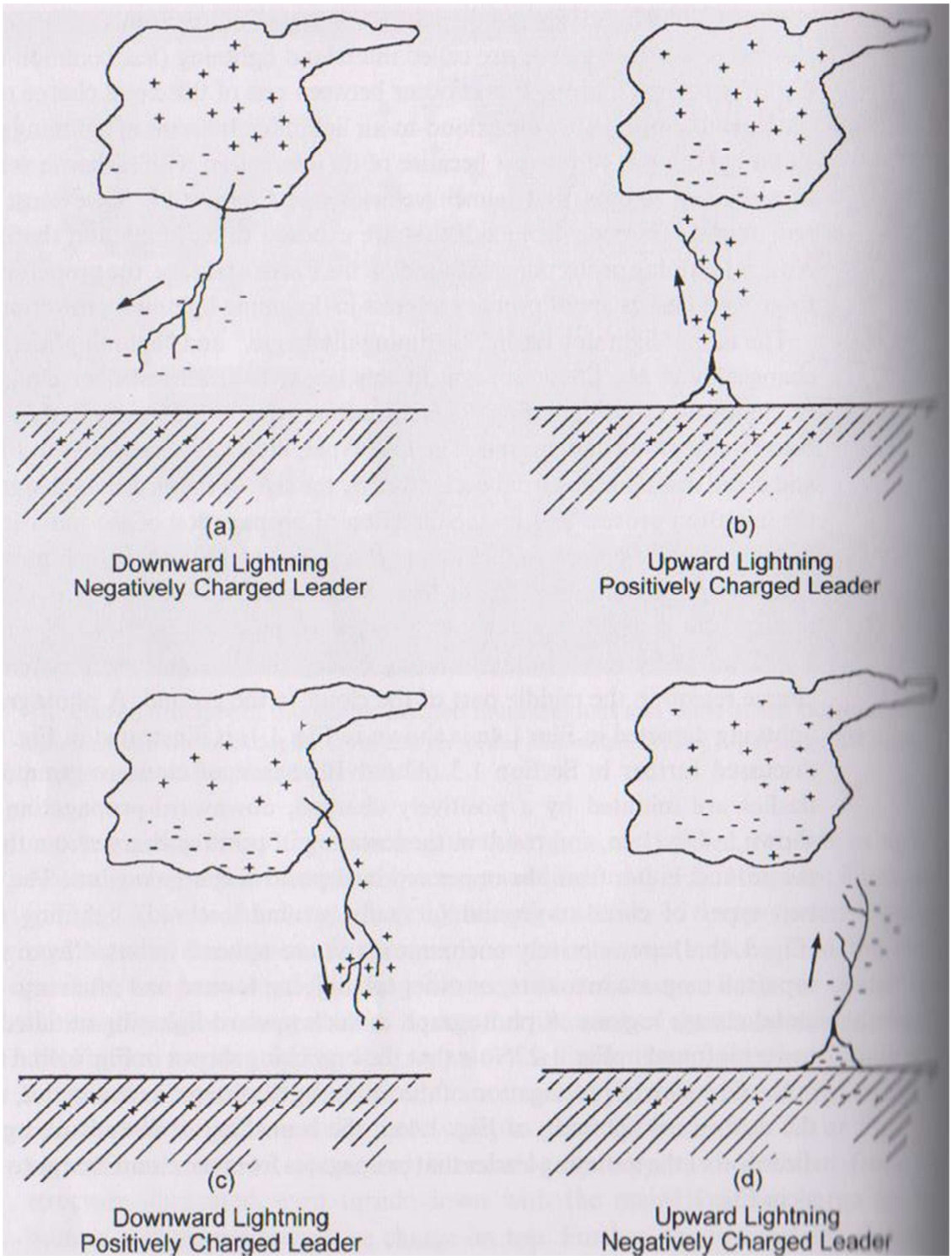

Figure 4.16. Diagram of the different types of CG lightning discharges: (a) downward traveling negative leader; (b) upward traveling positive leader; (c) downward traveling positive leader; and (d) upward traveling negative leader. The direction of the branching of the lightning leader indicates the direction of the leader [4].

4.2.2. IC Lightning Discharges

IC discharges have been studied much less than CG discharges, since IC discharges are typically blocked from view by the thunderstorm. Until the recent use of Lightning Mapping Arrays and satellite based lightning detectors, the true scale and rate of IC discharges within a thunderstorm were only crudely estimated [3, 43, 61]. IC lightning is now known to make up between 75-90% of all lightning discharges in a thunderstorm system and can be greater than 10 km in length without any part of the leader being outside the thunderstorm [3, 61].

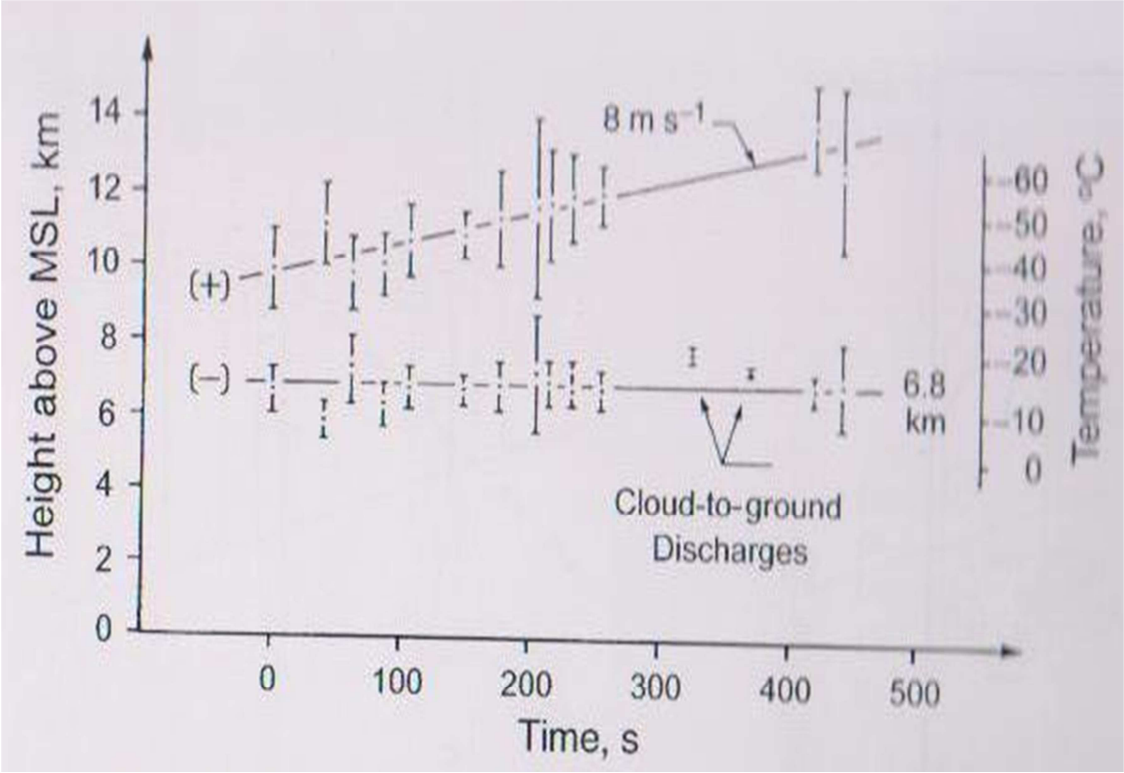

Figure 4.17. Origination locations of lightning discharges from a small thunderstorm: The solid lines are the location of the main positive (upper) and negative (lower) charge centers. The points are lightning discharges with one sigma error bars. The positive charge center altitude increased in time, since the thunderstorm was still developing. The majority of lightning discharges were IC discharges with only two CG discharges reaching the ground [3].

IC lightning transfers large amounts of electric charge throughout the thunderstorm cell (intracloud) and possibly to other thunderstorm cells (intercloud) or to large space charges in the atmosphere (air discharge). An IC discharge is typically initiated within either the main positive or negative charge center of the thunderstorm cell [8, 20, 25, 62]. Figure 4.17 is a plot of the initiation location of IC and CG lightning discharges within a small, developing Floridian thunderstorm [20]. CG lightning typically originates near the lower main negative charge center and is much rarer than IC lightning [20].

IC lightning is very common while the thunderstorm cell is in the cumulus and early mature developmental phases, with approximately five to ten IC lightning discharges for every CG lightning discharge [3]. In Figure 4.17, there was an almost constant amount of IC lightning in a thunderstorm cell, then very little when the CG lightning discharges occurred. Afterward the CG discharges stopped and the thunderstorm cell enters the dissipating stage and IC lightning began again [3].

4.3. Lightning Flash Rates

Worldwide, there are on average 81 lightning discharges per second being recorded by weather satellites. Thunderstorms are not distributed evenly across the globe, with the majority of them occurring over coastal land areas near the equator [1], as can be seen in Table 4.2. The highest lightning discharge rates in the world can be found over Central Africa and the Amazon Jungle in South America, with some particular regions having as many as 100 lightning discharges per square kilometer per year [1]. Lightning discharges over the ocean are generally less frequent than over land, especially as compared with land masses near the equator or coastal regions, by a ratio of 4:1 [63].

Table 4.2: Median Lightning Discharge Rates for Different Regions of the Earth [1].

Geographic Location	Discharge Rate discharges km^{-2} $year^{-1}$	Geographic Location	Discharge Rate discharges km^{-2} $year^{-1}$
North America	2.50	Indonesia	15.00
U.S. Gulf Coast	19.60	North Atlantic	2.30
South America	24.50	South Atlantic	0.29
North Africa	5.00	North Pacific	1.30
Central Africa	28.60	South Pacific	2.00
Asia	2.40	Indian Ocean	0.51

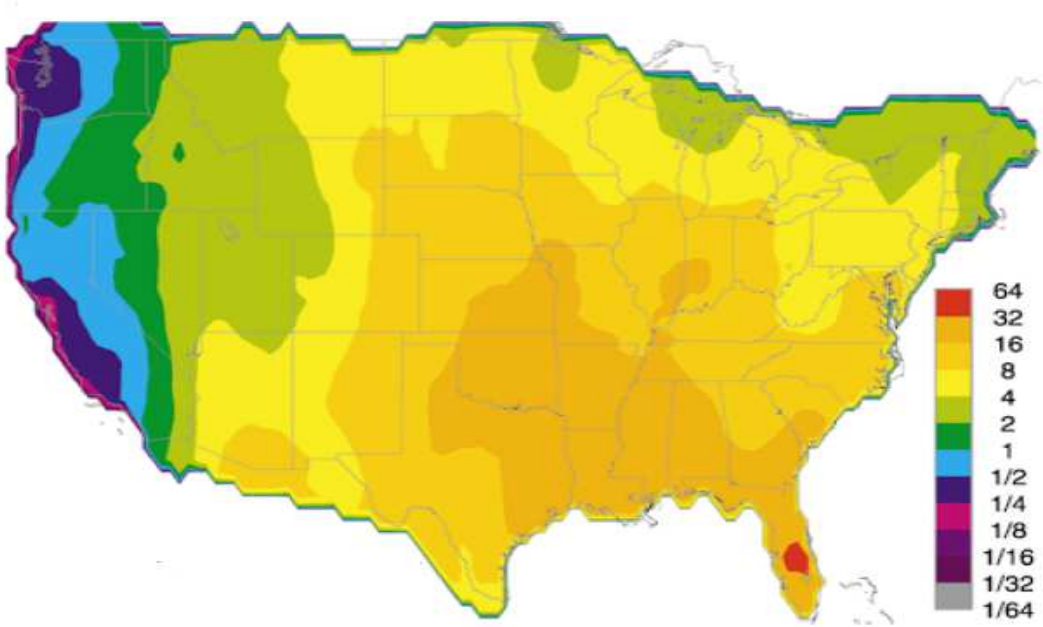

Figure 4.18. Diagram of the mean lightning discharge rate (CG + IC discharges km^{-2} $year^{-1}$) over the continental United States between May 1995 and April 1999 [64].

Throughout the United States there is great variation in the lightning discharge rate between different geographic regions, as shown in Figure 4.18 [64]. The Gulf region, especially central Florida, has the greatest concentration of lightning discharges within the continental United States. The Midwest, South East, Texas, and Oklahoma have the next highest lightning discharge concentrations. Thunderstorm systems in Florida tend to contain dozens of small thunderstorms compared to the single, large (and generally severe) thunderstorm cells that can affect more inland areas like Oklahoma [2]. There is little lightning activity in the Northern and Western parts of the continental United States, with <0.1 lightning discharges per square kilometer per year along the Pacific coast. On average, 25 to 30 million CG lightning discharges occur over the continental United States every year [64].

The mean CG lightning discharge rate for North America is approximately 2.0 discharges per square kilometer per year, which means that approximately every 250 years, a typical single story house will be struck by lightning [4]. In Oklahoma, the mean CG discharge rate is between 3-6 discharge per square kilometer per year, so a single story house should be struck by lightning every 80-160 years. In central Florida, the average time between lightning strikes on a single story home is only 50 years [4].

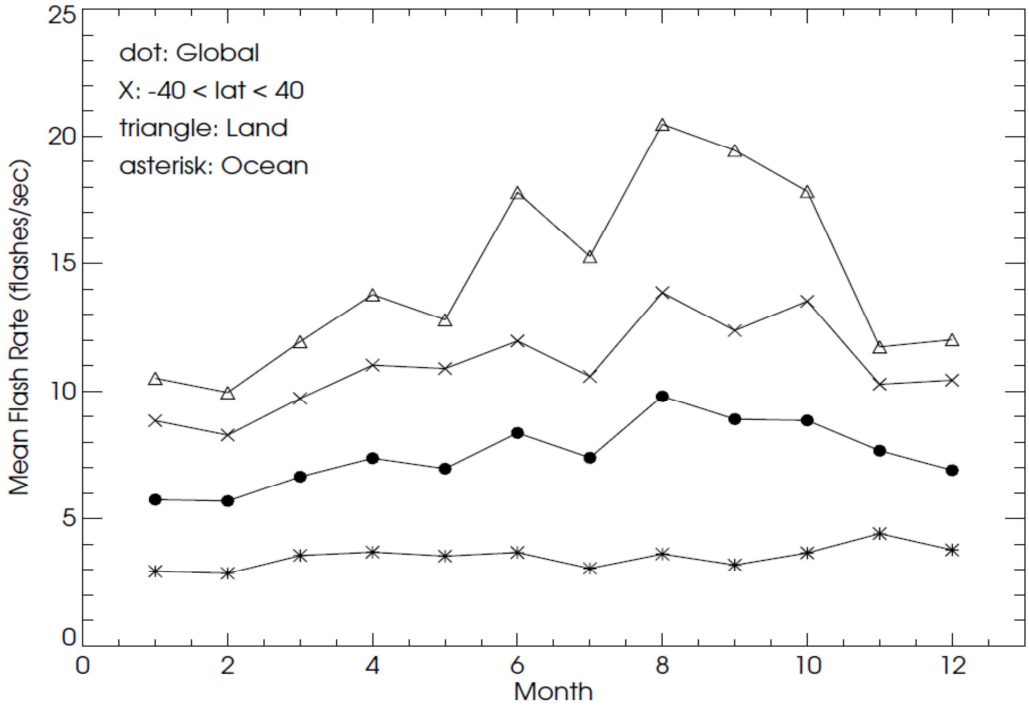

Figure 4.19. Diagram of the mean lightning flash rate as a function of month over the entire Earth (dots), between ± 40° latitude (x's), all land masses (triangles), and oceans (asterisks). A lightning flash is considered the same as a lightning discharge [1].

The number of thunderstorms around the globe varies throughout the year, especially over continental regions. Figure 4.19 is a plot showing the average lightning discharge (flash) rate as a function of the month over different regions of the Earth. The lightning discharge rate peaks in August over land masses and slowly decreases to a low between November and February. Over the oceans, the lightning discharge rate is fairly constant throughout the year [1].

The mean number of lightning discharges by month over the continental United States can be seen in Figure 4.20. July is the peak month for lightning activity in the continental United States with much less lightning activity between November and February [2]. Compared to the mean monthly global lightning discharge rate in Figure 4.20, the monthly lightning activity within the continental United States is closer to a Gaussian distribution [1, 2].

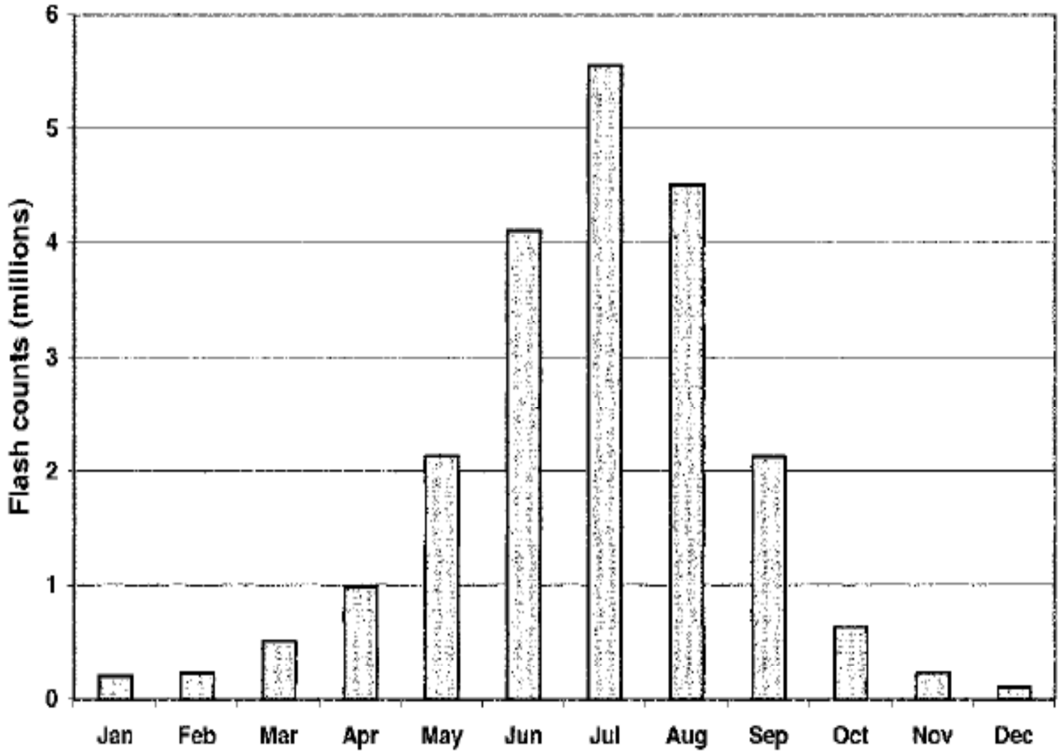

Figure 4.20. Average number of CG lightning flashes by month over the continental United States. A lightning flash is considered the same as lightning discharge [2].

Historically, CG lightning has been used to calculate lightning discharge rate for both individual thunderstorms and for a whole geographic regions, such as the lightning discharges rates shown in Figure 4.20 [1, 2, 3, 20]. However, newer satellite lightning flash rate data includes both IC and CG lightning discharges [1]. In a typical thunderstorm over the continental United States, the average ratio of IC to CG lightning is 2.94 ± 1.28 (central Oklahoma has a IC to CG ratio ~3.0) [64], i.e. ~75% of all lightning discharges are IC lightning. From a single severe thunderstorm over Florida, the total discharge rate (IC + CG) was >567 discharges min^{-1}, but the CG discharge rate was 12 discharges min^{-1} [63].

4.4. Anatomy of a CG Lightning Discharge

In long spark experiments, the distance between the electrodes is typically only a few meters and the electrodes are charged by a large AC current [51, 53]. As the electric field

strength rises with the current, a discharge occurs between the two metal electrodes, which ultimately short circuits the field [51]. In lightning discharges, the two electrodes are replaced by a charge center within a thunderstorm and the ground (for CG lightning) or another charge center (for IC lightning) that are several kilometers apart. The physical size (scale of km) of the charge centers makes it unlikely that a single lightning discharge will neutralize all the electrical charge of the charge center. The remaining electric charge in the charge center allows the lightning discharge to continue to develop after the initial discharge, unlike a long spark [3,20]. The development of a lightning discharge is illustrated in Figure 4.21.

A lightning discharge begins as a leader during what is called lightning initiation [10]. Unlike long spark leaders that were discussed in Section 4.1.4, a lightning discharge develops a special bipolar leader which is discussed in Section 4.4.1. The lightning leader then travels through the atmosphere until it reaches the conductive ground (CG lightning) or a charge center with the opposite polarity as the leader (IC lightning). The leader creates a conducting pathway between the originating charge center and the other terminal end during attachment [3, 20]. The attachment process initiates a strong current, called a return stroke that travels along the conductive pathway formed by the preceding leader. The return stroke current is large enough to heat the air to produce a bright flash (lightning) and a strong low-frequency sound (thunder). The return stroke also neutralizes electric charge at both ends of the conducting pathway [3, 20].

After the return stroke, the conducting pathway will slowly cool down and decrease in conductivity. A relatively weak current travels along the conducting pathway for many milliseconds and is known as a continuing current. Also, the remaining electrical charge in the originating charge center begins to rearrange itself (J processes) and starts to redevelop into a lightning leader (K processes). The continuing current, J, and K processes will be discussed in more detail in Section 4.4.4 [3]. A K process can produce a propagating lightning leader which will try to follow along the path of the original lightning leader. If the conducting pathway is still conductive, the leader is called a dart leader due to its fast propagation speed. When the dart leader reaches the ground or charge center, another return stroke is initiated [3].

A cycle of dart leaders and additional return strokes continues until the originating charge center (and possibly other adjacent charge centers [43]) no longer has enough electric charge to initiate a lightning leader [3]. These additional return strokes occur too quickly for the human eye to resolve except for a possible flicker in the brightness of the original lightning discharge if the time between them is greater than about 16 ms [3].

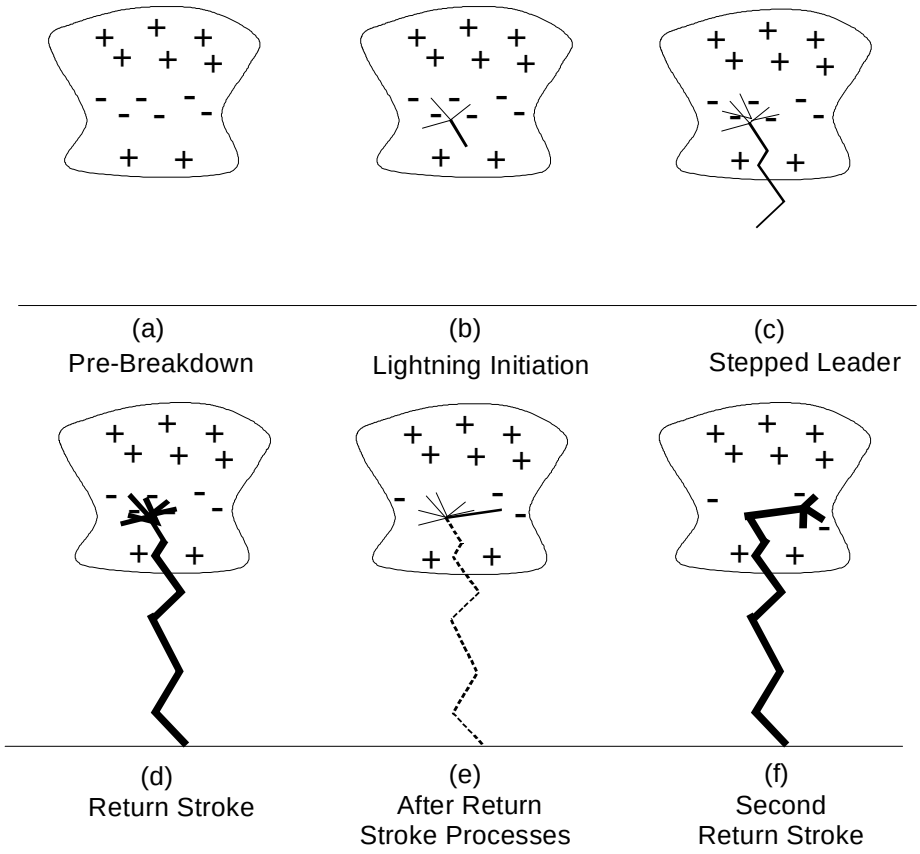

Figure 4.21: Diagram describing the development of a negative CG lightning discharge: (a) The pre-breakdown step is where the thunderstorm cell becomes electrified and the dipole/tripole electric charge structure develops. (b) The CG lightning is initiated by the creating of a bipolar discharge consisting of a positive streamer system and a negative leader. (c) The negative leader leaves the thunderstorm through a series of steps and is called a stepped leader. (d) When the stepped leader reaches the ground, a conducting pathway forms between the ground and the main negative charge center. A large current travels up the conducting pathway from the ground to the main charge center producing a bright flash (i.e. lightning) and a loud sonic boom (i.e. thunder). This large current is called a return stroke and neutralizes a portion of the main negative charge center. (e) After the return stroke, the conducting pathway remains slightly conducting allowing small amount of continuing current to travel along it. Streamers and leaders continue to form in the negative charge center. (f) A new negative leader travels down the conductive pathway, initiating another return stroke. Steps (e) and (f) both continue for as long as the conducting pathway does not dissipate [Adapted from 3, 44].

With the exception of lightning initiation and attachment, the development of lightning discharges has been well documented with high speed video, broadband filed antenna, electric field mills, and other modern detection methods, such as lightning mapping arrays [3, 20]. Lightning mapping arrays are one of the few methods to detect the short (< 1 ms [3, 20]) lightning initiation process located deep within a thunderstorm [43]. For this reason, I used data from the OKLMA for my research to infer where and when a lightning discharge was initiated in the atmosphere.

4.4.1. Lightning Initiation

As stated in Section 3.4, hydrometeors can undergo point discharges in the strong electric fields of a thunderstorm. A hydrometeor is polarized in an electric field, with opposite ends of the hydrometeor having different polarities. If the ambient electric field is strong enough to generate both positive and negative streamers, both will form around the same hydrometeor as can be seen in the photograph in Figure 4.22 [20, 50].

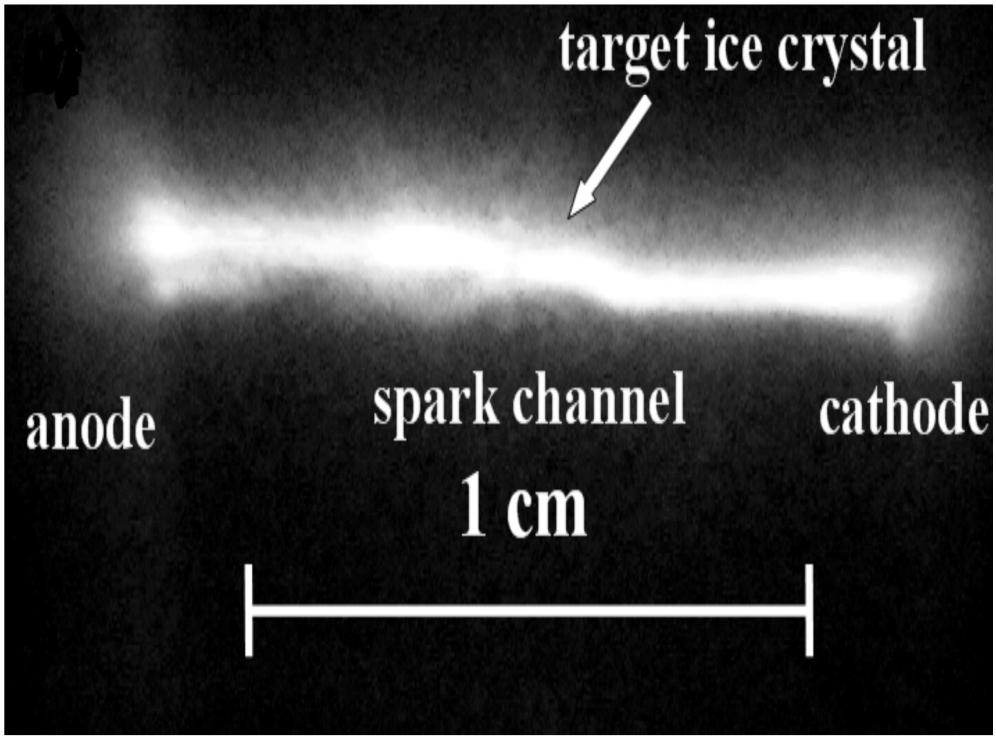

Figure 4.22. Photograph of an ice particle discharging from both polarized ends in a long spark experiment [50].

Lightning mapping arrays have found that lightning leaders are typically bipolar in nature, where there are both positive and negative streamers and leaders being formed by the discharge [43]. These bipolar leaders occur for both CG and IC lightning discharges as illustrated in Figure 4.23 [43]. Lightning discharges typically originate within the lower main negative charge center of the thunderstorm where a positive streamer system develops to provide the current needed for a negative leader [20, 43]. This negative leader either travels upward toward the upper main positive charge center to become an IC lightning discharge or downward toward the lower positive charge center to become a CG lightning discharge. Sometimes an upward negative leader turns around and becomes what is called a hybrid discharge [43].

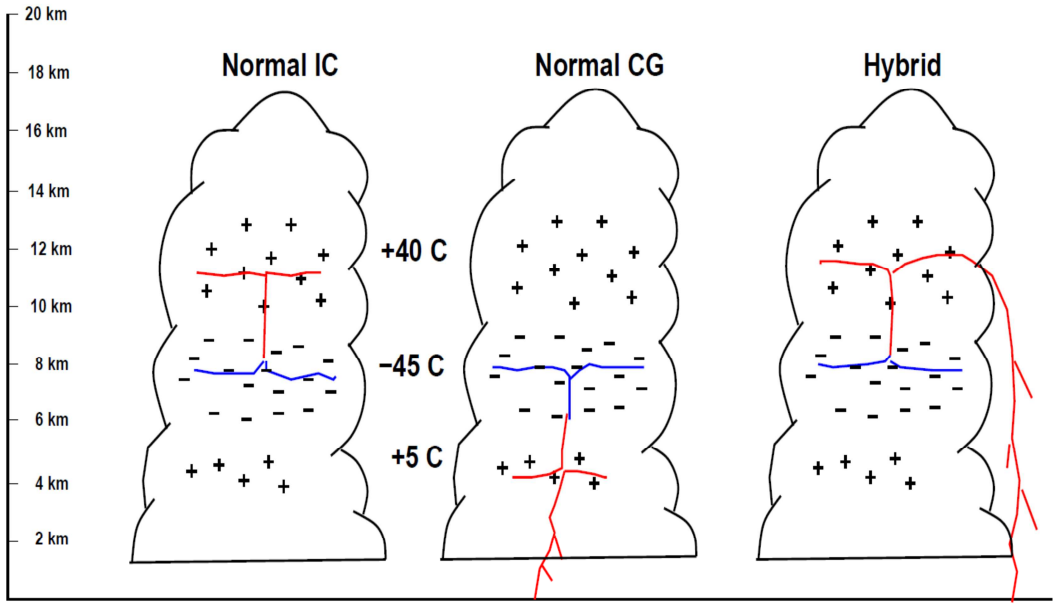

Figure 4.23. Diagram of negative IC and CG lightning in a standard dipole/tripole thunderstorm: The blue lines represent the positive streamers, while the red are negative streamers. In a normal IC discharge, the positive streamers generate a bipolar lightning leader in the main negative charge region, which propagates toward and eventually discharges in the main positive charge center. The positive streamers also start in the main negative charge center for a CG, but the negative leader advances downward toward the lower positive charge center. The atmosphere below a thunderstorm is typically positively charged, due to point discharges, which helps to direct the downward negative leader to the ground in a CG lightning discharge. It is also possible for an upward traveling negative leader to change directions and travel toward the ground to be a CG lightning discharge. Sometimes these lightning leaders that change directions are called hybrid discharges [43]

The conventional lightning initiation model describes how a hydrometeor can initiate a bipolar lighting leader in a strong electric field, which is described in detail in section 4.4.1.1 [10]. Positive leader discharges, especially during extreme weather, have been observed to be unipolar and develop through currently unknown mechanisms [3, 20].

4.4.1.1. Conventional Lightning Initiation Model

The conventional lightning initiation model begins with a hydrometeor located within the maximum electric field region of an active thunderstorm. The hydrometeor polarizes in the electric field and has two edges at different polarities. The bound charge (and any free charges) collects on the surface of the polarized hydrometeor [10, 20]. Since the required electric field to generate positive streamers is 2-3 times weaker than that is required to generate negative streamers [51], a positive point discharge develops first near the polarized hydrometeor. The positive point discharge begins to generate positive streamers which ionize the air surrounding the hydrometeor and create a supply of free electrons. The free electrons will accelerate toward the positive point discharge and the hydrometeor. As negative charge accumulates near the hydrometeor, the ambient electric field is further enhanced allowing the hydrometeor to initiate a negative point discharge and generate negative streamers. All the free charge generated by both the positive and negative streamers is enough to heat the air and create a leader [10]. A diagram of the above process can be seen in Figure 4.24.

The majority of lightning discharges are observed to start with a negative leader [54], so the negative streamer system transforms into a negative leader. The negative leader propagates through the atmosphere according to long spark theory (Section 4.1.4) with one exception: the presence of the positive streamer system. The positive streamer continues to generate negative current, which strengthens the negative leader. Also, the negative leader is generating a positive current, which strengthens the positive streamer system. This feedback between the negative leader and positive streamer system allows both electrical discharges to expand further in the atmosphere, which is why both the positive and negative discharges branch in Figure 4.23. Without this feedback loop, a leader would dissipate in the weaker electric field regions of the thunderstorm [10, 43].

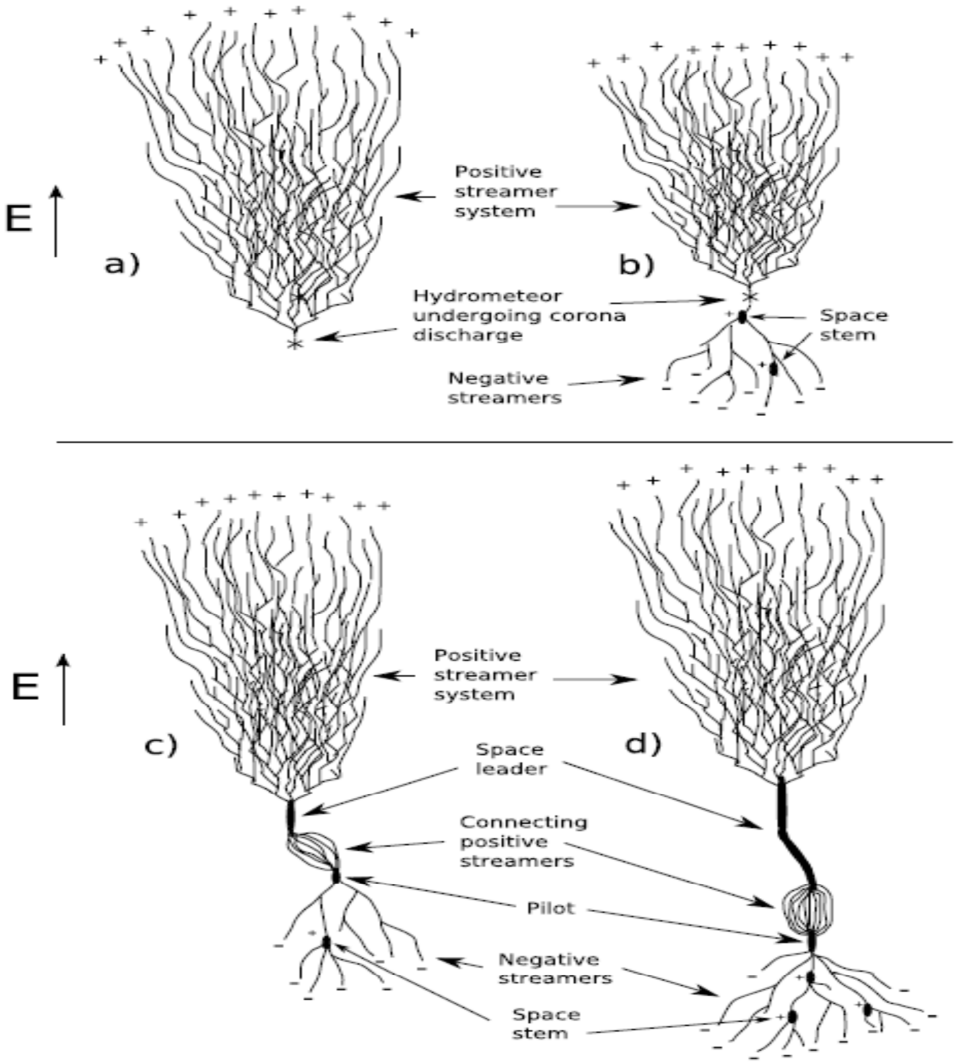

Figure 4.24. Diagram of the formation of a bipolar lightning discharge: (a) A hydrometeor undergoes a point (corona) discharge and develops a positive streamer system. (b) The free electrons generated by the positive streamers further enhance the ambient electric field to generate a negative streamer system on the other side of the hydrometeor. (c) The negative streamer system develops into a negative leader. (d) The positive streamer system and negative leader strengthen each other through a feedback loop, which helps both to expand further into the atmosphere [10].

The main problem with the conventional lightning discharge model is that the required strength of the ambient electric field to initiate a positive point discharge is much higher than the electric fields measured in a typical thunderstorm. Ground based studies with ice hydrometeors in thunderstorm conditions (pressure, humidity, temperature, etc.) have found that a minimum of ~400 kV m^{-1} electric field strength is required for streamer

generation [50]. The average maximum electric field observed in an active thunderstorm is 130 kV m^{-1} [20], which is a factor ~2-3 weaker than the minimum required for positive streamer generation. Once the positive streamer system is established, the lightning discharge can develop within the weaker fields of a thunderstorm, but the initial electric field strength must first be strong enough to initiate the process.

4.4.2. Leader Propagation

After a lightning leader is initiated, the leader begins to propagate both within and outside the thunderstorm. Negative leaders, which are the most common type of lightning leader [54], propagate through the atmosphere via a process called stepping, as discussed in Section 4.1.4. Figure 4.25 is a photograph taken by a high speed camera of a lightning leader stepping in the atmosphere.

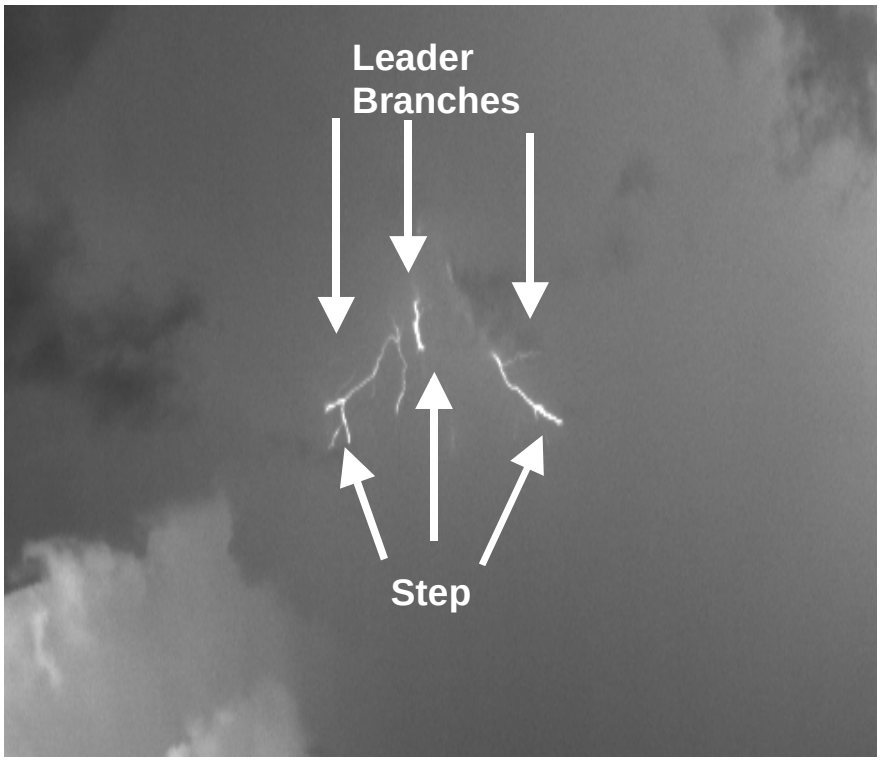

Figure 4.25. Photograph showing the branches and steps of a lightning discharge in the atmosphere [65].

The bright sections of the lightning leaders seen in Figure 4.25 are the steps. Each branch of the lighting leader propagates independently of any of the other branches [60]. Each step is ~10 m in length and occurs every 20-50 μs [3, 20]. The stepping of the lightning leader causes the zig-zag appearance of a lightning discharge. The lightning leader takes several milliseconds to propagate from the bottom of the thunderstorm to the ground a few kilometers below [3]. Positive leaders propagate in a continuous manner through the atmosphere compared to the discontinuous steps of a stepped leader. Without the need for stepping, positive leader are much straighter than stepped leaders, but both types of leader do branch in the atmosphere [3, 20, 55].

4.4.3. Return Stroke

As a CG lightning leader nears ground, the potential difference between the leader and the ground (~10 MV [10]) enhances the already enhanced electric field. This enhancement of the electric field causes objects near the ground (including trees, cars, buildings, and people) to generate streamers that propagate upwards towards the downward propagating stepped leader. Some of these streamers from the ground become upward-going leaders, one of which reaches the stepped leader, forming an ionized pathway from the leader to the ground. The process where a leader from the ground meets the downward traveling stepped leader is called attachment [3, 20]. The belief that only the tallest object will be struck by lightning comes from fact that taller objects are generally closer to the stepped leader. Thus upward going leaders originating from taller objects have less distance to travel in order to attach to the stepped leader. However, the first upward going leader (or leaders in case of lightning discharges that strike multiple locations [20]) that attaches to the downward-going stepped leader creates the ionized pathway, which is not necessarily the leader from the closest source [55]. A photograph of a return stroke and an unattached leader can be seen in Figure 4.26.

When the stepped leader reaches the ground, the ground and the charge center where the leader originated are connected by a conducting pathway. For negative CG lightning, a large current pulse travels up the leader channel from the ground to neutralize the charge center in the thunderstorm. This large current is called the return stroke [3, 20, 51]. The current of the return stroke of a natural lightning discharge averages 30 kA but can be >100 kA [20]. The strong current rapidly heats the air within the conducting pathway to temperature typically >31,000 K, or about twice the temperature of the surface of the sun [3, 20]. At these temperatures, the air molecules in the conducting channel begin to glow intensely. This intense glow is what is commonly called a lightning. The heated column

of air rapidly expands, which generates a loud sound wave, which is known as thunder [20]. The entire duration of a CG return stroke is ~75 μs [3].

Figure 4.26. Photograph showing the return stroke of a lightning discharge along with a streamer that did not attach to the return stroke [Adapted from 66].

4.4.4. Later Processes

The return stroke leaves the conducting pathway between the charge center and the ground. The residual charge in the charge center produces small current, typically <100 A [3], along the conducting pathway. This weak (relative to a return stroke) current continues to travel through the conducting pathway for up to 100 ms after a return stroke and is called the continuing current [3]. Continuing currents are fairly stable for the entire duration of the event with the exception of short millisecond variations called M-components (after the researcher who first studied the process) [3].

Compared to the return strokes, which only last for a few microseconds, longer duration continuing currents allow more total charge to be transferred to a struck object. It is the continuing current which heats up a material enough to leave burn marks or possibly to

catch fire. From a lightning protection perspective, often the continuing current, and not the return stroke, is what causes the most damage to structures and people [3, 20, 28].

A large portion of the negative charge center is neutralized after the return stroke, and that causes a large change in the ambient electric field, as seen in ground-based electric field measurements such as the one in Figure 3.15. Inductive charging processes begin to recharge the neutralized region and the residual negative charge begins to redistribute itself. The rapid changes to the electric field due to the redistribution of electric charge after a return stroke are called J-processes (for junction processes) [3, 61].

During the electric charge redistribution process, streamers and leaders can develop near the conducting pathway. These streamers and leaders slightly distort the ambient electric field, which can be measured on the ground. These distortions in the electric field measurement are called K-processes (after the German word “kleine” for small) [3].

The combination of the J and K processes cause the ambient electric field to return to its pre-lightning discharge state in ~30 ms [3]. With the strong electric field restored, K-process streamers and leaders expand into other regions of the thunderstorm, possibly into other neighboring charge centers [3, 61]. Eventually, one of the leaders starts to travel down the original stepped leader’s conducting pathway, which will generate another return stroke [3, 20].

4.4.5 Dart Leaders and Multiple Return Stroke Discharges

A leader generated during a K-process might start to travel down the conducting pathway to the ground. Since the pathway is already established, the leader can quickly travel to the ground and is called a dart leader [3, 20]. If too much time passes before the dart leader is generated, segments of the pathway lose their conductivity and the dart leader must propagate via stepping. When this occurs, the leader is called a dart-stepped leader [3]. When the dart or dart-stepped leader reaches the ground, another return stroke occurs (with typical current of 1 kA) [3]. A photograph of a return stroke from a dart leader is shown in Figure 4.27.

The dart leader only travels along the main branch of the original stepped leader and typically does not branch [3]. Without needing to stepped through the atmosphere, the dart leader reaches the ground in ~1/10 the time of the original stepped leader (~1 ms) [3]. The return stroke of the dart leader also does not travel along the branches of the original, so in general only the main channel glows brighter in subsequent return strokes [3].

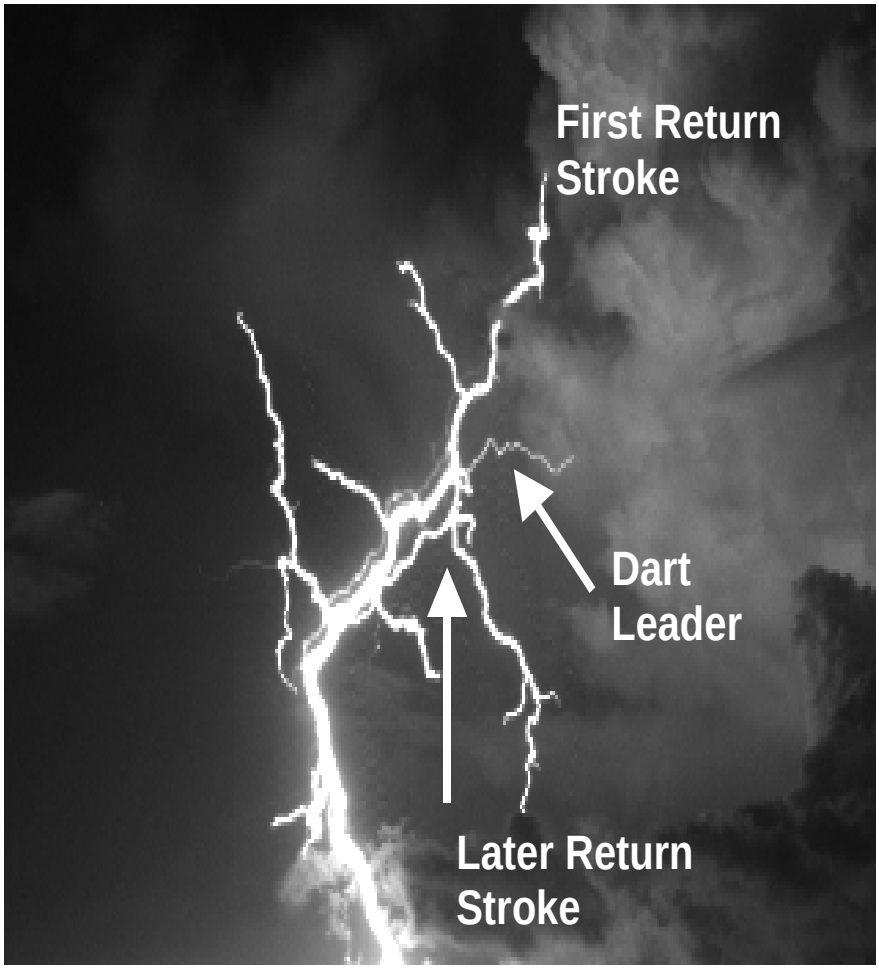

Figure 4.27. Photograph of multiple return strokes. A dart leader travels through the charge center and eventually arrives to and propagates along the conducting pathway of the original stepped leader. The dart leader follows the most direct route to the ground, typically not illuminating branches not connected to the ground [65].

As long as the charge center can be reestablished before the conducting pathway cools and loses its conductivity, the continuing current, J-processes, K-processes, dart leaders and dart-stepped leaders will continue to occur [3]. Lightning discharges are commonly indexed by how many return strokes (typically shortened to just strokes [3, 20]) occurred over the entire duration of discharge. More than 80% of all negative CG lightning discharges have multiple return strokes, with the average being three stokes per lightning discharge [3, 56]. Positive CG lightning discharges typically only have a single stoke [3].

CHAPTER V

GALACTIC COSMIC RAYS

In very distant and currently unknown [32, 67] astrophysical processes, a large population of very energetic particles are produced and emitted into interstellar space. These energetic particles (electrons, positrons, hydrogen nuclei, alpha particles, and other heavy ions up to Uranium) travel through interstellar space, possibly undergoing interactions along the way, and eventually reach Earth. These particles are called Galactic Cosmic Rays (GCR) [11, 67, 68, 69]. When GCR penetrate the Earth's atmosphere, they undergo nuclear interactions in the Earth's atmosphere generating large numbers of secondary particles, including pions (neutral and charged), kaons, neutrons, protons, muons, electrons, positrons, and photons [11, 12, 67, 68]. These secondary cosmic rays propagate and interact with the atmosphere over a large spatial volume and are collectively called an extensive air shower (EAS) [11, 12, 67, 68]. The majority of particles in an EAS range out, i.e. loses all their kinetic energy, or decay before reaching the ground. The major exceptions are secondary muons and neutrons, which are commonly measured on the ground [12, 70]. Interactions between the secondary cosmic rays and the atmospheric nuclei are responsible for generating many of the aerosols found at thunderstorm altitudes and creating radioisotopes such as ^{7}Be and ^{14}C [11, 71]. Secondary cosmic ray electrons have been hypnotized to generate a special type of long duration electron avalanche called a relativistic runaway electron avalanche (RREA) that may be responsible for initiating lightning discharges [2, , 9, 10, 72].

5.1. Primary Galactic Cosmic Rays

The Earth's atmosphere is under constant bombardment by Galactic Cosmic Rays (GCR). GCR are made up of electrons, positrons, protons, helium nuclei, and other heavy ions that are generated in distant astrophysical processes [67, 69]. Table 5.1 lists the fraction of each type of GCR primary particles measured at the top of the Earth's atmosphere.

Table 5.1: The distribution of GCR primaries at the top of the atmosphere [73, 74].

Primary		Percent (%)
Baryons		98
	Protons	87
	Helium Nuclei	12
	Heavy Ions (Z >3)	1
Leptons		2
	Electrons	90
	Positrons	10

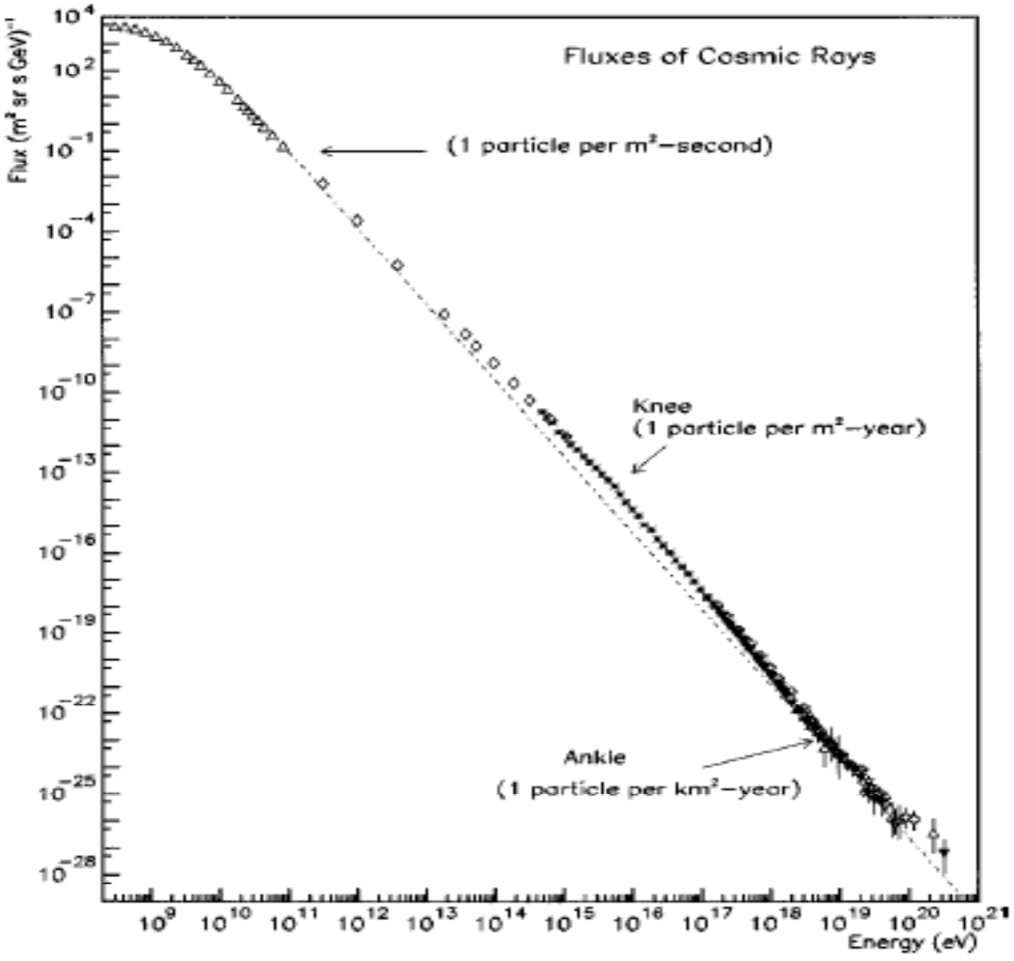

Figure 5.1: The differential flux of all GCR primaries at the top of the atmosphere [75].

GCRs propagate through the interstellar medium where they undergo collisions and nuclear interactions, and, if charged, are deflected by galactic magnetic fields [11, 32]. GCR primaries that arrive in the solar system also interact with the Sun's and Earth's magnetic fields before reaching the Earth's atmosphere [11, 32]. The more energetic the GCR, the less the particle is affected by the magnetic fields. The differential flux of all the GCR at the top of the Earth's atmosphere is shown in Figure 5.1.

GCR that reach the Earth range in energy from 10^6 to 10^{20} eV with the peak flux occurring at 10^9 eV (1 GeV) [69, 73, 75]. The flux decreases with increasing particle energy via a power law with an index of -2.71 [69]. Experiments have found that the power law index decreases around 10^{15} eV in what is called the Knee region and increases again around 10^{19} eV at the Ankle region [69, 75].

5.2. Extensive Air Showers (EAS)

After entering the Earth's upper atmosphere, a GCR primary will ultimately undergo a nuclear interaction with an air molecule in the atmosphere, generating many secondary particles. These secondary particles are typically very energetic and can initiate hadronic and electromagnetic cascades in the atmosphere. These secondary particle cascades generate many more secondary particles and photons. All the secondary particles from a single GCR primary are collectively called an extensive air shower (EAS) [12, 67]. The components of an EAS are illustrated in Figure 5.2.

The core of an EAS is the hadronic component which is typically made up protons, neutrons, pions, kaons, and their associated antiparticles. The largest component of an EAS is the electromagnetic component made up of electrons, positrons, and photons generated from electromagnetic cascades. The muonic component consists of muons and antimuons from charged pion decays and can penetrate deep underground [22].

EAS have a thin parabolic disk shape, called a shower front [12], with a disk thickness of only a few meters and a radius of up to approximately ten kilometers [12]. The center of the shower front is called the shower core [12] and is the location of the hadronic component and the highest energy secondary electrons [12, 68]. The shower core of the EAS travels in the same direction as the original GCR primary in the Earth's atmosphere [12, 76]. A diagram of the different regions of an EAS is shown in Figure 5.3. Figure 5.4 is an image of the particle tracks of the secondary cosmic rays from an EAS initiated from a vertical 10^{12} eV GCR proton primary.

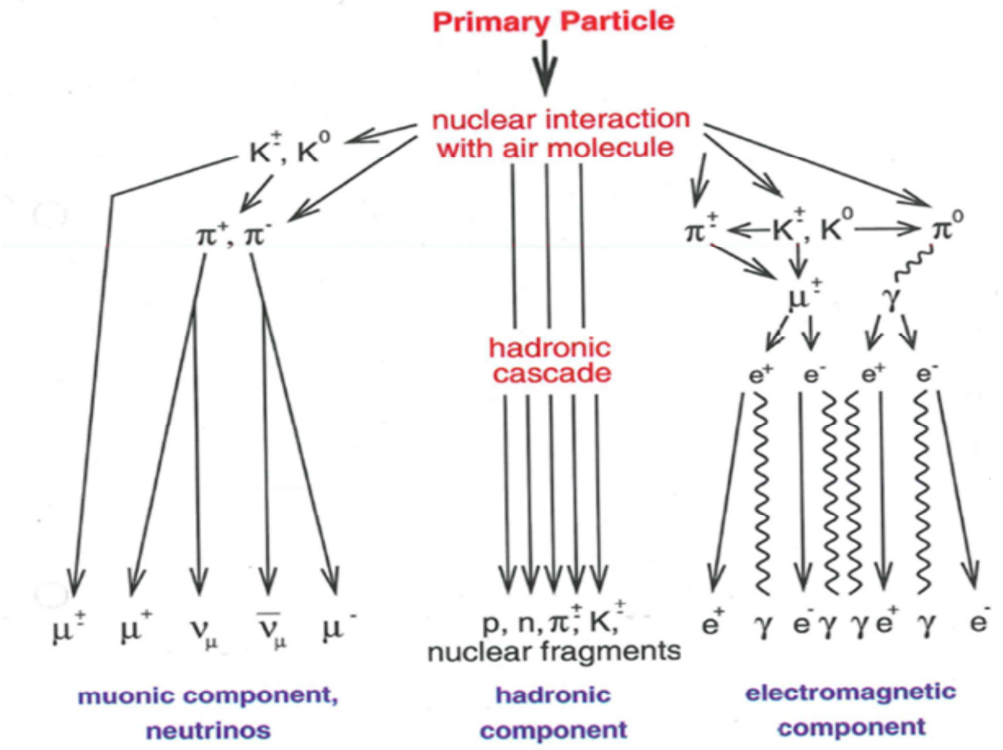

Figure 5.2: The components of an EAS [77].

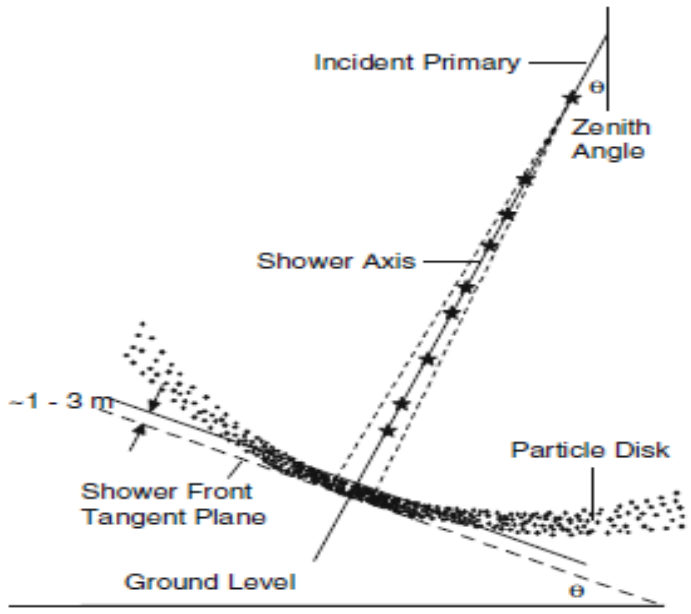

Figure 5.3: Diagram of an EAS as it travels through the atmosphere [12].

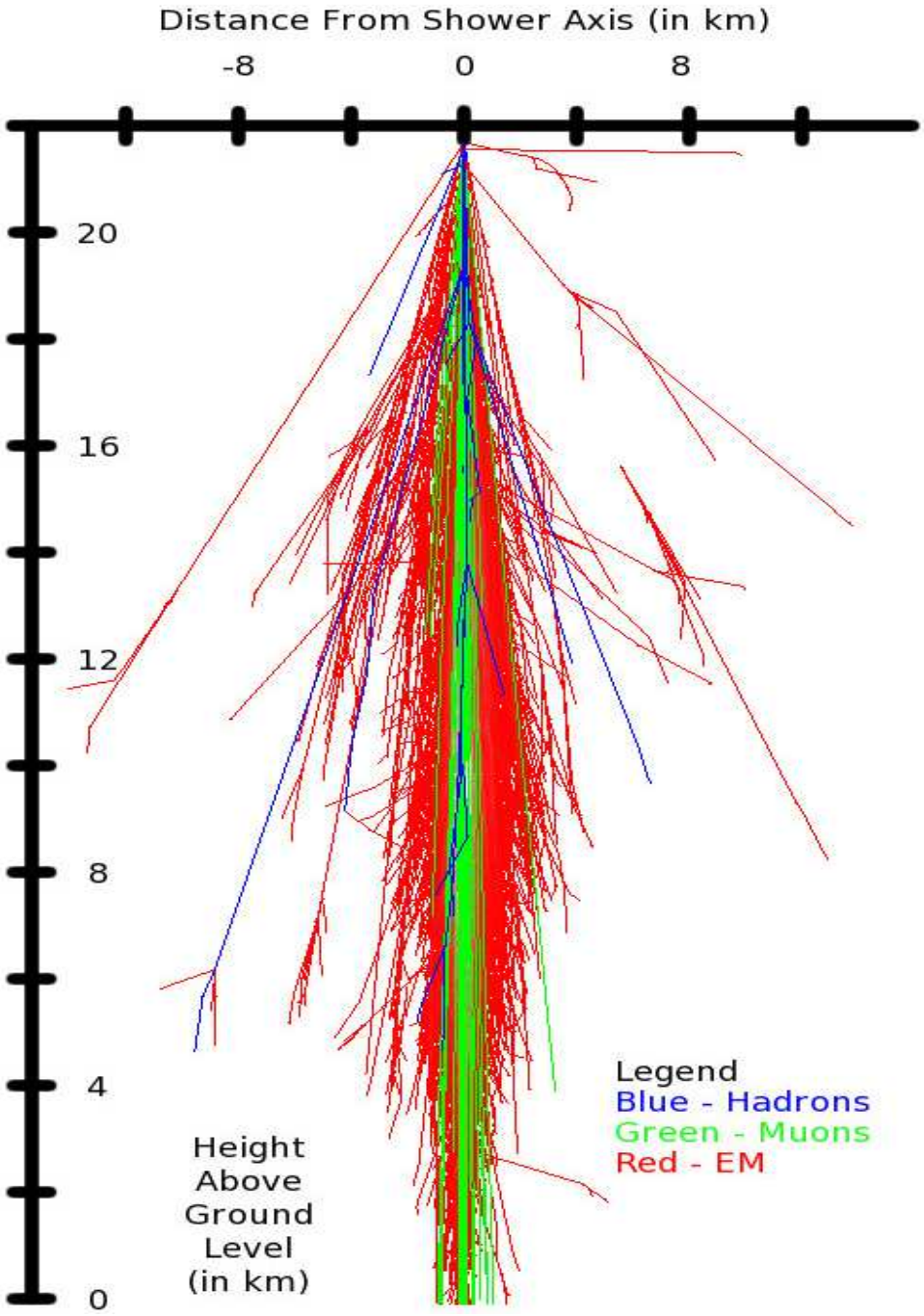

Figure 5.4: The secondary particle tracks from a vertical 10^{12} eV GCR proton primary. The blue tracks represent the hadronic component of the EAS, green tracks represent secondary muons, and red tracks represent the electromagnetic component of the EAS. This plot was generated using the shower plot feature in the CORSIKA 6.690 Cosmic Ray Monte Carlo code [13].

5.2.1. Hadronic Component

The hadronic component of an EAS is created by the nuclear interactions and collisions between the GCR primary and air nuclei. Due to the extreme energy of the GCR primary, a series of hadronic cascades develop from each collision, producing many secondary hadrons, i.e. particles made up of quarks and anti-quarks [12, 22, 68, 76]. The first such collisions typically occur high in the atmosphere (altitude ~24 km in the EAS shown in Figure 5.4) and is what initiates the EAS. The most common particles created from these collisions are protons, neutrons, pions (neutral and charged), and charged kaons, with other more exotic particles and antiparticles also possible [12, 22, 68, 76].

With the exception of protons, the hadrons are unstable and decay into other secondary particles. Table 5.2 lists the half-lives and decay reactions of the typical hadrons found in an EAS. As charged particles, secondary protons ionize the surrounding air and range out before arriving at the ground [78]. The only hadrons that can be measured reliably on the ground are secondary neutrons due to their long half-lives [12, 79].

Table 5.2: Half-lives and decay products of typical secondary hadrons found in an EAS. In the table, *l* stands for one type of lepton: electron or muon [79, 80].

Particle	Half-Life (s)	Decay Products (Branching Ratio)	
Protons (p)	Stable	None	
Neutrons (n)	880.0 ± 0.9	$n \rightarrow p + e^- + \overline{\nu_e}$	
Charged Pions ($\pi^{\pm}$)	(2.6033 ± 0.0005) x 10^{-8}	$\pi^+ \rightarrow \mu^+ + \nu_\mu$	
		$\pi^- \rightarrow \mu^- + \overline{\nu_\mu}$	
Neutral Pions (π^0)	(8.52 ± 0.18) x 10^{-17}	$\pi^0 \rightarrow 2\gamma$	(~99%)
		$\pi^0 \rightarrow e^+ + e^- + \gamma$	(~1%)
Kaons ($K^{\pm}$)	(1.2380 ± 0.0021) x 10^{-8}	$K^+ \rightarrow \mu^+ + \nu_\mu$	(~65%)
		$K^- \rightarrow \mu^- + \overline{\nu_\mu}$	(~65%)
		$K^+ \rightarrow \pi^0 + l^+ + \nu_l$	(~10%)
		$K^- \rightarrow \pi^0 + l^- + \overline{\nu_l}$	(~10%)
		$K^{\pm} \rightarrow \pi^{\pm} + \pi^0$	(~20%)
		$K^{\pm} \rightarrow \pi^{\pm} + \pi^{\pm} + \pi^{\mp}$	(~5%)

Hadrons are found in the core of the EAS and are responsible for generating both the electromagnetic and muonic components of the EAS. Being created via interactions between the GCR primary and the air nuclei, the hadrons are the most energetic of the

secondary particles [81]. The electromagnetic component is initiated when a neutral pion decays into two high energy gamma-ray photons and the muonic component is generated through the decay of charged pions or kaons [12, 22, 68].

5.2.2. Electromagnetic Component

The electromagnetic component is initiated by gamma-ray photons produced in the decay of neutral pions produced by the hadronic component [12, 68]. These gamma-ray photons are typically generated with $>10^9$ eV and quickly undergo pair production to create an electron positron pair. The electron positron pair creates additional secondary electrons via ionization and secondary photons via bremsstrahlung and positron annihilation [70]. At these high energies, positrons act similar to electrons and are more likely to ionize the surrounding air molecules than undergo annihilation [70]. All secondaries continue to generate additional secondaries via ionization, bremsstrahlung, pair production, and positron annihilation until the energy of the secondary particles becomes too low for the above process [70]. This cycle of secondary electron, positron, and photon generation is called an electromagnetic cascade [12, 70]. Figure 5.5 is a diagram of the various processes in an electromagnetic cascade.

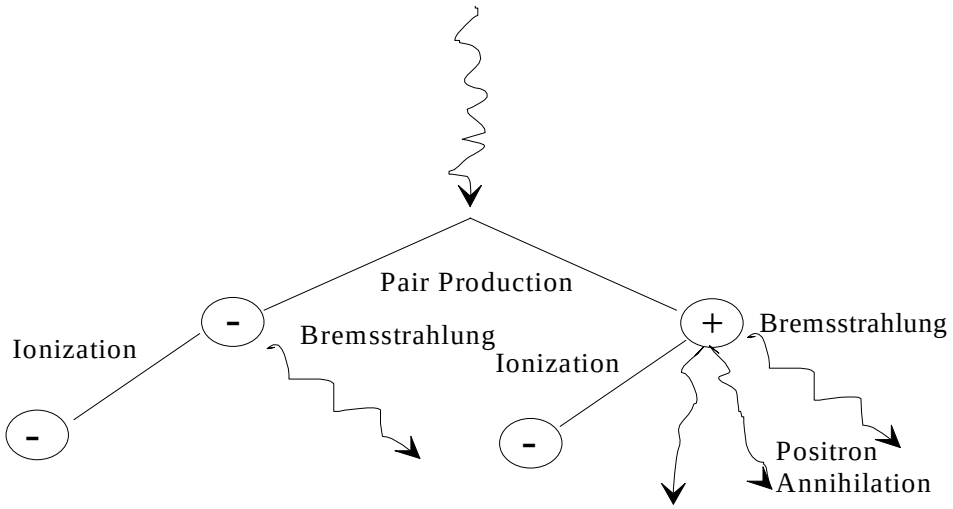

Figure 5.5: Diagram of the different processes in an electromagnetic cascade [Adapted from 12].

Each EAS is made up of several electromagnetic cascades which produce the majority of the secondaries in the EAS. Electromagnetic cascades are also responsible for scattering the EAS secondaries away from the shower core and creating the shower front [12]. However, as the electromagnetic cascades begin to lose energy, the total number of EAS secondaries begins to decrease. The atmospheric depth where the EAS has the largest number of total secondaries is called shower maximum [12]. The depth of the shower maximum depends on the initial energy of the EAS primary with higher energy primaries having their shower maxima lower in the atmosphere [12, 70]. A more detailed look at electromagnetic cascades can be found in *Rossi* & *Greisen* (1948) or Section 7.1 [70].

5.2.3. Muonic Component

The muonic component is created by the decay of charged pions and kaons into muons and antimuons [12]. Muons are leptons like electrons, but are ~200 times more massive and are also unstable (half-life of $\sim 2.2*10^{-6}$ s) [82] and decay into an electron (positron) and an anti-neutrino (neutrino) [82]. Being the decay products of high energy secondary hadrons, secondary muons are typically $>10^9$ eV and, due to time dilation, can reach deep underground before decaying [12, 22].

Muons do not produce as much bremsstrahlung radiation as electrons, due to their larger mass [70], so the dominate form of energy loss for muons in the atmosphere is ionization [12, 70]. Because of this, muons generate very few high energy secondaries and are considered to leave the shower core where they were produced, and to scatter out into the shower front [12]. Secondary muons also reach the ground and can be detected by a muon detector array to infer the passage of an EAS through the atmosphere [12, 22].

5.3. The Role of Secondary Cosmic Rays in the Atmosphere

The passage of high energy particles through the atmosphere has many effects on the chemistry and electrical properties of the atmosphere. All three EAS components have a direct effect on the atmosphere.

Secondary hadrons, especially protons and neutrons, can undergo various nuclear interactions and collisions with the nuclei in the atmosphere. Through these nuclear interactions, radioisotopes such as ^{7}Be and ^{14}C, are produced which are eventually

brought down to the ground by precipitation [71]. Secondary neutrons and muons can both reach the ground and provide ~9% of the background radiation dose [22, 83].

Secondary electrons, positrons, and muons leave a trail of ionized molecules and free electrons in the atmosphere. The constant flux of GCRs produces enough ionizing secondaries to leave the atmosphere in permanent weakly ionized state, especially at altitudes below twenty kilometers [24]. The global electric circuit requires this atmospheric ionization in order to function and to produce the fair weather electric field [30, 31]. The fair weather electric field is believed to be responsible for the initial charge generation in a thunderstorm [20, 30, 31], so cosmic rays do play a role in thunderstorm charge generation. Also, the constant ionization of the atmosphere provides a supply of free electrons for electron avalanches to initiate in strong electron fields, which is the first step in generating an electrical breakdown in the atmosphere [51].

Secondary GCR ionizing radiation also leaves large concentrations of ions in the atmosphere. These ions interact chemically with the other atmospheric atoms and molecules forming larger and more complex molecules and ions. Many of these complex molecules become aerosols and allow hydrometeors to form in the atmosphere [20, 24, 25, 27]. According to the conventional lightning initiation model, lightning is initiated by hydrometers undergoing point discharge in the strong thunderstorm electric field [10, 20]. Without hydrometeors, which are both the electric charge carriers of and lightning initiation locations within a thunderstorm, there would be no lightning, so cosmic rays do play a role in conventional lightning discharges [10, 24].

GCRs are known to play a role in generating the fair weather electric field and the creation of aerosols with the atmosphere which are both important in thunderstorm development, but theorists also believe that secondaries from $>10^{14}$ eV GCR primaries may be directly responsible for lightning initiation. According to *Gurevich et al.* [9], relativistic electrons can be accelerated in the electric fields found within thunderstorms and begin to run away, i.e. the electron gains more energy by accelerating in the electric field than is lost to ionization and bremsstrahlung [9, 72]. These runaway electrons no longer decelerate in the atmosphere and instead are accelerated to higher energies. Since the kinetic energy of the electron is not decreasing with distance, runaway electrons produce more secondary electrons and photons over a much longer distance than do non-runaway electrons. This increase in the number secondary electrons and photons over a long distance by a single runaway electron is called a relativistic runaway electron avalanche (RREA), due to their similarity with the much smaller scale electron avalanches [10]. RREAs have been theorized to generate enough secondary electrons to either directly generate a lightning streamer, in the RREA lightning initiation model [9], or to generate a strong localized electric field to allow a charged hydrometeor to initiate a lightning leader, in the hybrid model [10, 50].

Currently, there is no experimental evidence for either the RREA or hybrid lightning initiation models. One of the objectives of OSU and OU collaboration is to correlate nearby lightning discharges with the passage of EASs initiated by high energy cosmic ray primaries. A positive correlation between lightning discharges and the passage of EASs would provide evidence in support of the RREA and hybrid lightning initiation models. The collaboration is using the OKLMA to determine when a lightning discharge is initiated near a four muon telescope detector in Norman, OK. The muon telescope detector array detects the passage of a large EAS through the atmosphere via coincident measurements in the four ground based cosmic ray muon detectors. The time between a lightning initiation and the passage of a EAS is compared in order to find if the two events are coincident with one another. Figure 5.6 displays a lightning discharge that is coincident with an EAS.

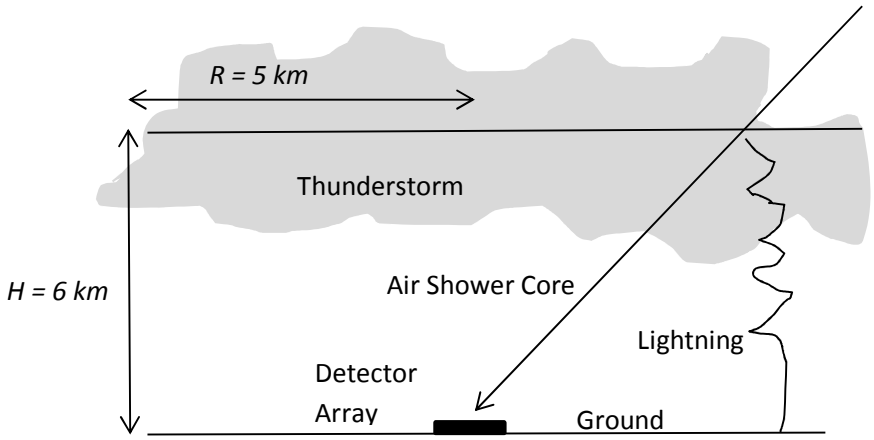

Figure 5.6: Diagram of an EAS passing through an active thunderstorm. The core of an EAS (Arrow) travels through the region where a lightning discharge (jagged Line) occurred before reaching the muon telescope detector array (black rectangle) on the ground.

CHAPTER VI

RELATIVITIC ELECTRONS IN THE ATMOSPHERE

The Earth's atmosphere is constantly being bombarded by GCR primaries which generate large numbers of secondary particles and photons in EASs. The majority of secondary particles produced in an EAS are relativistic (>1 MeV) electrons [12, 70]. As charged particles, these relativistic electrons ionize the atmosphere generating ions and other low energy free electrons. The constant flux of GCRs ensures that the Earth's atmosphere is always in a weakly ionized state due to all the relativistic electrons produced in EASs.

The vast majority of interactions between electrons of all energies and atmopsheric nuclei are soft collisions which produce low energy, free electrons through ionization. Soft collisions also leave the bound electrons in an excited state which eventually de-excite giving low energy, excitation photon [76, 84, 85]. For relativistic electrons, hard collisions and bremsstrahlung radiation become the dominate energy loss mechanisms. Hard collisions, called Mott Scattering [84], which are direct collisions between electrons that transfers a large amount of kinetic energy from the relativistic electron to atomic electron. These hard collisions are responsible for generating high energy secondary electrons in the atmosphere. Bremsstrahlung photons are high energy gamma-ray photons that are generated by the rapid deceleration of the relativistic electron near a nucleus [12, 76, 84, 85].

Electrons are charged particles and are accelerated in ambient electric fields, such as those found within an active thunderstorm. Depending on the strength and direction of the electric field, a relativistic electron can be accelerated enough to overcome the energy losses from soft and hard collisions, and bremsstrahlung. When this happens, the relativistic electron becomes a runaway electron and no longer ranges out in the atmosphere [9]. These runaway electrons generate long lived, high energy electron avalanches called relativistic runaway electron avalanches (RREA) and which may to be responsible for lightning initiation [9, 10, 50, 72].

6.1. Relativistic Electrons in the Fair Weather Atmosphere

The majority of free electrons in the atmosphere are <100 eV and are produced via ionization collisions with high energy secondary electrons generated in EASs. These low energy electrons quickly range out, i.e. lose all kinetic energy and recombine with the surrounding material. Relativistic electrons, >1 MeV, can travel several meters through the atmosphere before ranging out. However, relativistic electrons lose energy in the atmosphere via three processes: soft collisions, hard collisions, and bremsstrahlung.

6.1.1. Soft Collisions

The vast majority of interactions between a charged particle and its surrounding medium are soft collisions, where small amounts energy is lost to ionize atomic electrons from the medium. Typically in a single soft collision, <100 eV is transferred between the relativistic electron and atomic electrons [86]. An illustration of a soft collision between a relativistic electron and an atomic electron is shown in Figure 6.1.

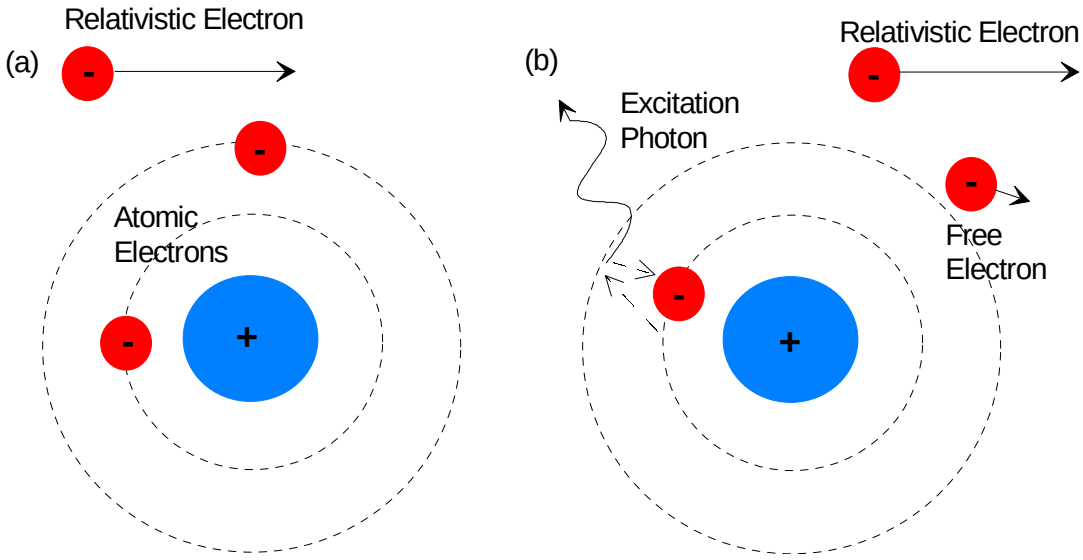

Figure 6.1: Diagram of (a) before and (b) after a soft collision. (a) The relativistic electron travels near an atom and interacts via the Coulomb force with the bound electrons. (b) The bound electrons are either excited and produce a excitation photon or ionized and become a free electron.

Relativistic electrons transfer only a small portion of their energy and momentum in a soft collision, so the relativistic electron continues on its original path. The ionized electron scatters away from the relativistic electron and becomes a free electron. Depending on the energy of the free electron, the free electron can also ionize other nuclei in the atmosphere [35, 58].

In air, the majority of nuclei are either nitrogen or oxygen which have electron binding energies of 15.6 and 12.2 eV, respectively [14, 43, 51]. However, most of the energy lost by the relativistic electrons is lost to rotational and vibrational excitations of N_2 and O_2 molecules. The average energy lost by a relativistic electron to produce a free electron in dry air is ~34 eV [56]. The difference between the amount of energy lost by a relativistic electron in a soft collision and the electron binding energy is divided between the production of excitation photons and kinetic energy of the free electron. Monte Carlo simulations have shown that free electrons typically have <10 eV of kinetic energy in fair weather conditions [32]. Long spark studies have found that excitation photons play a role similar to free electrons in ionizing the air within an electron avalanche [51, 55].

6.1.2. Hard Collisions

Rarely, the relativistic electron will collide directly with a bound electron in what is called a hard collision [84]. In a hard collision, a relativistic electron transfers a large amount of energy, which could be all the kinetic energy of the relativistic electron, to the bound electron which ionizes and leaves the atom with the original relativistic electron [84]. Figure 6.2 is an illustration of a hard collision between a relativistic electron and a bound electron.

The initial energy of the relativistic electron is divided between the colliding electrons, which is much greater than the binding energy of the air molecules, so that high energy electrons leave the molecule and propagate through the atmosphere. Due to the uncertainty principle, during a collision, the relativistic and bound electrons are indistinguishable from one another, so for calculations, the electron with the greatest kinetic energy after the collision is assumed to be the original relativistic electron. This assumption artificially limits the kinetic energy of the ionized secondary electron to half the kinetic energy of the initial relativistic electron [76, 84].

Energy losses from soft and hard collisions are typically grouped together under the term ionization or collisional losses. Hard collisions produce high energy secondary electrons and soft collisions are responsible for low energy secondary electrons in an EAS [12, 76, 84].

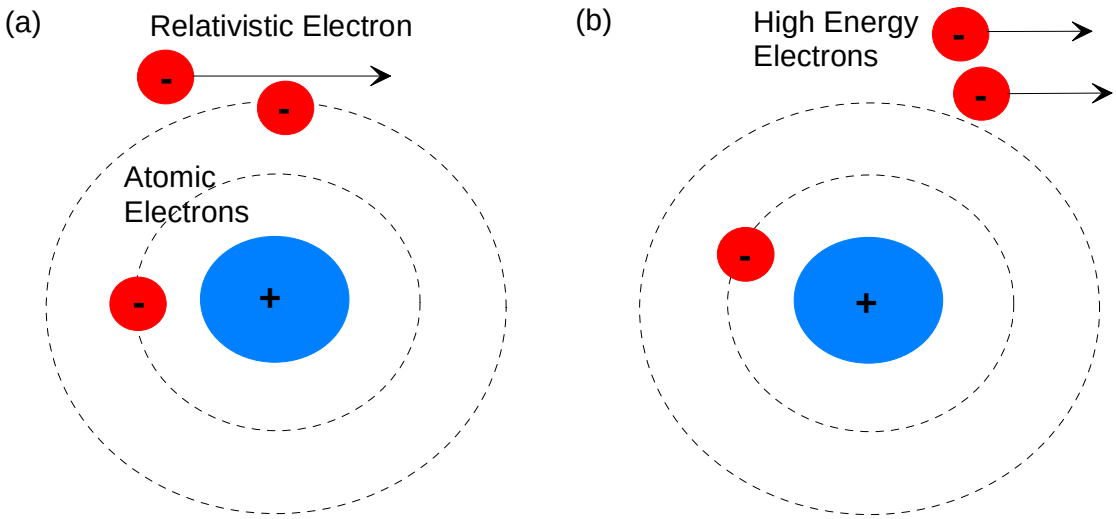

Figure 6.2: Diagram of (a) before and (b) after a hard collision. (a) A bound electron is in the direct path of a relativistic electron. (b) The relativistic electron and atomic electron collide and both electrons travel away from the air nucleus with a share of the initial energy of the relativistic electron.

6.1.3. Bremsstrahlung

Very high energy electrons, >10 MeV, can travel near atmospheric nuclei and generate high energy gamma-rays through bremsstrahlung. These gamma-rays range in energy from few keV to the total kinetic energy of the incident relativistic electron, with typical photons being <1% of the kinetic energy of the relativistic electron [84]. Figure 6.3 shows a diagram of bremsstrahlung.

Gamma-rays are generated via bremsstrahlung when a relativistic electron travels near a nucleus. The relativistic electron is attracted to the positively charged nucleus by the Coulomb force, which causes the relativistic electron to rapidly slow down. The amount of kinetic energy lost by the relativistic electron takes the form of the bremsstrahlung photon [76, 84].

Bremsstrahlung is the dominate form of energy loss for >80 MeV electrons in the atmosphere [12]. For EASs that have their shower maximum, high energy secondary electrons within the shower core produce gamma-rays. The gamma-rays scatter away from the shower core and initiate electromagnetic cascades that create and then widen the

shower front [12]. In the literature, the energy loss to bremsstrahlung is called radiative energy loss [85].

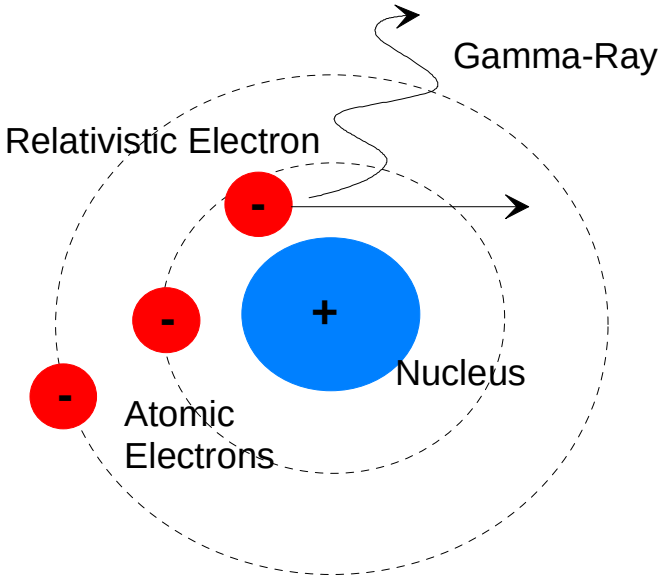

Figure 6.3: Diagram of a relativistic electron producing a gamma-ray via bremsstrahlung. The relativistic electron travels near a nucleus. Due to the Coulomb force, the relativistic rapidly decelerates and produces a high energy gamma-ray.

6.1.4. Electron Stopping Power and Range in the Atmosphere

The total amount of energy lost by a charged particle per unit distance in a material due to the different types of interactions is called the stopping power. The stopping power for electrons includes the energy losses due to soft collisions, hard collisions, and the production of bremsstrahlung photons.

For electron <80 MeV, ionization (both hard and soft) collisions make up the dominate form of energy loss in the atmosphere [12]. The average amount of energy lost to ionization collisions by electrons of all energies traveling through a material is given by

the Bethe-Bloche formula:

$$-\left(\frac{dE}{dx}\right)_{ion} = \left(\frac{e^2}{4\pi\varepsilon_0}\right)^2 \frac{2\pi N_0 z\rho}{mc^2\beta^2 A}\left[ln\left(\frac{E(E+mc^2)\beta^2}{2I^2mc^2}\right) + (1-\beta^2) - ln(2)\left(2\sqrt{(1-\beta^2)} - 1 + \beta^2\right) + \frac{1}{8}\left(1-\sqrt{1-\beta^2}\right)^2\right], \quad (6.1)$$

where, E is the kinetic energy the electron, x is the distance the electron travels through a material, e is the charge of an electron, ε_0 is the permittivity of free space, N_0 is Avogadro's number, z is the atomic number of the material, ρ is the density of the material, m is the mass of an electron, c is the speed of light, $\beta = v/c$, v is the velocity of the electron, A is the atomic mass of the material, and I is the mean ionization potential of the material [85]. The negative sign indicates that the electron is losing energy while traveling through the material. Ionization collisions are stochastic processes, so the Bethe-Bloche formula calculates the average amount of energy an electron loses to both soft and hard collisions as it travels through a material. The average amount of energy lost to just hard collisions is determined from the Mott scattering cross section:

$$\sigma(E,W) = \left(\frac{e^2}{4\pi\varepsilon_o}\right)^2 \frac{2\pi N_o z\rho}{mc^2\beta^2 A} dW \left\{\frac{1}{EW^2} - \frac{1}{EW(1-W)}\frac{mc^2(2E+mc^2)}{(E_e+mc^2)^2} + \frac{1}{E(1-W)^2} + \frac{T}{(E+mc^2)^2}\right\} \quad (6.2)$$

where σ is the Mott scattering cross section, W is ratio of the primary and secondary electron energies [84]. It should be noted that the energy losses determined from Mott scattering are already included in the Bethe-Bloche formula.

For >80 MeV electrons, the dominate form of energy loss in the atmosphere is the production of bremsstrahlung photons. The average amount of energy lost to the production of bremsstrahlung photons is given by

$$-\left(\frac{dE}{dx}\right)_{brem} = \left(\frac{e^2}{4\pi\varepsilon_0}\right)^2 \frac{\alpha z^2 N_0 (E+mc^2)\rho}{m^2c^4 A}\left[4ln\left(\frac{2(E+mc^2)}{mc^2}\right) - \frac{4}{3}\right], \quad (6.3)$$

where α is the fine structure constant [84]. Bremsstrahlung is a stochastic process where photons can be created with up to the kinetic energy of the electron, so to accurately determine the number and energy of the secondary photons, Monte Carlo simulation is required. However, the total kinetic energy lost by the electron to bremsstrahlung is accurately described by equation (6.3).

The total amount of energy lost by an electron while traveling through a material is given by,

$$\left(\frac{dE}{dx}\right)_{tot} = \left(\frac{dE}{dx}\right)_{ion} + \left(\frac{dE}{dx}\right)_{brem}. \tag{6.4}$$

Equation (6.4) is generally referred to as the electron stopping power in a material with equation (6.1) describing the collisional stopping power and equation (6.3) describing the radiative (bremsstrahlung) stopping power. In a compound material, such as air, the total stopping power is calculated from the stopping power for each of the materials that make up the compound:

$$\left(\frac{dE}{dx}\right)_{compound} \rho_{compound}^{-1} = \sum_i \omega_i \left(\frac{dE}{dx}\right)_i \rho_i^{-1}, \tag{6.5}$$

where the index i represents each of the materials that make up the compound and ω_i is the mass fraction of the i^{th} material within the compound [84]. In gaseous materials, the low energy bonds between molecules can be ignored when calculating stopping power [87].

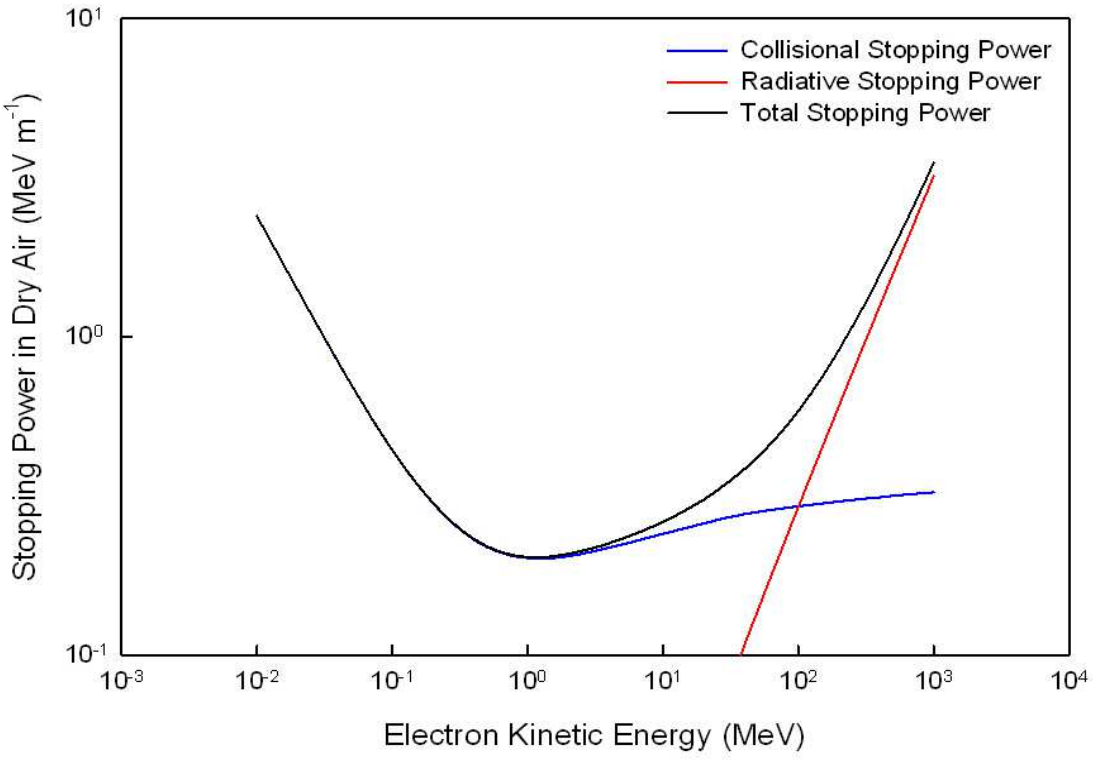

Figure 6.4: Plot of the electron stopping power in dry air near sea level [26].

The stopping power for electrons in dry air at sea level is shown in Figure 6.4. The electron stopping power decreases with increasing electron kinetic energy reaching a minimum at ~1 MeV. For <1 MeV electrons, the stopping power is completely due to collisional energy losses. Above the minimum ionizing energy of ~1 MeV, collisional energy losses increase with electron kinetic energy. This causes the total stopping power to also rise. At electron energies >10 MeV, radiative energy losses become appreciable and become the dominate form of energy losses in air for >80 MeV electrons [12, 85].

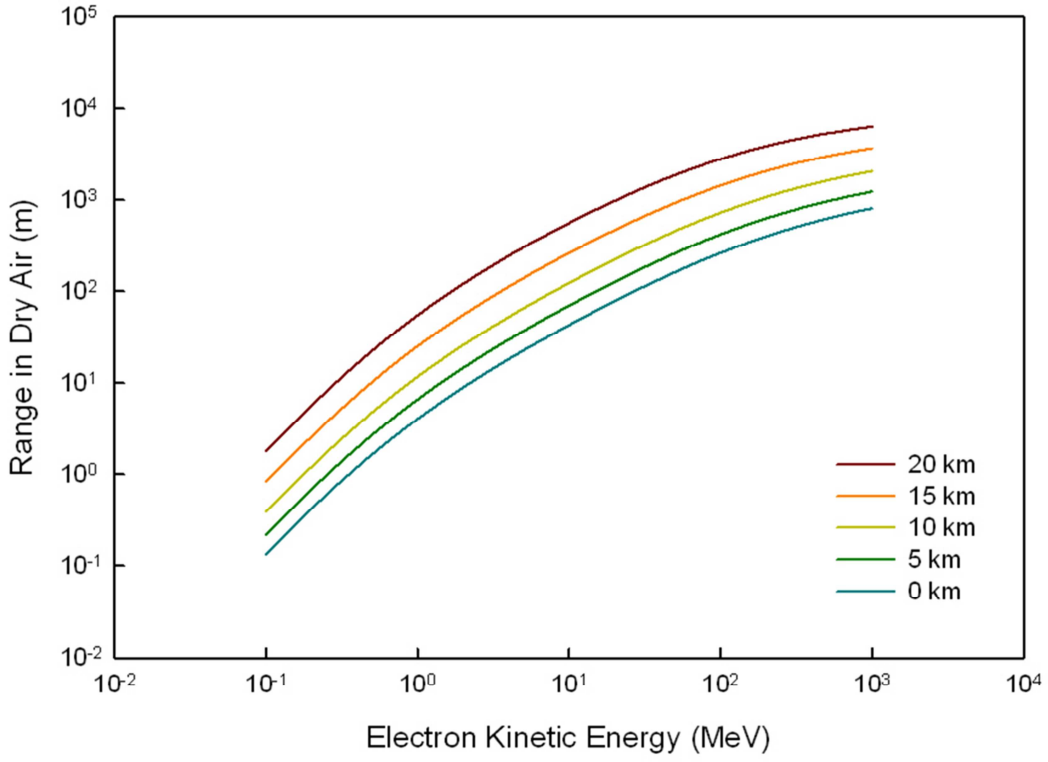

Figure 6.5: Plot of the range of electrons in dry air at listed altitudes [20, 26].

As an electron travels through a material, it loses energy, quantified by its stopping power, and slows down. The average distance the electron would travel in the material before losing all of its kinetic energy is called the range [84]. Theoretically, the range of an electron can be determined analytically by solving equations (6.1) and (6.3) for the distance *x*. Because equations (6.1) and (6.3) both depend logarithmically with the electron kinetic energy, an analytic solution for the range of an electron can not be derived. However, the range of the electron can be determined numerically by assuming that the electron loses energy at a constant rate over a small distance, and counting how many of these short distances it takes for an electron to lose all of its kinetic energy [85]. An electron that reaches the end of its range is said to range out. An electron that has

ranged out has lost all of its kinetic energy and assumed to recombine with the atoms in material. The range of an electron in dry air at different altitudes is shown in Figure 6.5. Figures 6.4 and 6.5 were both calculated assuming that the electrons were in a fair weather atmosphere and not in the strong ambient electric field typically found within an active thunderstorm.

High in the atmosphere, relativistic electrons travel between 10 m, for a 1 MeV electron, to 1 km, for a 100 MeV electron, before losing all their kinetic energy and ranging out. Near the ground, the range of relativistic electrons is an order of magnitude shorter, ranging from between a meter for a 1 MeV electron to ~100 m for a 100 MeV electron. According to Figure 6.5, relativistic electrons produced at lightning initiation altitudes of 4-8 km range out before reaching the ground in fair weather conditions. In thunderstorm conditions, the relativistic electrons are accelerated in the ambient electric field of the thunderstorm, which has a large effect on both the range and kinetic energy of the relativistic electron.

6.2. Relativistic Electrons in Thunderstorm Conditions

Thunderstorms introduce two changes to the fair weather atmosphere that affect the passage of relativistic electrons: strong electric fields and increased water content in the air. Relativistic electrons are charged particles and accelerate in external electric fields. Although the fair weather electric field (~100 V m^{-1}) accelerates electrons in the atmosphere, it is not strong enough to affect the propagation of relativistic electrons. However, strong electric fields found within active thunderstorms (~130 kV m^{-1}) are sufficient to have an effect on the stopping power and range of relativistic electrons in the atmosphere [9]. Depending on the direction of the electric field, electrons will either be accelerated or decelerated by the electric field. Figure 6.6 illustrates the regions within a typical dipole/tripole thunderstorm where a downward traveling electron is accelerated or decelerated by the ambient electric fields.

The increased water content within the thunderstorm changes the elemental composition of the atmosphere, which affects the stopping power and range of the relativisitic electrons. Within a thunderstorm, the air contains more water in various states than the U.S. Standard Atmosphere [7, 88], so the stopping power for electron inside a thunderstorm is slightly lower than in fair weather conditions [26]. Table 6.1 shows the mean ionization potential, *I,* and elemental mass fractions for fair weather and thunderstorm conditions used in this work.

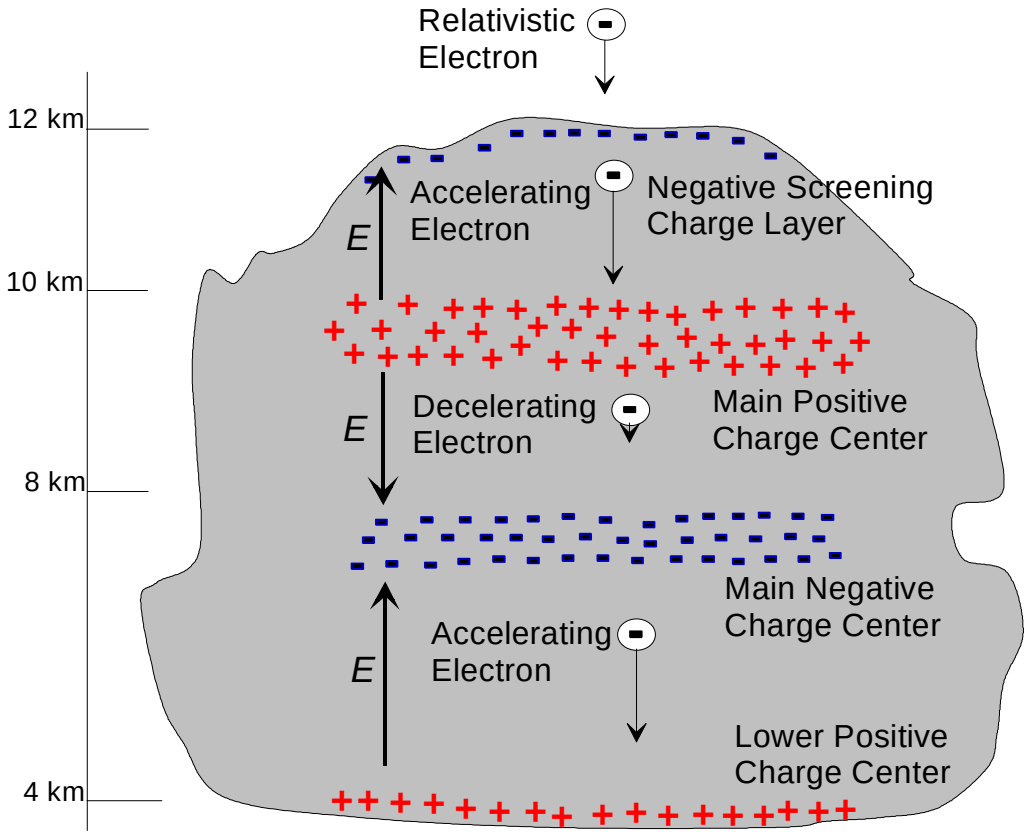

Figure 6.6: Diagram of regions within a typical thunderstorm where downward traveling relativistic electrons are accelerated or decelerated in ambient electric field. The length of the thin arrows represents the velocity of the relativistic electron. The altitude scale is only approximate [3].

Table 6.1: Mean ionization potential, I, and elemental mass fractions ω_i for fair weather and thunderstorm conditions in the atmosphere [7, 85, 88].

Element	I (eV)	Fair Weather ω_i	Thunderstorm ω_i
H	19.2	0.0000	0.0012
N	82.0	0.7617	0.7721
O	95.0	0.2262	0.2174
Ar	188.0	0.0121	0.0093

The stopping power of an electron in a strong electric field is given a modified version of equation (6.5) as,

$$\left(\frac{dE}{dx}\right)_{electron}(h) = \left(\frac{dE}{dx}\right)_{compound}(h) + e\varepsilon(h), \tag{6.6}$$

where the compound used in the stopping power is either dry air (fair weather conditions) or moist air (thunderstorm conditions), and ε is thunderstorm's electric field at altitude h. The electron stopping power depends on the altitude because the atmospheric density also depends on the altitude. The electron stopping power in a material is defined as the amount of energy lost by an electron traveling through the material, so a positive, upward directed electric field will cause a downward traveling electron to accelerate in the atmosphere. Inside a thunderstorm with a typical dipole/tripole electric charge structure, electrons traveling toward the ground are accelerated above the main positive charge center and between the main negative and lower positive charge centers. The ambient electric field between the main positive and negative charge centers causes an electron that is traveling towards the ground to decelerate. According to Section 4.2, CG lightning typically originates near the negative charge region where the ambient electric fields changes direction.

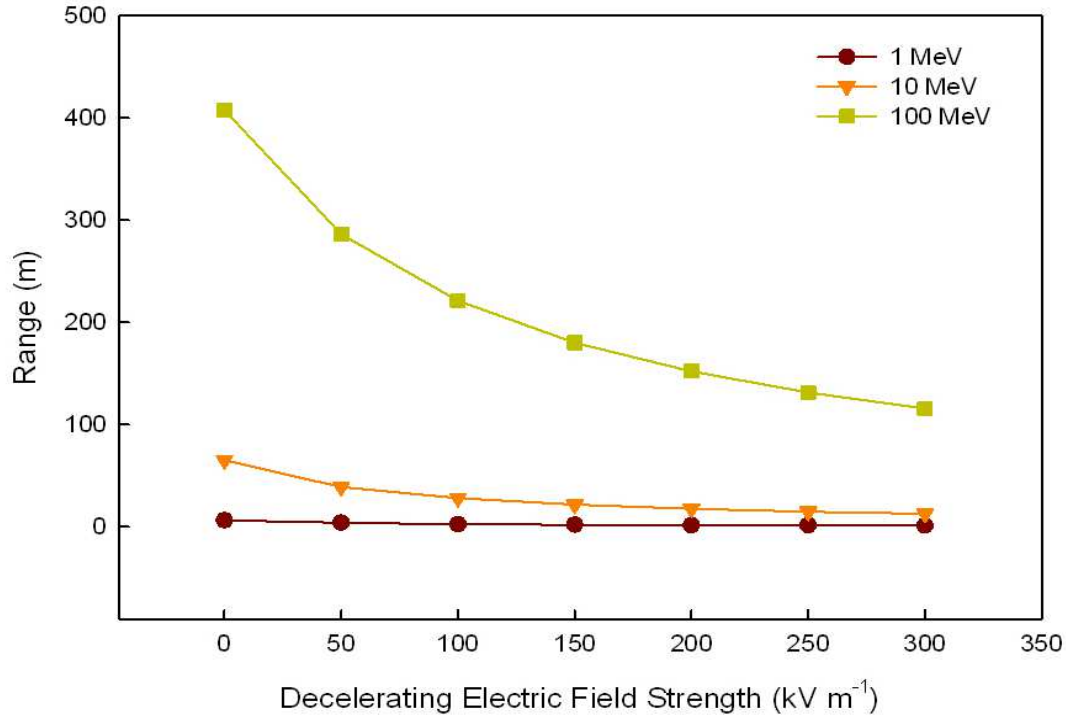

Figure 6.7: Plot of the range of electrons in moist air at an altitude of 6 km in the listed constant electric field.

In a decelerating electric field, electrons lose energy quicker than an electron in a zero electric field region. The strength of the decelerating electric field effectively adds to the stopping power of the electron without producing additional secondaries. This causes the electron to produce fewer secondaries and to have a much shorter range. Figure 6.7 shows the range of relativistic electrons as a function of decelerating electric field strength. The range of an electron in thunderstorm conditions decreases by approximately an order of magnitude in a constant 300 kV m^{-1} decelerating electric field compared to the range in an electric field free region.

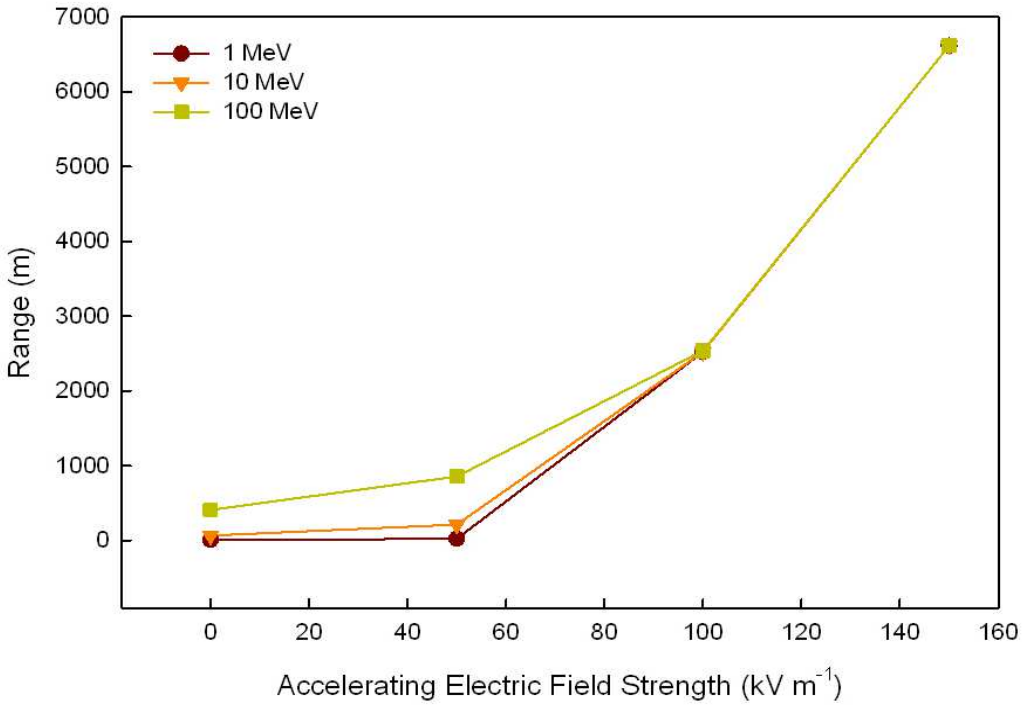

Figure 6.8: Plot of the range of electrons in moist air at an altitude of 6 km as a function of the magnitude of an accelerating electric field.

The situation is vastly different for electrons in accelerating electric fields. Accelerating electrons have greater kinetic energies and extended ranges than electrons in an electric field free region. Having greater kinetic energy, accelerated electrons will produce more secondaries, especially more high energy secondary electrons through hard collisions. If the electric field is sufficiently strong, the accelerated electron can run away, i.e. have a limitless range, in the electric field [9]. Figure 6.8 shows the range of electrons in different strength, constant, accelerating electric fields. Once an electron runs away in an

electric field, the range of the electron is determined by the strength and length of the accelerating electric field region and not the energy of the runaway electron.

Runaway electrons generate large amounts of secondaries, mostly low energy electrons and photons, in relativistic runaway electron avalanches (RREA) [9]. RREAs are theorized by *Gurevich et al.* [9] to produce a sufficient number of high energy electrons to initiate a lightning discharge.

6.2.1. Runaway Electrons

Runaway electrons are electrons which have a limitless range in a material due to being accelerated by a strong electric field. There is a minimum kinetic energy required for an electron to run away in the atmosphere that is dependent both on the altitude and strength of the electric field as shown in Figure 6.9. Any electron above the minimum runaway energy will not range out in the atmosphere.

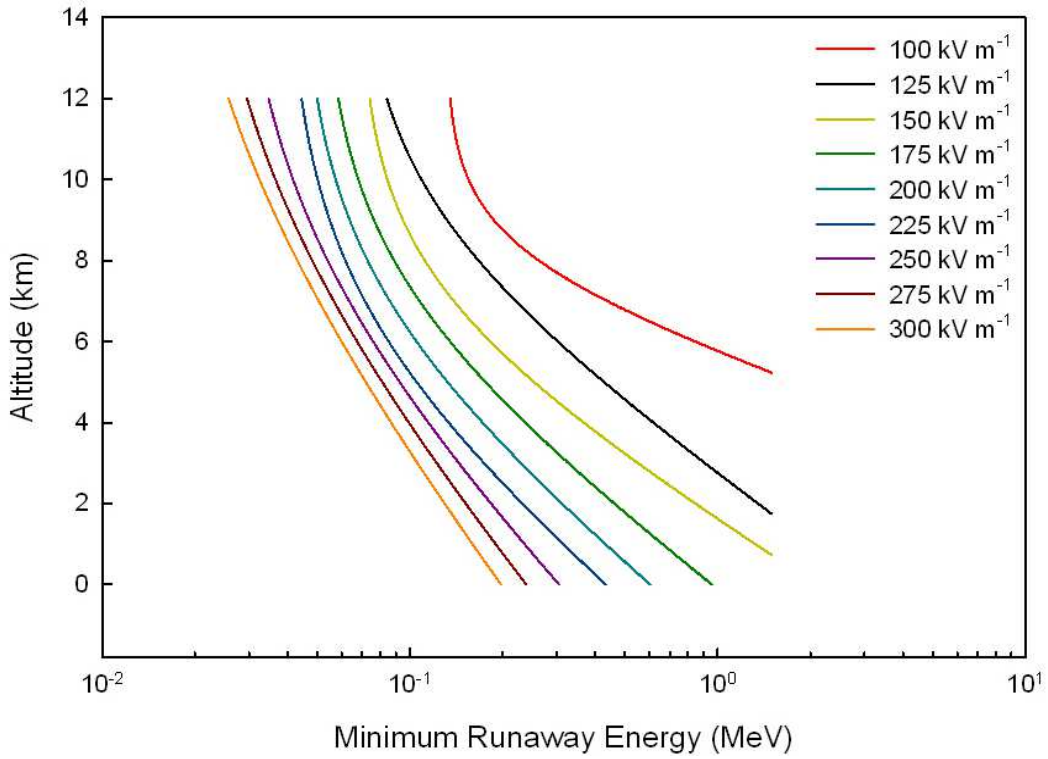

Figure 6.9: Plot of the minimum electron kinetic energy required for an electron to run away in the listed accelerating electric field strengths.

In Figure 6.4, the stopping power of a >1 MeV electron increases with electron kinetic energy, so that there is a maximum electron kinetic energy where the energy gain by being accelerated in the electric field is greater than the stopping power. The kinetic energy of a runaway electron where the energy gained by being accelerated in the electric field and the stopping power is called the equilibrium runaway energy, E_{eq}, and is shown for various electric field strengths in Figure 6.10. Runaway electrons below the equilibrium runaway energy will increase in energy with distance until the runaway electron reaches the equilibrium runaway energy. Runaway electrons above the equilibrium runaway energy will decrease in energy with distance until the runaway electron reaches the equilibrium runaway energy. Regardless, both accelerating runaway electrons ($E < E_{eq}$) and decelerating runaway electrons ($E > E_{eq}$) will not range out in the atmosphere. Figure 6.11 shows the three energy regions: low energy, accelerating runaway, and decelerating runaway, of electrons at an altitude of 6 km in a 300 kV m^{-1} accelerating electric field.

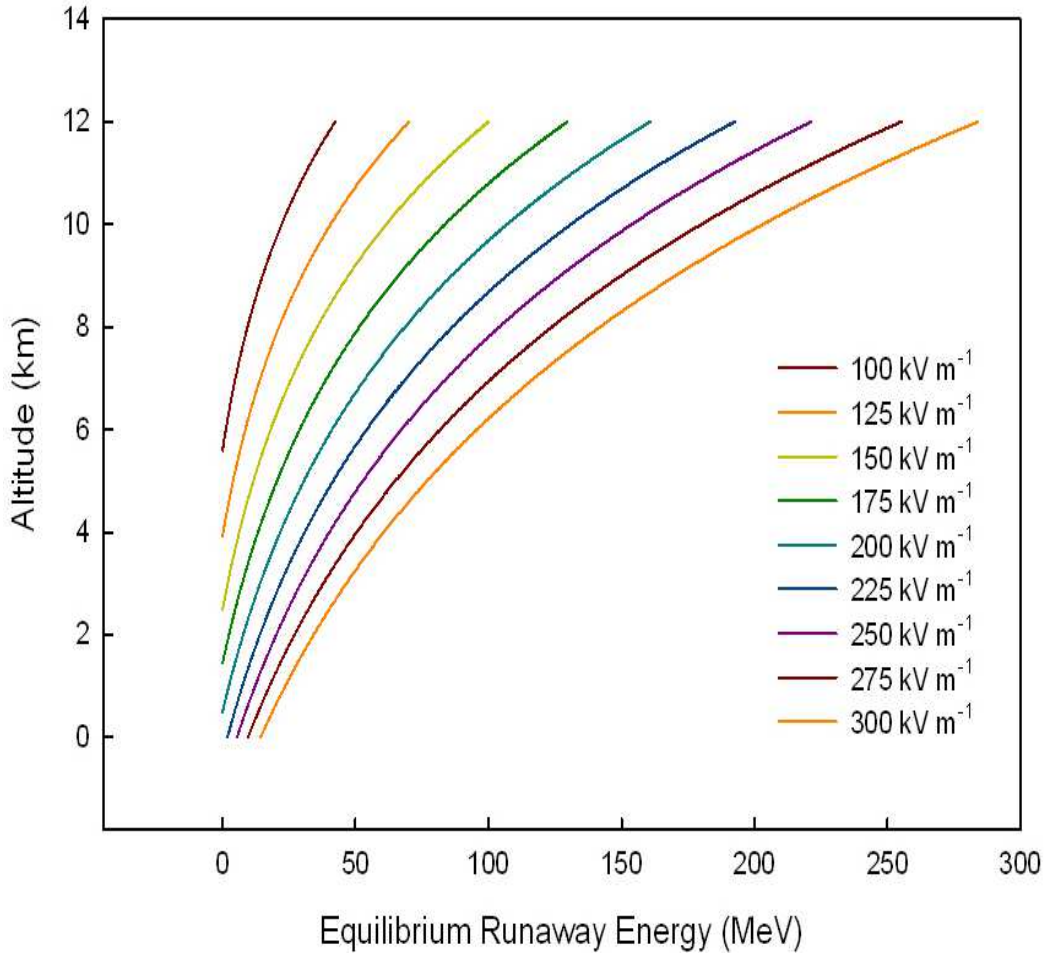

Figure 6.10: Plot of the equilibrium runaway energy for listed electric field strengths.

Electrons will only continue to run away as long as the strong electric field region exists. Outside the electric field region, the former runaway electrons will lose energy to ionization and bremsstrahlung and will range out just like a typical electron. Runaway electrons only have a limitless range while inside a strong electric field region.

In *Gurevich et al.* [9] only accelerating runaway electrons are considered to be runaway electrons since the energy gained by accelerating in the electric field is greater than the stopping power of the electron. I will be using the definition that runaway electrons have a limitless range in the atmosphere, since both accelerating and decelerating runaway electrons are able to initiate RREAs.

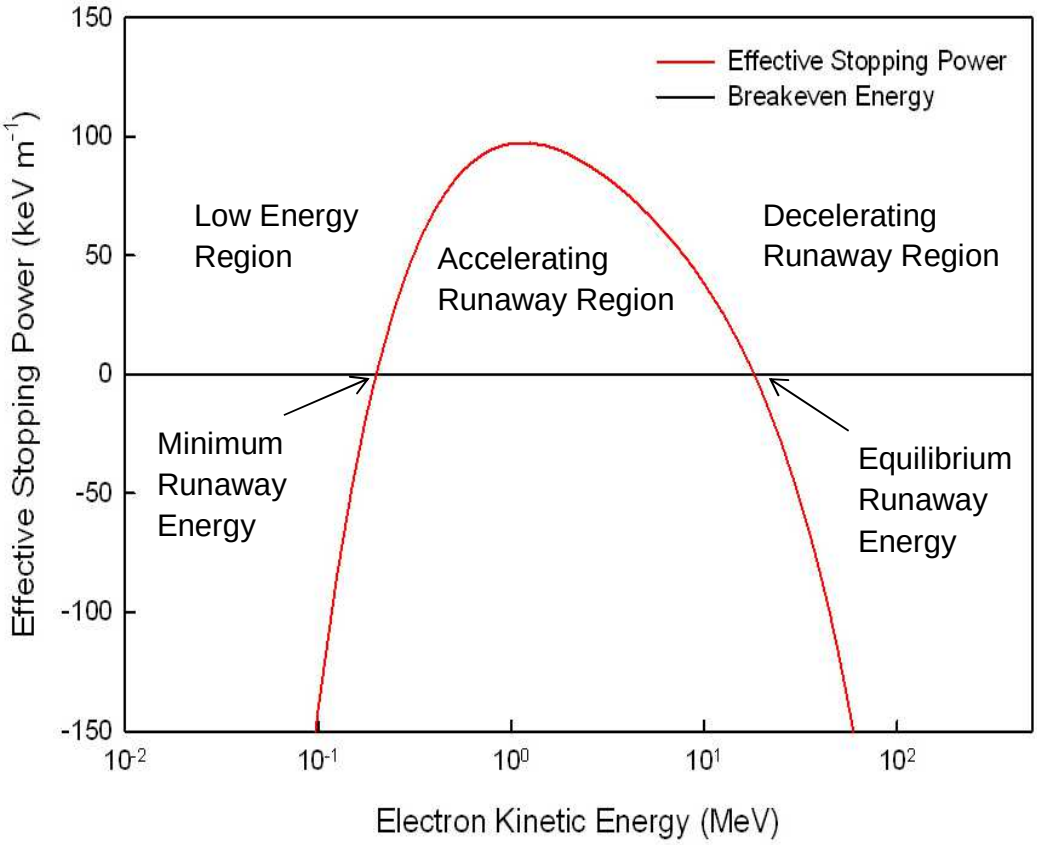

Figure 6.11: Diagram of the different regions of a relativistic electron in a 300 kV m^{-1} accelerating electric field at an altitude of 6 km in a 3% moist air by mass atmosphere. The effective stopping power is calculated by equation (6.6).

6.2.2. Relativistic Runaway Electron Avalanches

All electrons that travel through a material produce secondaries through ionization and bremsstrahlung regardless of the presence of electric fields. The total number of secondaries (both low and high energy) increase with electron kinetic energy and range. Thus, electrons in strong accelerating electric fields will produce more secondaries since the primary electron has both higher energy and longer range. Figure 6.12 shows the difference in the number of high energy secondary electrons produced by a single runaway electron with the equilibrium runaway energy.

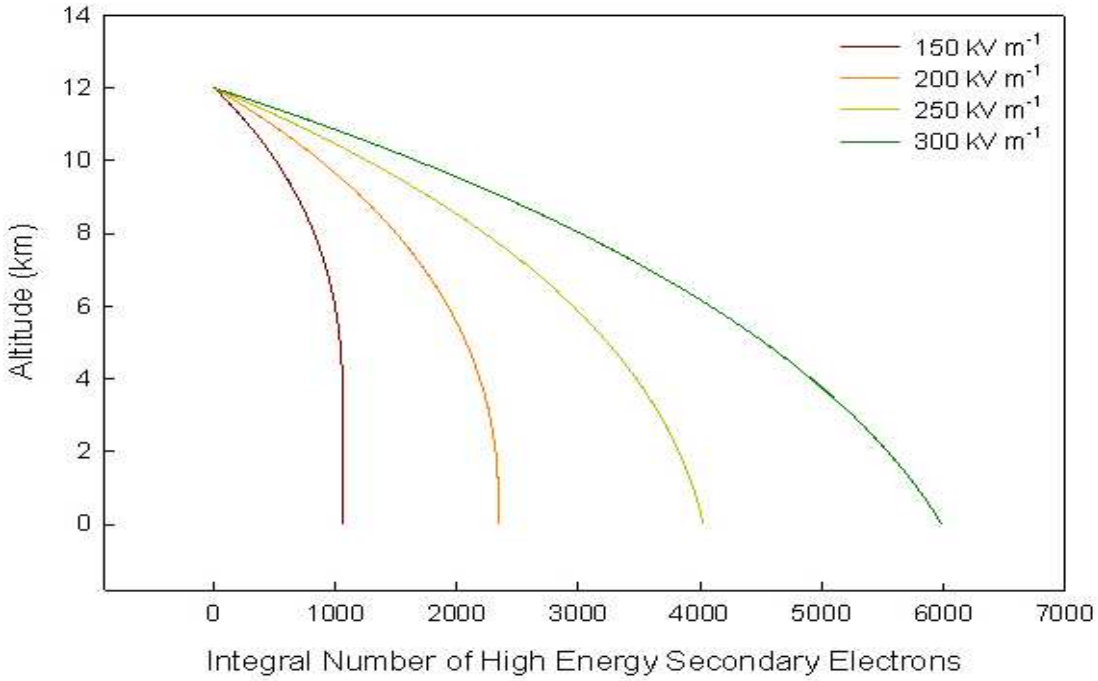

Figure 6.12: Plot of the integral number of high energy secondary electrons produced by a single primary electron with equilibrium runaway kinetic energy in the listed constant accelerating electric fields.

If a runaway electron is at least twice the minimum runaway energy, then that runaway primary could produce secondary electrons with enough energy to also run away in the electric field. Since the air density decreases with altitude, the closer to the ground the relativistic electron is, the stronger the electric field needs to be in order to produce additional runaway secondary electrons as shown in Figure 6.13.

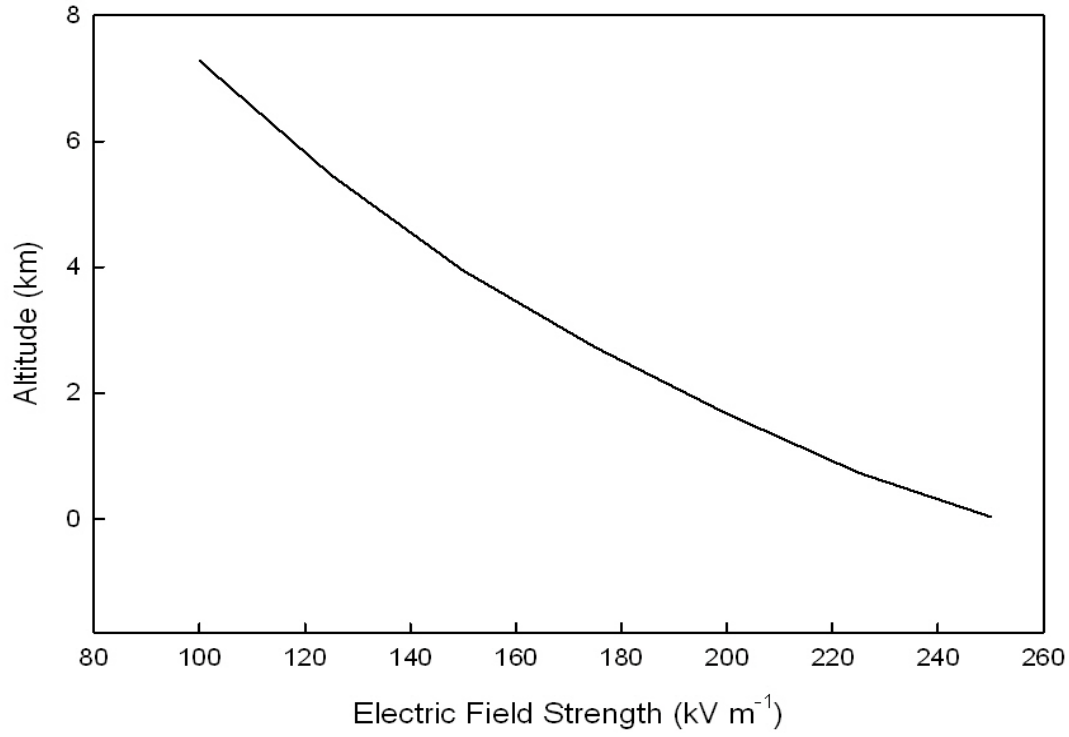

Figure 6.13: Plot of the minimum electric field required for a runaway electron to produce runaway secondary electrons in the atmosphere.

Runaway electrons do not range out, so all primary and secondary runaway electrons continue to propagate through the entire strong electric field region. As the runaway electrons travel through the strong electric field region, large quantities of low energy electrons are produced along with a smaller number of high energy, runaway electrons. The low energy electrons will slowly scatter away and eventually recombine with the atoms in the atmosphere, but the high energy runaways will continue on producing even more secondaries. This slowly growing core of runaway electrons that produces a plasma of low energy electrons forms a RREA [9, 51].

Figure 6.14 shows the evolution of a RREA in a strong electric field region. A runaway electron primary enters the strong electric field region and initiates a RREA. The runaway primary begins to produce a plasma of low energy secondary electrons and also a few runaway secondary electrons which initiate their own RREAs. As the primary and secondary runaway electrons continue propagate through the strong electric field region, the total number of RREAs and the magnitude of the low energy electron plasma increases in size and density. Once outside the strong electric field region, all the RREAs begin to attenuate and eventually all the electrons begin to range out.

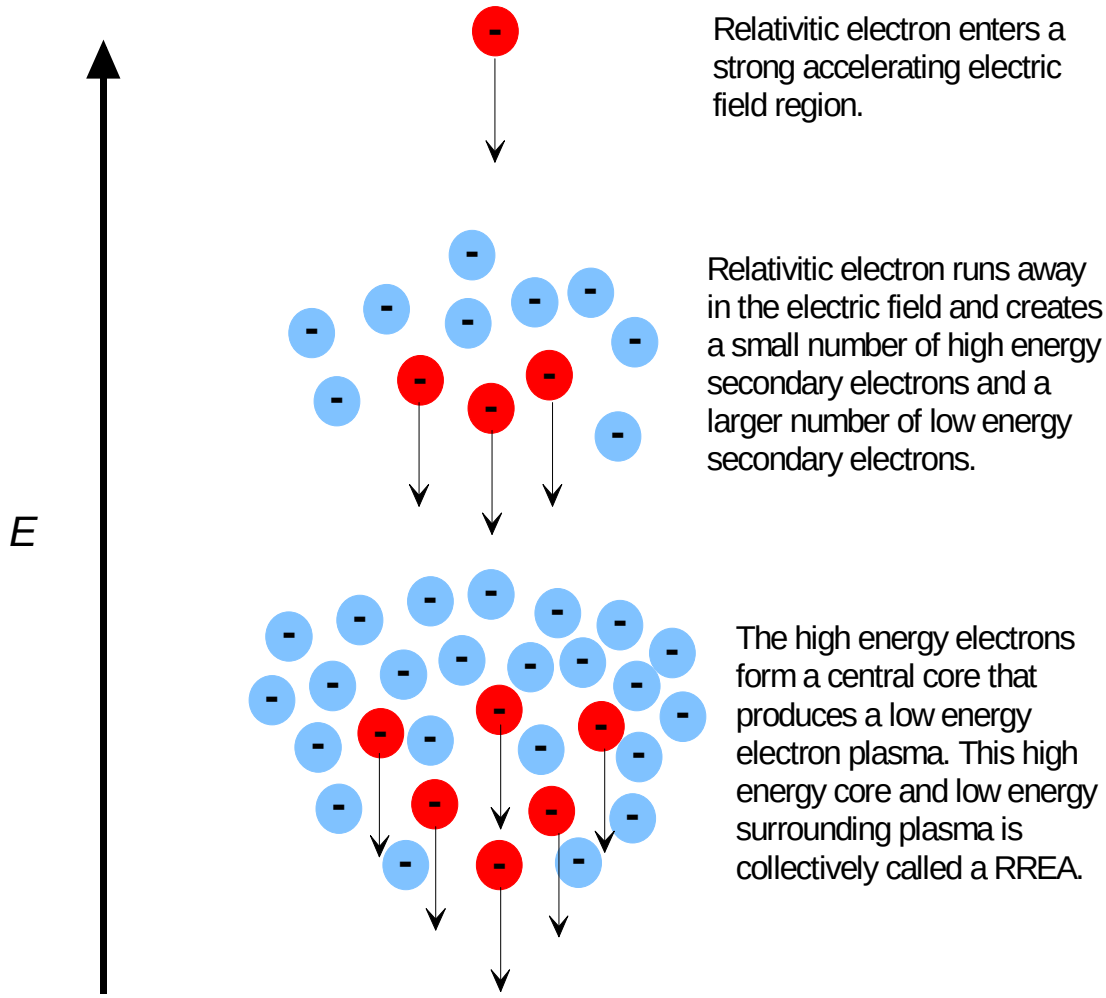

Figure 6.14: Diagram of the formation of an RREA. A relativistic electron enters a strong, accelerating electric field, *E*, region and runs away in the electric field. The runaway electron generates a small number of high energy secondary electrons and a large number of low energy secondary electrons. The high energy secondary electrons also run away in the electric field and generate additional high energy and low energy secondary electrons. The runaway electrons form a small ionizing core, which is surrounding by a plasma of low energy electrons, creating a RREA.

According to *Gurevich et al.* [9], RREAs will be able to directly generate a streamer, which eventually develops into a leader via the conventional lightning discharge model. This is called the RREA lightning initiation model [9, 10]. In *Petersen et al.* [10], the low energy electron plasma created by RREAs locally enhances the ambient electric field,

which allows nearby hydrometeors to initiate a lightning discharge via the conventional lightning discharge model. The lightning initiation model proposed in *Petersen et al.* [10] is called the hybrid lightning initiation model.

6.3. Relativistic Runaway Electron Avalanche (RREA) Lightning Initiation Model

Secondary electron densities within the core of a $>10^{15}$ eV proton primary initiated EAS can be much greater than the electric charge densities typically measured within the main charge centers of a thunderstorm [20, 22, 76]. When a large EAS travels through an active thunderstorm, the strong electric field causes the shower core electron density to grow due to the increased kinetic energy of the secondary electrons and the presence of runaway electrons. The EAS shower front travels near the speed of light and quickly leaves the thunderstorm, leaving behind a plasma of low energy secondary electrons. This charged plasma polarizes in the ambient electric field. The atmosphere surrounding a point discharge is also a polarized plasma, which is able to generate streamers. *Gurevich et al*. [15] theorized that the polarized plasma from RREAs could also generate streamers just like point discharges but in typical thunderstorm electric fields [15]. Once streamers are generated, a leader would develop by the same mechanism as in the conventional lightning discharge model. The theory that the low energy electron plasma created by RREAs could generate streamers in typical thunderstorm electric fields is called the RREA lightning initiation model [9, 10, 15]. A diagram of the RREA lightning initiation mechanism is shown in Figure 6.15. Once streamer formation begins, the lightning discharge develops just like in the conventional lightning discharge model as described in Section 4.4.1.1. [10, 15]. The major difference between the RREA and conventional lightning initiation models is that the RREA model does not require a hydrometeor to undergo a point discharge in order to generate a streamer [10, 15].

Monte Carlo simulations [16, 17, 89] have determined that an initial ambient electric field of 200-300 kV m^{-1} is required for a RREA to generate a dense enough low energy electron plasma to modify the electric field for a lightning leader to develop. 200-300 kV m^{-1} electric fields are greater than the average maximum thunderstorm electric field of 130 kV m^{-1}, but electric fields of those strengths have been measured before within thunderstorms. In addition, 200-300 kV m^{-1} electric fields are approximately an order of magnitude weaker than the 3000 kV m^{-1} that is required for long spark initiation [9, 10, 17]. The breakdown electric field threshold for a RREA initiated discharge also decreases with altitude. At 6 km only an electric field of 167 kV m^{-1} is required to initiate a lightning discharge [17, 20, 21].

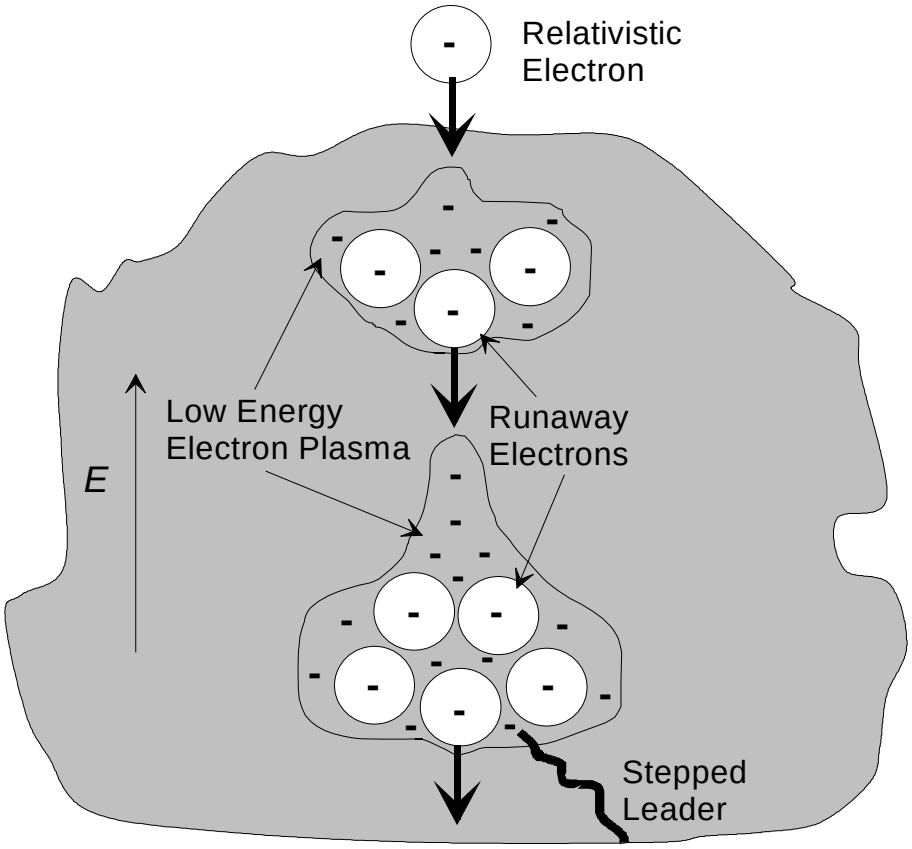

Figure 6.15: Diagram of the RREA lightning initiation model. A RREA develops in an active thunderstorm, producing a large number of low energy secondary electrons. The low energy electrons form a charged plasma which is dense enough to develop a streamer system and eventually a stepped leader [Adapted from 9 and 15].

Currently, there is no definitive experimental evidence that lightning discharges are caused by EASs and accompanying RREAs. The best experimental evidence for the RREA lightning initiation model comes from balloon-borne electric field mills measurements where there is a lightning discharge whenever the ambient electric field gets near the RREA threshold electric field [15, 89]. Results from four such experiments are shown in Figure 6.16. These balloon borne experiments only measured the ambient electric fields, so these experiment could not verify if EAS or RREA were responsible for these lightning discharges [21, 89]. Experimental proof of the RREA lightning discharge model would require measuring both the passage of an EAS and the initiation of a lightning discharge.

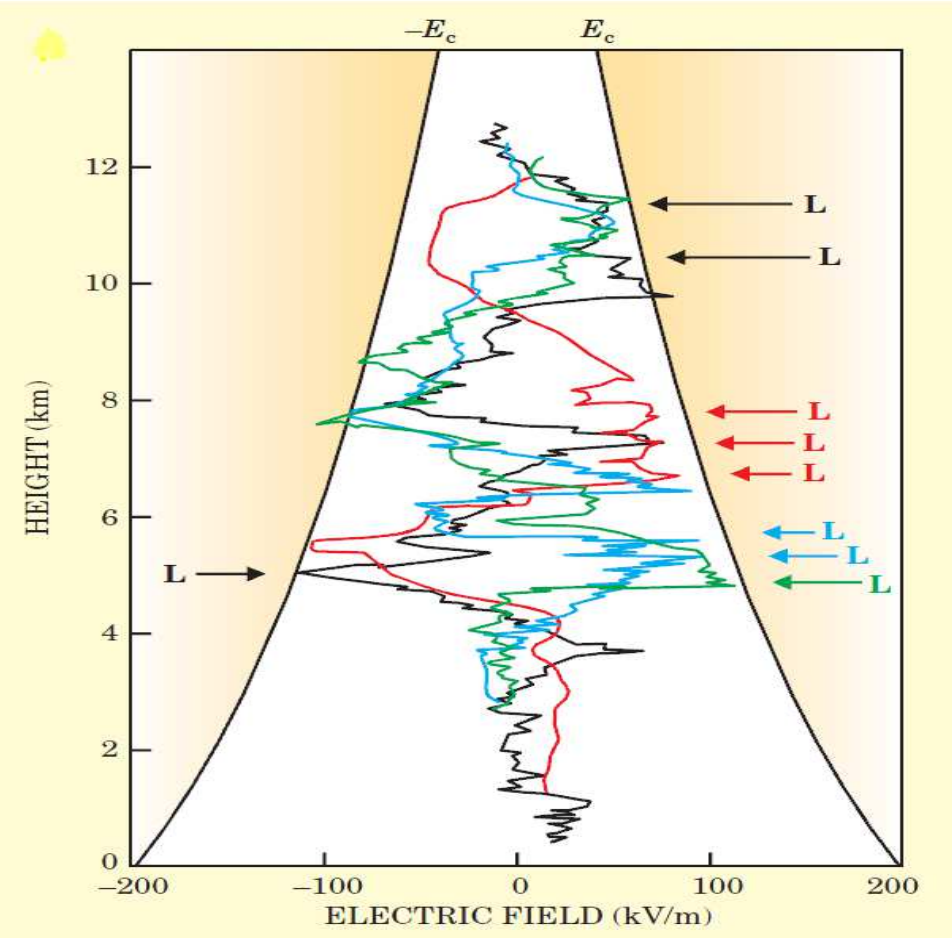

Figure 6.16: Four balloon-borne electric field measurements (colored lines) within an active thunderstorm. In the plot, E_c is the minimum electric field required to produce runaway secondary electrons and L (colored arrows) shows when a lightning discharge occurred near the balloon [89].

6.4. Hybrid Lightning Initiation Model

The main problem with the conventional discharge model is that the required electric fields to initiate a point discharge and generate streamers are at least 2-3 times larger than those typically measured within an active thunderstorm [10, 20]. As seen in the RREA lightning initiation model, EAS and RREAs leave behind a plasma made up low energy electrons in strong electric field regions. Along with being polarized by the strong electric field, this plasma could also enhance the electric field within a small localized region, such as the region surrounding the EAS shower core [10]. Hydrometeors within this

enhanced electric field region could undergo point discharges and generate streamers according to the conventional discharge model [10, 20]. *Petersen et al.* [10] was the first to theorize that the low energy electron plasma generated by RREA could enhance the ambient electric fields to allow the conventional discharge model to function in typical electric: the hybrid lightning initiation model.

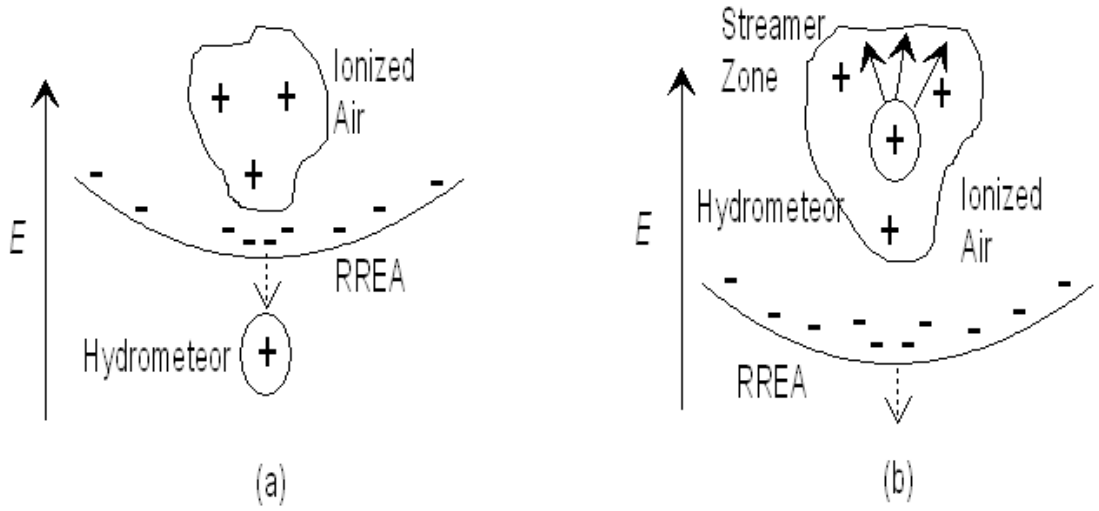

Figure 6.17: Diagram of the hybrid lightning initiation model. (a) An EAS travels through the atmosphere leaving behind an ionized plasma. (b) A charged hydrometeor undergoes a point discharge in the ionized air, which then develops into a lightning leader via the conventional lightning initiation model [10].

Figure 6.17 is a diagram showing the steps of the hybrid lightning initiation model. The hybrid lightning initiation model begins when an EAS enters a high electric field region and RREAs begin. The EAS shower front travels past a charged hydrometeor, which does not undergo a point discharge in the ambient electric field. Behind the shower front is the low energy electron plasma generated by the RREAs, which surround the charged hydrometeor. Due to the presence of the low energy electron plasma, the local electric field is enhanced, allowing the hydrometeor to undergo a point discharge, develop a streamer system, and generate a leader in the ambient electric field [10].

Macroscopically, the RREA and hybrid lightning discharge models look very similar: an EAS travels through a strong electric field region and a lightning discharge develops [9, 10]. Discriminating between the RREA and hybrid models experimental would be very difficult (e.g. did the streamers originate from a hydrometeor or not). This needs to be

considered in any future experiments to prove exclusively either the RREA or hybrid lightning initiation models. In the current experiment being performed by the OSU and OU collaboration, any correlation between the passage of EAS and nearby lightning discharges supports both the RREA and hybrid lightning initiation models.

One assumption that both the RREA and hybrid lightning initiation model make is that there are enough relativistic electrons traveling through the atmosphere in order to generate a dense enough low energy electron plasma to modify the ambient electric fields and initiate a lightning discharge [9, 10]. In the early stages of the OSU/OU experiment, it was discovered that that has been very few measurements of the electron flux at altitudes below 12 km, which were summarized in *Daniel and Stephens* [90]. A major portion of my research was to determine if there were sufficient number high energy electrons in the atmosphere to account for all lightning discharges within a typical thunderstorm. Due to the lack of measurements of the electron flux at thunderstorm altitudes, I used the cosmic ray Monte Carlo code CORSIKA 6.790 [13] to simulate the development of EASs and then calculated the resulting electron flux in a fair weather atmosphere.

CHAPTER VII

CORSIKA MONTE CARLO SIMULATIONS

The RREA and hybrid models both require populations of high energy EAS secondary electrons at thunderstorm altitudes, between 4 and 8 km, in order to initiate a lightning discharge. There are very few experimental measurements in the literature regarding the flux of EAS secondary electrons in the atmosphere at any altitude. Of the few published results, most are measurements from balloons at the top of the atmosphere at altitudes a above 16 km as summarized by *Daniel and Stephens* in 1974 [90]. *Daniel and Stephens* is also the most referenced source to present any measurements or model calculations on the secondary electrons fluxes and energy spectrum below 12 km, i.e. thunderstorm altitudes. Due to the lack of secondary electron measurements and calculations at thunderstorm altitudes over the past 40 years, researchers have had to simply assume a secondary electron flux and energy spectra in the atmosphere as inputs into the RREA or hybrid models [9, 10, 15, 16, 17, 18, 22, 89]. One of the objectives of this research is to model the secondary electron environment at thunderstorm altitudes, and to determine if there are enough high energy electrons in the atmosphere to initiate a lightning discharge.

In order to obtain data on the secondary electrons at thunderstorm altitudes, the cosmic ray Monte Carlo code CORSIKA (COsmic Ray SImulations for KAscade) 6.970 was used to simulate the development of EASs in the lower atmosphere under fair weather conditions [13]. A Monte Carlo code was chosen to simulate the secondary electron environment, because of the lack of secondary electron measurements in the atmosphere. CORSIKA was originally developed to simulate EASs in the atmosphere for the cosmic ray experiment Kascade-Grande, based in Karlsruhe, Germany, but has been since modified for use in many different experiments such as IceCube or the Pierre Auger Projects [13, 91, 92]. Results from CORSIKA have been verified in both cosmic ray and accelerator experiments [13, 93, 94, 95] and can be used to generate a more realistic secondary electron environment, flux and energy spectrum in the fair weather atmosphere.

7.1. Overview of CORSIKA

CORSIKA is a Monte Carlo computer code that simulates the development of an EAS in the Earth's atmosphere. Monte Carlo codes use random numbers to determine the probability of a particle undergoing an interaction, e.g. particle collisions or decays, in the atmosphere and the momenta of all products of that interaction. CORSIKA simulates the development of an EAS from primary protons, heavy ions up to iron, electrons, and photons of energies between 10^6 and 10^{20} eV. The program tracks all the secondaries in an EAS including secondary hadrons, leptons, and photons. For each secondary produced in an EAS, CORSIKA records the location, energy, and direction of travel between each of its interactions. Because of the vast number of possible particle interactions (especially particle decays), CORSIKA only simulates interactions that have >1% probability of occurring, i.e. CORSIKA does not simulate extremely rare events such as producing the Higgs boson [13].

In order to properly simulate hadronic interactions for the entire primary cosmic ray energy range, CORSIKA uses two different hadronic interaction generators. Hadronic generators are computer routines that simulate hadronic particle interactions. One generator handles hadrons >80 GeV and the other handles hadrons <80 GeV. CORSIKA is packaged with five different high energy (>80 GeV) hadronic generators and two low energy (<80 GeV) hadronic generators that were developed connection with several accelerator experiments and detailed in the CORSIKA documentation [13]. This work used the QGSJET-II event generator [96] for high energy and GHEISHA event generator [97] for low energy hadronic interactions. QGSJET-II (Quark Gluon String model with JETs version 2) uses quantum chromodynamics (QCD) and super string theory to model collisions between quarks and gluons, the force carrier for the strong force, at high center of mass energies [98]. QGSJET-II also includes the physics for hadronic jet, i.e. hadronic shower, production [13, 96]. Recent results from the Large Hadron Collider have verified the lowest energy portions of the QGSJET-II model [93]. The low energy hadronic generator GHEISHA uses particle cross section data experimentally measured in various particle accelerator experiments to simulate strong interactions between particles [13]. GHEISHA was used previously in the particle transport code GEANT3 [13]. Electromagnetic interactions are simulated with EGS4 (Electron Gamma Shower version 4) in CORSIKA [99]. EGS4 simulates all the interactions between electrons and gamma photons such as ionization, bremsstrahlung, and pair production [100]. The hadronic generators and electromagnetic physics packages are chosen when CORISKA is first complied. In order to change any of the event generators, a fresh build of CORSIKA must be compiled.

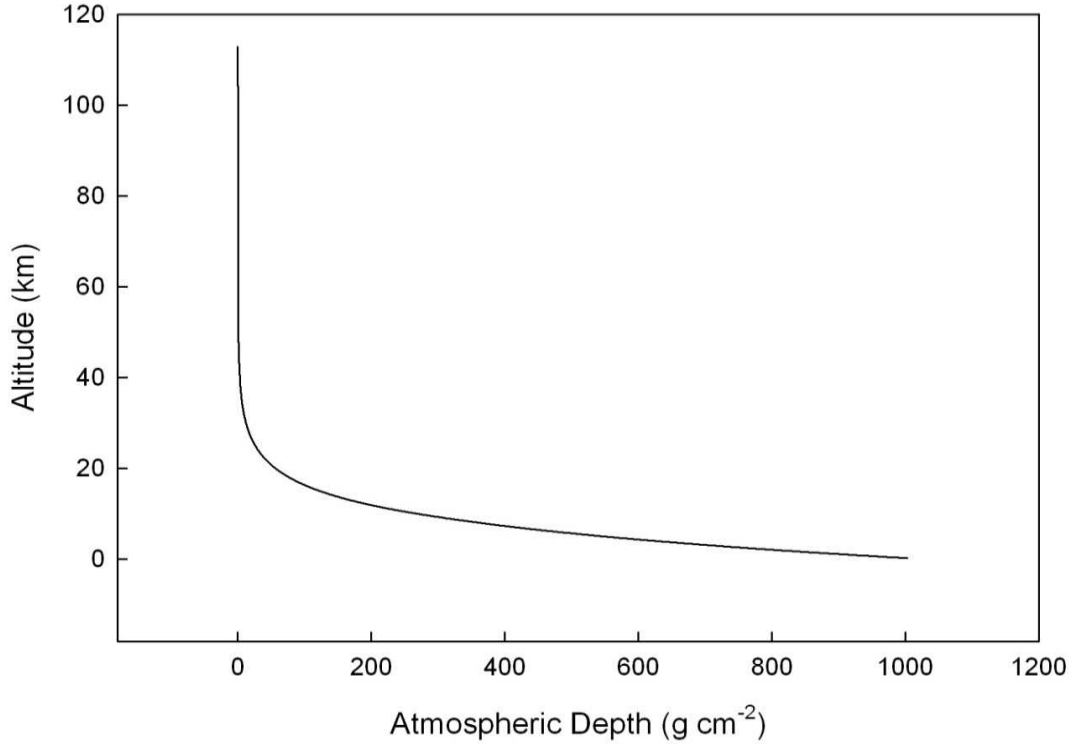

Figure 7.1: Altitude as a function of Atmospheric Depth of the 1976 U.S. Standard Atmosphere parameterized for CORSIKA 6.970 [13].

An accurate description of the development of an extensive air shower in the atmosphere requires CORSIKA to use a detailed parameterization of both the atmosphere and the geomagnetic field of the location where EAS is being simulated. By default, CORSIKA uses the 1976 U.S. standard atmosphere model for the fair weather atmosphere [7, 13]. The 1976 U. S. standard atmosphere model is a parameterization consisting of 78.1% N_2, 21.0% O_2, and 0.9% Ar [7, 13]. CORSIKA also divides the entire atmosphere into five regions based on how the atmospheric density changes with altitude: 0-4 km, 4-10 km, 10-40 km, 40-100 km, and >100 km altitude. For the atmospheric regions below 100 km, the altitude, *h*, is related to atmospheric depth, *d*, via the exponential relationship,

$$d(h) = a_i + b_i e^{-\frac{h}{c_i}}, \tag{7.1}$$

where a_i, b_i, and c_i are fitted parameters for the i^{th} atmospheric region. For the region

above 100 km, atmospheric depth and altitude are related via the linear relationship,

$$d(h) = a_j - b_j \frac{h}{c_j}, \tag{7.2}$$

where the >100 km atmospheric region is the j^{th} atmospheric region. From this parameterization, the entire atmosphere has a depth of 1034 g cm^{-2} with the top of the atmosphere at an altitude of 112.8 km [13]. Figure 7.1 shows a plot of altitude as a function of the atmospheric depth. CORSIKA uses the geomagnetic field determined from IGRF 11 [33]. For this work, the geomagnetic field for Oklahoma City, OK (35° 28' 56.28" N 97° 32' 6.72" W) was determined from the IGRF 11 model and used as an input for CORSIKA. Both the atmosphere and geomagnetic field can be changed through a user command on the CORSIKA input file.

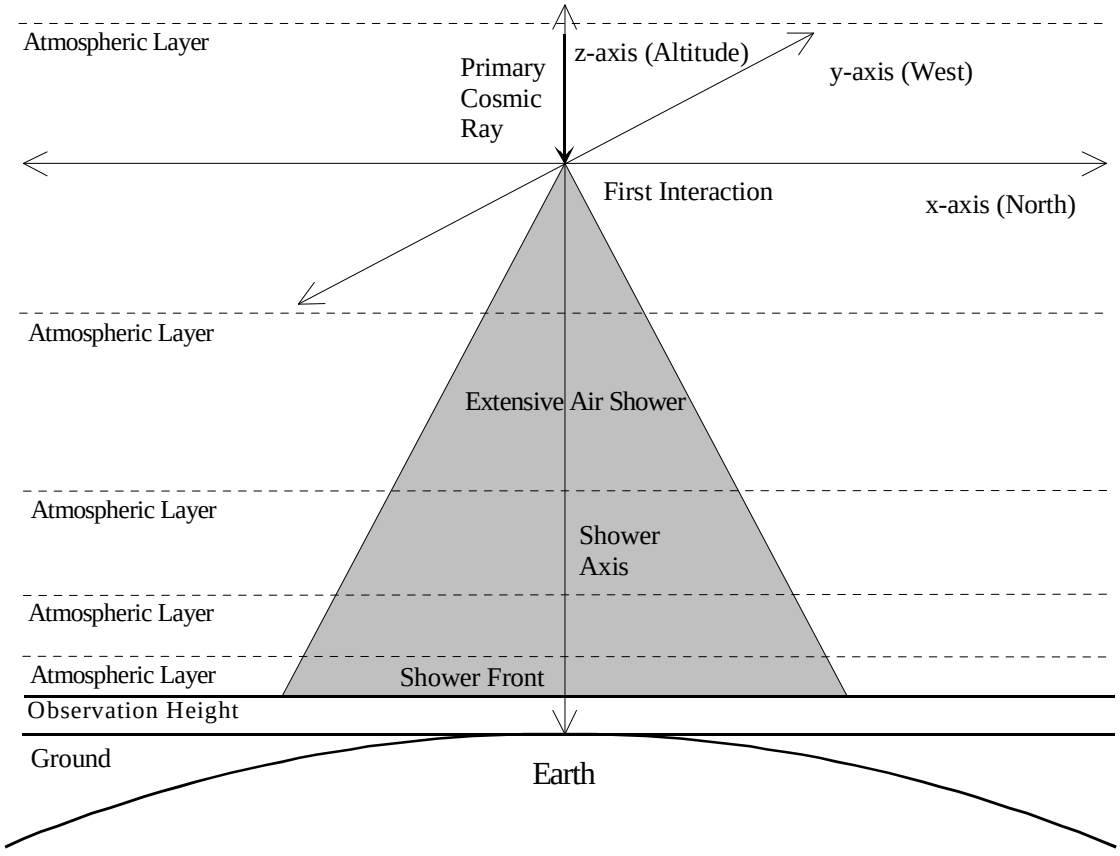

Figure 7.2: Geometry used in CORSIKA cosmic ray simulations. CORSIKA uses magnetic North and West for the x and y directions [Adapted from 13].

CORSIKA simulates the path of the cosmic ray primary particle from the top of the atmosphere to the altitude of first interaction, i.e. when the cosmic ray primary first undergoes a nuclear interaction with an atmospheric atom or molecule. After the first interaction, CORSIKA simulates all the interactions of the cosmic ray primary and secondary particles through the rest of the atmosphere to a user defined observation level. A diagram of the atmospheric geometry used in CORSIKA is shown in Figure 7.2. CORSIKA uses Cartesian coordinates to describe the locations of the EAS particles relative to the shower axis. Corsika 6.790 uses magnetic North as the positive x-direction, magnetic West for the positive y-direction and the z-axis is along the shower axis with the origin being the location of first interaction [6]. Magnetic North and West are determined from the local geomagnetic fields calculated in IGRF 11 [33].

7.2. CORSIKA Simulation Inputs

Each CORSIKA simulation requires an input file made up of a series of commands, which are detailed in the CORSIKA 6.970 user guide [101] in order to correctly run the simulation. The input file is a small text file of less than two dozen lines that contains all the information needed by CORSIKA to simulate EASs. Each line in the input file is a different command, which controls a different aspect of the simulation. These input commands can be divided into three main tasks: defining the cosmic ray primary, EAS propagation through the atmosphere, and simulation outputs. Figure 7.3 shows the commands found in a typical input file used in this work. The different colors of the input file show the different types of CORSIKA commands: red are commands related to defining the cosmic ray primary, blue commands control EAS development and propagation, green commands are related to generating output files, and black commands are not used in this work but are still required by CORSIKA to run properly.

The first type of CORSIKA commands are used to define the primary cosmic ray that will be generating the EAS in the atmosphere. CORSIKA requires that the particle type (proton, heavy ion, electron, or gamma photon), initial energy, number, and zenith angle of the primary cosmic ray. According to the flux of cosmic ray primaries at the top of the atmosphere, listed earlier in Table 5.1, ~90% of all cosmic ray primaries are protons [73, 74]. The flux of helium and heavy ion cosmic ray primaries are not sufficient to generate the lightning discharge rates observed in mesoscale and severe thunderstorms [3, 68]. Proton cosmic ray primaries are frequent enough to account for the largest lightning discharge rates ever recorded in a thunderstorm system [3]. For this reason, only primary proton initiated EASs were considered in this work.

```
RUNNR   610000                          run number
EVTNR   1                               number of first shower event
NSHOW   10                              number of showers to generate
PRMPAR  14                              particle type of prim. particle
ESLOPE  -2.7                            slope of primary energy spectrum
ERANGE  1.E6  1.E6                      energy range of primary particle
THETAP  00.  00.                        range of zenith angle (degree)
PHIP    -180.  180.                     range of azimuth angle (degree)
SEED    1   10   0                      seed for 1. random number sequence
SEED    2   0   0                       seed for 2. random number sequence
OBSLEV  000000                          observation level (in cm)
FIXCHI  0.                              starting altitude (g/cm**2)
MAGNET  22.5  45.8                      magnetic field central OK
HADFLG  0  0  0  0  0  2                flags hadr.interact.&fragmentation
ECUTS   0.1  0.1  0.0005  0.0005        energy cuts for particles
MUADDI  T                               additional info for muons
MUMULT  T                               muon multiple scattering angle
ELMFLG  T   T                           em. interaction flags (NKG,EGS)
STEPFC  1.0                             mult. scattering step length fact.
ARRANG  0.                              rotation of array to north
LONGI   T  1.  T  T                     longit.distr.&step size & fit & out
ECTMAP  1.E3                            cut on gamma factor for printout
MAXPRT  10                              max. number of printed events
DIRECT  ./                              output directory
DATBAS  F                               write .dbase file
PAROUT  T F                             write DAT file
USER    you                             user
DEBUG   F  6  F  1000000                debug flag and log.unit for out
EXIT                                    terminates input
```

Figure 7.3: CORSIKA commands from an input file for a 10^{15} eV proton primary simulation used in this work. See the text for the meaning of the different colors.

The majority of cosmic ray primaries measured at the top of the atmosphere are proton primaries of energy <1 GeV. Less than 1 GeV cosmic ray primary protons are affected by the geomagnetic field and are deflected to large zenith angles [32]. EASs of large zenith primaries develop near the top of the atmosphere and attenuate above thunderstorm altitudes. However, EASs initiate from >10 GeV primary proton are not as affected by the geomagnetic field and are able to reach thunderstorm altitudes even near the equator where the effect of the geomagnetic field is at its strongest [12, 20, 32, 69, 71]. From satellite measurements, the majority of lightning discharges also occur near the equator in coastal regions [1]. For those reasons, the minimum primary proton cosmic ray energy used in this work was 10 GeV (10^{10} eV). At the other energy extreme, the flux of $>10^{17}$ eV proton primaries are typically measured in units of square kilometers per year, which is too low to explain typical lightning discharge rates [3, 69]. The maximum lightning discharge rate ever recorded is 120 discharges per minute in a single

thunderstorm cell and corresponds to an maximum primary cosmic ray flux of ~5 PeV ($5.0 * 10^{15}$ eV) [69]. To account for more typical lightning discharge rates, this work assumes that maximum primary proton energy that could generate a lightning discharge is 10 PeV (10^{16} eV).

Table 7.1: Energies and number of cosmic ray proton primaries simulated in this work.

Primary Energy (eV)	Number of Primaries
10^{10}	10000
10^{11}	10000
10^{12}	10000
10^{13}	1000
10^{14}	1000
10^{15}	100
10^{16}	50

Table 7.1 lists all the primary proton energies that were simulated in CORSIKA for this work. A range of primary proton energies were simulated in order to determine the minimum energy required to produce an EAS with enough high energy secondary electrons to initiate a lightning discharge, or to determine if the background ambient flux of secondary electrons, i.e. secondary electrons from the constant flux (of mostly lower energy) cosmic ray primaries, is sufficient. The method of calculating ambient flux from the individual energies of EAS simulations is discussed in Chapter 8. There is a large amount of variation between EASs of the same energy [76], so each primary proton energy was simulated a number of times as listed in Table 7.1 in order to obtain a statistical average. Because the number of EAS secondaries increases linearly with primary proton energy [68], i.e. there are roughly ten times more EAS secondaries for 100 GeV than 10 GeV EASs, and that computer time also increases linearly with the number of EAS secondaries [76], fewer simulations of higher energy EASs were performed than lower energy EASs. The total computer time for 10000 10^{10} eV proton primary EAS simulations was <30 seconds but 50 10^{16} eV proton primary EAS simulations was >10 days. The number of simulations was chosen so that the error of the average of each simulation was <20%.

The primary cosmic rays are assumed to arrive isotropically at the top of the atmosphere [11]. Due to the geometry of the atmosphere, EASs that develop at larger zenith angles must pass through a greater depth of atmosphere in order to reach the same point in the atmosphere as a lower zenith angle EAS [11]. The development of an EAS is affected by

the amount of atmosphere the EAS secondaries must travel through [76]. Thus large zenith angle EASs arrive later in their development at an observation level than smaller zenith angle EASs. For the primary proton energies simulated, vertical, i.e. 0° zenith angle, EASs typically reach shower maximum at lightning initiation altitudes of 4 to 8 km. Below shower maximum, EASs begins to attenuate as the secondaries begin to range out or get absorbed by the atmosphere. The shower maximum of large zenith angle EASs are above and are very attenuated at lightning initiation altitudes. Small zenith angle EASs still reach shower maximum at higher altitudes than vertical EASs, but because of the exponential nature of atmospheric density, the difference is not as severe as high zenith angles [102]. Experimental measurements have found that the typical variation between EASs affects in the number of EAS secondaries more significantly than zenith angle for EAS with <40° zenith angles [103]. For these reasons, all EAS simulated in for this work were assumed to be vertical.

The propagation of the cosmic ray primary and secondaries through the atmosphere is controlled by the second type of CORSIKA commands. This type of commands includes how the atmosphere and local magnetic field are defined, the initial values of the random number generator seeds, and cosmic ray secondary energy cutoffs. Since this work only uses the default atmosphere used in CORSIKA, Figure 7.2 does not include any commands for modifying the atmosphere. The geomagnetic field varies more with location than does the atmosphere [7, 33], so the local geomagnetic field must be included in each CORSIKA input file.

CORSIKA uses randomly generated numbers to determine stochastic interactions between particles. A more thorough description of how CORSIKA generates random numbers and uses them to describe particle interactions is presented in the CORSIKA physics guide [13]. However, CORSIKA does require that an initial random number be chosen by the user and is included in the input file. This initial random number is called a seed in CORSIKA [13]. CORSIKA actually requires the user to define two random number seeds, one for hadronic generators and another for generating secondary particles [102]. Due to a how CORSIKA uses the second random number seed in computations, the authors of CORSIKA suggest that the second random seed always be set to zero [101]. For this work, only the first random number seed was modified for each simulation.

The amount of computer time required for CORSIKA to complete a simulation is linearly related to the number of secondaries produced in the EAS [77]. The number and energy of the EAS secondaries increases with cosmic ray primary energy [12]. As the energy of secondaries increases, more types of interaction become possible. For example, the dominate forms of energy loss for 1 MeV electrons are soft collisions, for 10 MeV electrons are soft and hard collisions, and for 100 MeV electrons are soft and hard

collisions and bremsstrahlung [12, 70]. Higher energy interactions also produce more high energy secondaries, such as secondary electrons from hard collisions or photons from bremsstrahlung. The majority of secondaries are not produced with sufficient energy to greatly affecting the development of the rest of EAS. In an effort to decrease computer time, CORSIKA only propagates EAS secondaries above a user defined energy threshold, i.e. only monitor higher energy secondaries that could affect the development of the EAS. Any EAS secondaries below these energy thresholds, or cutoff energies, are removed from the EAS and its energy assumed to be deposited to the local atmosphere. In this work, the cutoff energies, typically written as E_{cut} are 500 keV for electrons and photons and 100 MeV for hadrons and muons. The chosen cutoff energies used in this work were the lowest allowed by CORSIKA [101].

Another method to lower the computer time is to divide the all EAS secondaries into several energy bins and only propagate a single secondary from each energy bin. All secondaries of the same energy are then assumed to propagate in the same manner as the simulated EAS secondary. This method of approximating the propagation of multiple EAS secondaries with a single simulated EAS secondary is called thinning [102]. CORSIKA uses a thinning algorithm to drastically reduce the computer time for simulations of very high energy EASs [13]. Typically, the thinning algorithm is used with secondary electrons and photons that are <100 MeV [102]. Simulations of the highest energy cosmic rays (>10^{19} eV) require using thinning algorithm to limit computer time to a reasonable period (<1 year) [104, 105, 106]. This work focuses on the production of <100 MeV secondary electrons, which are affected the most by the thinning algorithm, so the thinning algorithm was not used in this work.

The last type of CORSIKA commands involves how CORSIKA generates outputs. The majority of these commands tell CORSIKA what types of outputs to write to the hard drive and include the longitudinal and lateral particle distributions. The different types of outputs from CORSIKA are discussed in Section 7.4. For these output commands, the user must define the different observation levels in the atmosphere of the simulation. An observation level is the altitude at which data from the simulation is written to a file. CORSIKA simulates the EAS down to the observation level, writes EAS secondary data to the output file, and either continues to simulate the EAS to the next observation level or ends the simulation at the lowest observation level. CORSIKA has two output types that requires the user to define observation levels: the longitudinal and lateral EAS distributions. Longitudinal output contains a small amount of data (<1 Mb per simulation), so the longitudinal observation levels were assigned as every 1 g cm^{-2} of the atmosphere in this work. In contrast, the lateral distribution output files could be quite large (>20 Gb per simulation), so the lateral distribution observations levels for this work were every 2 km of altitude from the ground up to 12 km. Table 7.2 lists the altitudes and depths in the atmosphere where the lateral distributions were determined for this work.

The 2 km lateral distribution observation levels were chosen as a compromise to monitor the development of EASs throughout thunderstorm altitudes and having too much data to store or analyze.

Table 7.2: List of altitudes and depths in the atmosphere where the EAS secondary lateral distribution was determined in CORSIKA [13].

Altitude (km)	Atmospheric Depth (g cm^{-2})
12	198
10	271
8	365
6	483
4	631
2	813
0	1034

7.3. Simulating an EAS with CORSIKA

CORSIKA runs via a command line on a Linux operating system, without the assistance of a graphical user interface. Routines within CORSIKA use both FORTRAN and C libraries which are not located on most Window operating system computers, thus CORSIKA is only supported for Linux systems [102]. From the command line, the user links the simulation's input file (described in Section 7.2) to a complied version of the CORSIKA program and begins the simulation.

The first type of commands in the CORSIKA input file lists the energy and number of cosmic ray primaries that are to be simulated in a single run of the program. CORSIKA simulates one EAS at a time from the proton primary entering Earth's atmosphere until every EAS secondary particle either ranges out or reaches the lowest observation level. Figure 7.4 is a flow chart of the major steps in a CORSIKA EAS simulation. The simulation begins with CORSIKA generating a list of all EAS secondaries (hadrons, muons, electrons, and photons) currently in the EAS. Initially, this list of EAS secondaries only includes the proton primary, but eventually includes all EAS secondaries that do not instantly decay, such as neutral pions [13, 80], or drop below the cutoff energy, such as low energy electrons from soft collisions [56, 70, 76, 84, 102]. CORSIKA records the current location, components of momenta, and the time the

particle was created relative to the first interaction (primary protons are considered to have been created at the time of first interaction) [94]. Every time an EAS secondary is used by CORSIKA, these recorded parameters are updated.

CORSIKA selects an EAS secondary from the EAS secondary list to propagate, or transport, through the atmosphere. The CORSIKA commands from the input file that control how the EAS develops in the atmosphere are followed in this portion of the simulation. The distance the EAS particle is transported is determined by the mean free path, half-life of an unstable particle or the distance to the next user defined observation level. Along this distance, CORSIKA takes into account ionization losses (which for secondary electrons is the amount of energy lost to soft collisions), multiple scattering, deflection in the geomagnetic field, and the probability of the particle undergoing an interaction (such as a hard collision or bremsstrahlung for secondary electrons) or particle decay. CORSIKA determines the interaction cross section and decay constant via lookup tables are built into CORSIKA [13]. Each hadronic generator uses its own lookup tables that are supplied by the original authors of those routines [13].

Once the probability of an interaction or decay is calculated, CORSIKA uses a set of random numbers based on the first random seed of the input file to determine if the particle undergoes an interaction or a particle decay. The method on how CORSIKA uses the random numbers to determine which type of interaction or decay is explained in detail in the CORSIKA Physics Guide [13] and the documentation of the hadronic generators [95, 96]. If the particle undergoes an interaction or decay, CORSIKA uses random numbers from the second random number seed to determine the initial momentum of any secondaries produced, subject to conservation laws and the physics of the interaction or decay. The location, momentum, and time are then either recorded for any newly generated EAS secondaries and updated for the original EAS secondary if still present. CORSIKA then checks to determine if all of the remaining EAS secondaries are above the cutoff energy, e.g. CORSIKA checks that secondary electrons produced during a hard collisions are >500 keV. If a secondary is below the cutoff energy, the secondary is discarded, but the energy of that secondary is still removed from the total energy of the interaction.

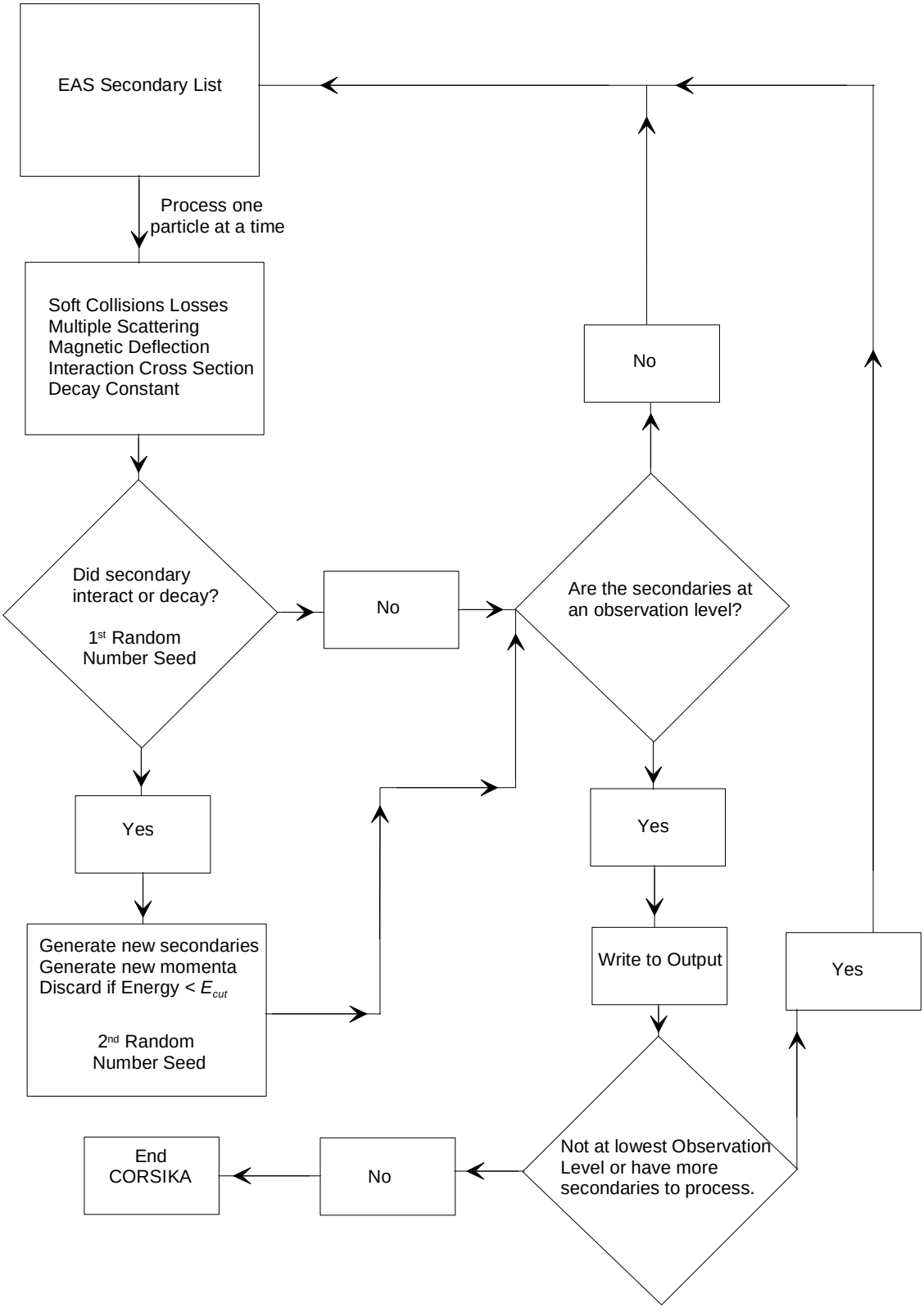

Figure 7.4: Flowchart for how CORSIKA simulates an EAS.

Regardless of whether or not an interaction or decay occurred, the location of the EAS secondary (and any newly created EAS secondaries) is checked to determine if it is at an observation level. If the EAS secondaries are not at an observation level, the information of the EAS secondaries is returned to the list of EAS secondaries and another EAS secondary is selected from the list to be transported through the atmosphere. Otherwise, the information of the EAS secondaries is written to an output file. The particular data that is written to a file depends on which type of output was selected by the user in the input file. The different output files and what information they collect are discussed in Section 7.4. If the EAS secondaries are not at the lowest observation level as defined by the user, the EAS secondaries are returned to the EAS particle list and another EAS secondary is selected to be transported through the atmosphere.

At the lowest observation level, CORSIKA first discards all EAS secondaries that had their information written to an output file and then loops back to the list of EAS secondaries. If the EAS secondary list is empty, i.e. all the EAS secondaries have reached the lowest observation level, CORSIKA ends the simulation for that EAS. CORSIKA will then initiate entirely new EAS simulation with a primary proton entering at the top of the atmosphere.

7.4. CORSIKA Simulation Outputs

The last type of command contained in the CORSIKA input file is used to define which of type of output files are created by the CORSIKA routines described in Section 7.3. For this work, two types of CORSIKA output files were used: text and DAT files. The text output file is human-readable and includes the simulated EAS longitudinal distributions. The DAT file is generated as a binary file and includes the EAS lateral distributions. Figure 7.5 shows a flow chart of how the CORSIKA data was used to determine EAS secondary distributions in the atmosphere. As mentioned in Section 7.2, the longitudinal and lateral distributions contain different amounts of information on the EAS secondaries and describe different aspects of EAS development.

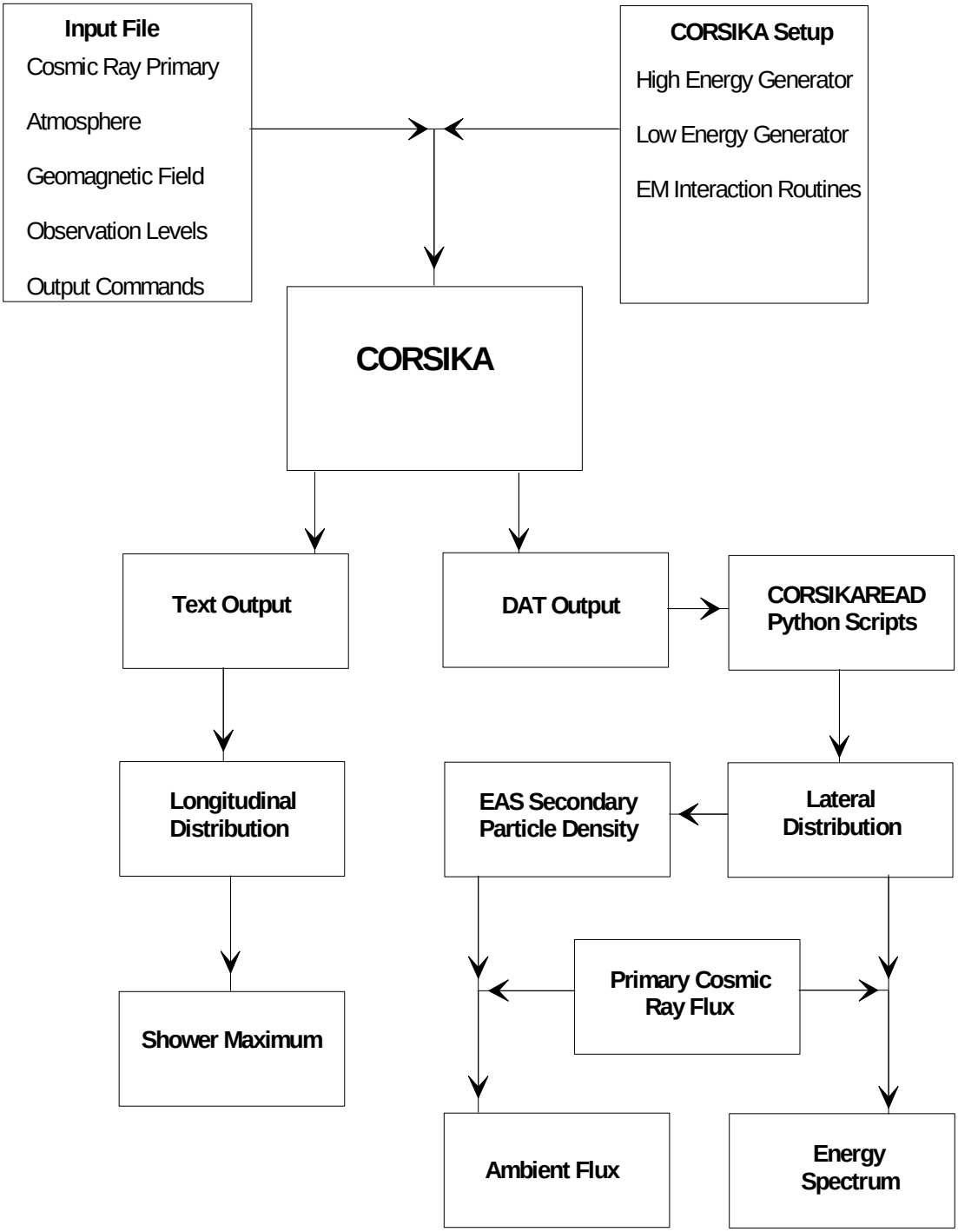

Figure 7.5: Flowchart for generating fair weather EAS secondary data from CORSIKA.

The longitudinal distribution is the number of secondary particles in an EAS located at an observation level

$$n_{long} = n(h, E_o), \tag{7.3}$$

where n_{long} is the longitudinal distribution, n is the number of EAS secondaries, h is the altitude determined from solving equations (7.1) and (7.2) for the altitude from a known atmospheric depth, and E_o is the primary proton's initial energy. Longitudinal distributions are typically divided into different particle types, such as secondary electron longitudinal distribution. No information about the energy or radial distribution of the secondary particles can be inferred from the longitudinal distribution. Longitudinal distributions are typically used to determine the atmospheric depth of EAS maximum [12].

The DAT file is converted to a human-readable via the program CORSIKAREAD, which is included with CORSIKA 6.970 distribution. The converted DAT file lists the position (x and y) relative to the shower core and components of momentum (p_x, p_y, and p_z) for every EAS secondary at an observation level. A typical DAT file from 10^{16} eV primary proton initiated EAS can be >20 Gb in size, so several custom Python scripts were used to parse through the human-readable DAT files. The Python scripts separated the different particle types, converted the relative position to a radial distance from the shower core, and converted components of momentum into energy. The secondary particles were then separated into a two-dimensional array with 0.1 logarithmic divisions in both radial distance and kinetic energy. This two-dimensional array is the lateral distribution of the EAS and is given symbolically as,

$$n_{lat} = n(r, E, h, E_o), \tag{7.4}$$

where n_{lat} is the EAS lateral distribution, r is the EAS secondary's radial distance, and E is the EAS secondary's energy. From the lateral distribution, both the fair weather particle density and energy spectrum of an EAS can be determined.

During the early development of the RREA model [9, 89], only the secondary electron longitudinal distribution was considered to be enough information to explain all lightning discharges in the atmosphere. The typical assumption was that a single EAS initiated by a 10^{16} eV proton primary produced up to 10^8 >1 MeV secondary electrons that are capable to run away in the strong electric field region of a typical thunder, and these runaway electrons produce enough RREAs to initiate a lightning discharge [89]. The main issue with this assumption was that the density and energies of these 10^8 high energy electrons various drastically between the EAS shower core and the edges of the EAS shower front, which is not shown in a longitudinal distribution [12]. As the RREA model was furthered

developed, *Carlson et al.* [16] determined through simulations that the different energy EAS secondaries (including gamma photons and muons) produce different amounts of runaway secondary electrons and *Dwyer and Smith* [18] found that runaway electrons are accelerated to an equilibrium energy. Also, the *Petersen et al.* [10] hybrid model only requires a large concentration of high energy secondary electrons near a charged hydrometeor, not across the entire EAS shower front. From the results of those three studies, the secondary electron lateral distribution contains more of the required information than the longitudinal distribution needed to explain how high energy secondary electrons initiate lightning discharges in the atmosphere.

CHAPTER VIII

FAIR WEATHER SECONDARY ELECTRON ENVIRONMENT

The fair weather cosmic ray secondary electron environment, i.e. the cosmic ray secondary electron flux and energy spectrum, is a required input for both the RREA and hybrid lightning initiation models [9, 10]. In previous work, the secondary electron environment was assumed to have some simple distribution, e.g. all EAS secondary electron having energies between 100 keV to 10 MeV [9]. In order to generate a more realistic distribution of the fair weather secondary electron environment, EASs were simulated using the cosmic ray Monte Carlo code CORSIKA. The fair weather secondary electron environment used in this work was determined from the longitudinal and lateral particle distribution output files generated by CORSIKA.

8.1. EAS Secondary Electrons in a Fair Weather Atmosphere

The different components (hadronic, electromagnetic, and muonic) and how they develop within an EAS was previously described in Chapter 5, but a more detailed description is required to understand the secondary electron distributions generated by CORSIKA. The following qualitative description of the development of an EAS comes from the theory of hadronic and electromagnetic cascades. More details about hadronic and electromagnetic cascades in the atmosphere can be found in cosmic ray text books such as *Grieder* [12], *Dorman* [22] and *Gaisser* [68].

An EAS is a high energy particle shower made up a single hadronic cascade and multiple electromagnetic cascades. The hadronic cascade is initiated at first interaction, when the primary cosmic ray collides with an atom in the atmosphere, producing a number of high energy secondary hadrons. Due to the momentum of the cosmic ray primary, the secondary hadrons produced in the first interaction continue to travel along the same path as the cosmic ray primary, i.e. along the shower axis. The secondary hadrons continue to interact along the shower axis and develop the hadronic cascade.

The hadronic cascade continues along the shower axis until the primary cosmic ray and secondary hadrons lose their kinetic energy and range out, for charged particles, or decay, for unstable particles. One type of particle produced by the hadronic cascade is neutral pions. Neutral pions are unstable and quickly decay into a pair of high energy gamma-rays. These gamma-rays initiate electromagnetic cascades and are responsible for generating the electromagnetic component in an EAS.

8.1.1. Electromagnetic Cascades

Electromagnetic cascades are made up of secondary electrons, positrons, and gamma-rays that are created through a combination of nuclear and electromagnetic interactions. The different interactions that occur in electromagnetic cascades were previously described in Section 5.2.2. In EASs, electromagnetic cascades are initialized by high energy gamma-rays produced by the decay of neutral pions, which are themselves produced by the hadronic cascade. A diagram of an electromagnetic cascade is shown in Figure 8.1.

An individual electromagnetic cascade contains only as much energy as the initial gamma-ray. The initial gamma-ray undergoes pair production and splits its energy (not necessarily evenly) between the secondary electron and positron. Being highly energetic themselves, the secondary electron and positron quickly generate additional secondaries through hard collisions with bound electrons and bremsstrahlung. Each time a new secondary is produced, the total energy of the electromagnetic cascade is divided again. While the electromagnetic cascade secondaries have sufficient energy to generate new high energy secondaries, the electromagnetic cascade is its developing stage. The top portion of Figure 8.1 shows the developing stage of an electromagnetic cascade.

After many interactions, the secondaries will no longer possess sufficient energy to produce new secondaries. The electromagnetic cascade eventually reaches a maximum number of secondaries, which is called electromagnetic shower maximum (another name for electromagnetic cascades is electromagnetic showers [70]). Beyond electromagnetic shower maximum, the number of electromagnetic cascade secondaries begins to attenuate when the secondary electrons begin to range out, secondary positrons undergo positron annihilation, and secondary photons are absorbed by the atoms and molecules of the atmosphere as shown in Figure 8.1.

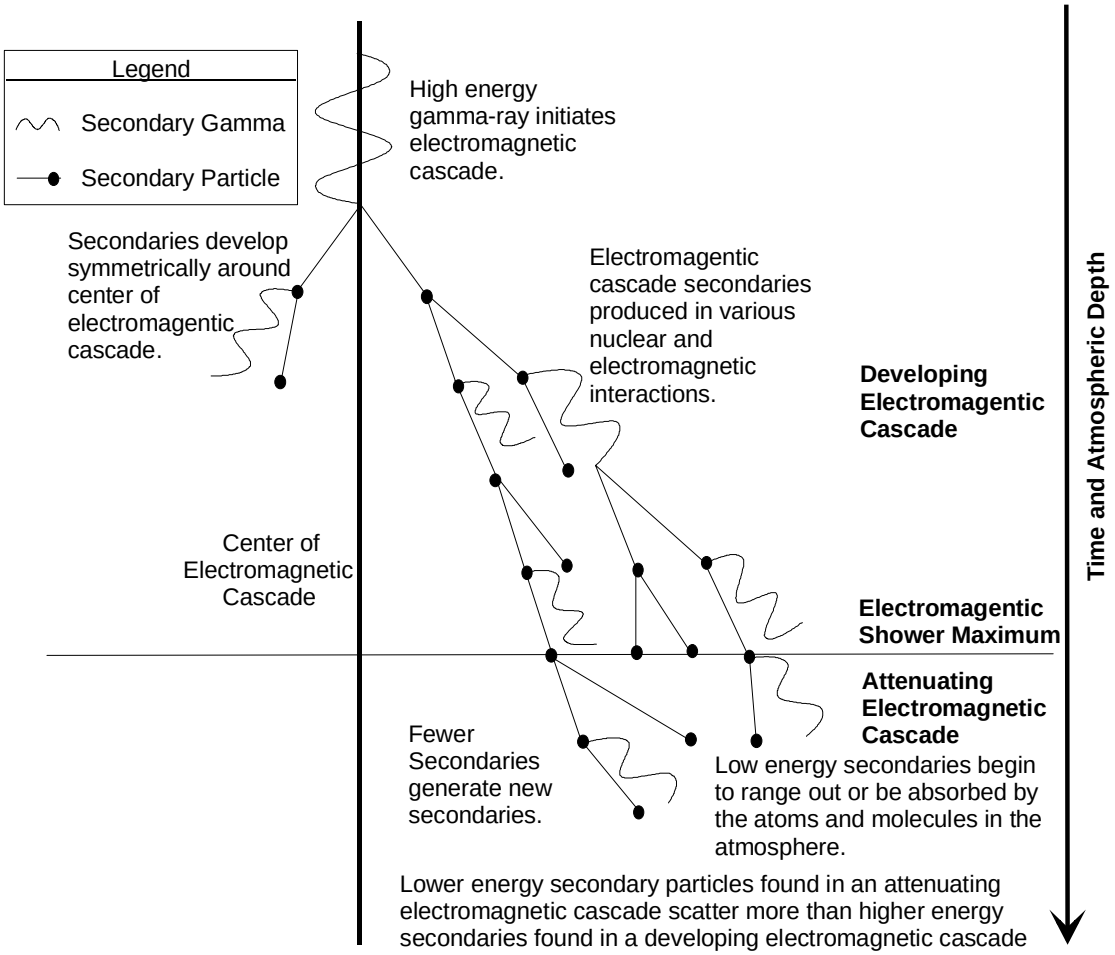

Figure 8.1: Diagram of an electromagnetic cascade in the atmosphere. Due to space constraints, only a representative sample of the secondaries in a developing electromagnetic cascade was shown interacting in the atmosphere. The distance of the electromagnetic cascade secondaries are from the center of the electromagnetic is not drawn to scale [Adapted from 77].

While an electromagnetic cascade propagates through the atmosphere, there is a small probability that the secondary electrons and positrons will deviate slightly, i.e. scatter, from their path after an interaction, such as a soft collision. The probability of scattering decreases with secondary particle energy, but never goes to zero. As the secondary electrons and positrons undergo multiple interactions (which also lowers their kinetic energy), the cumulative probability of scattering from its original path also increases and scattering is virtually assured before the secondary particle ranges out or undergoes positron annihilation.

A scattered secondary particle travels laterally away from the center of electromagnetic cascade. As an example, in Figure 6.5, the range of a 100 MeV secondary electron (typically produced early in an electromagnetic cascade) at lightning initiation altitudes is ~1 km. If that 100 MeV secondary electron scattered a total of 1° over its entire range, the secondary electron would range out ~20 m laterally from the center of the electromagnetic cascade. A difference of 20 m over a range of a 1 km is insignificant for a single secondary electron, but every electromagnetic cascade secondary produced by the scattered electron will be produced at some lateral distance from the rest of the electromagnetic cascade. Figure 8.1 shows that after each interaction, the electromagnetic cascade secondaries are propagate farther and farther away from the center of the electromagnetic cascade. By the time of the electromagnetic shower maximum is reached, electromagnetic cascade secondaries are spread out over an area of several square kilometers around the center of the electromagnetic cascade.

The secondary electrons from attenuating electromagnetic cascades are typically found far away from center of the electromagnetic cascade. In attenuating electromagnetic cascades that have propagated well past their electromagnetic shower maximum, there are few if any secondary electrons left around the center of the electromagnetic cascade due to scattering. Because the electromagnetic cascades develop symmetrically around the center of the electromagnetic cascade, the secondary electrons are distributed laterally in a ring around the center of the electromagnetic cascade.

8.1.2. Secondary Electrons in an Extensive Air Shower

The distribution of secondary electrons in an EAS is determined by the combination of all the secondary electrons generated by the multiple electromagnetic cascades that make up the electromagnetic component of the EAS. Figure 8.2 shows a diagram of the density of secondary electrons along the shower front at different stages of the development of an EAS. The EAS propagates downward through the atmosphere, so the lower the shower front disk is in Figure 8.2, the lower in the atmosphere and the more time the EAS had to develop.

Starting with the top shower disk in Figure 8.2, the first electromagnetic cascades are initiated in the region in the shower axis called the shower core. The secondaries of these developing electromagnetic cascades are initially have not undergone a sufficient number of interactions to scatter. Thus all the secondary electrons generated in a recently initiated EAS are found in the shower core.

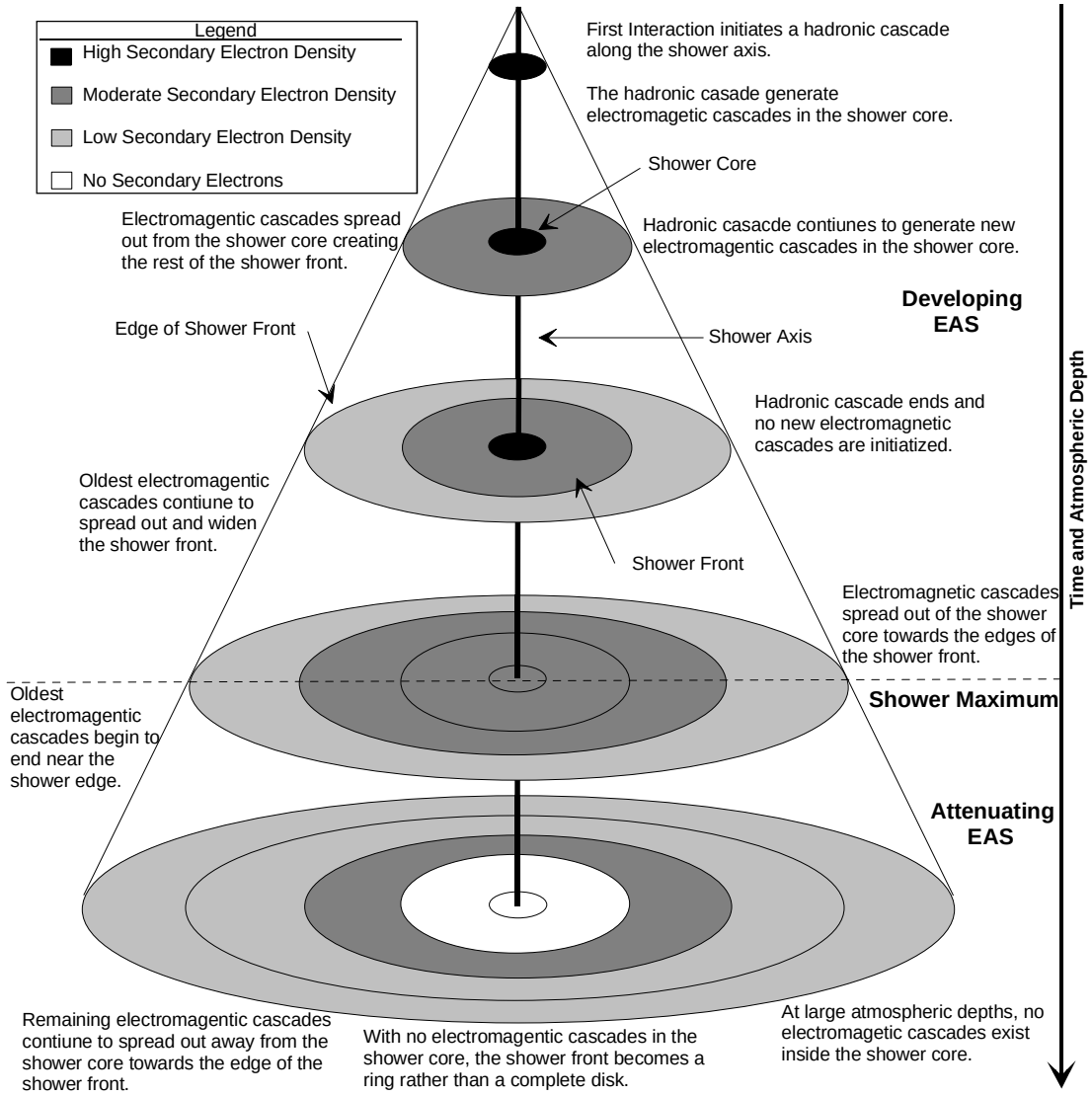

Figure 8.2: Diagram of the secondary electron density across the shower front at different stages in the development of an EAS in a fair weather atmosphere. The different rings of the shower front roughly scale logarithmically with radial distance, with the center oval being the shower core. Darker shades of grey represent higher relative secondary electron density [Adapted from 12, 76].

As the EAS continues to propagate downward through the atmosphere, the initial electromagnetic cascades also continue to develop, producing many more secondary electrons. As the secondary electrons of those initial electromagnetic cascades undergo multiple interactions, they scatter outside the shower core and expand the shower front as shown in the second shower front disk in Figure 8.2. The hadronic cascade continues to

develop along the shower axis and generate more neutral pions, which initiates additional electromagnetic cascades in the shower core. Because new electromagnetic cascades continue to develop in the shower core, the density of secondary electrons within the shower core remains high.

Like the electromagnetic cascade secondaries, the hadronic cascade secondaries eventually do not have sufficient energy to produce additional secondary hadrons, include neutral pions. Once the production of neutral pions stops, no additional electromagnetic cascades are initiated within the EAS. The third shower front disk in Figure 8.2 represents the shower front of an EAS after the hadronic cascade no longer produces neutral pions. Secondary electrons from the oldest electromagnetic cascades, which are now transitioning from developing to attenuating electromagnetic cascades, continue to scatter away from shower core towards the edge of the shower front. The secondary electrons from the majority of electromagnetic cascades have scatter outside the shower core and populated the rest of the shower front. The recently initiated electromagnetic cascades still have the majority of their secondary electrons within the shower core. There are more secondary electrons outside the shower core than inside, but due to the expanding area of the shower front, the secondary electron density decreases with distance from the shower core.

The electromagnetic cascades continue to develop with the EAS as it propagates further through the atmosphere. Without new electromagnetic cascades being initiated in the shower core, the number of secondary electrons within the shower core begins to decrease as they continue to interact and scatter out into the rest of the shower front. The secondary electrons within the shower front continue to interact and scatter from the shower core towards the edge of the shower front. This causes the secondary electrons density to become fairly uniform across a large portion of shower front as shown in the fourth disk of Figure 8.2. The secondary electron density decreases near the edge of the shower front due to the lowest energy secondary electrons from the oldest electromagnetic cascades are starting to range out in the atmosphere.

While the electromagnetic cascades develop in the atmosphere, the total number of secondaries (mostly secondary gamma-rays, electrons, and positrons) in the EAS increases with atmospheric depth. While the total number of secondaries in the EAS increases with atmospheric depth, the EAS is in the developing stage. Once the majority of secondary electromagnetic cascades within the EAS transition to the attenuating stage and their secondaries begin to range out, the total number secondaries in the EAS at any one time reaches a maximum. The altitude at which the total number of EAS secondaries reaches this maximum is called the shower maximum. The electromagnetic shower maximum is the maxima for a single electromagnetic cascade and the shower maximum is the maxima for the entire EAS high energy particle shower.

As the EAS propagates past shower maximum, the EAS enters the attenuating stage of development. In the attenuating stage, the total number of secondaries in the EAS decreases with atmospheric depth. The electromagnetic cascades in an attenuating EAS are also in their attenuating stage of development. The secondary electrons in attenuating electromagnetic cascades are distributed in lateral rings centered on the center of the electromagnetic cascade. This causes the secondary electrons density to be concentrated towards the outer edge of the shower front and very few or even no secondary electrons within the shower core as shown in the fifth shower front disk in Figure 8.2. The EAS continues to propagate through the atmosphere until all of its secondaries range out or are absorbed by the atoms and molecules in the atmosphere or reaching the ground.

8.2. Fair Weather EAS Secondary Electron Distributions

The previous section presented only a qualitative description of the development of an EAS in the atmosphere. Due to the complexities of mathematically modeling hadronic cascades, there is currently no fully analytic theory of the development of an EAS in the atmosphere [107]. As the energy of the hadrons increases, more interaction channels, i.e. possible types of interactions, become available and each with their own cross section. Since these interaction channels are not necessarily scalars of one another, e.g. one channel would be a neutral pion and the next would be a neutron, the only practical way to determine which interaction channel occurs is to use random numbers [12, 108]. For this reason, a Monte Carlo code such as CORSIKA was used to produce realistic simulations of EASs in the atmosphere.

From the different outputs from CORSIKA, the fair weather secondary electron longitudinal distribution, density, and energy spectrum has been determine for EASs initiated by several different cosmic ray primary proton energies that are important to the RREA lightning initiation model.

8.2.1. Fair Weather Secondary Electron Longitudinal Distribution

The longitudinal distribution is the total number of energetic secondary electrons at an arbitrary altitude regardless of electron energy or location in the shower front of a particular EAS. Figure 8.3 shows the longitudinal distribution of secondary electrons from EASs initiated by cosmic ray primary protons of various energies in fair weather conditions as determined by CORSIKA.

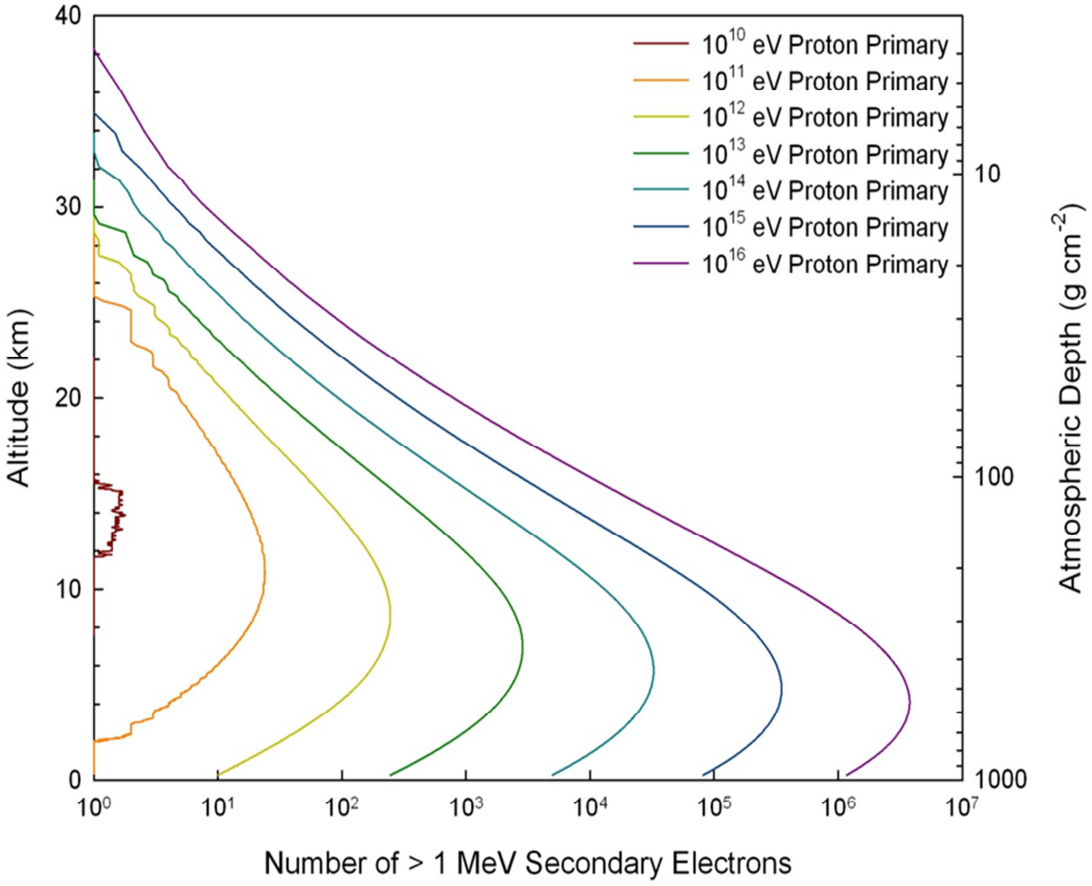

Figure 8.3: Average secondary electron longitudinal distribution of a single EAS with listed initial primary proton energy as determined by CORSIKA simulations.

For all cosmic ray primary proton energies, the number of >1 MeV secondary electrons first increases exponentially as the EAS travels through the atmosphere towards the ground until reaching a maximum and then quickly decreases until the EAS dissipates or reaches the ground. Each of the EASs in Figure 8.3 follows the qualitative description of the different stages in the development of an EAS shown in Figure 8.2. The only major differences that primary proton energy has on each of the EASs shown in Figure 8.3 is that EASs initiated by higher energy cosmic ray primaries generate more >1 MeV secondary electrons and have their shower maxima at a lower altitude than do lower energy cosmic ray primaries. From Figure 8.3, for every order of magnitude increase in the primary proton energy, the number of >1 MeV secondary electrons at shower maximum also increases by approximately an order of magnitude.

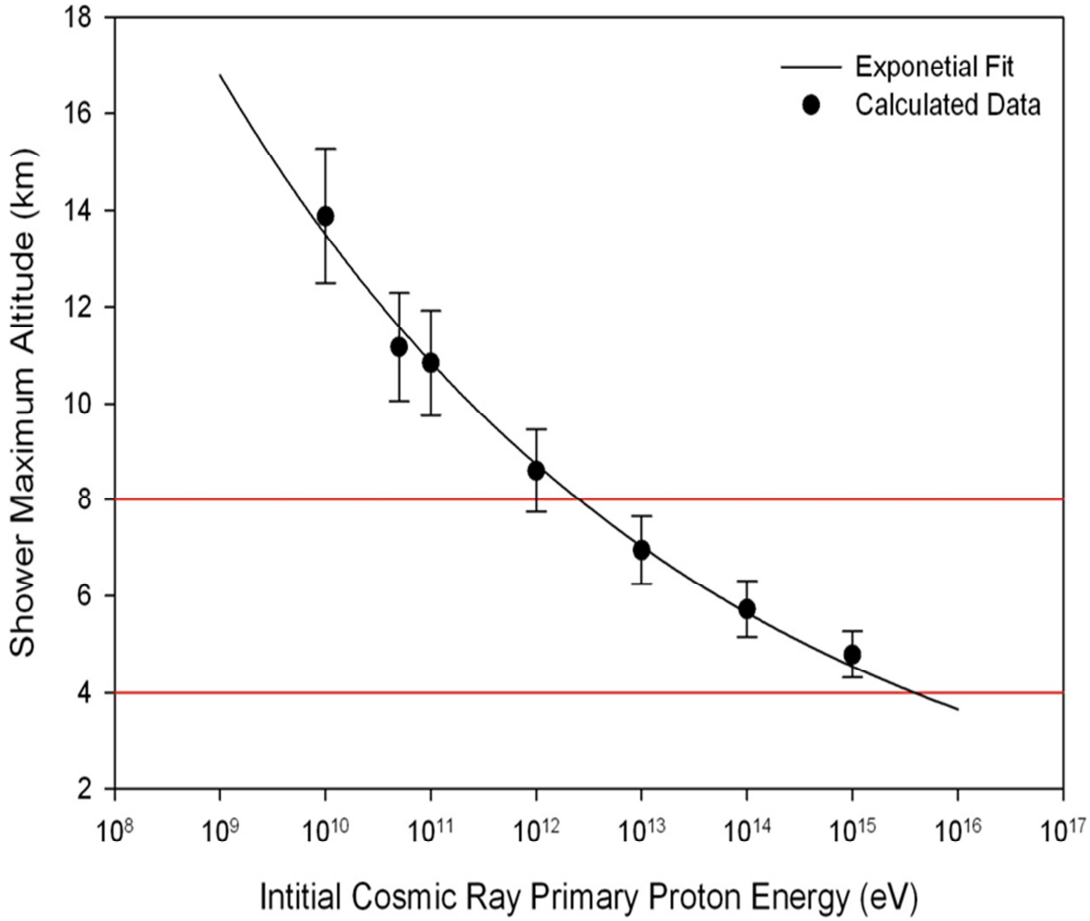

Figure 8.4: Shower maximum altitude as a function of initial cosmic ray primary proton energy. Typical lightning initiation altitudes lie between the two horizontal red lines.

As seen in Figure 8.2, the dividing line between a developing EAS and an attenuating EAS is the shower maximum. Figure 8.4 shows the altitude of shower maximum for each of the EASs shown in Figure 8.3. Figure 8.4 shows that the altitude of shower maximum decreases with increasing cosmic ray primary proton energy. EASs initiated by cosmic ray primary protons between 10^{12} and 10^{16} eV have their shower maximums at lightning initiation altitudes of 4 to 8 km. Therefore, EASs initiated by cosmic ray primary protons of those energies are typically still developing, and creating more secondary electrons with distance when they enter an active thunderstorm.

8.2.2. Fair Weather Secondary Electron Density

The fair weather secondary electrons density is calculated from the lateral distribution function, which was determined from CORSIKA's DAT output files. From equation (7.4), the secondary electron lateral distribution, n_{lat}, is a function of the radial distance from the shower axis, r, the total secondary electron energy (kinetic plus rest mass energies), E, the initial energy of the cosmic primary proton that generates the EAS, E_o, and the altitude of the observation level, h, which is symbolically written as,

$$n_{lat} = n(r, E, E_o, h). \tag{8.1}$$

The lateral distribution is divided into a two dimensional array in both radial distance and secondary electron energy for each of the primary proton energies listed in Table 7.1 and observation levels listed in Table 7.2. For this work, r varies between 10^{-1} and 10^{4} meters (10 cm to 10 km) and E varies between 10^{6} and 10^{11} eV (1 MeV to 100 GeV) in 0.1 logarithmic bins. Since all simulated EASs were vertical (see Chapter 7), the secondary electron distributions are also be assumed to be cylindrically symmetric about the shower axis [57, 58, 96].

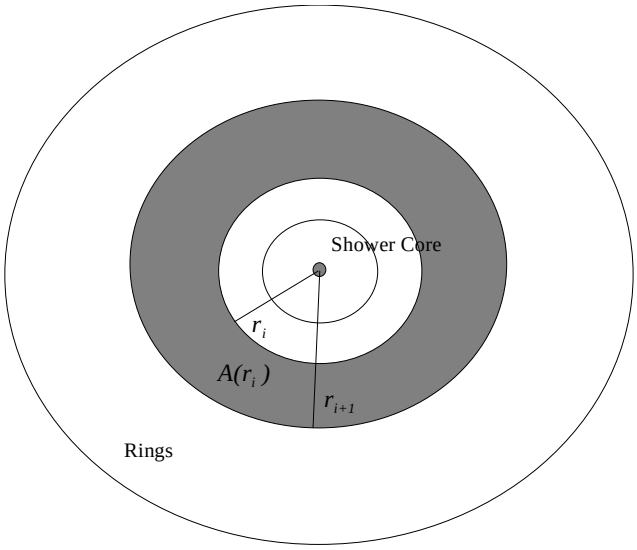

Figure 8.5: Diagram used to calculate the shaded area *A(r)* of the shower front as seen from above, i.e. EAS traveling into the paper.

From the secondary electron lateral distribution, the secondary electron density for a single EAS, d_{EAS}, is calculated by,

$$d_{EAS}(r, E_o, h) = \int_{10^6 eV}^{10^{11} eV} \frac{n_{lat}(r, E, E_o, h)}{A(r)} dE, \tag{8.2}$$

where *A(r)* is the area of the circular ring centered on the EAS shower axis that has an inner radius of *r*. A diagram of how *A(r)* is calculated is shown in Figure 8.5. The area, *A(r)*, is calculated by dividing the entire cross sectional area of an EAS shower front into circular rings, each with a radius of one of the values of the radial distance *r*. Since *r* has discrete values, *A(r)* for the i^{th} ring is given by,

$$A(r_i) = (r_{i+1}^2 - r_i^2)\pi. \tag{8.3}$$

Figures 8.6 through 8.8 show the fair weather density of >1 MeV secondary electron as a function of radial distance from the shower axis at different observation level altitudes. Each of the major ticks on the horizontal axis of Figures 8.6 to 8.8 corresponds to the next larger ring on the shower fronts shown in Figure 8.2. The secondary electron density is the average number of >1 MeV secondary electrons passing through arbitrary point in the atmosphere from a single EAS. Figure 8.6 shows the secondary electron density for EASs at an altitude of 12 km, the altitude of tops of most severe thunderstorms [3]. Figure 8.7 displays the fair weather secondary electron density in the middle of the lightning initiation altitudes of 4 to 8 km. Finally, Figure 8.8 shows the secondary electron density on the ground.

From the different stages of EAS development shown on Figure 8.2, EASs initiated by the three highest energies (10^{14} to 10^{16} eV) correspond to developing EASs where the hadronic cascade just ended at all three observation levels. According to Figure 8.4, all three of these EASs should be past their shower maxima in Figure 8.8. The only explanation for this discrepancy is that electromagnetic cascades of EASs initiated by higher energy cosmic rays must generate higher energy secondary electrons that stay in the shower core longer than the EAS assumed in Figure 8.2.

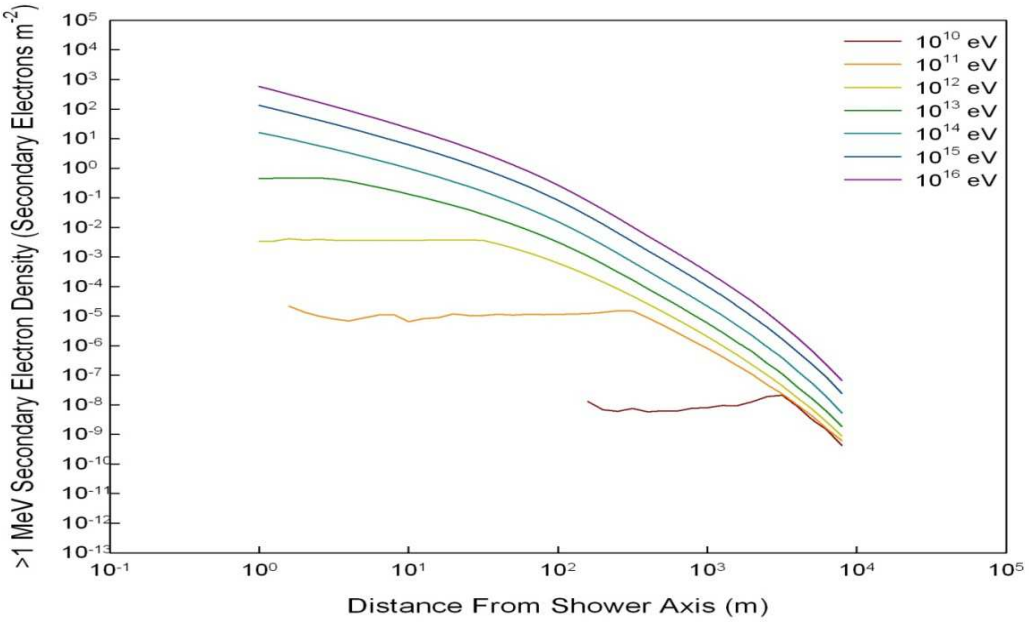

Figure 8.6: Fair weather density of >1 MeV secondary electrons at an altitude of 12 km from a single EAS initiated by the listed cosmic ray primary protons as a function of distance from the shower axis, based on CORSIKA simulated data.

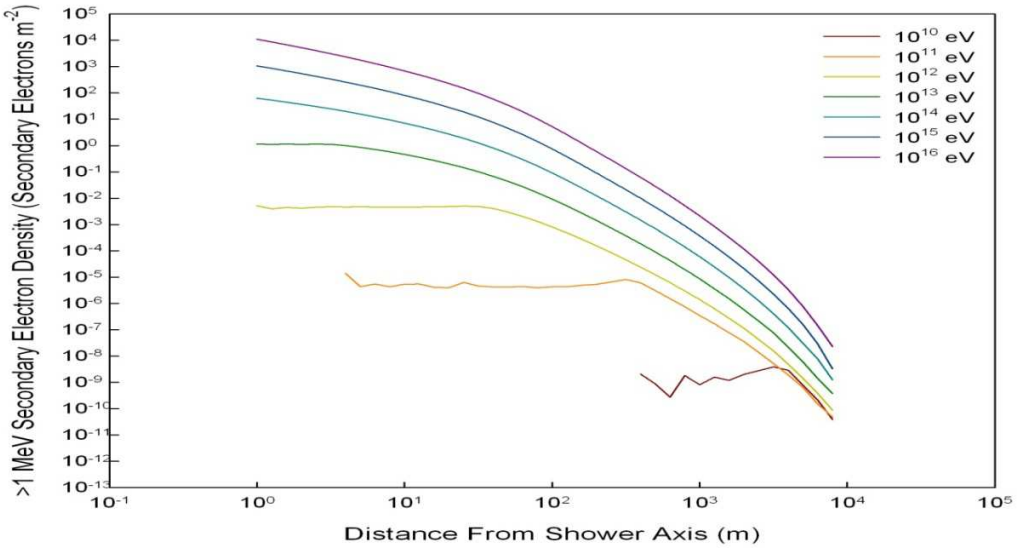

Figure 8.7: Fair weather density of >1 MeV secondary electrons at an altitude of 6 km from a single EAS initialed by the listed cosmic ray primary protons as a function of distance from the shower axis, based on CORSIKA simulated data.

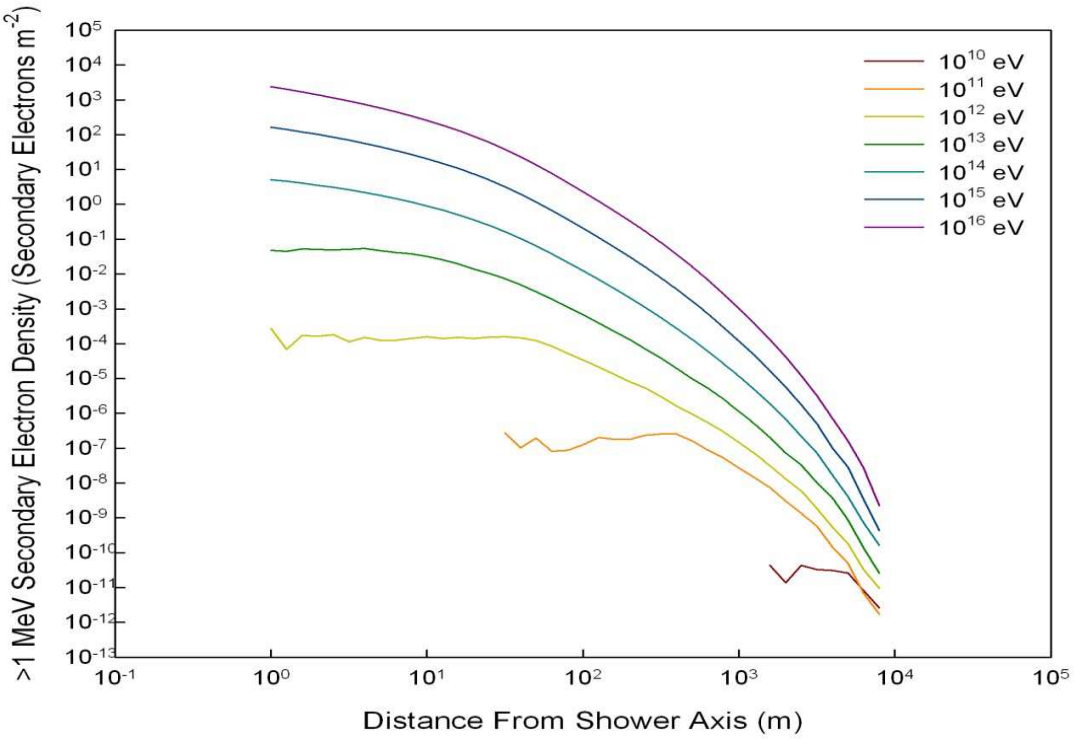

Figure 8.8: Fair weather density of >1 MeV secondary electrons on the ground from a single EAS initialed by the listed cosmic ray primary protons as a function of distance from the shower axis, based on CORSIKA simulated data.

EASs initiated by cosmic ray primary protons between 10^{12} and 10^{13} eV in Figures 8.6 to 8.8 correspond to EASs near their shower maxima in Figure 8.2. Even at the observation level on the ground, these EASs still have disk shaped shower fronts and not the ring shape shower fronts (i.e. no secondary electrons in the shower core) found at later stages of an attenuating EAS. However, EASs initiated by cosmic ray primary protons between 10^{10} and 10^{11} eV show the late stages of an attenuating EAS at all three observation levels in Figures 8.6 to 8.8.

Overall, Figures 8.6 to 8.8 show that the highest secondary electron density is found near the shower axis in a developing EAS. Only EASs initiated by the highest energy cosmic ray primaries are still developing at lightning initiation altitudes of 4 to 8 km. EASs initiated by low energy cosmic ray primaries are near or pass their shower maxima at lightning initiation altitudes. EASs initiated by $<10^{12}$ eV cosmic ray protons have traveled so far past their shower maxima that by lightning initiation altitudes, they are in the late stages of an attenuating EAS, having a ring shaped shower front and no secondary electrons are near the shower axis.

8.2.3. Fair Weather Secondary Electron Energy Spectrum

The secondary electron energy spectrum of an EAS is calculated from the lateral distribution described by equation (8.1) by selecting the radial distance from the shower axis, energy of cosmic ray primary proton that initiated the EAS, and the observation level altitude. Figure 8.9 shows the secondary electron energy spectra 10 m from the shower axes of different energy EASs at an altitude of 6 km from the CORSIKA simulations, i.e. in the first ring outside the shower core in Figure 8.2.

Each of the secondary electron energy spectra shown in Figure 8.9 follow the same trend where the number of secondary electrons increases with secondary electron energy from 1 MeV to a broad maximum near 100 MeV followed by a long decreasing tail for high secondary electron energies. Other than absolute value of the number of secondary electrons, the energy spectra for the each of the EASs initiated by different energy primary protons are almost identical. The nearly identical secondary electron energy spectra mean that the same range of secondary electrons energies can be found in an EAS at the same stage of development, regardless of the initial energy of the EAS. The energy of the primary cosmic ray that initiated the EAS just determines the total number of secondary electrons.

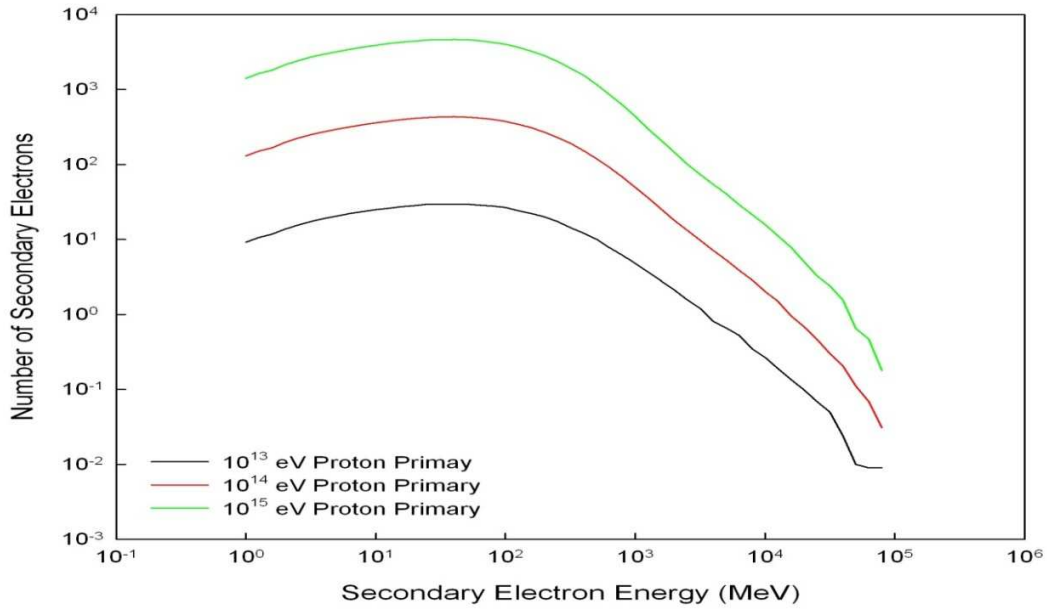

Figure 8.9: Secondary electron energy spectra 10 m from the shower axis of an EAS initiated by a cosmic ray proton primaries of the listed energies at an altitude of 6 km as derived CORSIKA simulations.

Figure 8.10 shows the secondary electron energy spectra at an altitude of 6 km of a 10^{15} eV cosmic ray primary proton initiated EAS at different radial distances from the shower axis. Unlike the almost identical curves of Figure 8.9, the energy spectra shown in Figure 8.10 are quite different from one another. The secondary energy spectrum 1 m from the shower axis, i.e. in the middle of the shower core, gradually increases with secondary electron energy from 1 MeV to a broad maximum near 1 GeV before slowly decreasing at higher secondary electron energies. In the shower front at a distance of 100 m from the shower axis, the number of secondary electrons increases rapidly to a maximum near 10 MeV and slowly decreases at higher energy. Figure 8.9 does show that >100 MeV secondary electrons do exist throughout the EAS shower front along with secondary electrons of lower energies.

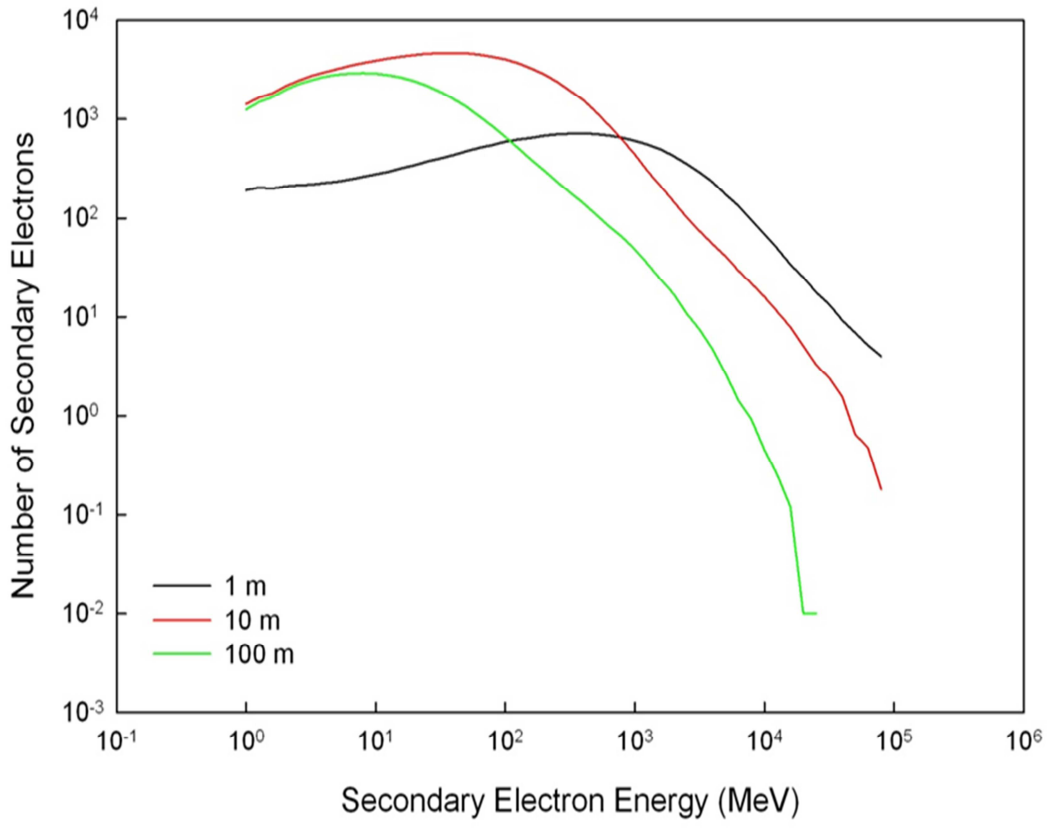

Figure 8.10: Secondary electron energy spectra at various distances from the shower axis of a 10^{15} eV proton primary EAS at an altitude of 6 km as derived from CORSIKA simulations.

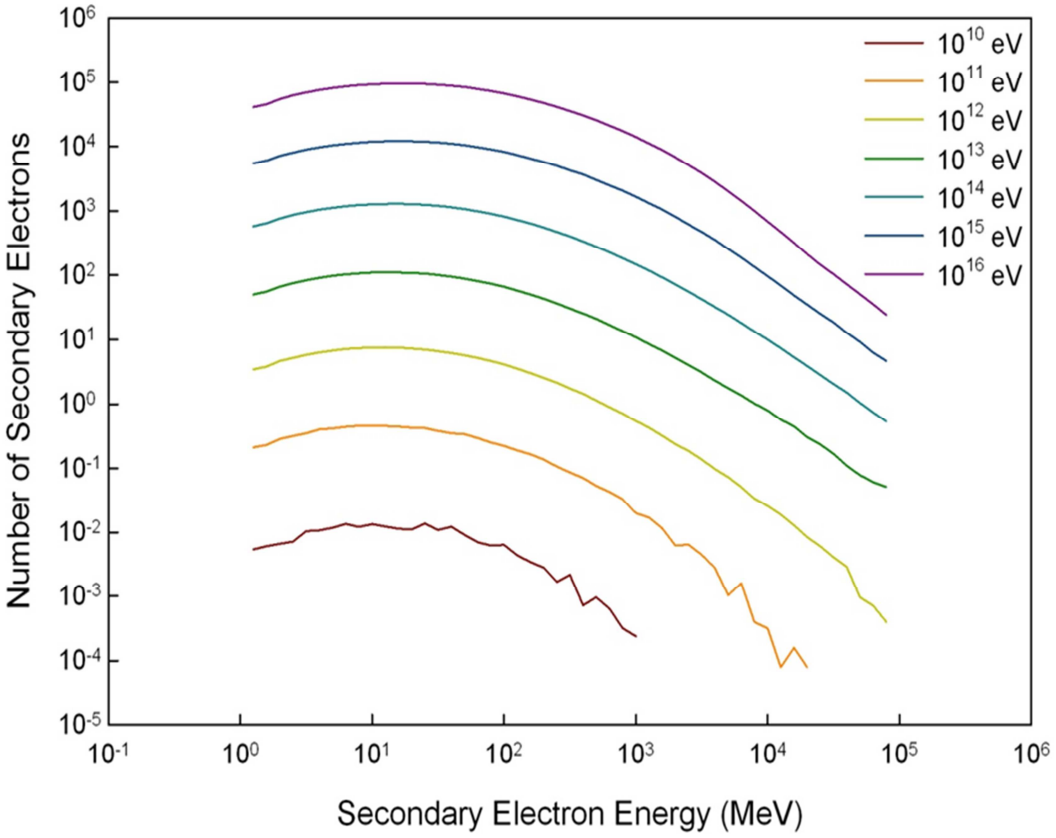

Figure 8.11: Secondary electron energy spectra of all the secondary electrons in an EAS of listed energy at an altitude of 6 km.

Figure 8.11 shows the secondary electron energy spectra of all the secondary electrons within an EAS of a given energy at an altitude of 6 km. The secondary electron energy spectra for Figure 8.11, ε_{EAS}, were calculated by,

$$\varepsilon_{EAS}(E, E_o, h) = \int_{10^{-1}m}^{10^{4}m} n_{lat}(r, E, E_o, h)dr. \tag{8.4}$$

For developing EASs, the secondary electron energy spectra look similar to the energy spectra from Figure 8.10, except that the high energy secondary electron tail decreases at a slower rate. Like the energy spectra shown in Figure 8.10, the secondary electron energy spectra are nearly identical, so the range of secondary electron energies is

approximately the same for all EASs of all energies. The number of secondary electrons of all energies increases with cosmic ray primary proton energy.

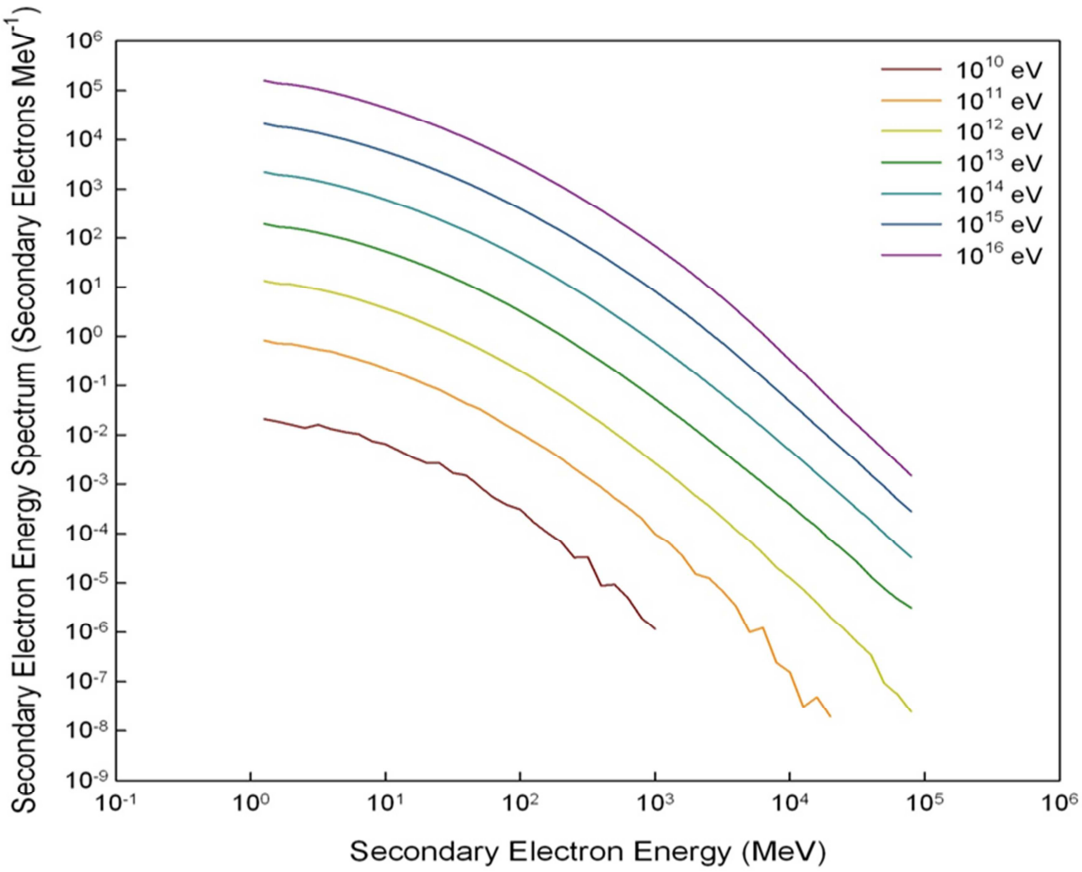

Figure 8.12: Differential secondary electron energy spectra of all the secondary electrons in an EAS initiated by cosmic ray primary proton of the listed energy at an altitude of 6 km. This is the differential form of the energy spectra shown in Figure 8.10.

The secondary electron energy spectra that are reported in the literature [11, 90] typically are not calculated by equation (8.4), but instead take the form of the differential energy spectrum given by,

$$\varepsilon_{diff}(E, E_o, h) = \int_{10^{-1}m}^{10^{4}m} \frac{n_{lat}(r, E, E_o, h)}{B(E)}\, dr, \tag{8.5}$$

where *B(E)* is the size of the energy bins in units of MeV used in the lateral distribution. The differential secondary electron energy spectrum is used instead of the energy

spectrum to remove the bias on the size the energy bins from calculations or measurements of the energy spectrum. Figure 8.12 shows a plot of the differential secondary electron spectra for the same EASs shown in Figure 8.7. The differential energy spectra rapidly decrease from a maxima at 1 MeV to approximately 10 MeV, before the decrease slows between 10 MeV and 1 GeV, and then decrease rapidly again above 1 GeV electrons. This trend describes all the differential energy spectra, as long as the EAS has secondary electrons of those energies. The differential secondary electron energy spectra show that the energy of the EAS only has an effect on the overall number secondary electrons in the EAS and little effect on the secondary electron energy distribution.

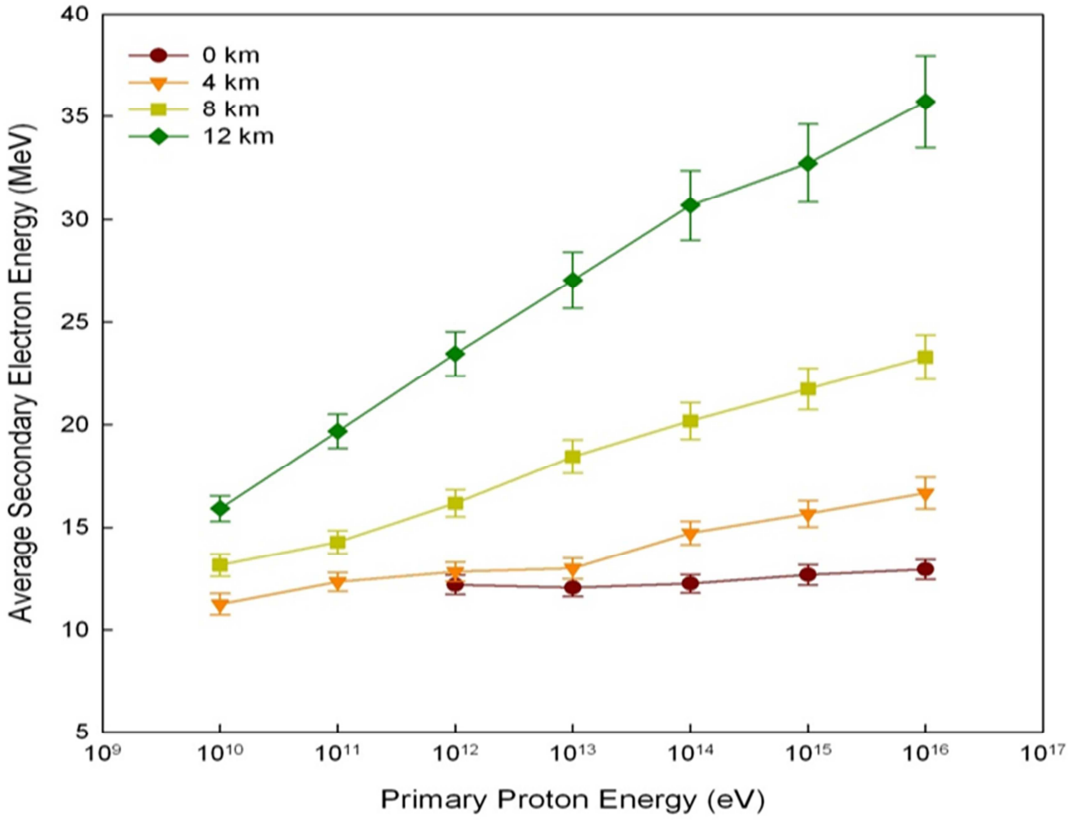

Figure 8.13: The average secondary electron energy as a function of primary proton energy at various altitudes. Error bars represent one sigma.

Other ways to look at the distribution of secondary electron energy is to observe how the average secondary electron energy changes with the energy of the initiating cosmic ray primary proton. The average secondary electron energy in an EAS, E_{avg}, as a function of

the cosmic ray primary proton energy was calculated from the lateral distribution function via,

$$E_{avg}(E_o,h) = \frac{\int_{10^6 eV}^{10^{11} eV} \int_{10^{-1} m}^{10^4 m} E n_{lat}(r,E,E_o,h) dr dE}{\int_{10^6 eV}^{10^{11} eV} \int_{10^{-1} m}^{10^4 m} n_{lat}(r,E,E_o,h) dr dE}. \quad (8.6)$$

Figure 8.13 shows the average secondary electron energy as a function of cosmic ray primary proton energy at thunderstorm altitudes. According to Figure 8.8, the average secondary electron energy for EASs well past their shower maximums is still >10 MeV. The average secondary electron energy increases with the initial energy of the cosmic ray primary proton that created the EAS. Due to the secondary electron energy being shown in log scale, this increase in the average secondary electron energy was not visible in Figure 8.9.

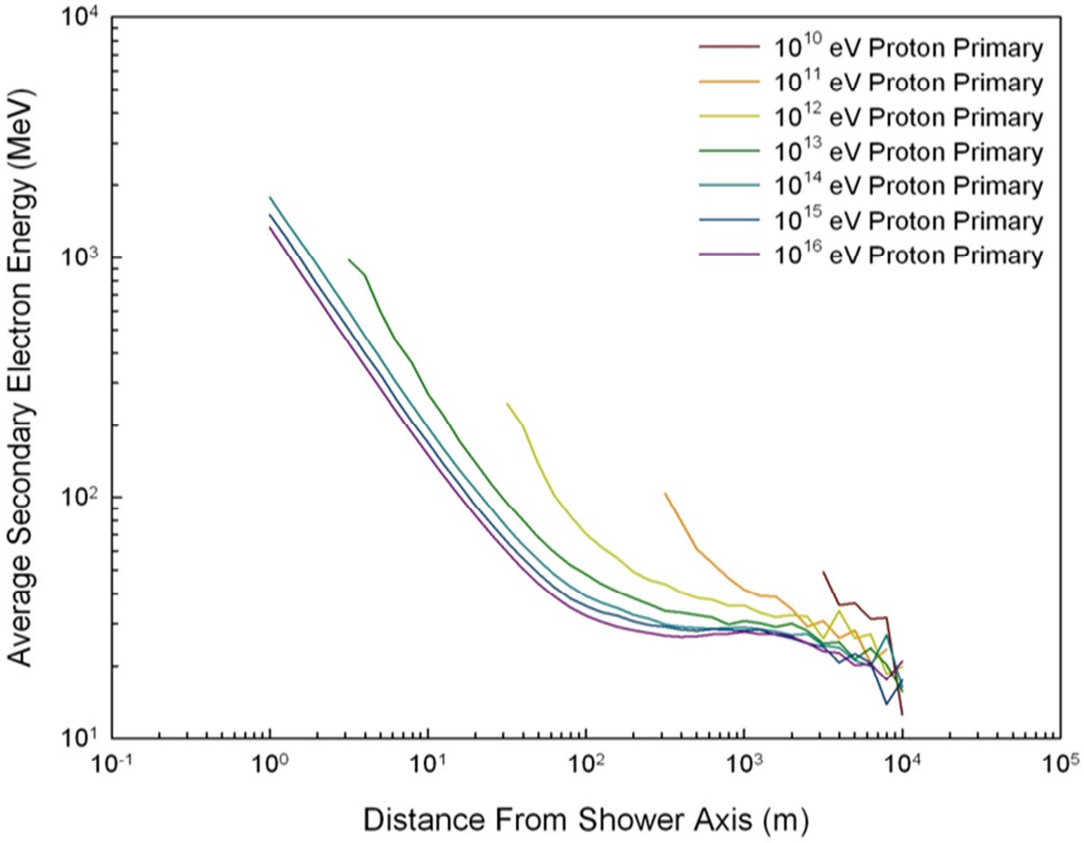

Figure 8.14: The average secondary electron energy at 6 km altitude for EAS of listed initial primary proton energies as a function of distance from the shower axis.

The qualitative description of EAS development in Section 8.1 states that lower energy secondary electrons are scattered farther from the shower axis towards the edge of the shower front than higher energy secondary electrons. The average secondary electron energy can be calculated as a function of radial distance, $E_{avg\,r}$, by,

$$E_{avg\,r}(r, E_o, h) = \frac{\int_{10^6 eV}^{10^{11} eV} E n_{lat}(r, E, E_o, h) dE}{\int_{10^6 eV}^{10^{11} eV} n_{lat}(r, E, E_o, h) dE}. \tag{8.7}$$

Figure 8.14 shows how the average secondary electron energy changes with radial distance. The average secondary electron energies shown in Figure 8.14 are based on the same results used to calculate the secondary electron density in Figure 8.7, which explains why the attenuating EASs do not have any secondary electrons near the shower axis. For developing EASs, the average secondary energy decreases from ~1 GeV to ~100 MeV in less than 10 m from the shower axis. Outside of the shower core region (~10 m from shower axis), the average secondary electron energy decreases at a slower rate from ~100 MeV to ~10 MeV at 1 km from the shower axis. For attenuating EASs past their shower maxima, the secondary electrons originating near the shower axis have either ranged out or scattered towards the edges of the shower front.

8.3. Fair Weather Ambient Secondary Electron Environment

Any measurement of the secondary electrons in the atmosphere will include secondary electrons from multiple EASs in various stages of development and not just a single EAS as discussed in Section 8.2. Using the geometry of an EAS (Chapter 7 and Section 8.1), primary cosmic ray flux (Figure 5.1), and the results from Section 8.2, the fair weather ambient secondary electron environment, i.e. flux and energy spectrum, are determined. Due to the stochastic nature of the arrival of cosmic ray primaries and individual processes within the EAS, the ambient secondary environment represents the average secondary electron distribution over a period a time.

8.3.1. Fair Weather Ambient Secondary Electron Flux

In order to determine the fair weather ambient flux of secondary electrons at a specific observation point in the atmosphere, the secondary electron density of each of the different EAS energies must be weighted by primary cosmic ray flux at the top of the atmosphere [68]. Assigning a weight to the secondary electron density to determine the ambient secondary electron flux is performed in three steps. The first step is to calculate the weighted secondary electron density, denoted w_{EAS}, by,

$$w_{EAS}(r, E_o, h) = \varphi_{primary}(E_o) d_{EAS}(r, E_o, h), \tag{8.8}$$

where $\varphi_{primary}$ is the cosmic ray primary proton flux measured at the top of the atmosphere. For this work, $\varphi_{primary}$ was taken from *Horandel* [69] as,

$$\varphi_{primary}(E_o) = (8.73 * 10^{-2}\ m^{-2} sr^{-1} s^{-1}) \left(\frac{E_o}{10^{12} eV}\right)^{-2.71}. \tag{8.9}$$

The second step is to convert the weighted secondary electron density into a weighted flux, i.e. the rate at which secondary electrons travel through the observation point. The weighted secondary electron flux, w_{flux}, is calculated from,

$$w_{flux}(r, E_o, h) = w_{EAS}(r, E_o, h) A(r). \tag{8.10}$$

The area *A(r)* has the same value as in equation (8.3) but now represents the area of a region where EAS are a distance *r* from an observation point. The observation point in the atmosphere is not necessarily along the shower axis of an EAS. The third step in determining the ambient secondary fluxes is to sum up the weighted secondary electron flux from all the EASs in the region surrounding the observation point in the atmosphere. The ambient secondary electron flux, $\varphi_{electrons}$, is given by,

$$\varphi_{electrons}(h) = \int_{10^{-1}m}^{10^{4}m} \int_{10^{10}eV}^{10^{16}eV} w_{flux}(r, E_o, h) dE_o dr$$

$$= \int_{10^{-1}m}^{10^{4}m} \int_{10^{10}eV}^{10^{16}eV} \int_{10^{6}eV}^{10^{11}eV} \varphi_{primary}(E_o) n_{lat}(r, E, E_o, h) dE dE_o dr. \tag{8.11}$$

The ambient secondary electron flux describes the constant rate of EAS secondary electrons in the atmosphere.

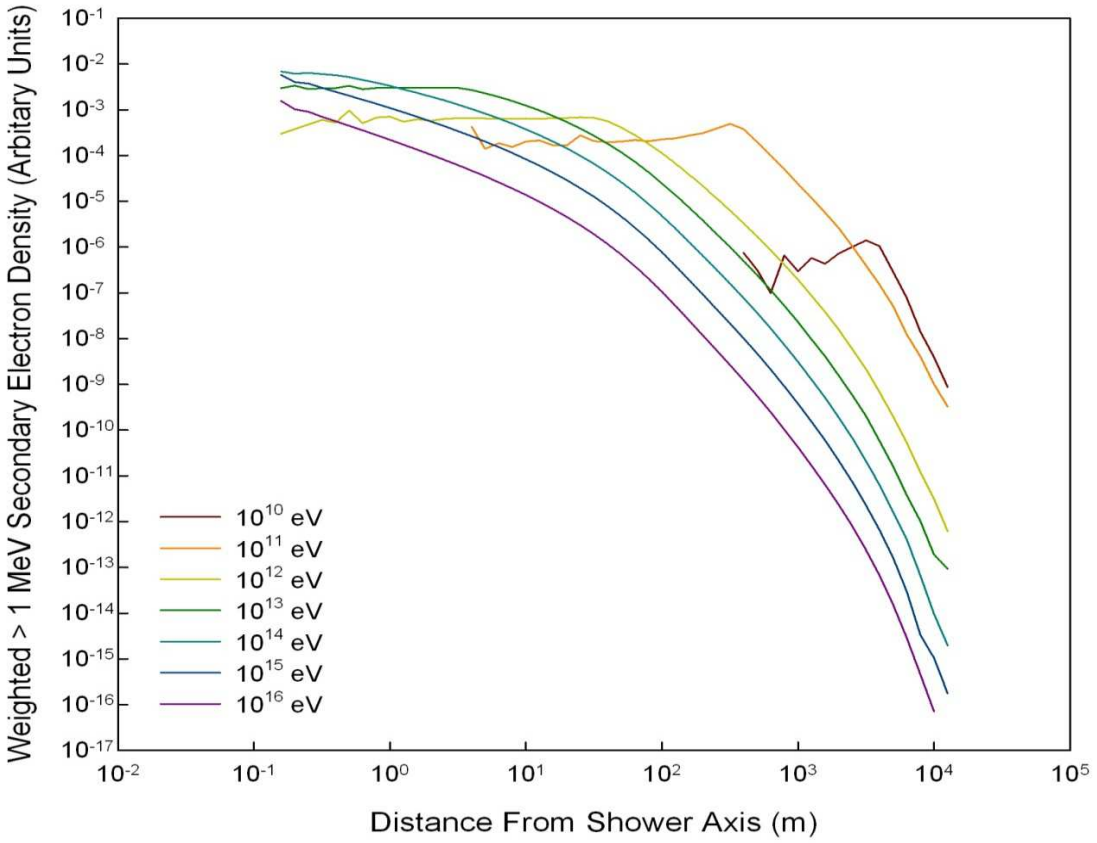

Figure 8.15: The weighted >1 MeV secondary electron density at a 6 km altitude for EASs initiated by cosmic ray proton primaries of listed energy. Data from Figure 8.7 was used to obtain these results.

Figure 8.15 shows the weighted secondary electron densities from the EASs shown in Figure 8.7. The weighted secondary electron densities describe which energy of EASs produce the most secondary electrons at a certain distance away from their shower axes. From Figure 8.15, 10^{13} to 10^{14} eV cosmic ray primary proton initiated EASs produce the most secondary electrons near their shower axes. This is because EASs of those primary proton energies occur relatively frequently in the atmosphere and that are near their shower maxima at an altitude of 6 km. Near the edge of the shower front, the majority of >1 MeV secondary electrons are generated from the numerous EASs initiated by lower energy cosmic ray primary protons that have developed well past their shower maxima and have ring shaped shower fronts. In general, EASs initiated by lower energy cosmic ray primaries make a greater contribution to the weighted secondary electron density, even though individual EAS initiated by higher energy cosmic ray primaries produce

many more secondary electrons at this altitude. The weighted secondary electron density is an intermediate calculation between the secondary electron density and the ambient secondary electron flux.

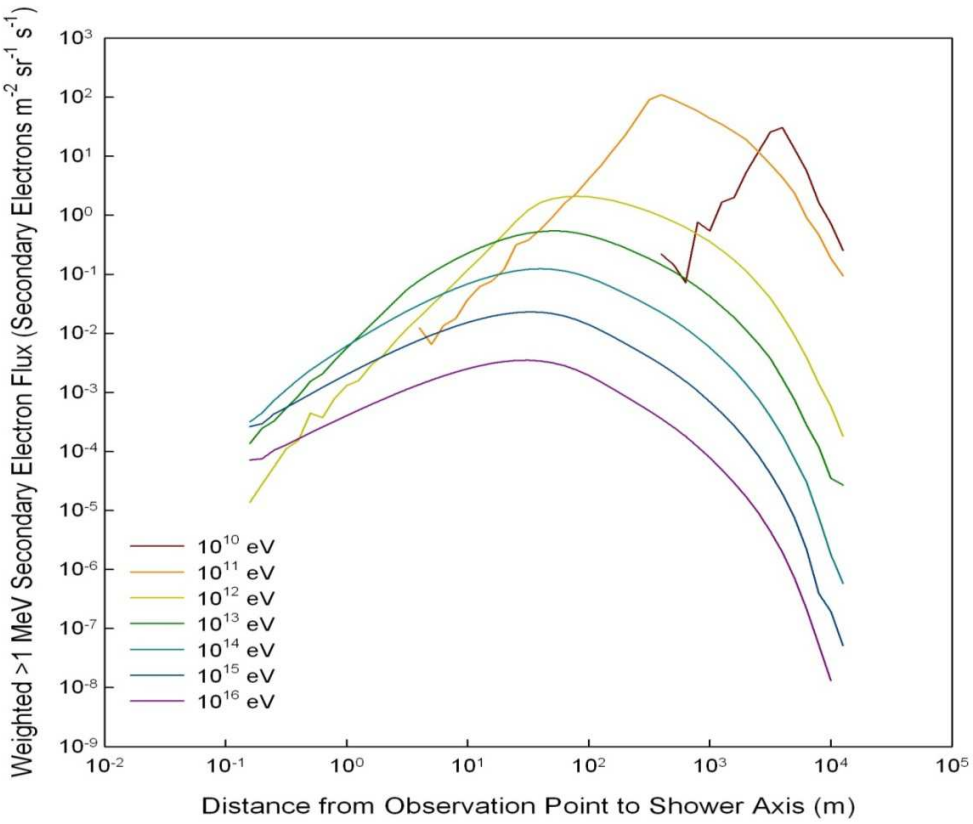

Figure 8.16: Weighted >1 MeV secondary electron flux at the observation point at an altitude of 6 km for EASs initiated by primary protons of listed energy. Data was calculated from the data the results shown in Figure 8.7.

The weighted secondary electron flux is the flux of secondary electrons at the observation point due to EASs that have their shower axes a certain distance away. Figure 8.16 shows the >1 MeV weighted secondary electron flux calculated from the >1 MeV secondary electron densities shown in Figure 8.7 and the weighted >1 MeV secondary electron densities shown in Figure 8.15. The distance used in Figure 8.16 is not the distance the electrons have to travel to reach the observation point in the atmosphere, but the distance the observation point is away from the shower axis of the EAS whose secondary electrons traveled through the observation point. Due to the flux of cosmic ray primaries being assumed to be isotropic at the top of the atmosphere [68, 70] and EASs having circular symmetry about the shower axis [103], the number of EASs that are a certain

distance away from an observation point is proportional to the area of a ring with the observation point at its center. Therefore as the distance between the observation point and the EAS increases, the total number of EASs that can have secondary electrons at the observation point increases. However, the secondary electron density decreases rapidly near the edge of the shower front, so the weighted secondary electron flux reaches a maximum then starts to decrease. Just like the weighted secondary electron density in Figure 8.15, lower energy EASs dominate the weighted secondary electron flux, especially at large distances between the observation point and the EAS shower axes

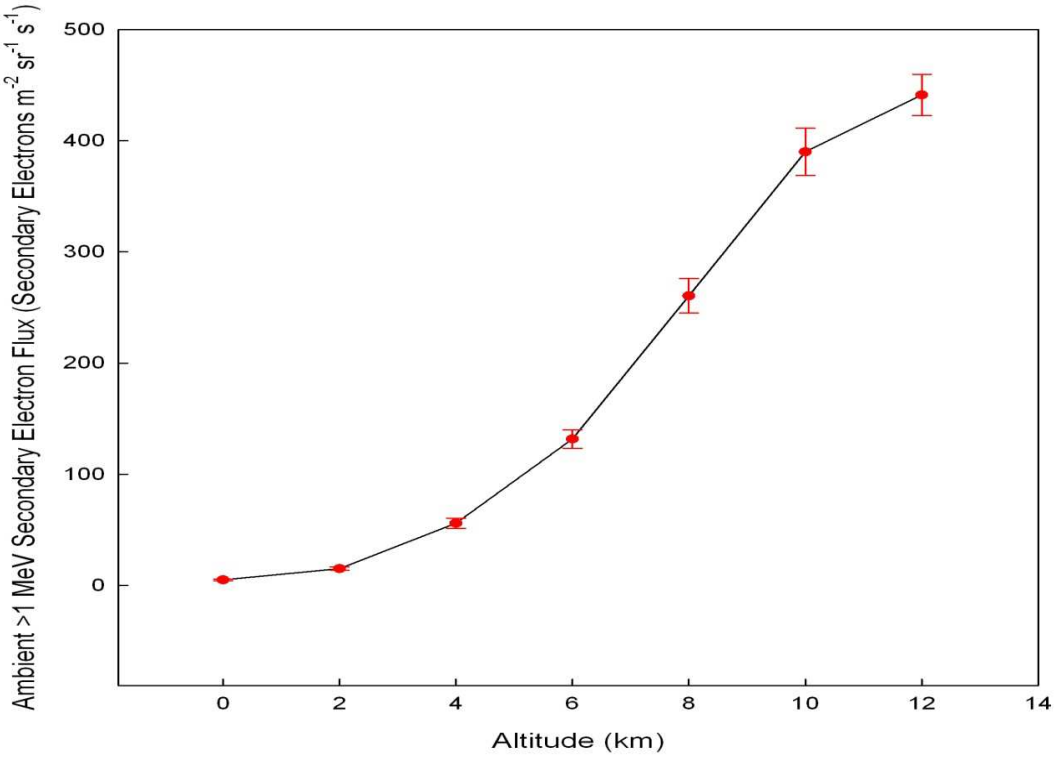

Figure 8.17: Fair weather ambient >1 MeV secondary electron flux as a function of altitude calculated from CORSIKA simulations. Error bars represent one sigma.

The fair weather >1 MeV ambient secondary electrons flux as a function of altitude is shown in Figure 8.17. The fair weather ambient secondary electron flux increases with altitude from ~5 secondary electrons m^{-2} sr^{-1} s^{-1} at the ground to ~300 secondary electrons m^{-2} sr^{-1} s^{-1} at 8 km and ~450 secondary electrons m^{-2} sr^{-1} s^{-1} at 12 km. The majority of secondary electrons that make up the ambient flux are secondaries from EASs initiated by lower energy cosmic ray primaries that have developed far away from the observation point. In ambient conditions, EASs generated by $>10^{15}$ eV proton primaries are rare events that briefly increase the number of secondary electrons well above ambient levels.

8.3.2. Fair Weather Ambient Secondary Electron Energy Spectrum

The fair weather ambient secondary electron energy spectrum describes the background energy distribution of secondary electrons due to the constant flux of EASs through the atmosphere. Like the secondary electron energy spectrum of an EAS described in Section 8.2.3., the ambient secondary electron energy spectrum is typically presented as the differential energy spectrum. The ambient differential secondary electron energy spectrum can be calculated by the same method used to calculate the ambient secondary electron flux in Section 8.3.1. The ambient differential secondary electron energy spectrum is calculated by,

$$\varepsilon_{ambient}(E,h) = \int_{10^{10}eV}^{10^{16}eV} \int_{10^{-1}m}^{10^{4}m} \frac{\varphi_{primary}(E_o) n_{lat}(r,E,E_o,h)}{B(E)} dr dE_o. \tag{8.12}$$

Figure 8.18 shows the fair weather ambient secondary electron energy spectrum calculated from the CORSIKA data used in this research. Like the ambient flux, the ambient secondary electron energy spectrum increases in absolute value with altitude. This is due to the ambient secondary electron flux being the integral with respect to secondary energy scaled by *B(E)* of the ambient energy spectrum. The ambient secondary electron energy spectra are almost identical, except for absolute value, to one another just like the energy spectra shown in Figure 8.12.

The ambient differential secondary electron energy spectrum is the distribution of secondary electron energies that are measured at the same observation point that was used to determine the ambient flux. The ambient differential energy spectra decreases at a faster rate for all secondary electron energies than does the differential energy spectra shown in Figure 8.12. This is because the ambient differential energy spectrum, just as the ambient flux, is dominated by EASs initiated by lower energy cosmic ray primaries. EASs initiated by lower energy cosmic ray primaries have far fewer secondary electrons, including fewer very high energy secondary electrons, than the less frequent high energy EASs initiated by higher energy cosmic ray primaries.

Previous experiments [89] have found that the ambient secondary electron energy spectrum could be fit by two different power law functions of the form

$$\varepsilon_{power\ law}(E,h) = a_i E^{\gamma_i}, \tag{8.11}$$

where a_i is a parameter to fit the absolute value of the differential flux and γ_i is the power law index of the i^{th} ambient secondary electron spectra. For the ambient secondary electron energy spectra plotted in Figure 8.18 in logarithmic scale on both axes, a power law fit would be a straight line. The first power law fits the secondary electron energies

between 10 MeV and 1 GeV and the other power law is fitted for secondary electrons >1 GeV. Table 8.1 lists the fitted power law indexes for both the 10 MeV to 1 GeV and the >1 GeV curves from the EAS data simulated by CORSIKA.

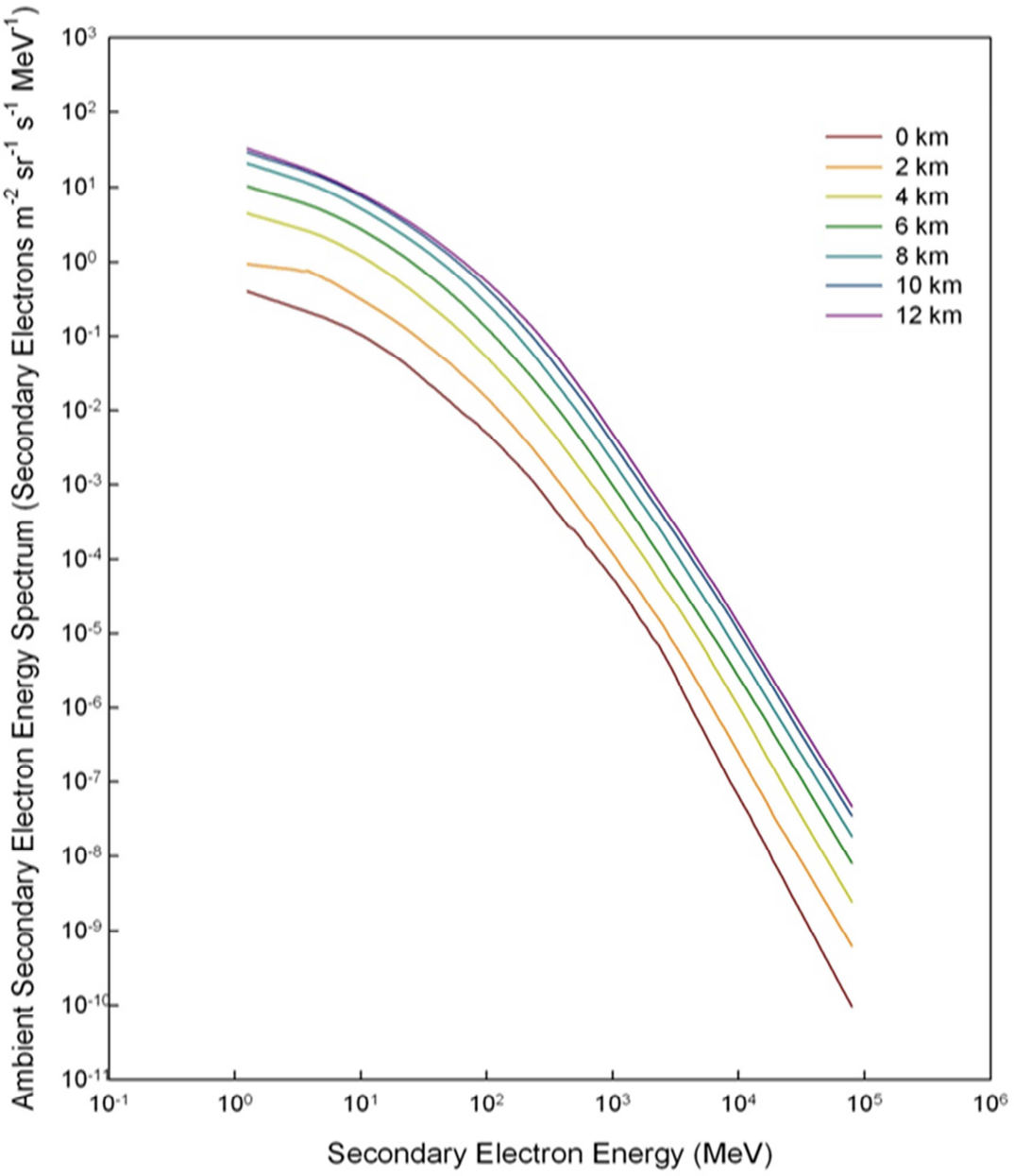

Figure 8.18: The fair weather ambient secondary electron energy spectrum at various altitudes as calculated from CORSIKA simulations.

Table 8.1: Fitted power law indexes of the ambient secondary electron energy spectra for 10 MeV to 1 GeV and >1 GeV secondary electron energies for different altitudes.

Altitude (km)	10 MeV to 1 GeV Power Law Index	> 1 GeV Power Law Index
0	-1.669 ± 0.060	-3.159 ± 0.085
2	-1.691 ± 0.056	-2.853 ± 0.039
4	-1.696 ± 0.046	-2.787 ± 0.050
6	-1.669 ± 0.048	-2.676 ± 0.025
8	-1.663 ± 0.059	-2.690 ± 0.019
10	-1.609 ± 0.055	-2.667 ± 0.026
12	-1.532 ± 0.054	-2.652 ± 0.025

8.4. Comparisons with Previous Results

All the results presented in the Sections 8.2 or 8.3 were calculated from secondary cosmic ray data generated using CORSIKA. CORSIKA was verified with cosmic ray and accelerator experiments [13, 93, 94, 95], which are typically trying to measure the highest energy EASs [93, 94]. This work is focused on 10^{10} to 10^{16} eV primary proton initiated EASs that are typically background events to current cosmic ray experiments such as Pierre Auger and Icecube projects [91, 109]. Thus, measurements of EASs initialized 10^{10} to 10^{16} eV cosmic ray proton primaries are typically not published.

The most frequently referenced paper on the ambient secondary electron energy spectrum for EASs initiated by $<10^{16}$ eV cosmic ray primaries is *Daniel and Stephens* from 1974 [90]. Even recently published cosmic ray reference texts [11] directly reuse the results from *Daniel and Stephens*. *Daniel and Stephens* was originally written as a review paper on all the balloon borne experiments that measured secondary electrons, positrons, and gamma photons in the atmosphere up to that time. *Daniel and Stephens* also presented model calculations of the ambient secondary electron flux in the atmosphere. However, the majority of secondary electron measurements where collected at the top of the atmosphere, well above the lightning initiation altitudes of 4 to 8 km.

The only direct comparison that can be made between the results published in *Daniel and Stephens* and this work's CORSIKA derived results are in the two power law fits of the ambient secondary electron energy spectrum near the ground. The absolute value of the differential flux calculated in this work and in *Daniel and Stephens* were within an order of magnitude of each other [90]. For the 10 MeV to 1 GeV secondary electrons, the power law index was approximately -2.0 and for >1 GeV secondary electrons, the power

index was determined to be -2.9 [90]. There is discrepancy (-1.7 vs. -2.0) in the value of the power law index between the differential flux calculated in this work and the measurements in *Daniel and Stephens* for the 10 MeV to 1 GeV power law. However, there was a close agreement (-3.1 vs. -2.9) in the power law indices for the greater than one GeV power law. No errors were reported with the power indexes in *Daniels and Stephens*, so there is no way of knowing how much of a discrepancy there was between the power laws calculated in this work and that from previous measurements [90].

Due to the lack of published results on the secondary electron environment at thunderstorm altitudes, the original authors of the RREA lightning initiation model had to assume a secondary electron distribution as an input parameter for the model. In a series of studies by *Gurevich et al.* [9, 15, 110], the theory of RREAs was developed, as described in Chapter 6, as a method to initiate a lightning discharge. One of the main findings was that the electron stopping power in air (Figure 6.4) had a minimum ~1 MeV. *Gurevich et al.* [9] proposed that only electrons near the minimum ionizing energy of 1 MeV would be able to run away in strong electric fields and generate RREAs. Thus, *Gurevich et al.* assumed that all the secondary electrons were approximately 1 MeV and could runaway together, similar to how the secondary electron longitudinal distribution was determined [89]. *Gurevich et al.* did not consider >10 MeV secondary electrons could run away in the electric field, because they still lost energy with distance.

There are two main problems with the assumed secondary electron energy distribution. First, the secondary electrons are spread out over several square kilometers, as is shown in Figure 8.7, and there is no way that all the electrons of an EAS could affect a small localized region, such as around a charged hydrometeor, at the same time. The second reason why the secondary electron distribution assumed in *Gurevich et al.* is unrealistic is that from the energy spectra plotted in Figure 8.11. The secondary electron energy spectrum shown in Figure 8.11 shows that there more >10 MeV secondary electrons than secondary electrons between 1 and 10 MeV at lightning initiation altitude of 4 to 8 km in an EAS. In Chapter 6, secondary electrons that were higher energy than the equilibrium runaway energy (Figure 6.10) still lost energy with distance, but were still accelerated in the electric field and will run away in strong electric fields. These secondary electrons were called decelerating runaway electrons due to the fact these electrons still lose kinetic energy, i.e. are decelerating, but still runaway in the strong electric field and produce RREAs. By not considering >10 MeV secondary electrons as possible runaway electrons, *Gurevich et al.* was removing a large population of runaway electrons from their model.

The fair weather secondary electron environment was calculated in this work as an input parameter into the RREA and hybrid lightning discharge models. However, a lightning discharge can occur if enough electric charge is collected into a small area to generate electric streamer system, regardless of whether it is in fair weather or thunderstorm

conditions [10]. From long spark theory, *Dawson and Winn* in 1965 [58] theoretically determined that a streamer will propagate through the atmosphere if 10^8 electrons reside within a sphere with a radius of 30 μm. *Dawson and Winn* calculated that density of low energy electrons would produce a strong enough electric field to ionized the surrounding ambient, no electric field atmosphere and generate a propagating streamer. There has not been an update of this calculation or computer model simulation of this process since *Dawson and Winn* [10, 20, 58]. A lightning leader is initiated by a series of propagating streamers (Section 4.1.4), so this work is using the electron density calculated by *Dawson and Winn* as a necessary condition for lightning initiation for the RREA model.

The density inside the core of an EAS initiated by a 10^{16} eV cosmic ray primary proton can reach ~10^5 electrons m^{-2}, according to Figure 8.7. Even assuming that the thickness of the shower core is <20 μm, which is not realistic [12], the number secondary electrons inside the 30 μm radius sphere is ~10^{-4}, which is twelve orders of magnitude too low to initiate an electric streamer. Therefore individual EASs and the ambient flux do not have sufficient number secondary electrons to initiate a lightning discharge in the fair weather atmosphere. However, the RREA model proposes that there are a sufficient number of runaway secondary electrons are generated by the fair weather "seed" electrons in the strong electric field regions of a thunderstorm to initiate a streamer.

CHAPTER IX

SECONDARY ELECTRON ENVIRONMENT IN THUNDERSTORM CONDITIONS

The cosmic ray secondary electron environment calculated from CORSIKA simulations discussed in Chapter 8 were generated assuming fair weather conditions, i.e. no strong electric fields. Thunderstorms produce strong electric fields up to several hundred kilovolts per meter [26], which affects the distribution of secondary electrons within an EAS. In thunderstorm electric fields, the secondary electrons initiate RREAs and generate more high energy secondary electrons than in fair weather conditions. The RREA model of *Gurevich et al.* [9] and the hybrid model of *Petersen et al.* [10] theorize that RREAs initiated by secondary electrons from EASs are sufficient to initiate a lightning discharge.

9.1. Production of Secondary Electrons in the Atmosphere

The electron stopping power in fair weather and thunderstorm conditions was discussed previously in Chapter 6. The change in the kinetic energy, ΔE, of a secondary electron after traveling a distance, Δx, in the atmosphere is given by,

$$\Delta E = \left(\frac{dE}{dx}\right)_{compound}(h)\Delta x + e\varepsilon(h)\Delta x, \tag{9.1}$$

where the stopping power is calculated from equation (6.5) for either dry air (fair weather) or moist air (thunderstorm conditions), e is the charge of an electron, and $\varepsilon(h)$ is the electric field at the altitude h. For this work, the change in kinetic energy of the EAS secondary electrons w calculated with equation (9.6) every meter, i.e. Δx = 1 m, inside the thunderstorm electric field region. The number of additional secondary electrons (both high and low energy) generated where calculated every time the energy of the EAS secondary electron is modified.

The number of high energy electrons, i.e. electrons able to run away in the electric field, was calculated by,

$$n_{High}(E, E_{min}) = \frac{\int_{E_{min}}^{E/2} E\sigma(E, E')dE'}{E_{min}}, \tag{9.2}$$

where $\sigma(E, E')$ is the Mott scattering cross section defined in equation (6.2), n_{High} is the number of additional high energy secondary electrons generated by a primary high energy electron and $E' = \frac{W}{E}$ and E_{min} is the minimum runaway energy for the particular altitude and electric field strength. The minimum runaway energy is the minimum kinetic energy required for an electron to run away in a given electric field strength and altitude. The number of low energy electron secondaries generated by the EAS secondary electrons is calculated from,

$$n_{Low}(E, E_{min}) = \frac{\left(\frac{dE}{dx}\right)_{ion} \Delta x - \int_{E_{min}}^{E/2} E\,\sigma(E, E')dE'}{E_{ion}}, \tag{9.3}$$

where $\left(\frac{dE}{dx}\right)_{ion}$ is the collisional stopping power defined in equation (6.1) and E_{ion} is the average energy lost by a primary electron to generate a single low energy secondary electron. For air, E_{ion} = 34 eV [41].

9.2. Relativistic Electrons in Constant Accelerating Electric Fields

According to equation (9.1), an energetic electron will gain energy with distance in an accelerating electric field relative to a similar electron in fair weather conditions. Figure 9.1 shows the energy of a 100 MeV electron starting at an altitude of 12 km as it travels downward through the atmosphere in various constant accelerating electric fields. In <100 kV m^{-1} electric fields, the electron loses energy with distance and eventually ranges out. In fair weather conditions (0 kV m^{-1}), the 100 MeV electron travels less than a kilometer at an altitude of 11 km before ranging out, but in a 100 kV m^{-1} constant electric field, a similar 100 MeV electron ranges out just below an altitude of 8 km. Even through the electron never gains more energy from being accelerated in the electric field than it loses to ionization and bremsstrahlung, the electron in the 100 kV m^{-1} electric field still travels three kilometers farther than in fair weather conditions.

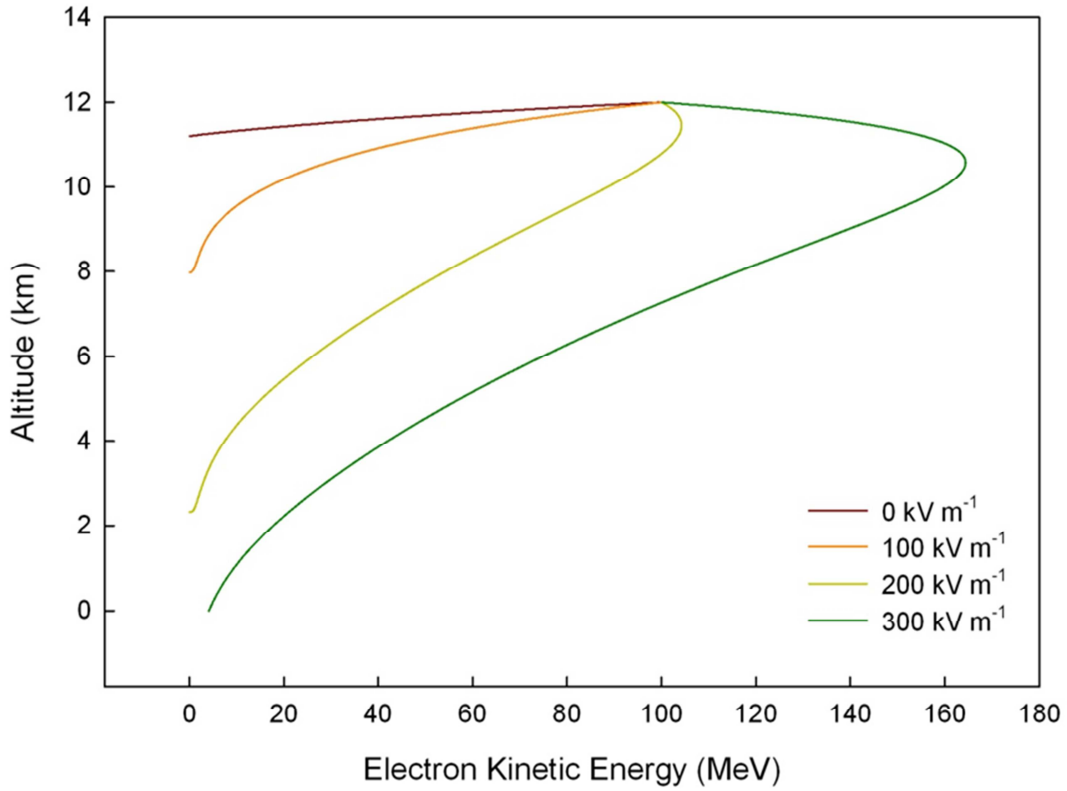

Figure 9.1: Plot of the kinetic energy of a 100 MeV electron starting at an altitude of 12 km and traveling downward through the atmosphere in listed constant, accelerating electric fields.

In >200 kV m^{-1} electric fields, the 100 MeV electron initially accelerates and gains energy with distance. The length of the acceleration region and the maximum energy the electron reaches depend on the strength of the electric field. The stronger 300 kV m^{-1} electric field accelerates the electron for a longer period, for a total acceleration length of ~1.5 km, and to a higher maximum energy of ~170 MeV. After accelerating to a maximum, the energetic electron begins to decelerate until the electron ranges out or reaches the ground. The energy of the electron as it is decelerating through the atmosphere is the same as the equilibrium runaway energy shown in Figure 6.10. The equilibrium runaway energy is the kinetic energy that all electrons above the minimum runaway energy obtain via accelerating if initially below or decelerating if initially above the equilibrium runaway energy. The equilibrium runaway energy depends on both the altitude and electric field strength.

In Figure 9.2, the equilibrium runaway energy does not depend on the initial energy of the electron. In Figure 9.2, the energies of several electrons of different initial energies are plotted as they travel downward through the atmosphere in a 300 kV m^{-1} accelerating electric field starting at an altitude of 12 km. Since all the electrons initially have less energy than the equilibrium runaway energy of a 300 kV m^{-1} electric field (~275 MeV according to Figure 6.10), they begin by first accelerating towards the equilibrium energy as they travel downward through the atmosphere. The higher initial energy electrons reach their respective equilibrium runaway energies first and begin to decelerate. All the electrons decrease in energy along with the equilibrium runaway energy and will have the same kinetic energy while in the constant accelerating electric field.

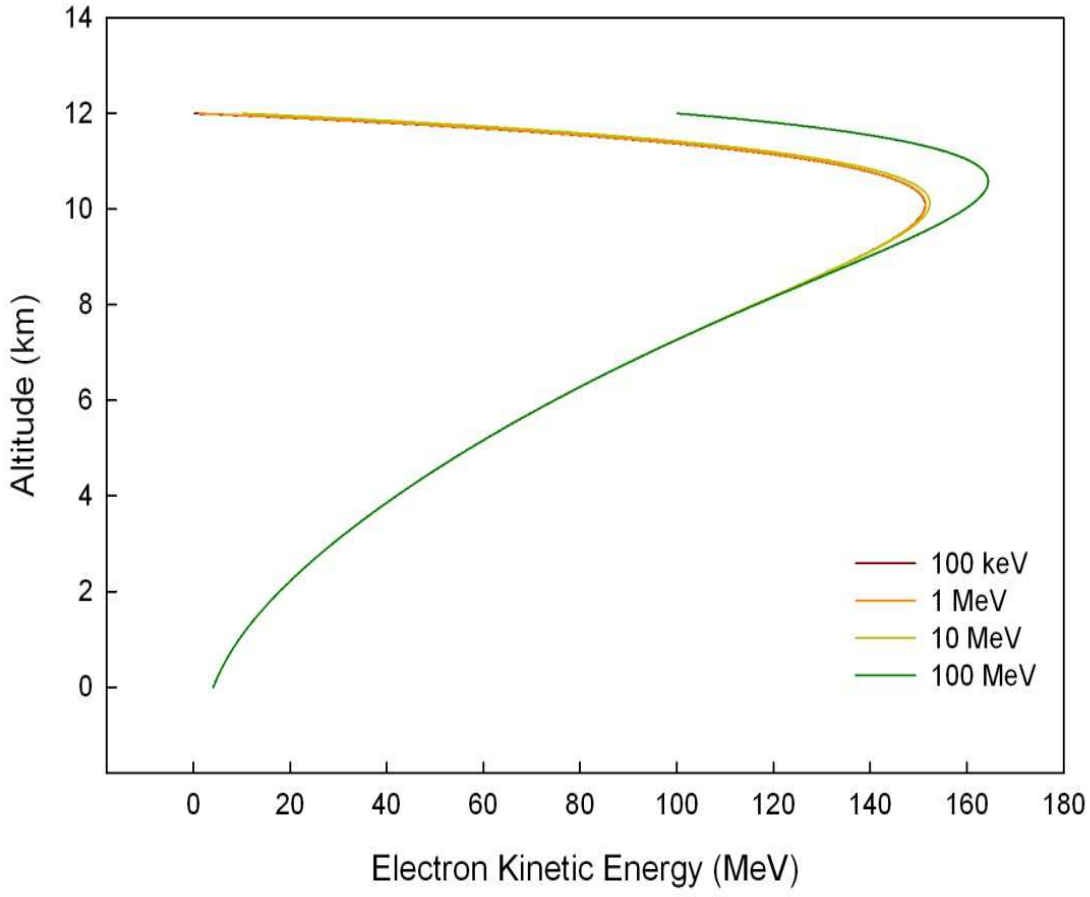

Figure 9.2: Plot of the energy of electrons of listed initial kinetic energies starting at an altitude of 12 km as they travel downward through the atmosphere in a 300 kV m^{-1} accelerating electric field.

The number of additional secondary electrons (both high and low energy) produced by a primary electron as it travels through the atmosphere depends on the kinetic energy of the primary electron. Figure 9.3 shows the number of >1 MeV secondary electrons directly produced by a primary electron of different initial energies in a 150 kV m^{-1} electric field. The number of >1 MeV secondaries increases with initial energy of the primary electron. However, the difference between the number of >1 MeV secondary electrons produce by a 1 MeV and a 1 GeV primary electron is ~100 over the 4 km distance of the lightning initiation region of a thunderstorm.

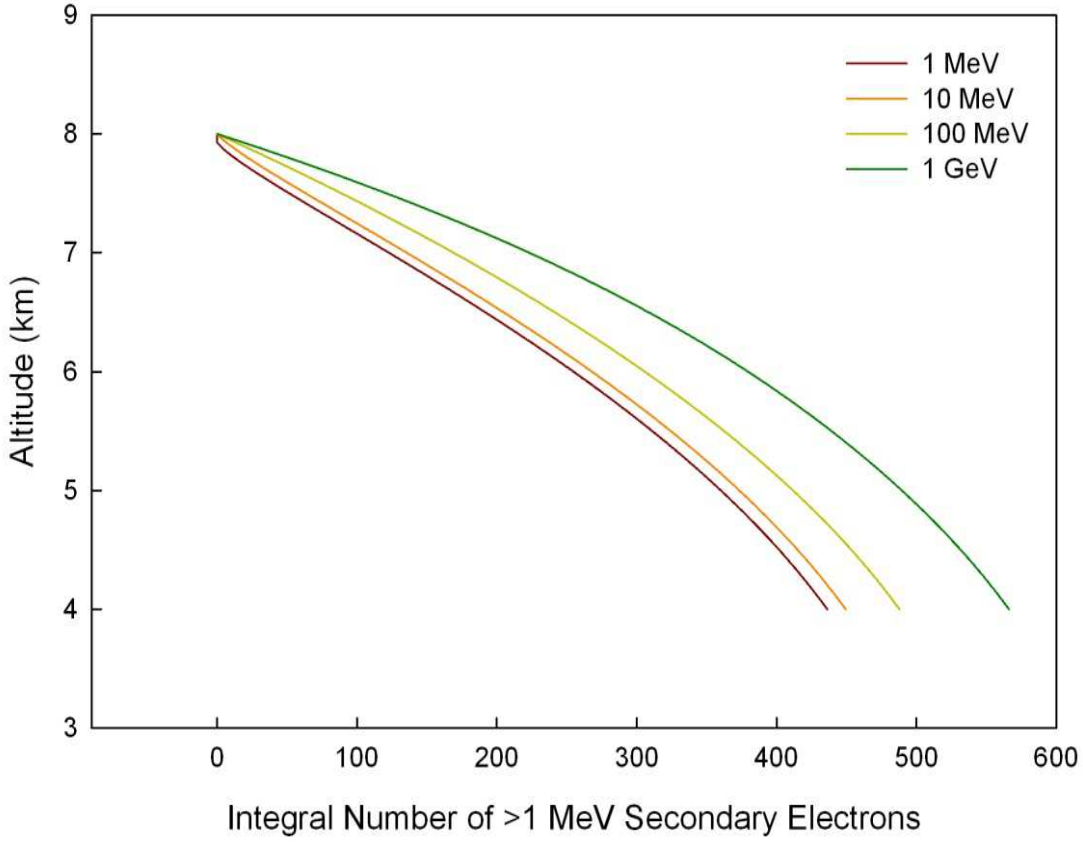

Figure 9.3: Integral number of >1 MeV secondary electrons produced by a primary electron of the listed initial energies traveling downward through the atmosphere at lightning initiation altitudes in a 150 kV m^{-1} electric field.

Figure 9.4 shows the number of <100 eV secondary electrons produced by a primary electron of different initial energies in a 150 kV m^{-1} electric field. The number of <100 eV secondary electrons in Figure 9.4 follow the same trend as the number of

>1 MeV secondary electrons in Figure 9.3. There is a slight increase (less than an order of magnitude) in the number of <100 eV secondary electrons produced by 1 MeV and 1 GeV primary electrons.

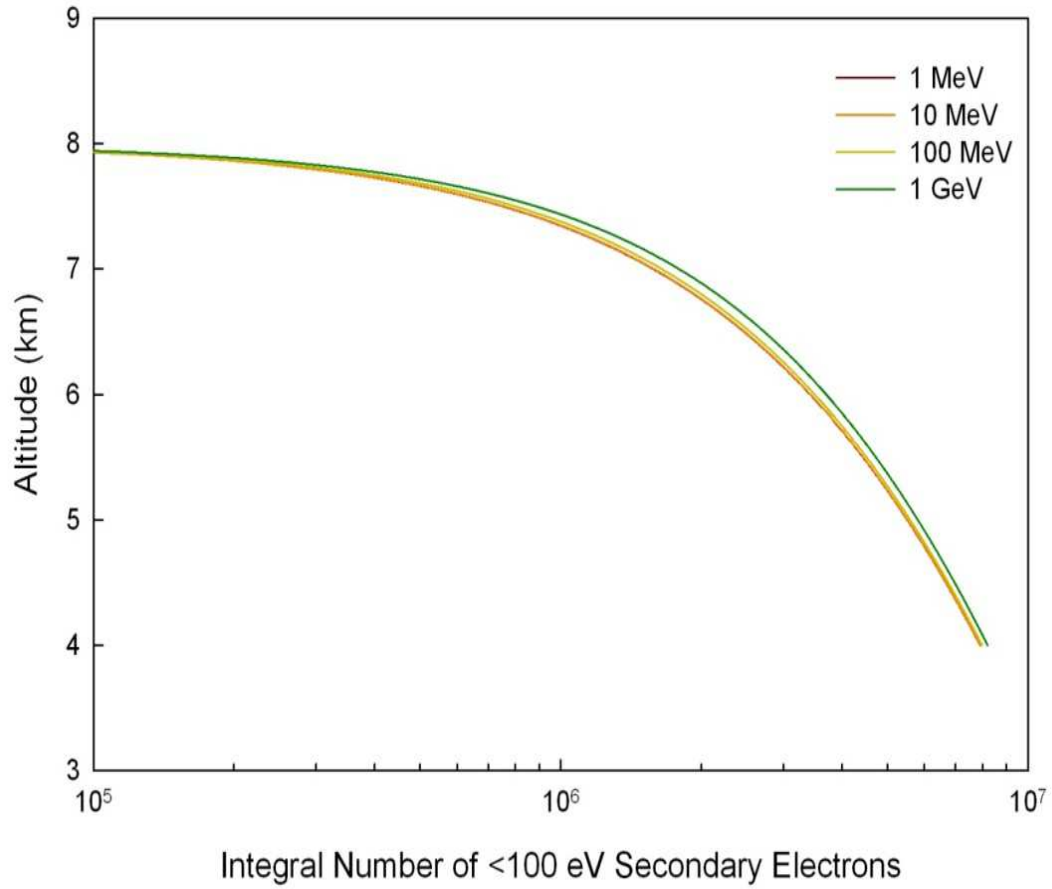

Figure 9.4: Integral number of <100 eV secondary electrons produced by a primary electron of the listed initial energies traveling downward through the atmosphere at lightning initiation altitudes in a 150 kV m^{-1} electric field.

Figure 9.3 shows only the number of >1 MeV secondary electrons that were directly produced by a seed electron. However in an RREA, >1 MeV secondary electrons themselves also function as seed electrons and generate additional high energy secondary electrons. Figure 9.5 shows the total number of >1 MeV secondary electrons produced in a 1 km long 150 kV m^{-1} electric field region starting at an altitude of 6 km by a 1 MeV seed electron. The number >1 MeV secondary electrons grows exponentially with the distance traveled through the atmosphere. The number of >1 MeV secondary electrons

increases by an order of magnitude over approximately every 200 m the RREA travels through the atmosphere. After accelerating for 1 km, the RREA has a similar number of electrons as found in the shower core of a 10^{16} eV cosmic ray primary proton initiated EAS at the same altitude.

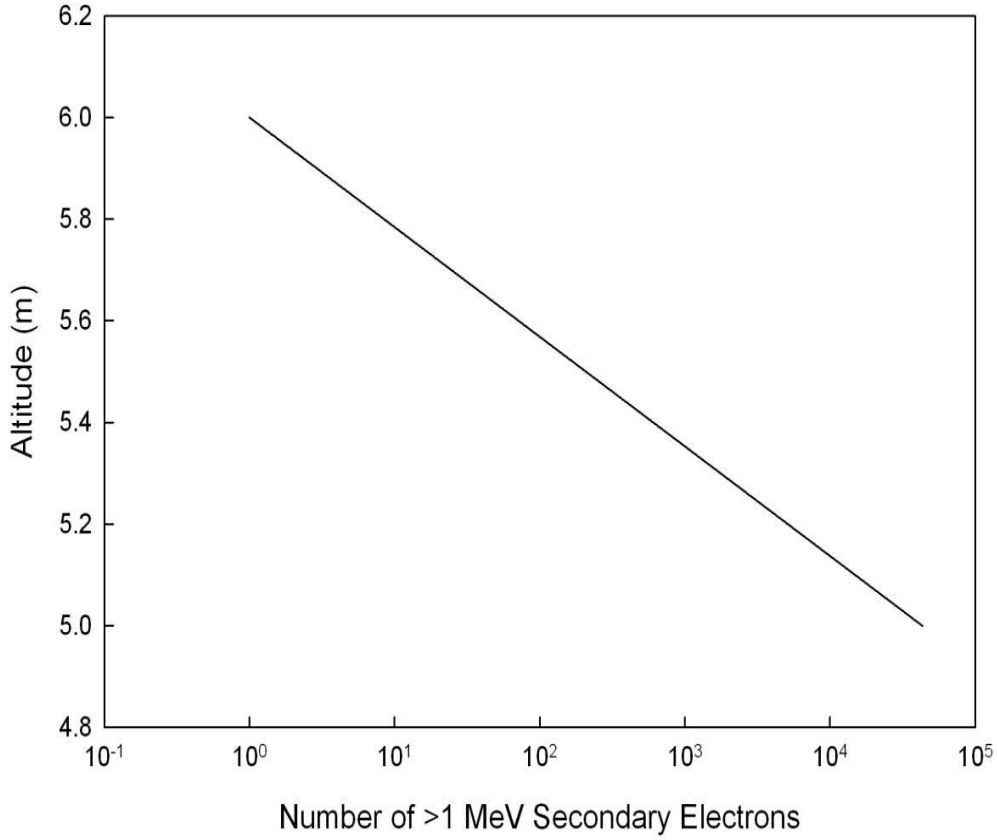

Figure 9.5: Total number of >1 MeV secondary electrons produced by a 1 MeV seed electron as it travels down through the atmosphere in a 150 kV m^{-1} accelerating electric field.

The distribution of secondary electrons within an EAS traveling through a strong electric field region of a thunderstorm is vastly different than for a EAS traveling in fair weather conditions. Even in electric fields as low as 100 kV m^{-1}, the secondary electrons lose less energy with distance and remain energetic over longer distances. In the maximum electric field regions of the thunderstorm, EAS secondary electrons can initiate RREAs, which are each capable of producing as many >1 MeV secondary electrons as are found in the EAS shower core.

9.3 Secondary Electrons in a Thunderstorm

The secondary electron distributions discussed in Section 9.2 only deal with the propagation of electrons through constant electric fields. The electric field within an active thunderstorm is not constant over the its spatial height. Figure 9.6 shows a parameterization of the vertical electric field measured within a thunderstorm by *Marshall et al.* [21]. The thunderstorm used in Figure 9.6 ranged in altitude between 4.0 and 7.5 km. Below 7 km, the electric field is always positive which represents an upward directed electric field. From Chapter 6, upward directed electric fields accelerate downward traveling secondary electrons in an EAS. The maximum electric field is reached at an altitude of 5.6 km of 175 kV m^{-1} and slowly decreases in strength to 150 kV m^{-1} at an altitude of 5.2 km. Below 5.2 km, the electric field rapidly decreases to 25 kV m^{-1}, which is not sufficient to support the development of RREAs.

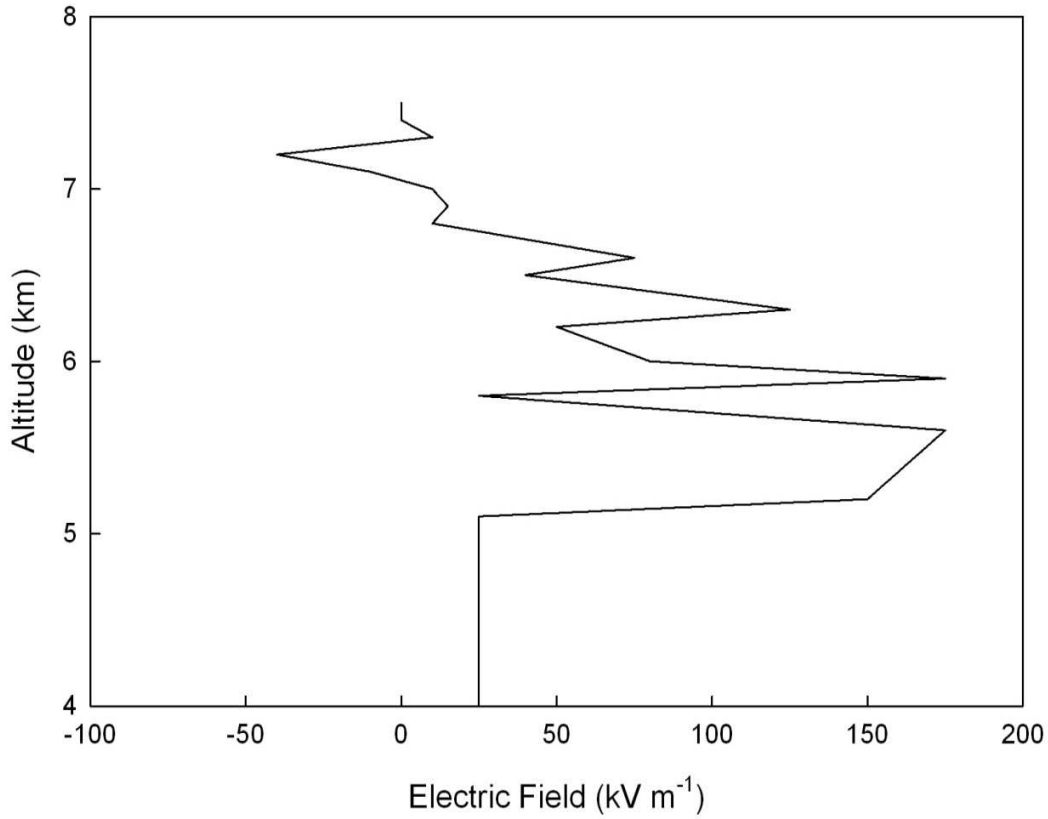

Figure 9.6: Parameterization of the vertical electric field measured in a thunderstorm by *Marshall et al.* [21]. A positive electric field represents an upward, accelerating electric field.

The number of >1 MeV secondary electrons that are generated in RREAs within the vertical electric field region shown in Figure 9.6, is determined from an initial population of seed electrons. The highest concentration of seed electrons in the atmosphere are found within the shower core of an EAS initiated by a high energy cosmic ray primary. For this work, all the secondary electrons within 10 m of the shower axis of an EAS initiated by a 10^{16} eV cosmic ray primary proton were chosen as the initial seed electron population. The fair weather differential energy spectrum of this initial population of seed electrons at 8 km is shown in Figure 9.7.

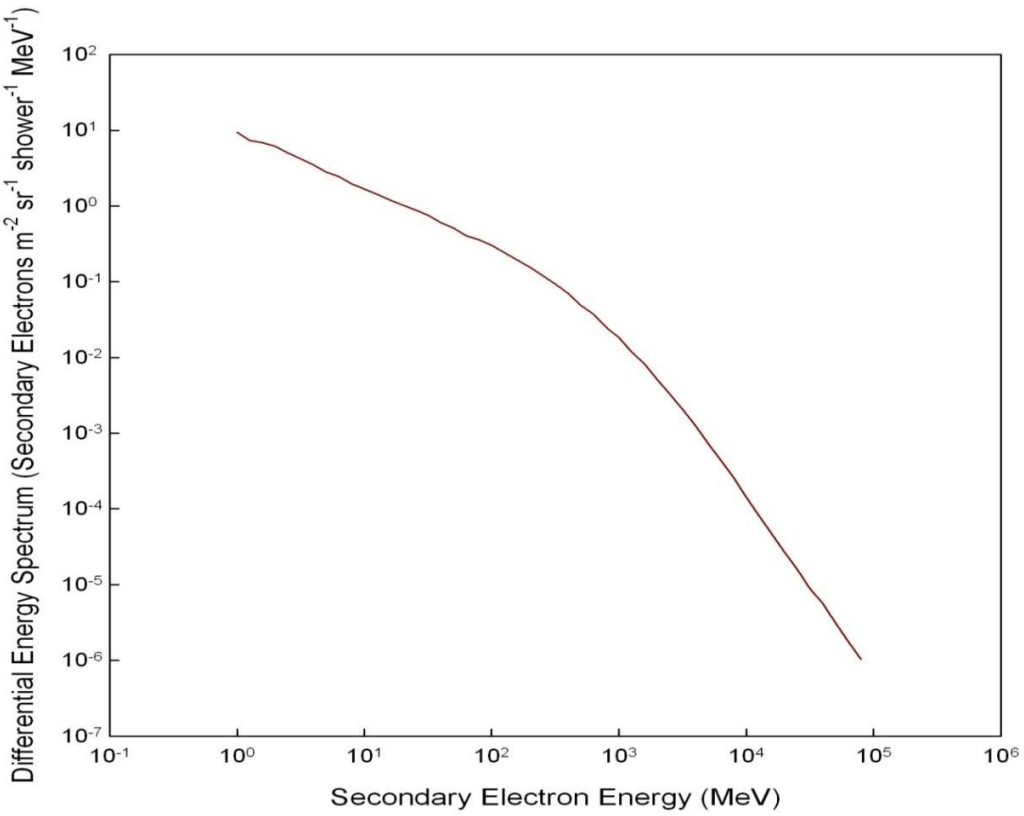

Figure 9.7: Fair weather differential energy spectrum of the secondary electrons within 10 m of the shower axis of an EAS initiated by a 10^{16} eV cosmic ray primary proton at an altitude of 8 km. The data used in this plot was generated by CORSIKA.

The initial seed electron population shown in Figure 9.7 begins at an altitude of 8 km and propagates downward through the vertical electric field described in Figure 9.6. While the seed electrons are traveling through the atmosphere, equations (9.6) and (9.7) are used to calculate the change in energy and flux in the number of seed electrons. Figure 9.8 shows the flux of >1 MeV secondary electrons at different altitudes within the

thunderstorm. As the seed electron population enters the thunderstorm, the total number of >1 MeV electrons increases because of being accelerated in the electric field. Between 8 and 6 km, the total number of >1 MeV seed electrons in the thunderstorm increases by an order of magnitude relative to that in fair weather conditions. The electric field between 8 and 6 km is not of sufficient strength to initiate RREAs, so the increase in the number of >1 MeV seed electrons is because the accelerated electrons are not ranging out as they would in fair weather conditions. Between 6 km and 5 km where the electric field reaches its maximum strength, the number of >1 MeV seed electrons increases another order magnitude to a total of two orders of magnitude relative to fair weather conditions. The electric field between 6 and 5 km is sufficient for the seed electrons to initiate RREAs. These RREAs are responsible for the increase in the number of >1 MeV seed electrons within the maximum electric field region. The number of >1 MeV seed electrons decrease below 5 km due to the weakening of the electric field.

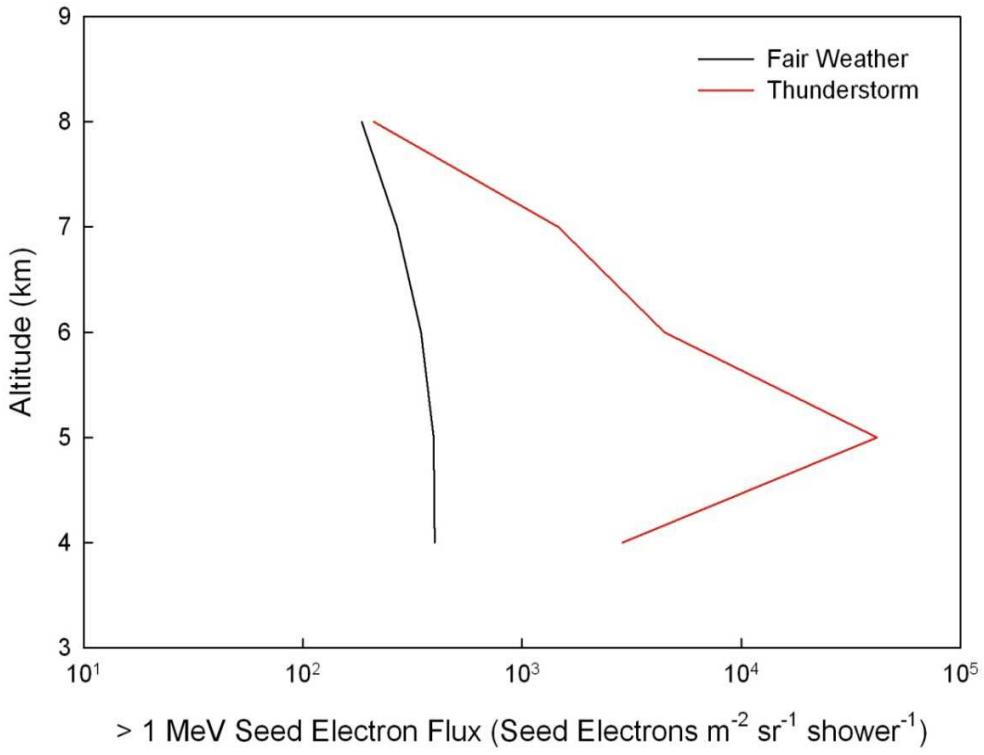

Figure 9.8: The flux of >1 MeV secondary electrons in both fair weather (black) and thunderstorm conditions (red) from an initial seed electron population of secondary electrons found within 10 m from of the shower axis of an EAS initiated by a 10^{16} eV cosmic ray proton primary.

Figure 9.9 shows the differential energy spectrum of seed electrons at an altitude of 5 km for both fair weather and thunderstorm conditions. There is a large enhancement in the number of lower energy electrons in thunderstorm conditions relative to fair weather conditions. These low energy electrons were produced in RREAs found between 6 and 5 km altitude. The enhancement in the number of seed electrons in thunderstorm conditions relative to the fair weather conditions in Figure 9.9 continues for all seed electron energies less than a 1 GeV.

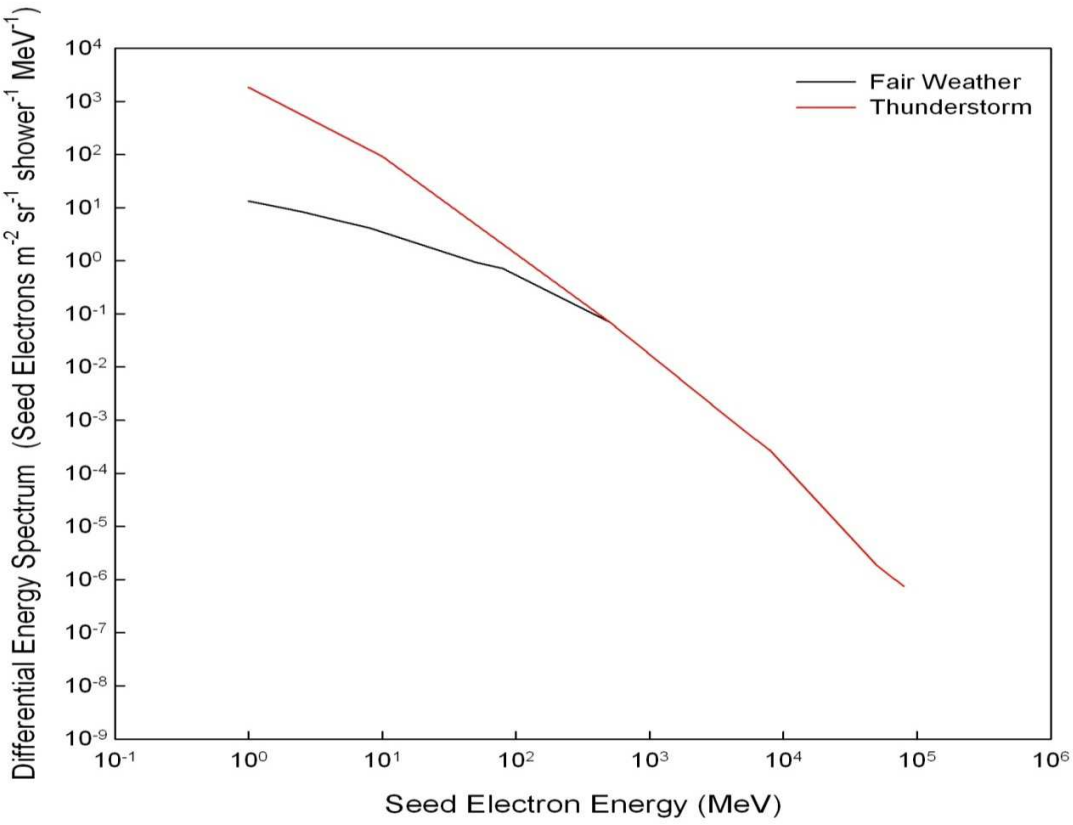

Figure 9.9: Differential energy spectrum of electrons at an altitude of 5 km in fair weather (black) and thunderstorm conditions (red).

According to Figure 9.5, the total number of >1 MeV seed electrons produced in RREAs that propagate through a 400 m acceleration region should be two orders of magnitude higher than the initial population of seed electrons. From Figure 9.8, the total number of >1 MeV seed electrons only increases one order of magnitude from 6 km to 5 km. However, the acceleration region of the electric field exists between 5.6 and 5.2 km. Below 5.2 km, the electric field rapidly weakens and no longer is sufficient to support the development of RREAs. According to Figure 9.9, the majority of the seed electrons

produced by the initial seed population are <10 MeV. These low energy seed electrons are the newest seed electrons generated by RREAs. From Figure 9.2, a 1 MeV secondary electron needs to accelerate for over 2 km in a constant accelerating electric field before reaching the equilibrium runaway energy. As the electric field weakens below 5.2 km, the newly created low energy seed electrons did not have enough energy or range to travel the additional 200 m distance needed to reach the altitude of 5 km. All the seed electrons that reach 5 km included in Figure 9.9 are ~20 MeV or greater at 5.2 km (according Figure 6.5). The number of seed electrons rapidly decreases outside the acceleration region.

9.4. Feasibility of the RREA and Hybrid Lightning Initiation Models

Assuming the actual maximum flux of >1 MeV seed electrons is an order of magnitude larger than shown in Figure 9.8, the maximum flux of >1 MeV secondary electrons within the thunderstorm described in Figure 9.6 is ~10^6 seed electrons m^{-2} sr^{-1} $shower^{-1}$. Because the seed electrons are being accelerated downward by the positive electric field, the solid angle of the seed electrons would be ~2π sr, so there could be up to ~10^7 >1 MeV seed electrons m^{-2} in the shower core of an EAS initiated by a 10^{16} eV cosmic ray primary proton. From equation (9.8), >1 MeV electrons produce ~10^4 low energy secondary electrons m^{-1}, thus the total flux of electrons is ~10^{11} electrons m^{-3}.

The RREA and hybrid models both require a large density of secondary electrons to initiate a lightning discharge, but the ways these secondary electrons are used by these models are different. As discussed in Chapter 6, the RREA model requires a large density of secondary electrons to produce streamers directly without first creating a point discharge. In the hybrid model, the secondary electrons enhance the local electric field around a charged hydrometeor. With a sufficient electric field enhancement, the hydrometeor would undergo a point discharge and eventually initiate a lightning discharge according to the conventional discharge model (Section 4.4.1.1).

9.4.1. Feasibility of the RREA Model

As discussed in Section 8.4, *Dawson and Winn* [58] theorized that 10^8 electrons concentrated within a sphere of a 30 μm radius are required to produce a propagating streamer in the atmosphere. Using this value as the criteria for initiating a lightning discharge for the RREA model, the ~10^{11} electrons m^{-3} generated in the thunderstorm in

Section 8.3 translates to only ~10^{-2} electrons within a sphere of a 30 μm radius. That is two orders of magnitude greater than the fair weather ambient secondary flux (Section 8.4), but still ten orders of magnitude too low to initiate a lightning discharge. The length of the acceleration region within the thunderstorm would have to be over 2 km in order to generate enough electrons to meet the criterion proposed by *Dawson and Winn*. The maximum electric field regions required to generate RREAs are rarely >1 km in length [20], so much stronger electric fields (>300 kV m^{-1}) than were measured in the thunderstorm used for Figure 9.6 would be required for the RREA model to generate lightning discharges in the atmosphere.

9.4.2. Feasibility of the Hybrid Model

The hybrid model proposed by *Petersen et al.* [10] suggests that the seed electrons form an ionized plasma in the atmosphere and enhance the local electric fields around charged hydrometers found throughout a thunderstorm. This localized enhancement of the electric field allows charged hydrometeors to initiate streamers in lower ambient electric fields strength. The amount of electric field enhancement required to initiate streamer varies greatly as a function of the physical characteristic of the hydrometeor (liquid droplet, jagged graupel, hail, etc.) and environmental conditions (temperature, water content, pressure, etc.). Measurements from hydrometeor experiments have found that an electric field enhancement of 100-200 kV m^{-1} could initiate a lightning discharge in the atmosphere [111]. An electric field enhancement of >100 kV m^{-1} is assumed as the lightning discharge initiation criteria for the hybrid model.

The amount of electric field enhancement created by the seed electrons depends on the geometry and charge density of the ionized plasma. Assuming that the relativistic seed electrons are traveling near the speed of light along the circular disk of the EAS shower front, the low energy electrons, which do not travel very far after being created, are left behind in a long cylindrical region. The base of the cylinder is the same area as the shower front of the seed electrons and is assumed in Section 8.3 to be a circle with a radius of 10 m for the initial seed electron population. Low energy electrons typically recombine with the atmospheric atoms and molecules in ~10^{-7} s [51]. This limits the height of the cylinder to ~30 m. The maximum electric field enhancement for this 10 m radius, 30 m tall cylindrical region with an electron density of 10^{11} electrons m^{-3} is 12 kV m^{-1}, which is not sufficient to initiate a lightning discharge according to the assumed criteria.

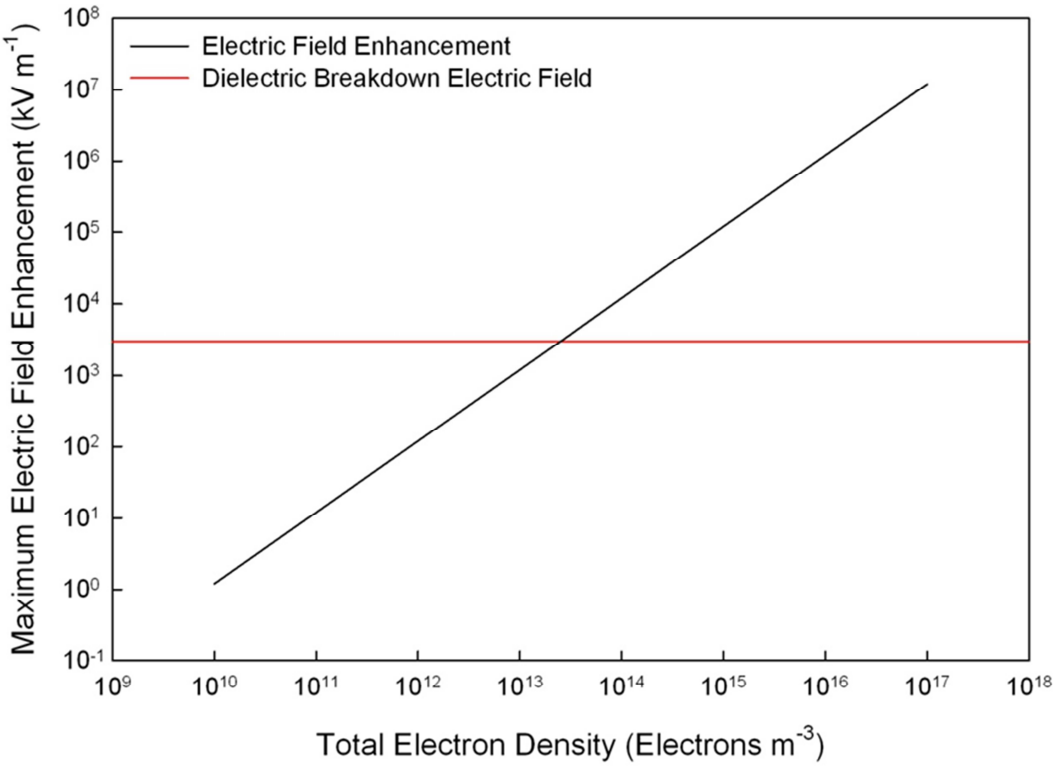

Figure 9.10: The maximum electric field enhancement as a function total electron density in a 10 m radius, 30 m long circular cylindrical region centered at an altitude of 6 km. The red line represents the dielectric breakdown electric field strength on the ground in dry air [51].

Figure 9.10 shows how the maximum electric field enhancement scales with electron density. Unlike the RREA model, one order of magnitude increase in the electron density would generate a maximum electric field enhancement of ~130 kV m^{-1}, which is sufficient to initiate a lightning discharge [111]. Also, the above calculation does not include the effect of high energy secondary electrons outside the shower core producing their own RREAs. Secondary electrons from outside the shower core RREAs expand the region of low energy secondary electrons and increase the overall electric field enhancement. If the acceleration region of the electric field in Figure 9.6 was to expand in length, to a total of ~600 m, maximum electric field enhancement due to the ionized plasma created by the low energy secondary electrons would be sufficient to allow streamer formation on most types of hydrometeors [10, 50].

CHAPTER X

EXPERIMENTAL VERIFICATION OF THE RREA AND HYBRID LIGHTNING INITIATION MODELS

Both the RREA and hybrid models require large concentrations of secondary electrons in order to initiate a lightning discharge. From Chapter 8, the largest concentration of secondary electrons at lightning initiation altitudes in fair weather conditions is inside the shower cores of EASs that were initiated by high energy cosmic ray primaries. In order to verify either the RREA or hybrid model, there must be a correlation between the passage of EASs initiated by high energy cosmic ray primaries through the thunderstorm and lightning discharges.

Due to the difficulties and dangers of sending radiation detectors into an active thunderstorm, ground-based radiation detectors are the preferred method to detect the passage of EASs initiated by high energy cosmic ray primaries. Figure 8.16 shows that the fair weather ambient >1 MeV secondary electron flux on the ground is ~5 secondary electrons m^{-2} sr^{-1} s^{-1}, which is lower than the number of energetic electrons and photons from terrestrial sources [112]. In addition to the secondary electrons, EASs produce secondary muons from the decay of charged pions and kaons. Secondary muons produced by EASs are highly relativistic and travel through the atmosphere and often deep underground before ranging out [11, 22].

Secondary muons reach the ground with >1 GeV of kinetic energy and can travel through most material, e.g. human bodies [83], without much energy loss. One method to discriminate secondary muons from other less penetrating forms of ionizing radiation, such as low energy photons and electrons from terrestrial sources, is to use two radiation detectors separated by a thick and dense material, e.g. lead. Because of the penetrating power of the secondary muons, they can travel through both detectors and the separating material, but lower energy electrons and photons either range out or are absorbed before traveling through both detectors and the separating absorber material. This method of detecting secondary muons is called the coincidence method, since the two radiation

detectors detect the secondary muon in coincidence with one another [113]. With the coincidence method, secondary muons can be detected and discriminated reliably on the ground.

Since secondary muons are created in the hadronic cascade of an EAS simultaneously with the electromagnetic cascades, the presence of secondary muons means that an EAS has developed within the atmosphere. The secondary electrons at lightning initiation altitudes from EASs range out before reaching the ground. However, the secondary muons that develop along with secondary electrons of the EAS do reach the ground and can be detected via the coincidence method. The secondary muons that are detected on the ground can be used as a proxy for secondary electrons at lightning altitudes from the same EAS.

In order to verify the RREA and hybrid models, an array of four ground-based cosmic ray muon detectors was developed to detect the passage of EASs initiated by high energy cosmic ray primaries through the atmosphere. The results from the detector array are then compared to the lightning initiation data from the Oklahoma Lightning Mapping Array (OKLMA) to determine if there is a correlation between the passage of EASs initiated by high energy cosmic ray primaries and lightning discharges. The ground-based cosmic ray muon detector array was deployed in Norman, OK in order to be near the center of the OKLMA's three dimensional lightning detection region.

10.1. Cosmic Ray Secondary Muons

Secondary muons were discussed briefly in Chapter 5. Secondary muon and anti-muons are the decay products of charged pions and kaons, which are produced in the hadronic cascade of the EAS. Charged pions and kaons are produced in many of the same interactions [12, 68] that generate the neutral pions. Being the decay products of hadronic cascade secondaries, all secondary muons are produced during the developing stage of an EAS, before the hadronic cascade ends (middle disk in Figure 8.2).

Secondary muons are leptons like electrons, but are approximately two hundred times heavier. As leptons, secondary muons are charged particles and lose energy via ionization and bremsstrahlung. Secondary muons are also able to produce electron positron pairs directly in the Coulomb field of a nucleus and to produce secondary hadrons through inelastic, photonuclear interactions due to their heavier mass [12, 114].

The muon stopping power, $\left(\frac{dE}{dx}\right)_{muon}$, in a material is generally written in the form of,

$$\left(\frac{dE}{dx}\right)_{muon}(E) = \left(\frac{dE}{dx}\right)_{muon\ ion}(E) + \left[b_{brem}(E) + b_{pair}(E) + b_{photo}(E)\right]E, \tag{10.1}$$

where E is the kinetic energy of the secondary, x is depth traveled by the muon in the material, $\left(\frac{dE}{dx}\right)_{muon\ ion}$, is the muon stopping power due to ionization collisions, b_i is the energy lost to bremsstrahlung, direct pair production, and photonuclear reactions, respectively [12]. Because muons have a larger mass than electrons, but are not as massive as protons, deriving an analytic expression to the ionization stopping power or the energy losses due to the other processes, requires the use of different nuclear models to approximate the muon, e.g. treating a muon as heavy ion for ionization collisions, but electron-like for bremsstrahlung [12, 70]. Energy loss equations that use approximations for modeling muon interactions typically deviate significantly from experimental measured and Monte Carlo simulated values [12, 70]. Experimental values of the muon stopping power in dry air at sea level are shown in Figure 10.1.

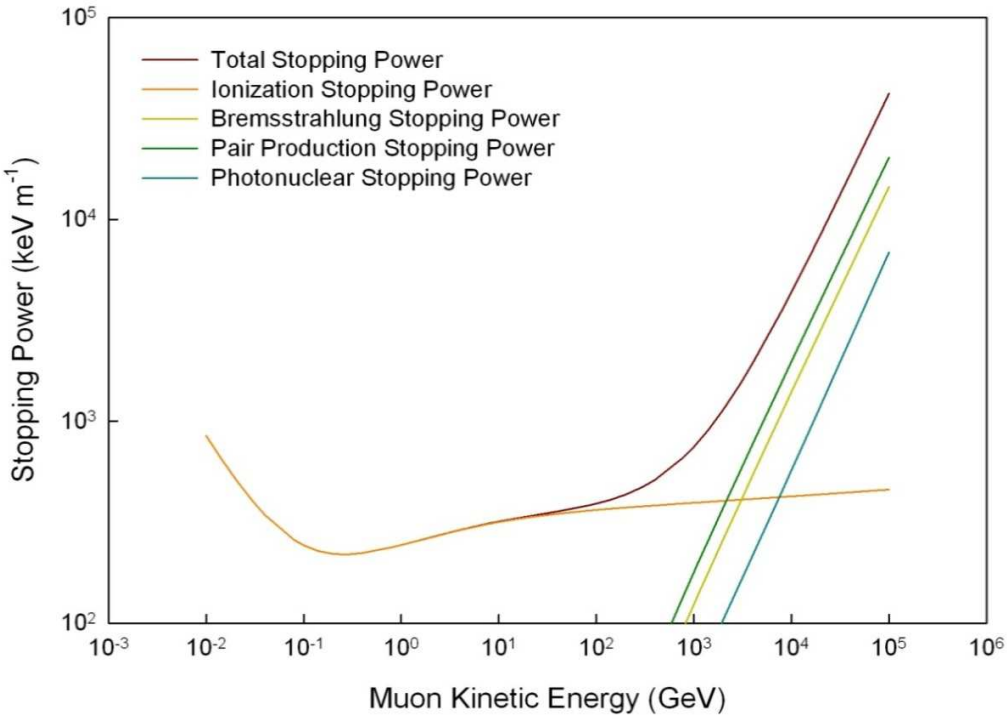

Figure 10.1: Muon stopping power in dry air at sea level [114].

In Figure 10.1, ionization energy losses dominate for < 1 TeV (10^3 GeV) muons in dry air. For >1 TeV muons, the energy losses to pair production, bremsstrahlung, and photonuclear interactions dominate the total muon stopping power . Between 100 MeV and 100 GeV, the total stopping slowly increases with muon kinetic energy due to relativistic effects. The stopping power for 1 TeV muons is ~1 MeV m^{-1}, meaning muons can travel hundreds to thousands of meters in air before ranging out. The range of muons in dry air at sea level is shown in Figure 10.2 [114]. According to Figure 10.2, 1 GeV muons have a >1 km range in the air at sea level. Due to this large range and low stopping power, >1 GeV muons are very penetrating and can travel through meters of material before significantly slowing down.

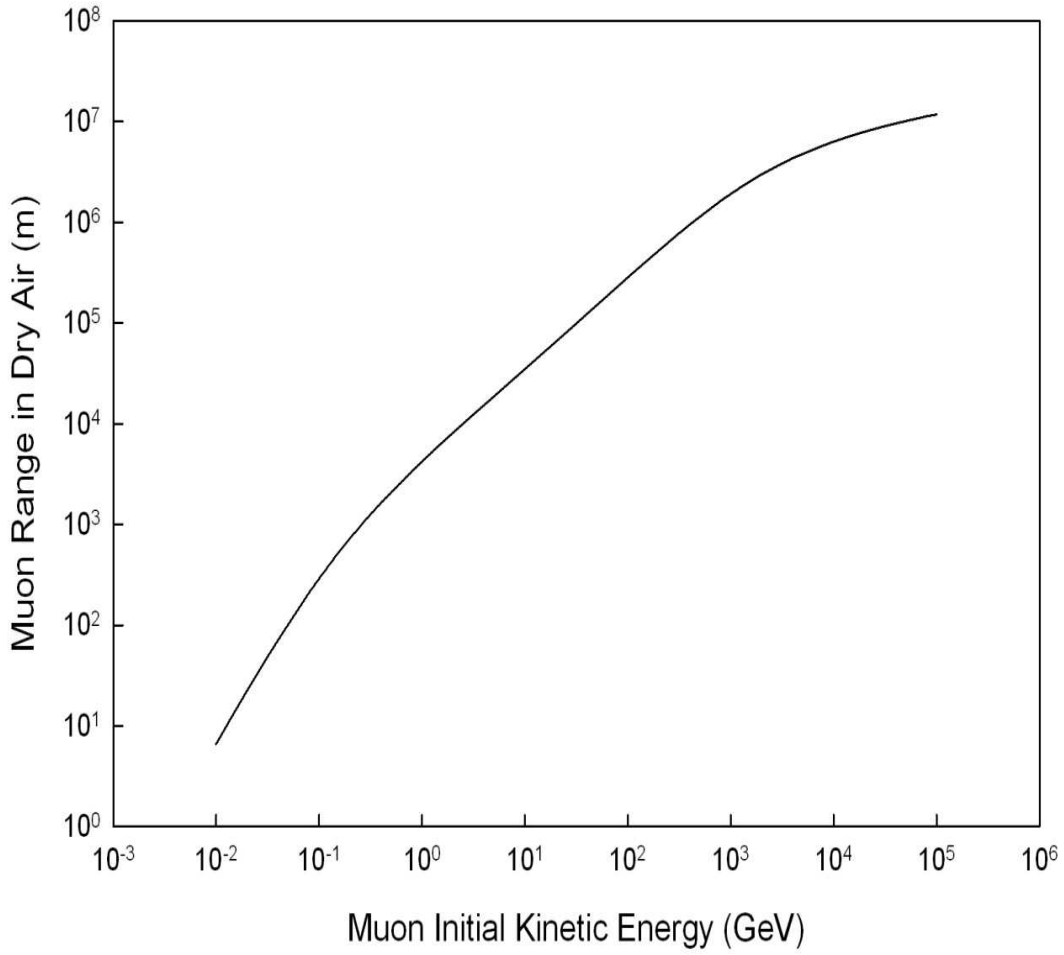

Figure 10.2: Range of muons in dry air at sea level as a function of the initial kinetic energy [114].

Monte Carlo methods are able to simulate the propagation of secondary muons through the atmosphere [12]. CORSIKA simulates all the secondaries produced in an EAS, not just secondary electrons. Using the same methods as for fair weather secondary electrons in Chapter 8, a lateral distribution function can be defined for secondary muons in fair weather conditions. From this secondary muon lateral distribution function, the different secondary particles distributions, such as the particle density and energy spectrum, can be calculated in the same manner as in Chapter 8. Figure 10.4 shows the secondary muon densities and Figure 10.5 shows secondary muon energy spectra on the ground from EASs that are initiated by different energy cosmic ray primary protons.

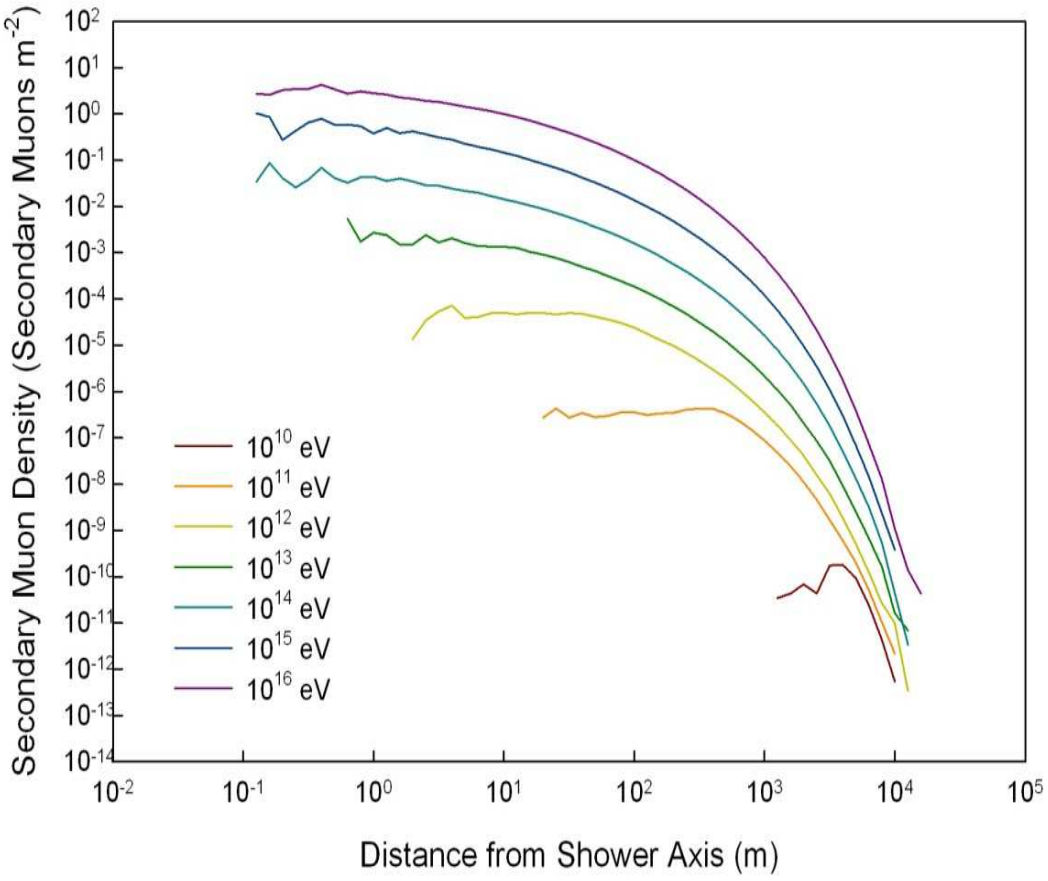

Figure 10.3: Fair weather secondary muon density on the ground from a single EAS initiated by the listed cosmic ray primary protons as a function of distance from the shower axis, based on CORSIKA simulated data.

Figure 10.3 shows the fair weather secondary muon density on the ground as a function of distance from the shower axis from EASs initiated by cosmic ray primary protons of listed energy. The fair weather secondary electron densities for the same set of EASs used in Figure 10.1 was shown in Figure 8.8. The secondary muon density is fairly uniform across the shower front up to ~100 m away from the shower axis. For distances >100 m from the shower axis, the secondary muon density decreases rapidly. As with the secondary electrons, the number of secondary muons produced in EASs scales with cosmic ray primary proton energy.

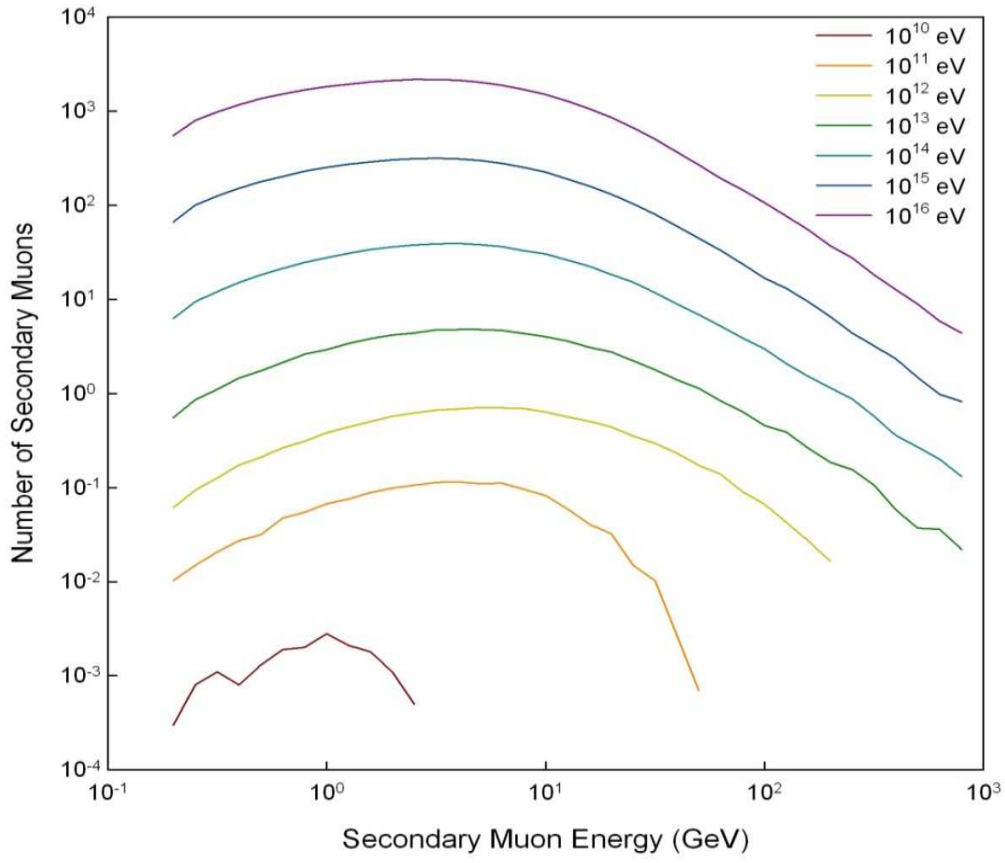

Figure 10.4: Fair weather secondary muon energy spectra of all the secondary muons in an EAS of listed cosmic ray primary proton energy on the ground, based on CORSIKA simulated data.

Figure 10.4 shows the fair weather secondary muon energy spectra of all the secondary muons in EASs initiated by different energy cosmic ray primary protons. For EASs initiated by $>10^{13}$ eV cosmic ray primary protons, the number of secondary muons

increases with energy from 100 MeV to a broad maxima at ~5 GeV before decreasing at higher energies. According to Figure 10.2, 5 GeV secondary muons have >10 km range in air on the ground. For EASs initiated by $<10^{12}$ eV cosmic ray primary protons develop higher in the atmosphere (Sections and 8.1 and 8.2) than do EASs initiated by higher energy cosmic ray primary protons, so their secondary muons must travel farther through the atmosphere to reach the observation level on the ground. By traveling a farther distance, the secondary muons that are measured on the ground are of lower energy than secondary muons from EASs initiated by higher energy cosmic ray primary protons. Thus, there are far fewer high energy secondary muons that reach the ground in EASs initiated by lower energy cosmic ray primary protons, than from higher energy protons.

10.2. Experimental Methods

The goal of this portion of my research is to test the RREA and hybrid models by correlating time- and location-resolved lightning initiation data from the OKLMA with time- and location-resolved cosmic ray muon count rate data from an array of four cosmic ray muon detectors located in Norman, OK.

10.2.1. Oklahoma Lightning Mapping Array (OKLMA)

The different processes of a CG lightning discharge discussed in Section 4.4 all involve the acceleration and movement of electric charge in the atmosphere. Accelerating electric charges generate electromagnetic radiation, so a lightning discharge is a source of electromagnetic radiation in the atmosphere. Due to the variation in the different lightning discharge processes, a lightning discharge generates a broad range of electromagnetic radiation frequencies [20].

The OKLMA is made up of 17 lightning mapping stations distributed throughout Central and Southwestern Oklahoma as shown in Figure 10.5 [115]. Each lightning mapping station is made up a VHF radio antenna, a GPS receiver, and a computer to store data as shown in Figure 10.6. The VHF radio antenna receives signal from 60-66 MHz (unused television channel 3) radiation events generated by lightning discharges [43]. These 60-66 MHz radiation events are time stamped to 50 ns accuracy with the signal from the GPS receiver and written to the hard drive of the computer. The time stamped data from all the lightning mapping stations are collected, and by using a time of arrival algorithm, the originating location of the radiation source can be determined. Depending on the

number of lightning mapping stations that measured the same radiation event (minimum of six stations) and strength of the signal, the originating location of the radiation source can be determined in two (orange region in Figure 10.2) or three dimensions (purple region in Figure 10.2) along with time of occurrence of the radiation source [43].

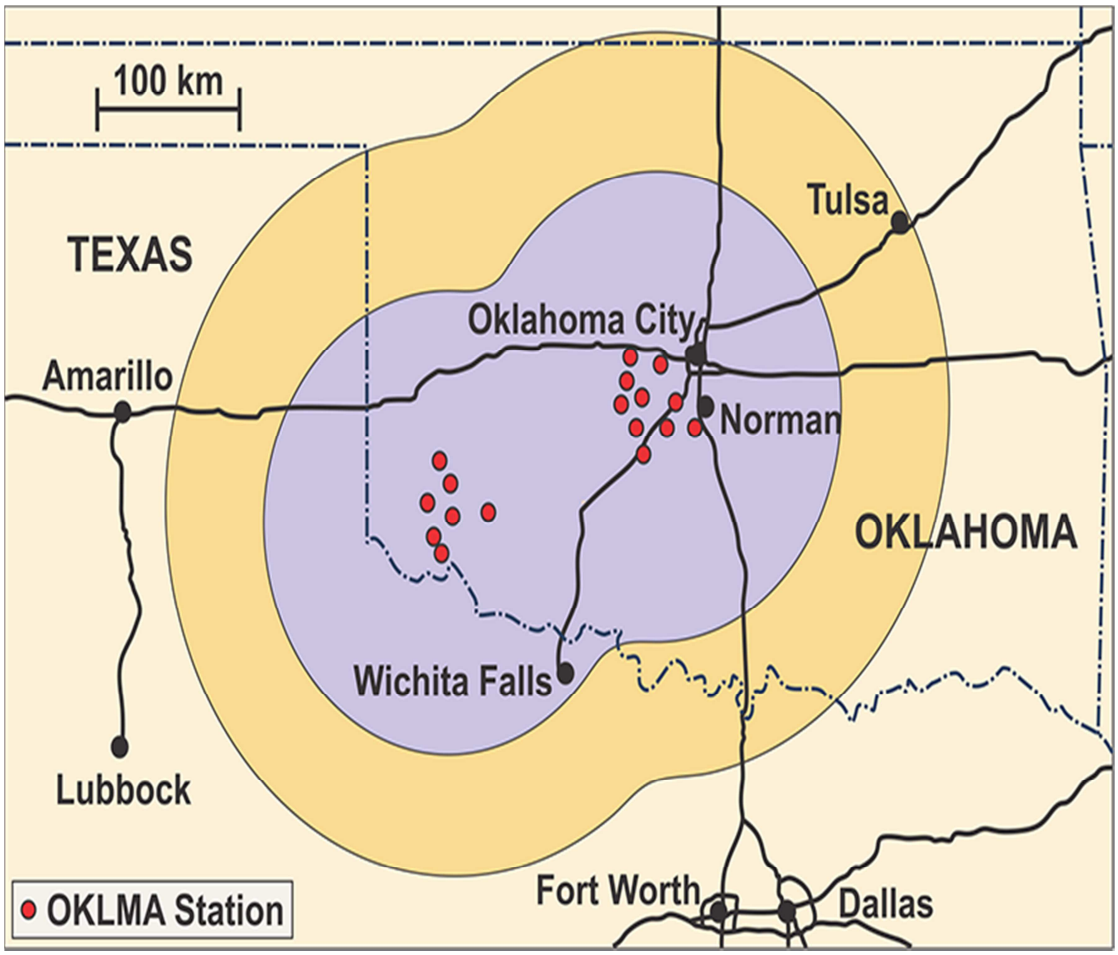

Figure 10.5: Map of the OKLMA lightning mapping station locations and coverage area. The purple region represents where the OKLMA can map lightning discharges in three dimensions and the orange region represents the region where lightning discharges are mapped in only two dimensions (no altitude information) [115].

Since electric charge is accelerated the entire length of the lightning discharge, VHF radiation events from the same lightning discharge are produced at multiple locations in the atmosphere. The lightning mapping stations receive each of these VHF radiation events and the time of arrival algorithm is robust enough to separate them. These multiple

VHF radiation events allow the entire length of the lightning discharge, including leader branches and J-processes, to be detected by the OKLMA. For this work, only the first VHF radiation event of a lightning discharge is used to indicate the time and location of lightning initiation.

Figure 10.6: Photograph of the equipment used in a lightning mapping array station. The 60-66 MHz radio antenna is shown on the left and both the GPS receiver and computer are located in the white enclosure on the right [116].

10.2.2. Cosmic Ray Muon Detectors

The cosmic ray muon detectors used in this work were developed and built by Aaron Ruse of the Oklahoma State University Radiation Physics Laboratory. The cosmic ray muon detectors use the coincidence method described in Section 8.1 to detect secondary muons. A brief description of the cosmic ray muon detectors is presented below. A more detailed description of the construction method, calibration, and equipment specifications can be found in *Ruse* [23].

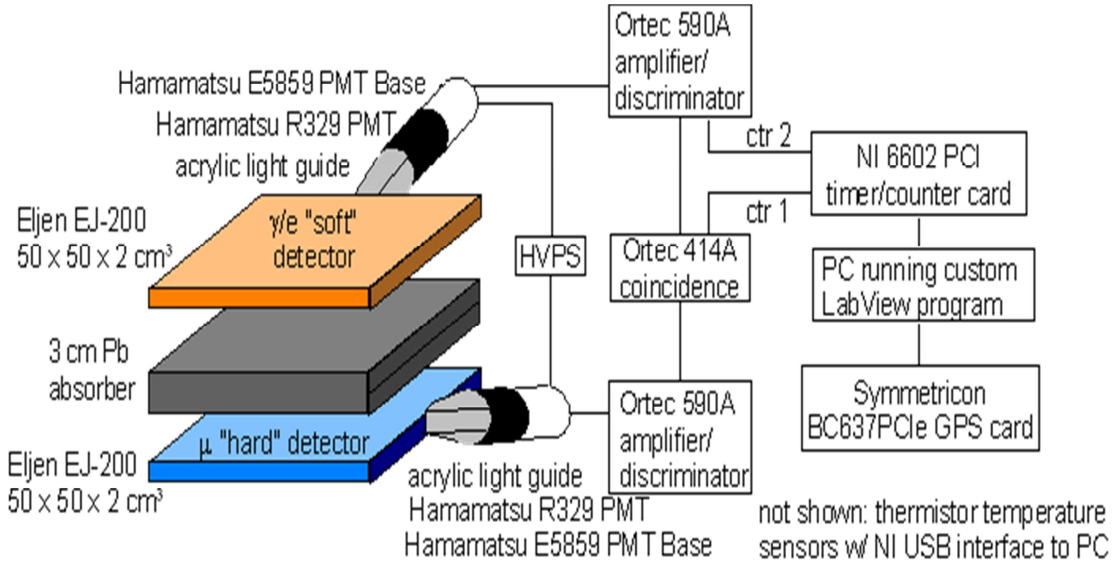

Figure 10.7: Diagram of the cosmic ray muon detector [23].

Figure 10.7 shows a diagram of the cosmic ray muon detector. Each of the four ground-based cosmic ray muon detectors contains two plastic scintillator paddles optically coupled, via acrylic light guides, to photomultiplier tubes (PMT). Plastic scintillators are an example of an organic scintillator. When a charged particle travels through plastic scintillator, the bound electrons of the molecules in the plastic are excited to a higher energy state. Unlike in an atom, the electron does not de-excite directly to a lower electron energy level, but instead de-excites in a series of transitions to different lower energy vibrational modes of the molecule before reaching the ground state. In organic scintillators, at least one of these transitions generates a photon of lower energy than electron gained via excitation. These photons scatter throughout the plastic scintillator. By using total internal reflection and lightning guides, the scattered photons are directed at the PMT, where they are converted into an electrical signal [117]. Each plastic scintillator paddle consists of a 50 cm x 50 cm x 2 cm sheet of Eljen EJ-200 plastic scintillator [118]. Hamamatsu R329-02 PMTs with E5859 bases are optically coupled to the plastic scintillator paddles. Each PMT is connected to a high voltage power supply (HVPS). To separate the “hard component”, i.e. penetrating secondary muons, from the “soft component”, i.e. low energy, electrons and photons, a 3 cm thick sheet of lead absorber is placed between the two scintillator paddles.

The electric signals from the PMTs pass to an Ortec 590A amplifer discriminator modules for amplification and discrimination to remove noise in the signal. The filtered signals from both the top and bottom scintillator paddles are then passed to an Ortec 414A coincidence module. Secondary muons travel through both plastic scintillator

paddles and the lead absorber, so the Ortec 414A coincidence module only sends out a pulse if signals arrive from within a few nanoseconds from each of the PMTs. Pulses from the Ortec 414A coincidence module are sent to a computer with a NI 6602 PCI counting card. The number of muons detected every 100 μs is written to a text file via custom Labview code. The output data are time stamped from the output signal of a Symmetricon BC637PCIe GPS time card also located in the computer. A photograph of a cosmic ray muon detector is shown in Figure 10.8.

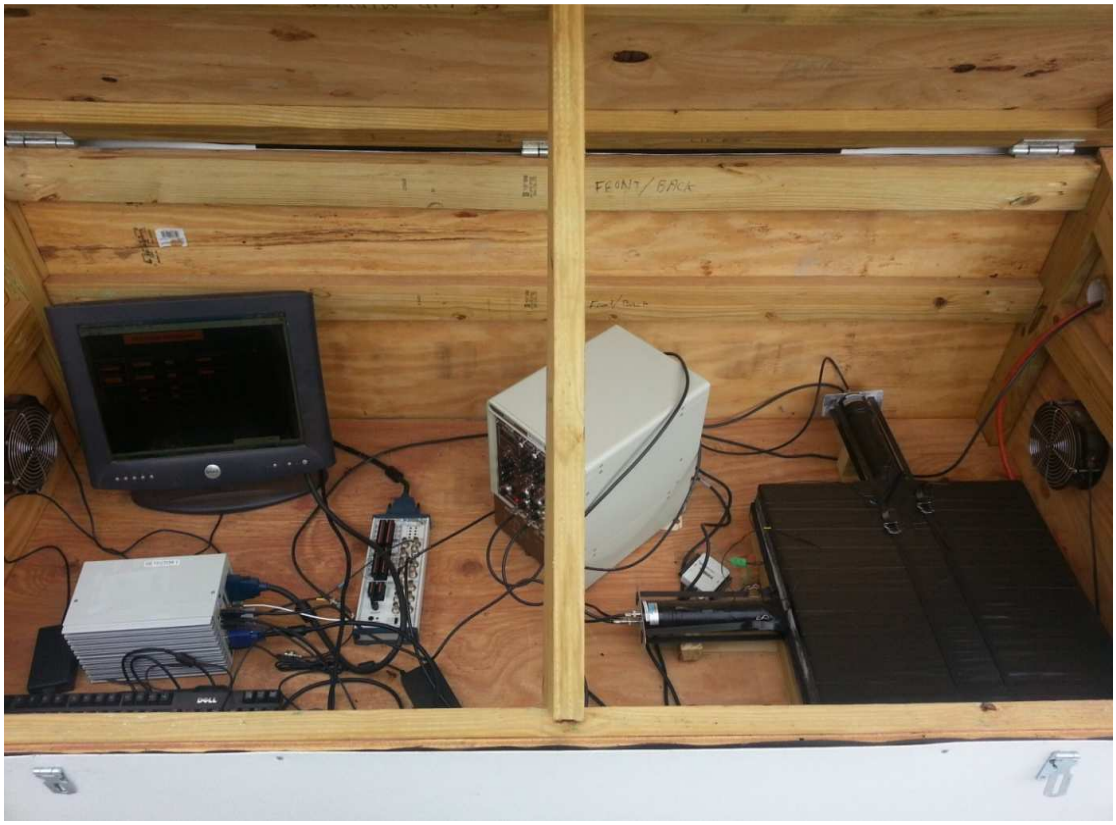

Figure 10.8: Photograph of a cosmic ray muon detector. The scintillator paddles are the large black object on the right side of the photograph. In the middle of the picture is the NIM module containing the amplifiers, discriminators, and coincidence units required to read out the signal from the scintillator paddles. The small grey box on the left side of the photograph is the computer containing the counting card, GPS card, and Labview software to collect and store the secondary muon data. Not shown is the GPS antenna, which is outside the wooden enclosure. The wooden enclosures protects the cosmic ray muon detector from the environment [23].

10.2.3. Cosmic Ray Muon Detector Array

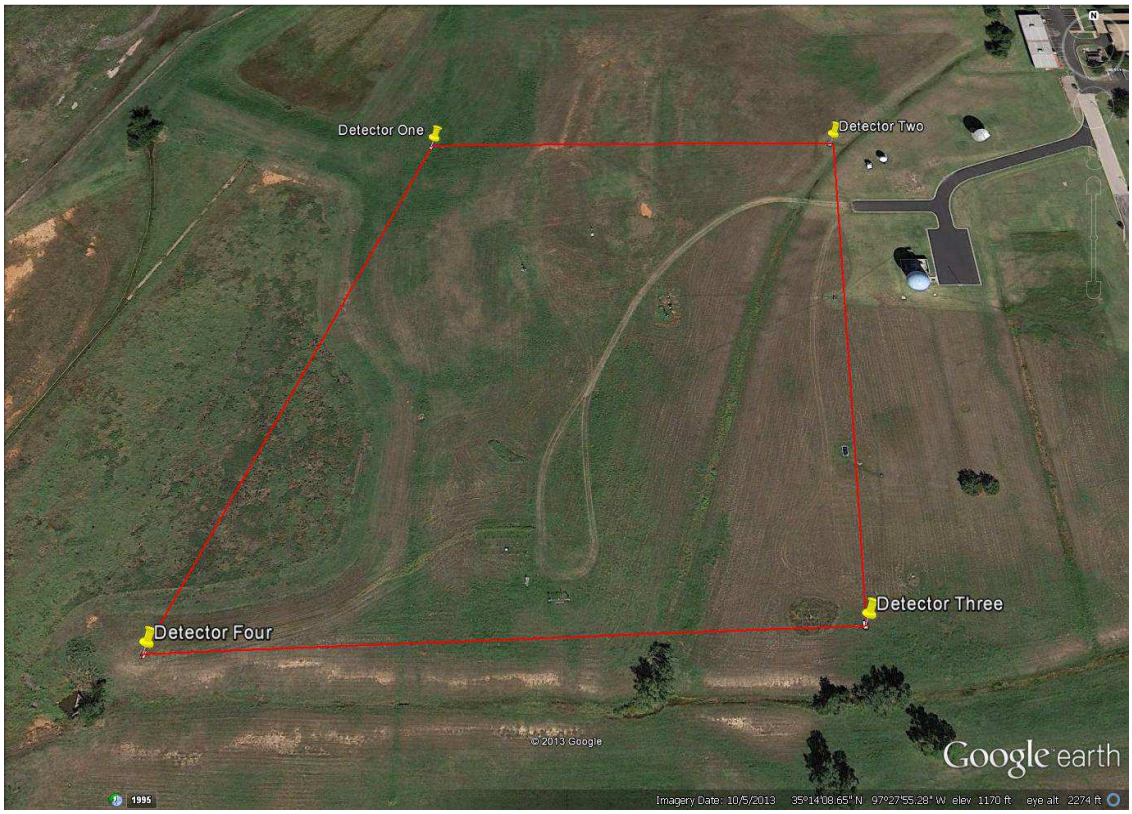

Figure 10.9: Image of the four cosmic ray muon detector array deployed in Norman, OK [119].

According to Figure 10.3, the density of secondary muons from EASs initiated by $<10^{15}$ eV cosmic ray primary protons is <1 secondary muons m^{-2} $shower^{-1}$ at all distances from the EAS. The cosmic ray muon detector described in Section 8.2.2 has a detection area of 0.25 m^2, so the likelihood of a single detector measuring a single muon from an EAS is low. However, the secondary muon density for EASs initiated by 10^{16} eV cosmic ray primary protons is >1 secondary muons m^{-2} $shower^{-1}$ for >100 m from the shower axis. For EASs initiated by high energy cosmic ray primaries, it is possible to measure secondary muons produced by one EAS at different locations hundreds meters away from one another. Thus, if several cosmic ray muon detectors are arranged over a large area and a majority of these detectors measure secondary muons in the same time interval, there is a high probability that an EAS initiated by a high energy cosmic ray passed through the area. This method of using the coincident measurement of secondary muons

in multiple detectors to detect the passage of EASs initiated by high energy cosmic ray primaries has been used in previous cosmic ray experiments [91, 120, 121, 122].

An array of four of the cosmic ray muon detectors described in Section 10.2.2 was deployed at the University of Oklahoma's School of Meteorology Test Field in Norman, OK (35° 14' 9.38" N 97° 27' 55.10" W). This region was chosen for the cosmic ray muon detector array in order to be within the three dimensional coverage area of the OKLMA. An image of the detector array is shown in Figure 10.9. The four detectors are arranged in a ~200 m square, with a detector in each of the corners. The time stamped data from each of the detectors are collected and processed in the OSU Radiation Laboratory in Stillwater. In order to analyze the ~5 Gb of data generated daily by each detector, a set of custom Python and C++ computer programs were developed to determine coincident secondary muon measurements between the four detectors. A minimum of three of the four cosmic ray muon detectors in the array must measure a secondary muon within the same 100 μs time bin in order for a coincident measurement to be considered an EAS event. The time and which coincident cosmic ray muons detectors detected the EAS are recorded for every EAS event for further analysis.

10.3. Experimental Results

In order to compare the lightning initiation data from the OKLMA and the EAS event data from the cosmic ray muon detector array directly, both data sets need to use the same time bins for their data. Because the lightning mapping stations time stamp the radiation event as soon as it records it, the OKLMA lightning initiation data are not binned and are listed by the time of the lightning discharge. Using a Python script, the first radiation source of every lightning discharge within 1 km of the center of the cosmic ray detector array is selected as a lightning initiation event. The time stamp of the lightning initiation event is then converted to the same time bins used for the EAS event data. Only lightning discharges within 1 km of the cosmic ray detector array are used in order to limit the range of EAS zenith angles to nearly vertical EASs that were assumed in the fair weather CORSIKA simulations. Also, with only four detectors in the array, there is no way to determine the zenith angle of the EAS with any degree of certainty. By restricting our analysis to only lightning discharges within 1 km of the center of the detector, we are only looking at the most ideal of conditions.

Figure 10.10 shows the number of lightning initiations that occurred with 1 km of the cosmic ray detector array for a thunderstorm on 19 May 2013. Because of lack of thunderstorms over the cosmic ray muon detector array the during the Fall of 2013 and Spring of 2014, the only data sets of thunderstorm conditions were from May and June of

2013. Those data sets used long 10 ms time bins instead of the current 100 μs time bins. Each black line shows the total number of secondary muons that were measured within a single time bin produced by a single EAS event. The red lines represent time bins that had at least one lightning initiation event.

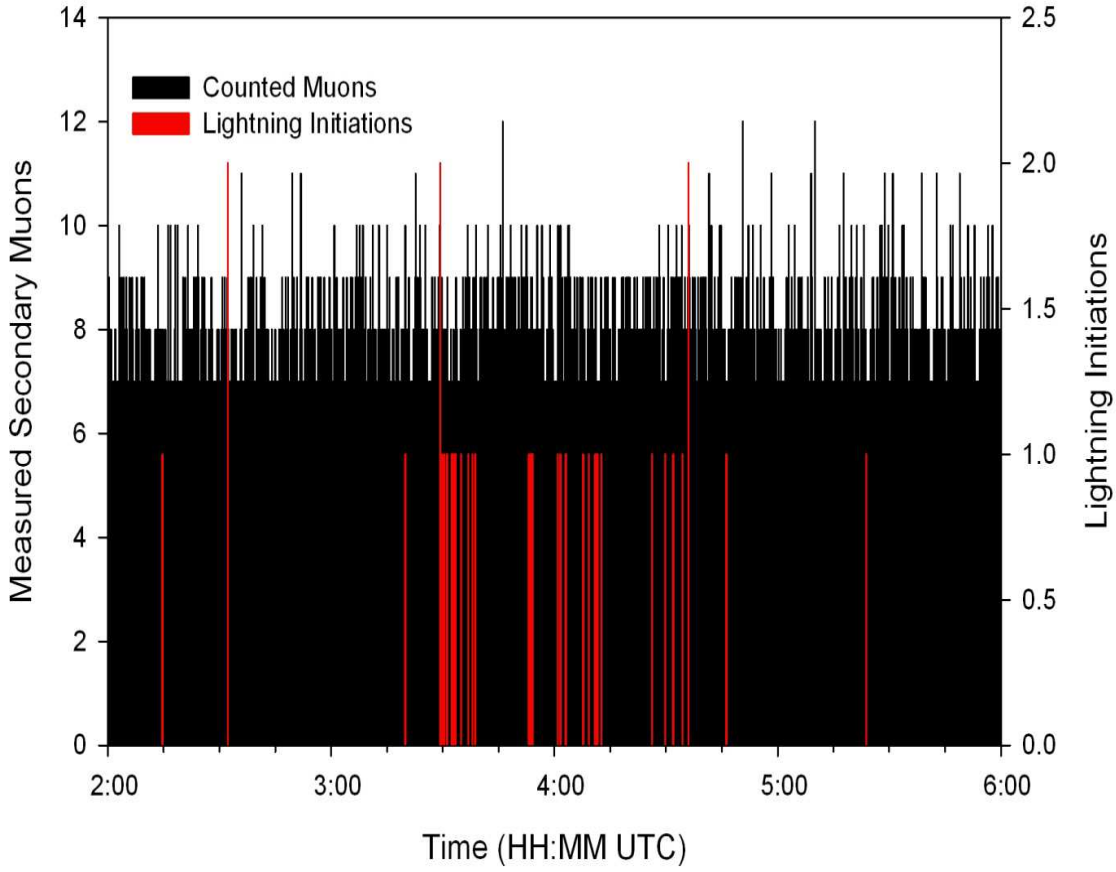

Figure 10.10: The distribution of EAS events and lightning initiation events within 1 km of the cosmic ray muon detector array for a thunderstorm on 5/19/2013. Each black line represents a single EAS event and the red lines are the number of lightning initiations within a single 10 ms time bin.

From Figure 10.10, it can be seen that the number of EAS events far outnumbers the number of lightning initiation events during this thunderstorm. EAS events are seen to occur at a constant rate regardless of the atmospheric weather conditions, whereas the lightning discharges occur in shorter 15 to 30 minute periods over the duration of the thunderstorm. To correlate EAS events with lightning initiations, the two data sets must be compared at a smaller time scale than an entire thunderstorm. Figure 10.11 shows

lightning initiations and EAS events on a 500 ms time scale, from the same thunderstorm shown in Figure 10.10. The EAS events still outnumber lightning initiations, but on this 500 ms time scale, individual EAS events can be observed. EAS events are stochastic in nature, so the time between EAS events is not constant. The pair of lightning initiations in Figure 10.11 occurred 40 ms after a pair of CREAS events.

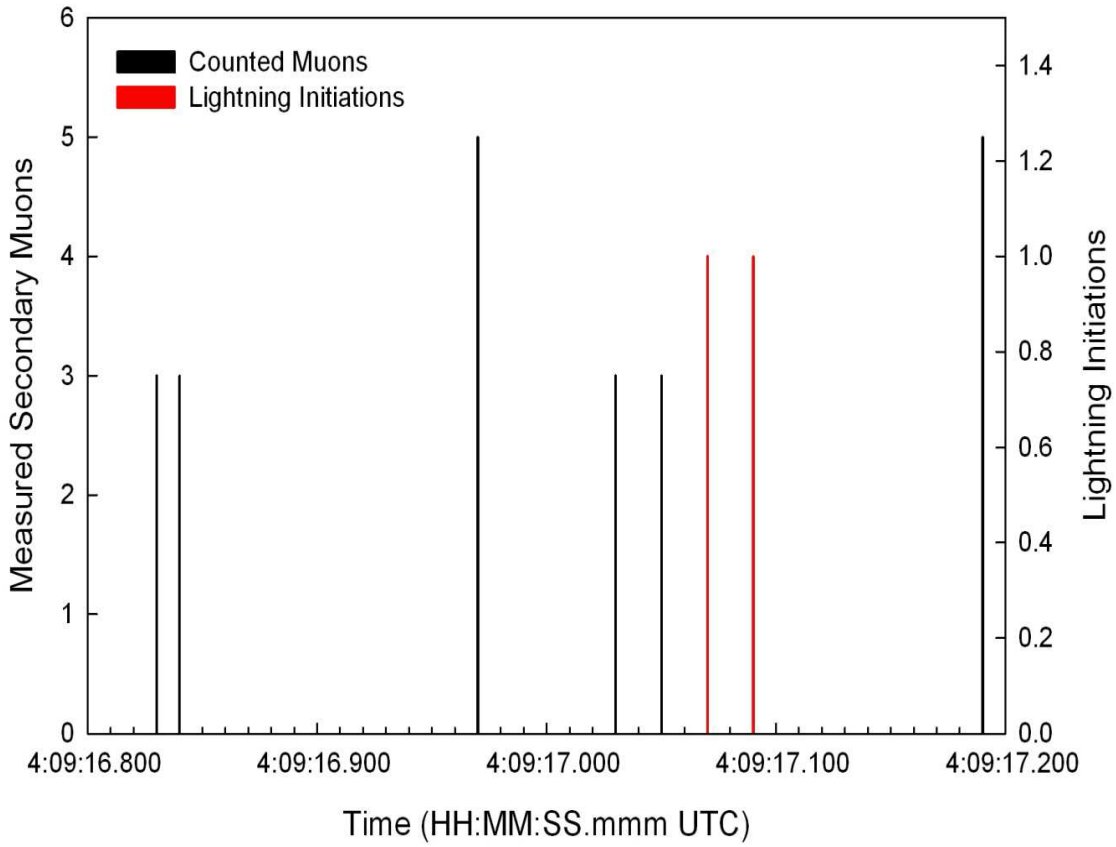

Figure 10.11: Plot of the EAS events and lightning initiation events within 1 km of the cosmic ray muon detector array for a thunderstorm on 5/19/2013. Each black line represents a single EAS event and the red lines are the number of lightning initiations within a single 10 ms time bin.

Figure 10.12 shows the distribution of the time between EAS events and lightning initiations that occurred within 1 km of the cosmic ray muon detector array. The data for Figure 10.12 were acquired from thunderstorms on 4/26/2013-4/27/2013, 5/16/2013-5/17/2013, and 5/18/2013-5/19/2013, which had a total of 310 lightning initiations within 1 km of the detector array. This is all the cosmic ray muon detector array data that have been collected during thunderstorm conditions during this time. Approximately 15% of

all lightning initiations occurred within 10 ms following a EAS event as detected by the cosmic ray muon detector array. The statistical significance of this result was compared to an average of 10 sets of simulated EAS events over the same time period. The simulated EAS occurred at the same frequency as the measured EAS events but the exact time bin was randomly determined. For the first eleven time bins (0-100 ms between the EAS event and a lightning initiation), $\chi^2 = 8.82$ (ten degrees of freedom), which means there is no significant difference between the measured and simulated EAS event data. For the first two time bins (0-10 ms between a EAS event and a lightning initiation), $\chi^2 = 3.02$ (one degree of freedom), which is statistically significant at the >90% confidence level. Therefore, it appears that the cosmic ray muon detector array is measuring statistically more EAS events coincident with lightning initiations than from an assumed random distribution of EAS events.

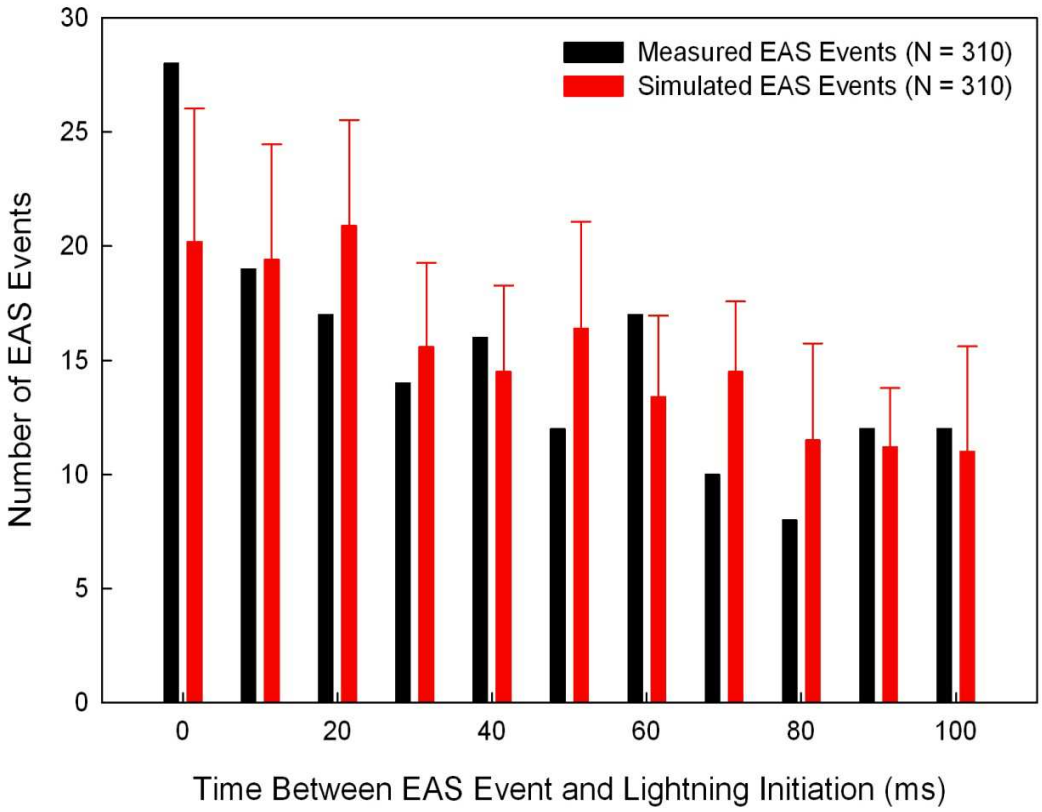

Figure 10.12: Plot of the time between EAS events and lightning initiation within 1 km of the cosmic ray muon detector array. The black bars represent actual EAS events measured by the cosmic ray muon detector array and the red bars represent randomly generated EAS events at the same average frequency. The error bars on the simulated EAS events represent 1σ. Data is from thunderstorms on 4/26/2013-4/27/2013, 5/16/2013-5/17/2013, and 5/18/2013-5/19/2013.

10.4. Discussion of Experimental Work

The current experimentally results show that the cosmic ray muon detector array is measuring more EAS events in coincidence with lightning initiation events within 1 km of the detector array than expected if the EASs occurred independent of lightning initiation. From the data collected from thunderstorms on 4/26/2013-4/27/2013, 5/16/2013-5/17/2013, and 5/18/2013-5/19/2013, the thunderstorms produced a total of 310 lightning initiations within 1 km of the detector. Approximately 15% of all lightning initiations were preceded within 10 ms by a EAS event measured by the cosmic ray muon detector array. Also, at >90% confidence level, the cosmic ray muon detector array measured statistically more EAS events than an assumed random EAS distribution of events in the 0-10 ms time bins. These preliminary results show that there may well be a correlation between EAS and lightning initiations. Since EASs generate the high energy electrons required by the RREA and hybrid models, these experimental results appear to support both of these models for lightning initiation.

However, the cosmic ray muon detector data analyzed in Section 10.3 were collected in 10 ms time bins which are much longer than the time required for a lightning discharge to be initiated within the atmosphere [3]. In November 2013, the cosmic ray muon detectors were upgraded to collect data in 100 μs time bins, a hundred times increase in resolution, in order to better correlate the passage of EASs through a thunderstorm and the initiation of nearby lightning discharges. As of the writing of this work, there have not been any cosmic ray muon detector array data collected at the 100 μs time resolution during a thunderstorm. As the experiment continues to collect data, the lightning initiation statistics that were presented in Section 10.3 will improve and should be able to show with better certainty if the passage of EASs through a thunderstorm is temporally correlated with nearby lightning initiations.

With only four cosmic ray muon detectors in the array, there is no way to determine with any certainty the directional information of the path of the EAS event. If the directional information of the EAS event could be determined from the detector array data, then it could be possible to follow the EAS shower front back into the thunderstorm and try to correlate the EAS event to specific lightning initiation. Correlating EAS events to specific lightning initiation events within the atmosphere would provide much stronger evidence in support of both the RREA and hybrid models than is found in the temporal correlation found in Section 10.3. However, to determine directional information for EAS events, the number of detectors within the array would have to be increased. Ground based cosmic ray experiments that measure the directional information of EASs typically have over a hundred detectors spread out over several square kilometers [120, 121]. For this experiment to prove that the passage of EASs through a thunderstorm cause lightning

initiation, the number of detectors in the array would need to be increased in order to determine the directional information of EAS events.

CHAPTER XI

DISCUSSION AND CONCLUSIONS

There are three research objectives in this work: 1) determining the fair weather secondary electron environment, 2) determined if there are sufficient numbers of secondary energetic electrons to initiate a lightning discharge in the atmosphere, and 3) to gather experimental evidence correlating the passage of GCR EASs through a thunderstorm with nearby lightning discharges. For the first objective, the secondary electron environment at thunderstorm altitudes (<12 km) was determined from longitudinal and lateral distributions simulated using the cosmic ray Monte Carlo Code CORSIKA 6.790. Using the secondary electron distributions and the geometry of an EAS, the fair weather secondary electron flux and energy spectra for both individual EASs and the ambient distribution of EASs were calculated. For the second objective, the secondary electrons inside the shower core of an EAS initiated by a 10^{16} eV cosmic ray primary proton were propagated through the vertical electric field profile measured in an actual thunderstorm. The number of secondary electrons within the EAS shower core was then compared to the lightning initiation criteria for both the RREA and hybrid models. For the third objective, secondary muons were measured by an array of four ground based cosmic ray muon detectors to determine the passage of EASs initiated by high energy cosmic ray primaries through the region above the detector array. The time of each EAS measured by the cosmic ray muon array is compared to the time of all lightning initiations as measured by the OKLMA to determine if there is a correlation between the two events.

11.1. The Fair Weather Secondary Electron Environment

From the EAS simulations carried out using CORSIKA 6.790, the secondary electron flux and energy spectra for both individual EASs and ambient distribution of the EASs in fair weather conditions were determined. The largest concentration of secondary electrons at lightning initiation altitudes (4-8 km) was found in the shower core of EASs

initiated by high energy cosmic ray primary protons. EASs initiated by a 10^{16} eV cosmic ray primary protons, the highest energy considered in this work, had a >1 MeV secondary electron density of ~10^5 electrons m^{-2} within its shower core at an altitude of 6 km. The fair weather ambient >1 MeV secondary electron flux at 6 km was found to be <10^3 electrons m^{-2} s^{-1}, which is approximately two orders of magnitude lower than the >1 MeV secondary electron density found within the shower core of a 10^{16} eV cosmic ray primary proton initiated EAS.

The fair weather secondary electron energy spectra showed that for developing EASs, the secondary energetic electrons ranged from 1 MeV to >100 GeV in the atmosphere. The average energy of the secondary electrons decreases with distance from the EAS shower axis from >1 GeV near the shower axis to ~100 MeV at 10 m from the shower axis to ~10 MeV near the edge of the shower front. The average energy of all the secondary electrons in an EAS was >10 MeV regardless of the altitude or energy of the initiating cosmic ray primary. EASs initiated by lower energy cosmic ray primaries dominate the ambient secondary electron energy spectrum at all altitudes. These low energy cosmic ray initiated EASs have far few of >100 MeV secondary electrons at lightning initiation altitudes than found in EASs initiated by higher energy cosmic ray primaries.

The fair weather ambient secondary electron energy spectrum on the ground calculated based on CORSIKA simulations agrees with the secondary electron energy spectrum reported in *Daniel and Stephens* [90] from 1974. *Daniel and Stephens* is still the most frequently referenced work on EAS secondary electrons in the fair weather atmosphere [11]. In *Daniel and Stephens*, there were no measurements of the secondary electrons at lightning initiation altitudes of 4 to 8 km, so this work could be considered as an update and expansion of the work by *Daniel and Stephens*.

Future work in determining the fair weather secondary electron environment would need to include the effect of non-vertical EASs and additional simulations of EAS initiated by lower energy cosmic ray primaries. One of the major assumptions used to calculate the secondary electron density and ambient flux was that all the EASs were vertical. For vertical EASs, the horizontal cross section of the shower front is a circle and the secondary electrons are distributed symmetrically around the shower axis. In non-vertical EASs, a horizontal cross section of the shower front would be an ellipse with the shower axis in the center of the ellipse. This would require that the secondary electron density be defined in a two-dimensional plane instead of the radial distance from the shower core. Including non-vertical EAS to the analysis would generate a more realistic secondary electron density and flux, but the analysis would be considerable more difficult than the analysis performed in this work.

Because the EASs initiated by the lowest energy cosmic ray primaries are in the attenuated stage of development at lighting initiation altitudes, these EASs have the

greatest variation in the number of secondary electrons at the chosen observation levels. For this reason, multiple EASs were simulated for each of the cosmic ray primary proton energy used in this work. However, due to the low number of secondaries and their higher flux, the error associated with EASs initiated by low energy cosmic ray primaries have a greater effect in the ambient secondary electron environment. By increasing the number of 10^{10} and 10^{11} eV cosmic ray proton simulations by an order of magnitude, the error associated with these EASs would be near the errors associated with the current number of 10^{16} eV simulations (~1%).

11.2. Lightning Initiation Models

From the analysis in Section 9.4, it was found that there was not a sufficient number of secondary electrons (both low and high energy) produced in the shower core of a 10^{16} eV cosmic ray primary proton initiated EAS to initiate a lightning discharge according to either the RREA or hybrid models. However, the required electron density needed to initiate a lightning discharge is vastly different between the two models, so it is best to discuss the models separately.

11.2.1. The RREA Model

The RREA model is the most well documented of the two lightning initiation models considered in this work. *Gurevich et al.* [9] originally proposed that the number of high energy secondary electrons produced in RREAs would be sufficient to directly generate a lightning discharge in the atmosphere. In *Gurevich et al.*, only ~1 MeV secondary electrons were considered to run away and generate RREAs in the strong electric field regions of the thunderstorm [9]. In this work, >1 MeV secondary electrons were considered to be able to run away in the strong electric field region. Using the streamer formation criteria of *Dawson and Winn* [58], this work showed that the total (both high and low energy) electron density produced in the vertical electric field profile from *Marshall et al.* [21] was approximately ten orders of magnitude too low to initiate a streamer that can develop into a lightning leader.

After *Gurevich et al.* proposed the RREA model [9], several research groups started to develop Monte Carlo codes to study RREAs. In these Monte Carlo codes, a number of monoenergetic electrons were introduced to a region of air with a strong external electric field. The monoenergetic electrons were then propagated through strong electric field

region following the interactions described in Chapter 6. All the particles that reach an observation level, both primaries and secondary particles, were counted and analyzed [16, 17, 18]. These monoenergetic electron simulations were then weighted by some parameterization to approximate an EAS.

Using their own electron Monte Carlo code, *Dwyer* [17] and *Dwyer and Smith* [18] found that electrons between 1 and 10 MeV could run away in a strong electric field, unlike the assumption made by *Gurevich et al* [9]. *Dwyer* [17] also found that runaway electrons had an average energy of 7.2 MeV regardless of the electric field strength. From energy spectra plotted in Figures 9.9, the secondary electron population ranges in energy from 1 MeV to >10 GeV, with only the newly generated secondary electrons being <10 MeV in an accelerating electric field region. As in *Gurevich et al.*, the results of *Dwyer* do not match with the range of secondary electron energies calculated in this work from CORSIKA simulations and model calculations.

Carlson et al. [16] used the Monte Carlo code GEANT4 to simulate RREAs after having determined the secondary electron environment with cosmic ray code AIRES, which is a cosmic ray Monte Carlo code similar to CORSIKA [123]. Secondary electrons up to 10 GeV were simulated in GEANT4 in *Carlson et al.* However, *Carlson et al.* only determined the efficiency of producing runaway electrons in the atmosphere, i.e. what fraction of secondary electrons produced runaway secondary electrons. *Carlson et al.* found that >1 MeV secondary electrons produced runaway secondary electrons, which is expected for any secondary electron greater than twice the minimum runaway energy, shown in Figure 6.9. However, *Carlson et al.* is unique because it was the only study of the RREA model that took into account >10 MeV secondary electrons.

In order for RREAs to initiate a lightning discharge directly, the density of secondary electrons (both high and low energy) would need to be increased by ten orders of magnitude. This could be accomplished by expanding the length of the strong accelerating electric field region to over a kilometer and increasing the strength of electric field to >300 kV m^{-1}. However, the average maximum electric field in a thunderstorm is 130 kV m^{-1} and the region of that electric field is typically <1 km [20]. Therefore, the RREA model as proposed by *Gurevich et al.* [9] is likely not responsible for initiating lightning discharges in typical thunderstorm conditions.

These results agree with the results of *Dwyer* [19] showing that the RREA model is not responsible for initiating most lightning discharges. *Dwyer* [19] proposed a Positron Feedback mechanism [17, 19] to produce a sufficient number of seed electrons to initiate a lightning discharge. The Positron Feedback mechanism causes secondary positrons that are produced along with the secondary electrons in an electromagnetic cascade are accelerated upward by the positive electric field. These accelerated positrons collide with electrons and annihilate, producing two photons. Since the kinetic energy of the positron

is also divided between the pair of photons, the secondary photons will have enough energy to initiate new electromagnetic cascades in the atmosphere. These new electromagnetic cascades develop behind the rest of the EAS shower front in the low energy secondary electron plasma. The secondary electrons from this new electromagnetic cascade generate more low energy secondary electrons which increases the electron density of the plasma. Secondary positrons from these new electromagnetic cascades are then accelerated upward by the ambient electric field and repeat the above process until a lightning discharge is initiated [17, 19]. Future work on the RREA model would include investigating the Positron Feedback mechanism proposed by *Dwyer*, since the RREA model proposed by *Gurevich et al.* is not sufficient to explain lightning initiation within the atmosphere.

11.2. The Hybrid Model

The hybrid model of lightning initiation proposed by *Petersen et al.* [10] hypothesizes that instead of directly initiating a lightning discharge the low energy electron plasma created by RREAs enhances the ambient electric field. Charged hydrometeors within this enhanced electric field region will undergo point discharge and initiate a lightning discharge according to conventional lightning discharge theory. From the analysis in Section 9.4, the electric field enhancement was only 12 kV m^{-1} from the total electron density calculated in this work. According to *Gurevich and Karashtin* [111], the required electric field enhancement to initiate a lightning discharge is between 100 and 200 kV m^{-1}, which is an order of magnitude larger than that calculated in this work. However, according Figure 9.10, the required electric field enhancement could be obtained by an electron density that was only an order of magnitude greater, unlike the ten orders of magnitude increased needed in the RREA model. This increase in the secondary electron density could be created in realistic conditions by a slight increase in the electric field strength and length of the acceleration region length [3, 21]. Thus it is possible for the hybrid model to may be able to explain for lightning discharges in the atmosphere.

Unlike the RREA model, there have been few previous studies of the hybrid model initiating lightning discharges in the atmosphere. The most referenced study on the hybrid model is *Gurevich and Karashtin* [111], which looked at the radio emissions before a lightning discharge was observed in the atmosphere. According to *Gurevich and Karashtin*, the radio pulses that occur before a lightning discharge are made from bipolar sources that are similar to the radio signals given off by hydrometeors in an enhanced electric field. Since the strength of the radio signal is proportional to electric field

enhancement, the strength of the radio signal could be used to determine the electron density of the plasma surrounding the hydrometeors. From their results, *Gurevich and Karashtin* estimate that EAS initiated by $>10^{12}$ eV cosmic ray primaries could enhance the electric field enough to cause several hydrometeors to breakdown simultaneously in the atmosphere. The result calculated in this work does not agree with the results of *Gurevich and Karashtin*. However, this work still shows that the hybrid model could be responsible for lightning discharges in the atmosphere.

Future work with the hybrid model could include calculating the electric field enhancement due to the low energy secondary electrons generated by high energy secondary electrons along the entire EAS shower front rather than just the secondary electrons within the shower core. The present work only calculated the electric field enhancement due to the low energy secondary electron plasma created by high energy secondary electrons within 10 m of the shower axis of a 10^{16} eV cosmic ray primary proton initiated EAS. This region has the largest secondary electron density of the entire shower front, but the majority of the secondary electrons in the EAS are found outside this region in the rest of the shower front. By including the low energy secondary electrons generated by the high energy secondary electrons, the low energy electron plasma will increase in size and can possibly increase the local electric field enhancement and possibly initiate multiple hydrometeors simultaneously as was reported in *Gurevich and Karashtin* [111].

11.3. Experimental Evidence of the Correlation of the Passage of EASs through a Thunderstorm and Lightning Initiation

In three thunderstorms that passed over the ground based cosmic ray muon detector array, a total of 310 lightning initiations were measured by the OKLMA within 1 km of the center of the detector array. Of those 310 lightning initiations, 47 (15%) of those lightning initiations were preceded by less than 10 ms by an EAS event measured by the cosmic ray muon detector array. Compared to a random distribution of EASs, the cosmic ray muon detector array measured more EAS that occurred within 10 ms of a lightning initiation at a >90% confidence level. These preliminary results do support that the passage of EASs through the thunderstorm are correlated to lightning initiations, but are not sufficient to represent verifiable proof.

In order to improve this experiment, the experiment needs to collect more data during active thunderstorms and with smaller time bins in the muon data. More data during thunderstorms would generate better statistics and the smaller time bins in the muon data

would remove falsely labeled EAS events. Both of these improvements are currently being implemented.

Another method to improve the experimental evidence would be to increase the number of cosmic ray muon detectors within the array. Currently, there are not enough detectors in the array to accurately determine the direction in which the EAS was traveling through the atmosphere. The OKLMA records the location, in three dimensions, in the atmosphere of every lightning initiation within its detection area. If the directional information of the EAS were known, then the path of the EAS could be traced back into the thunderstorm to determine if the EAS shower front traveled near any lightning initiation locations. With that sort of analysis, the passage of EASs through the thunderstorm and nearby lightning initiations would be much stronger evidence for a correlation between EASs and lightning initiation.

11.4. General Conclusions

There are three main conclusions that can be drawn from this work. The first conclusion is that there are numbers of >100 MeV secondary electrons within EASs initiated by high energy cosmic ray primaries. Because of their high energy, these secondary electrons do not gain energy with distance while running away in accelerating electric fields typically found at lightning initiation altitudes of 4 to 8 km. However, these >100 MeV secondary electrons are accelerated in the electric field and produce more runaway seed electrons that can run away in thunderstorm electric fields than ~1 MeV secondary electrons. Especially early on in the development of an RREA, these >100 MeV secondary electrons are producing the majority of the other seed electrons. Much of the previous work with the RREA model only assumed that up to 10 MeV seed electrons are able to initiate an RREA and do not consider the effect that these higher energy secondary electrons would have on RREA development [9, 14, 15, 16, 17, 18]. Any future work with RREAs should include the effects of these >100 MeV secondary electrons in order to generate a more realistic picture of the RREA environment within a thunderstorm.

The second conclusion is that the RREA model as proposed in *Gurevich et al.* [9] was shown not to be responsible for lightning initiation. The population of >1 MeV secondary electrons in the shower core of an 10^{16} eV cosmic ray primary proton initiated EAS as determined from CORSIKA simulations traveling through the vertical thunderstorm electric field profile measured by *Marshall et al.* [21], the total electron density was calculated to be approximately ten orders of magnitude too low to initiate a streamer in the atmosphere according to criteria calculated by *Dawson and Winn* [58]. Without stronger thunderstorm electric fields and longer acceleration regions, there are not a

sufficient number of >1 MeV secondary electrons to initiate a lightning discharge according to the RREA model. However, other lightning initiations models, e.g. the hybrid model [10] or Positron Feedback mechanism [19], which still require RREAs to generate a large number of secondary electrons could still be responsible for lightning initiation within the atmosphere. More work is needed to test these other lightning initiation models.

The last conclusion is that the results from the cosmic ray muon detector array experiment has shown that there is a correlation between the time an EAS event is detected by the array and a lightning discharge is initiated within 1 km of the detector array. With the current 310 recorded lightning initiations, there is a >90% probability that EASs are travelling through the thunderstorm when a lightning discharge is initiated. As the experiment continues to collect data, improved statistics are expected to strengthen the correlation between the passage of EASs through the thunderstorm and nearby lightning initiations. With the current four detectors in the cosmic ray muon detector array, there is no way to correlate specific EASs with any one lightning discharge initiation. The directional information, in addition to timing information, of the EAS events would need to be known with some certainty in order to correlate a particular EAS with a specific lightning initiation event. The cosmic ray muon detector array would require additional detectors in order to determine the directional information of the EAS events.

REFERENCES

[1] Light, T.E.L., S.M. Davis, W. Boeck, and A.R. Jacobson, "Global nighttime lightning flash rates and characteristics observed with the FORTE satellite", *Los Alamos National Laboratory Technical Report*, 2003.

[2] Uman, Martin A., *The Art and Science of Lightning Protection*, Cambridge University Press, 2008.

[3] Orville, Richard E., Gary R. Huffines,"Cloud-to-Ground Lightning in the United States: NLDN Results in the First Decade," *Mon. Wea. Rev.*, **129**, May 2001.

[4] Rakov, Vladimir A. and Martin A. Uman, *Lighting: Physics and Effects*, Cambridge University Press, Cambridge, 2003.

[5] Holle, R. L., R. E. Lopez, L. J. Arnold, and J. Endres, "Insured Lightning-Caused Property Damage in Three Western States", *J. App. Meteor.*, **35**, 1996.

[6] Jensenius, John S. Jr., "A Detailed Analysis of Recent Lightning Deaths in the United States", NOAA report, 2013.

[7] U.S. Standard Atmosphere, 1976, U.S. Government Printing Office, Washington D.C., 1976.

[8] Williams, Earle R., "C.T.R. Wilson versus G.C. Simpson: Fifty years of controversy in atmospheric electricity", *Atmospheric Research*, **91**, 2009.

[9] Gurevich, A. V., G.M. Milikh, and R. Roussel-Dupre, "Runaway electron mechanism of air breakdown and preconditioning during a thunderstorm", *Phys. Lett. A*, **165**, 1992.

[10] Petersen, Danyal, Matthew Bailey, William H. Beasley, and John Hallett, "A brief review of the problem of lightning initiation and a hypothesis of initial lightning leader formation", *J. Geophys. Res.*, **113**, 2008.

[11] Grieder, Peter, K. F., *Cosmic Rays at Earth*: *Researcher's Reference Manual and Data Book*, Elsevier, Amsterdam, 2001.

[12] Grieder, Peter K.F., *Extensive Air Showers: High Energy Phenomena and Astrophysical Aspects*, Vol. 1, Springer, Heidelberg, Germany, 2010.

[13] Heck, D., J. Knapp, J.N. Capdevielle, G. Schatz and T. Thouw, "CORSIKA: A Monte Carlo Code to Simulate Extensive Air Showers", *Report FZKA 6019*, 1998.

[14] Colman, J.J., R. A. Roussel-Dupré, and L. Triplett, "Temporally self-similar electron distribution functions in atmospheric breakdown: The thermal runaway regime", *J. Geophys. Res.*, **115**, 2010.

[15] Gurevich, A. V., K. P. Zybin, and R. A. Roussel-Dupre, "Lightning initiation by simultaneous effect of runaway breakdown and cosmic ray showers", *Phys. Lett. A*, **254**, 1999.

[16] Carlson, B.E., N. G. Lehtinen, and U. S. Inan, "Runaway relativistic electron avalanche seeding in the Earth's atmosphere", *J. Geophys. Res.*, **113**, 2008.

[17] Dwyer, J. R., "Relativistic breakdown in planetary atmospheres", *Physics of Plasmas*, **14**, 2007.

[18] Dwyer, J. R. and D. M. Smith, "A comparison between Monte Carlo simulations of runaway breakdown and terrestrial gamma-ray flash observations", *Geophy. Re. Lett*., **32**, 2005.

[19] Dwyer, J. R., "A fundamental limit on electric fields in air", *Geophys. Re. Lett.*, **30**, 2003.

[20] MacGorman, Donald R. and W. David Rust, *The Electrical Nature of Storms*, Oxford University Press, New York, 1998.

[21] Marshall, T.C., M. Stolzenburg, C.R. Maggio, L.M. Coleman, P.R. Krehbiel, T. Hamlin, R.J. Thomas, and W. Rison, "Observed electric fields associated with lightning initiation," *Geophy. Res. Lett.*, **32**, 2005.

[22] Dorman, Lev I, *Cosmic Rays in the Earth's Atmosphere and Underground*, Kluwer Academic Publishers Dordrecht, 2004.

[23] Ruse, Aaron, "Construction of a Muon Detector Array for the Correlation of Cosmic Ray Count Rates with Lightning Discharges", Oklahoma State Master's Thesis, May 2013.

[24] Viggiano, A.A. and Frank Arnold, "Ion Chemistry and Composition of the Atmosphere," *Handbook of Atmospheric Electrodynamics*, Vol 1, ed. Hans Volland, CRC Press, Boca Raton, 1995.

[25] Cairo, Francesco, "Atmospheric Thermodyamics", *Thermodynamics – Interaction Studies – Solids, Liquids, and Gases*, Ed. Juan Carlos Moreno Pirajajn, 2011.

[26] NIST, *ESTAR: Stopping Power and Range Tables for Electrons,* <http://physics.nist.gov/PhysRefData/Star/Text/ESTAR.html>

[27] Poschl, Ulrich, "Atmospheric Aerosols: Composition, Transformation, Climate, and Health Effects," *Angew. Chem. Int. Ed.*, **44**, 2005.

[28] Bouquegneau, Christian and Vladimir Rakov, *How Dangerous is Lightning?*, ed William Beasley, Dover Publications, Mineola, NY, 2010.

[29] Boltek Corporation, *EFM-100 Atmospheric Electric Field Monitor Installation/Operators Guide*, 2011.

[30] Rycroft, M.J., S. Israelsson, and C. Price, "The global atmospheric electric circuit, solar activity and climate change," *Journal of Atmospheric and Solar-Terrestrial Physics* **62**, 2000.

[31] Bering, Edgar A. III, Arthur A. Few, and James R. Benbrook, "The Global Electric Circuit," *Phy. Today,* **51**, 1998.

[32] Longair, Malcolm S., *High Energy Astrophysics,* Vol 1, 2nd ed., Cambridge University Press, Cambridge, England, 1992.

[33] International Association of Geomagnetism and Aeronomy, Working Group V-MOD, "International Geomagnetic Reference Field: the eleventh generation", *Geophy. J. Int.*, **183**, 2010.

[34] Song, Xiaodong and Paul G. Richards, "Seismological evidence for differential rotation of the Earth's inner core", *Nature*, **382**, 1996.

[35] Williams, Earle R., "Meteorological Aspects of Thunderstorms," *Handbook of Atmospheric Electrodynamics*, Vol I, Ed. Hans Volland, CRC Press, Boca Raton, 1995.

[36] Mason, John and Nigel Mason, "The physics of a thunderstorm," *Eur. J. Phys.* **24**, 2003.

[37] Rogers, Matt, "Cloud Formation," AIM Workshop Presentation 25 July 2006.

[38] Franklin, Benjamin, "A Letter from Mr. Franklin to Mr. Peter Collinson, F. R. S. concerning the Effects of Lightning," *Phil. Trans. Roy. Soc.*, **47**, 289, 1752.

[39] Simpson, George and F.T. Scrase, "The Distribution of Electricity in Thunderclouds," *Pro. Roy. Soc. A*, **161**, 906, 1937.

[40] Saunders, C.P.R., "Thunderstorm Electrification," *Handbook of Atmospheric Electrodynamics*, Vol 1, ed. Hans Volland, CRC Press, Boca Raton, 1995.

[41] Stolzenburg, Maribeth and Thomas C. Marshall, "Charge Structure and Dynamics in Thunderstorms," *Space Sci. Rev.*, **137**, 1-4, 2008.

[42] Feynman, Richard, Robert B. Leighton, and Matthews Sands, "Electricity in the Atmosphere," *The Feynman Lectures on Physics: Mainly Electromagnetism and Matter*, Vol 2, Addison-Wesley Publishing, Reading, MA, 1964.

[43] Rison, William, Paul Krehbiel, Ron Thomas, Time Hamlin, and Jeremiah Harlin, "3-Dimensional Lightning Observations Using a Time-of-Arrival Lightning Mapping System," Int. Lightning Detection Conf., 16–18 October 2002, Tucson, Vaisala, 2002.

[44] Beasley, William H., "Lightning Ontology and Phenomenology," Brown Bag Lectures on Lightning, 22 August 2005.

[45] Jackson, John David, *Classical Electrodynamics*, 3rd ed, John Wiley and Sons Inc., 1999.

[46] New Mexico Tech Physics Department, "Oklahoma LMA Realtime Data," <http://www.lightning.nmt.edu/oklma>

[47] Texas Weather Instruments, Inc., "WLS-8000 Instruction Manual, 1997.

[48] NOAA satellite Images.

[49] Boltek, "Storm Tracker Lightning Detection System", <http://www.boltek.com/stormtracker.html>.

[50] Petersen, Danyal A., *Laboratory Study of Electrical Discharges on Vapor Grown Ice Crystals Subjected to Strong Electric Fields*, Dissertation, University of Nevada-Reno, 2009.

[51] Bazelyan, E.M. and Yu. P. Raizer, *Spark Discharge*, CRC Press, Boca Raton, 1998.

[52] Loeb, Leonard B., "The Theory of the Electrical Breakdown of Gases at Atmospheric Pressure," *J. of Franklin Institute*, 1928.

[53] Ortega, P., P. Domens, A. Gilbert, B. Hutzler, and G. Riquel, “Performance of a 16.7 m air rod-plane gap under a negative switching impulse”, *J. Phys. D: Appl. Phys.* **27**, 1994.

[54] Petersen, Danyal, “Thunderstorm Electricity”, Presentation.

[55] Loeb, Leonard B., “The Mechanism of Lightning Discharge,” *J. of Franklin Institute*, 1948.

[56] International Commission on Radiation Units and Measurements, “Average Energy Required to Produce an Ion Pair”, *ICRU Report 31*, 1979.

[57] Beaty, William and Steven A. Ackerman, "What causes the strange glow known as St. Elmo's Fire? Is this phenomenon related to ball lightning?", *Scientific American*, September 1997.

[58] Dawson, G. A. and W. P. Winn, “A model for streamer propagation”, *Zeitschrift ftir Physik*, **183**, 1965.

[59] Nierneyer, L., L. Ullrich, and N. Wiegart, “The Mechanism of Leader Breakdown in Electronegative Gases”, *IEEE Transactions on Electrical Insulation*, **24**, April 1989.

[60] Bruce, C.E.R. and R.H. Golde, “The Lightning Discharge,” *J. Institution of Electrical Engineers-Part II: Power Engineering*, ed. W.K. Brasher, **88**, 6, December 1941.

[61] Shao, X. M. and P. R. Krehbiel, “The spatial and temporal development of intracloud lightning”, *J. Geophys. Res.*, **101**, 1996.

[62] Ogawa, Toshio, “Lightning Currents”, *Handbook of Atmospheric Electrodynamics*, Vol 1, ed. Hans Volland, CRC Press, Boca Raton, 1995.

[63] Williams, Earle, Bob Boldi, Anne Matlin, Mark Weber, Steve Hodanish, Dave Sharp, Steve Goodman, Ravi Raghavan, Dennis Buechler, “The behavior of total lightning activity in severe Florida thunderstorms,” *Atmospheric Research*, **51**, 1999.

[64] Boccippo, Dennis J., Kenneth L. Cummins, Hugh J. Christian and Steven J. Goodman, “Combined Satellite- and Surface-Based Estimation of the Intracloud–Cloud-to-Ground Lightning Ratio over the Continental United States”, *Mon. Wea. Rev.*, **129**, January 2001.

[65] Petersen, Danyal, Lightning Discharge Photographs.

[66] Uman, M.A., “The best lightning photo I have ever seen”, *Weatherwise*, **44**, 1991.

[67] Rao, M. V. S. and B. V. Sreekantan, *Extensive Air Showers*, World Scientific, Singapore, 1998.

[68] Gaisser, Thomas K., *Cosmic Rays and Particle Physics*, Cambridge University Press, New York, 1990.

[69] Horandel, Jorg R., "On the knee in the energy spectrum of cosmic rays", *Astroparticle Physics*, **19**, 2003.

[70] Rossi, Bruno and Kenneth Greisen, "Cosmic Ray Theory", *Rev. Mod. Phys.*, **13**, 1941.

[71] Reedy, Robert C., "Nuclide Production by Primary Cosmic-Ray Protons", *J. Geophys. Res.*, **92**, 1987.

[72] Dwyer, Joseph R., Martin A. Uman, Hamid K. Rassoul, Maher Al-Dayeh, Lee Caraway, Jason Jerauld, Vladimir A. Rakov, Douglas M. Jordan, Keith J. Rambo, Vincent Corbin, and Brian Wright, "Energetic Radiation Produced During Rocket-Triggered Lightning", *Science*, **299**, 2003.

[73] Simpson, J. A., "Elemental and Isotopic Composition of the Galactic Cosmic Rays", *Ann. Rev. Nucl. Part. Sci.*, **33**, 1983.

[74] Picozza, P. and L. Marcelli, "Electron cosmic ray measurements in space", *Astroparticle Physics*, **53**, 2014.

[75] Cronin, James W., "Cosmic rays: the most energetic particles in the universe", *Rev. Mod. Phys.*, **71**, 1999.

[76] Rossi, Bruno, *High-Energy Particles*, Prentice-Hall, Inc., Englewood Cliffs, NJ, 1952.

[77] Heck, Dieter, Tanguy Pierog, Gevorg Poghosyan, and Ralph Engel, "Challenges of simulating air showers at ultra-high energy," Computational Methods in Science and Engineering Workshop (SimLabs@KIT 2010), Karlsruhe, Nov. 29-30, 2010.

[78] NIST, *PSTAR: Stopping Power and Range Tables for Protons*, <http://physics.nist.gov/PhysRefData/Star/Text/PSTAR.html>

[79] Beringer J. et al. (Particle Data Group), "Baryons", Phys. Rev. D86, 010001, 2012.

[80] Beringer J. et al. (Particle Data Group), "Mesons", Phys. Rev. D86, 010001, 2012.

[81] Greisen, Kenneth, "Cosmic Ray Air Showers", *Annu. Rev. Nucl. Sci.*, 1960.

[82] Beringer J. et al. (Particle Data Group), "Leptons", *Phys. Rev.*, **D86**, 010001, 2012.

[83] Bushberg, Jerrold T., J. Anthony Seibert, Edwin M. Leidholdt Jr., and John M. Boone, *The Essential Physics of Medical Imagining*, 2nd ed, Lippincott Williams and Wilkins, Philadelphia, 2002.

[84] Staub, H., H. Bethe, J. Ashkin, N.F. Ramsey, and K.T. Bainbridge, *Experimental Nuclear Physics*, Vol 1, ed. E. Segre, John Wiley & Sons, Inc., New York, 1953.

[85] International Commission on Radiation Units and Measurements, "Stopping Powers for Electrons and Positrons", *ICRU Report 37*, 1984.

[86] Turner, J. E., H. G. Paretzke, R. N. Hamm, H. A. Wright and R. H. Ritchie, "Comparative Study of Electron Energy Deposition and Yields in Water in the Liquid and Vapor Phases", *Rad. Res.*, **92**, 1, 1989.

[87] Ziegler J. F., J. P. Biersack, and M. D. Ziegler, *SRIM: The Stopping and Range of Ions in Matter*. SRIM Co., 2008.

[88] MacGorman D.R., W. D. Rust, T. J. Schuur, M. I. Biggerstaff, J. M. Straka, C. L. Ziegler, E R. Mansell, E. C. Bruning, K. M. Kuhlman, N. R. Lund, N. S. Biermann, C. Payne, L. D. Carey, P. R. Krehbiel, W. Rison, K. B. Eack, and W. H. Beasley, "TELEX The Thunderstorm Electrification and Lightning Experiment". *Bull. Amer. Meteor. Soc.*, **89**, 2008.

[89] Gurevich, Alexander V. and Kirill P. Zybin, "Runaway Breakdown and the Mysteries of Lightning", *Physics Today*, May 2005.

[90] Daniel, R.R. and S. A. Stephens, "Cosmic-Ray-Produced Electrons and Gamma Rays in the Atmosphere", *Rev. Geophys. & Space Phys.*, **12**, 1974.

[91] The IceCube Collaboration, "IceTop: The surface component of IceCube", *Nuc. Inst. & Meth. Phys. Res. A*, **700**, 2013.

[92] S. Riggi, S., A. Insolia, G. Medina-Tanco, and E. Trovato,"Reconstruction of muon tracks in a buried plastic scintillator muon telescope (BATATA)", *Nuc. Inst. & Meth. Phys. Res. A*, **688**, 2012.

[93] d'Enterria, David, Ralph Engel, Tanguy Pierog, Sergey Ostapchenko, and Klaus Werner, "Constraints from the first LHC data on hadronic event generators for ultra-high energy cosmic ray physics", *Astroparticle Physics*, **2**, 2011.

[94] Milke, J., T. Antoni, W. D. Apel, F. Badea, K. Bekk, A. Bercuci, H. Blumer, H. Bozdog, I. M. Brancus, C. Buttner, A. Chilingarian, K. Daumiller, P. Doll, R. Engel, J. Engler, F. Febler, H. J. Gils, R. Glasstetter, A. Haungs, D. Heck, J. R. Horandel, K.-H. Kampert, H. O. Klages, G. Maier, H. J. Mathes, H. J. Mayer, M. Muller, R. Obenland, J. Oehlschlager, S. Ostapchenko, M. Petcu, H. Rebel, A. Risse, M. Risse, M. Roth, G. Schatz, H. Schieler, J. Scholz, T. Thouw, H. Ulrich, J. van Buren, A. Vardanyan, A. Weindl, J. Wochele, and J. Zabierowski, "Investigation of hadronic interaction models with the KASCADE experiment", *Nuc. Phys. B. (Proc. Suppl.)*, **151**, 2006.

[95] Apel, W. D., A. F. Badea, K. Bekk, J. Blumer, H. Bozdog, I. M. Brancus, K. Daumiller, P. Doll, R. Engel, J. Engler, H. J. Gils, R. Glasstetter, A. Haungs, D. Heck, J. R. Horandel, K.-H. Kampert, H. O. Klages, H. J. Mathes, H. J. Mayer, J. Milke, J. Oehlschlager, S. Ostapchenko, M. Petcu, T. Pierog, H. Rebel, A. Risse, M. Risse, M. Roth, G. Schatz, H. Schieler, H. Ulrich, J. van Buren, A. Weindl, J. Wochele and J. Zabierowski, "Test of interaction models up to 40 PeV by studying hadronic cores of EAS", *J. Phys. G: Nucl. Part. Phys,*. **34,** 2007.

[96] Ostapchenko, S., "QGSJET-II: towards reliable description of very high energy hadronic interactions", *Nuc. Phys. B (Proc. Suppl.)*, **151**, 2006.

[97] Fesefeldt, H., *Report PITHA-85/02*, 1985.

[98] Engel, Ralph, "Modeling of Hadronic Interactions", presented at CORSIKA School at Ooty, India on December 17-20, 2010.

[99] Nelson, W.R., H. Hirayama and D.W. Rogers, *Report SLAC 265*, 1985.

[100] Bielajew, A. F., H. Hirayama, W. R. Nelson, and D. W. O. Rogers, "History, overview and recent improvements of EGS4", *Report NRC-PIRS-0436*, 1994.

[101] Heck, D. and T. Pierog, *Extensive Air Shower Simulation with CORSIKA: A User's Guide*, 2010.

[102] Heck, D, "The SLANT Option of the Air Shower Simulation Program CORSIKA," *FZKA Report 7082*, 2004.

[103] Sima, O., H. Rebel, A. Haungs, G. Toma, C. Manailescu, C. Morariu, J. C. Arteaga, K. Bekk, M. Bertaina, J. Blumer, H. Bozdog, I. M. Brancus, A. Chiavassa, F. Cosavella, V. de Souza, P. Doll, R. Engel, M. Finger, R. Glasstetter, C. Grupen, D. Heck, T. Huege, K. H. Kampert, D. Kang, H. J. Mathes, H. J. Mayer, J. Oehlschlager, M. Roth, J. Wochele, M. Wommer, and J. Zabierowski, "Restoring the azimuthal symmetry of lateral distributions of charged particles in the range of the KASCADE-Grande experiment", *Nuc. Inst. & Meth. Phys. Res. A*, **638**, 2011.

[104] Capdevielle, J. N., C. Le Gall , and Kh. N. Sanosyan, “Simulation of extensive air showers at ultra-high energy using the CORSIKA Monte Carlo code”, *Astroparticle Physics*, **13**, 2000.

[105] Song, C., Z. Cao, B. R. Dawson, B. E. Fick, P. Sokolsky, and X. Zhang, “Energy estimation of UHE cosmic rays using the atmospheric fluorescence technique”, *Astroparticle Physics*, **14**, 2000.

[106] Risse, Markus and Dieter Heck, “Energy release in air showers”, *Astroparticle Physics*, **20**, 2004.

[107] Matthews, J., “A Heitler model of extensive air showers”, *Astroparticle Physics*, **22**, 2005.

[108] Krane, Kenneth S., *Introductory Nuclear Physics*, John Wiley & Sons, Inc., 1988.

[109] de Mello Neto, J. R. T. (Pierre Auger Collaboration), “Measurements of cosmic rays at the highest energies with the Pierre Auger Observatory”, *Advances Space Res.*, **53**, 2014.

[110] Gurevich, A. V., G.A. Mesyats, K.P. Zybin, A.G. Reutov b, V.G. Shpak, S.A. Shunailov, M.I. Yalandin, “Laboratory demonstration of runaway electron breakdown of air”, *Phys. Lett. A*, **375**, 2011.

[111] Gurevich, A. V. and A. N. Karashtin, “Runaway Breakdown and Hydrometeors in Lightning Initiation”, *Phys. Rev. Lett*, **110**, 2013.

[112] National Council on Radiation Protection and Measurements (NCRP), “Exposure of the Population in the United States and Canada from National Background Radiation”, *NCRP Report 94*, 1987.

[113] Rossi, Bruno, *Cosmic Rays*, McGraw-Hill Book Company, New York, 1964.

[114] Groom, Donald E., Nikolai V. Mokhov, and Sergei I. Striganov, “Muon Stopping Power and Range Tables 10 MeV–100 TeV”, *Atomic Data and Nuclear Data Table*s, **78,** 2001.

[115] NOAA National Severe Weather Laboratory, “Oklahoma Lightning Mapping Array Data”, <http://www.nssl.noaa.gov/projects/lma.php>.

[116] New Mexico Tech Physics Department, “LMA Hardware,” <http://www.lightning.nmt.edu/lma>

[117] Tsoulfanidis Nicholas, *Measurement and Detection of Radiation*, 2nd ed., Taylor and Francis, Washington D.C., 1995.

[118] Eljen Technology,“ EJ-200 Plastic Scintillator”,<www.eljentechnology.com>.

[119] Google, Google Earth, 2014 <http://www.google.com/earth/>.

[120] N. Budnev, N., D. Chernov, O. Gress, E. Korosteleva , L. Kuzmichev, B. Lubsandorzhiev, G. Navarra, L. Pankov , V. Prosin, Yu. Semeney, C. Spiering, R. Wischnewski, and I. Yashin, “Tunka-25 Air Shower Cherenkov Array: The main results”, *Astropart. Phys.*, **50**-**52**, 2013.

[121] Chiavassa, A., W. D. Apel, J. C.Arteaga-Velázquez, K. Bekk, M. Bertaina, J. Blümer, H. Bozdog, I. M.Brancus, E. Cantoni, F. Cossavella, C. Curcio, K. Daumiller, V. de Souza, F. Di Pierro, P. Doll, R. Engel, J. Engler, B. Fuchs, D. Fuhrmann, H. J. Gils, R. Glasstetter, C. Grupen, A. Haungs, D. Heck, J. R. Hörandel, D. Huber, T. Huege, K. H. Kampert, D. Kang, H. O. Klages, K. Link, P. Łuczak, M. Ludwig, H. J. Mathes, H. J. Mayer, M. Melissas, J. Milke, B. Mitrica, C. Morello, J. Oehlschläger, S. Ostapchenko, N. Palmieri, M. Petcu, T. Pierog, H. Rebel, M. Roth, H. Schieler, S. Schoo, F. G. Schröder, O. Sima, G. Tomae, G. C. Trinchero, H. Ulrich, A. Weindl, J. Wochele, and J. Zabierowski,“Latest results from the KASCADE-Grande experiment”, *Nuc. Instrum. Methods A*, **742**, 2014.

[122] Tinyakov, P.,“Latest results from the telescope array”, *Nuc. Instrum. Methods A*, **742,** 2014.

[123] Sciutto, S. J., “Air Shower Simulations with the AIRES System”, *Proceedings of the 26th International Cosmic Rays Conference in Salt Lake City, Utah*, August 17-25, 1999.

VITA

Nathan Carl Lindy

Candidate for the Degree of

Doctor of Philosophy

Thesis: THE ROLE OF COSMICS RAYS IN LIGHTNING INITIATION

Major Field: Physics

Biographical:

Education:

Completed the requirements for the Doctor of Philosophy in Physics at Oklahoma State University, Stillwater, Oklahoma in July, 2014.

Completed the requirements for the Bachelor of Science in Mathematics at Grand Valley State University, Allendale, Michigan in 2008.

Completed the requirements for the Bachelor of Science in Physics at Grand Valley State University, Allendale, Michigan in 2007.